DESIGN OF A SEMI-ACTIVE STEERING SYSTEM FOR A PASSENGER CAR

Design, Analysis and Control of an Innovative and a Safe Semi-Active Steering System for a Passenger car

By

Masri Bin BAHAROM

submitted for the degree of Doctor of Philosophy

School of Engineering, Design and Technology

University of Bradford

July 2008

Design of a Semi-Active Steering System for a Passenger Car

ABSTRACT

This thesis presents research into an improved active steering system technology for a passenger car road vehicle, based on the concept of steer-by-wire (SBW) but possessing additional safety features and advanced control algorithms to enable active steering intervention. An innovative active steering system has been developed as 'Semi-Active Steering' (SAS) in which the rigid steering shaft is replaced with a low stiffness resilient shaft (LSRS). This allows active steer to be performed by producing more or less steer angle to the front steered road wheels relative to the steering wheel input angle. The system could switch to either being 'active' or 'conventional' depending on the running conditions of the vehicle; e.g. during normal driving conditions, the steering system behaves similarly to a power-assisted steering system, but under extreme conditions the control system may intervene in the vehicle driving control. The driver control input at the steering wheel is transmitted to the steered wheels via a controlled steering motor and in the event of motor failure, the LSRS provides a basic steering function. During operation of the SAS, a reaction motor applies counter torque to the steering wheel which simulates the steering 'feel' experienced in a conventional steering system and also applies equal and opposite counter torque to eliminate disturbance force from being felt at the steering wheel during active control operation.

The thesis starts with the development of a mathematical model for a cornering road vehicle fitted with hydraulic power-assisted steering, in order to understand the relationships between steering characteristics such as steering feel, steering wheel torque and power boost characteristic. The mathematical model is then used to predict the behaviour of a vehicle fitted with the LSRS to represent the SAS system in the event of system failure. The theoretical minimum range of stiffness values of the flexible shaft to maintain safe driving was predicted.

Experiments on a real vehicle fitted with an LSRS steering shaft simulator have been conducted in order to validate the mathematical model. It was found that a vehicle fitted with a suitable range of steering shaft stiffness was stable and safe to be driven. The mathematical model was also used to predict vehicle characteristics under different driving conditions which were impossible to conduct safely as experiments.

Novel control algorithms for the SAS system were developed to include two main criteria, viz. power-assistance and active steer. An ideal power boost characteristic curve for a hydraulic power-assisted steering was selected and modified and a control strategy similar to Steer-by-Wire (SBW) was implemented on the SAS system.

A full-vehicle computer model of a selected passenger car was generated using ADAMS/car software in order to demonstrate the implementation of the proposed SAS system. The power-assistance characteristics were optimized and parameters were determined by using an iteration technique inside the ADAMS/car software. An example of an open-loop control system was selected to demonstrate how the vehicle could display either under-steer or over-steer depending on the vehicle motion.

The simulation results showed that a vehicle fitted with the SAS system could have a much better performance in terms of safety and vehicle control as compared to a conventional vehicle. The characteristics of the SAS system met all the requirements of a robust steering system. It is concluded that the SAS has advantages which could lead to its being safely fitted to passenger cars in the future.

Keywords: steer-by-wire, active steering, innovative, power-assisted steering, steering control, flexible shaft, steering intervention, system failure, safety features.

ACKNOWLEDGEMENTS

I would like to thank my supervisors Dr. Khalid Hussain and Prof. Andrew. J. Day for all their help and guidance in ensuring the success of this research. I would also like to thank Mr. Chhibubhai Mistry who helped me with the preparation and experimental work, and also to all the technicians who were involved in the fabrication of parts.

Thanks to the management of the University Technology PETRONAS, Malaysia who had selected and trusted me to pursue my studies and paid my monthly allowances.

Finally, I want to thank my family members, wife and children, and also friends who have provided endless moral support.

Table of Contents

List of Figures

List of Tables

Nomenclatures

Mathematical Modelling of a Cornering Vehicle Fitted with Hydraulic Power Assisted Steering

F_x, F_y, F_z	(N)	Longitudinal, Lateral and Vertical forces
F_{rack}	(N)	Steering rack output force
M_y, M_z	(Nm)	Pitch and Yaw moments
Subscript x, y, z		In the directions of x, y, z
Subscripts F, R		Front and Rear
Subscript LF, RF, LR, RR		Left Front, Right Front, Left Rear, Right Rear
m, m_s, m_u	(kg)	Total vehicle mass, sprung mass, unsprung mass
a, b	(m)	Distance from centre of garavity (c.g) to front contact patch, rear contact patch
h, θ_r	(m,rad)	Height of sprung mass to the roll axis, Slope of the roll axis
δ, δ_{sw}	(rad)	Average front wheel steer angle, steering wheel angle
V_x, V_y, r, a_y	(m/s,rad/s,m/s^2)	Longitudinal speed, lateral velocity, yaw velocity, lateral acceleration
I_{xx}, I_{zz}, I_{xz}	(kg-m^2)	Roll, yaw and x-z product moment of inertias
$\alpha, \kappa, \gamma, \phi$	(rad)	Lateral slip angle, long. slip ratio, camber angle, roll angle
C_ϕ, K_ϕ	(N-s/rad, N/rad)	Suspension damping constant, spring stiffness constant
α_V	(rad)	Valve deflection angle
t	(m)	Pneumatic trail
Subscripts t, r		Corresponds to pneumatic trail and residual moments
ΔF	(N)	Load transfer
T	(N)	Track width
Ω, R_e	(rad/s, m)	Wheel angular velocity and rolling equivalent radius
τ_a	(Nm)	Steering assist torque
$\tau_{sw}, \tau_r, \tau_{fw}$	(Nm)	Total torque on steering wheel, column/pinion and front wheels
K_t, B_t, K_r, B_r	(Nm/rad, Nm-s/rad)	Torsion and Column/Pinion stiffness and damping

I_{sw}, I_r, I_{sa}	(kg-m^2)	Moment of inertia of steering wheel, column and steering assembly
δ_r, ℓ_{rack}	(rad,m)	Pinion rotation angle, rack displacement
P, A_p, r_{eff}	(N/m^2,m^2,m)	Hydraulic pressure, piston area, and pinion effective radius
B_{sw}, B_{rack}	(N-s/m)	Damping of steering wheel and rack assembly

Detailed and Simplified Mathematical Modelling

δ_{sw}	(rad)	Steering wheel angle
δ_F	(rad)	Average Front Steered Wheel Angle
δ_p	(rad)	Pinion Rotation Angle
m	(kg)	Total vehicle mass
a,b	(m)	Distance from c.g. to front contact patch, rear contact patch
V_x	(m/s)	Vehicle Longitudinal Speed
I_{zz}	(kg-m^2)	Yaw moment of inertia
G		Steering Ratio
$\tau_f; F_{cf}$	(Nm, N)	Friction torque on steering wheel; Friction force
K_t	(Nm/rad)	Steering Shaft Torsion Stiffness
B_t	(Nm-s/rad)	Steering Shaft Damping Coefficient
B_{Fw}	(Nm-s/rad)	Front Wheel Assembly Damping Coefficient
I_{Fw}	(kg-m^2)	Moment of Inertia of Front Wheel Assembly
β	(rad)	Side-slip Angle
$r, \dot{r}$	(rad/s,rad/s^2)	Yaw Velocity, Yaw Acceleration
a_y	(m/s^2)	Total Lateral acceleration
M_{zF}	(Nm)	Self-Aligning Moment
C_{MaF}	(Nm/rad)	Self-Aligning Moment Coefficient
$C_{FaF}; C_{FaR}$	(N/rad)	Front and Rear Cornering Coefficients
α_F	(rad)	Front Slip Angle

Modelling of semi-Active Steering

δ_{sw}	(rad)	Steering wheel angle
δ_{pm}	(rad)	Power motor angle
δ_{rm}	(rad)	Reaction motor angle
δ_F	(rad)	Average Front Steered Wheel Angle
δ_p	(rad)	Pinion Rotation Angle
P	(N/m^2)	Hydraulic pressure
$P_{\min}$	(N/m^2)	Minimum hydraulic pressure
α	(rad)	Deflection angle between steering wheel and pinion rotation
V_x	(m/s)	Vehicle forward speed
τ	(Nm)	Torque
$\tau_{\min}$	(Nm)	Minimum torque
K_f	(Nm/rad)	Constant for feel torque
K_{LSRS}	(Nm/rad)	Constant for low stiffness resilient shaft (LSRS)
R		Output to input ratio
m	(Nm/rad)	Slope of power boost characteristic curve
d	(deg)	Distance between the first and second line of curves
α_0	(deg)	The starting point of the first curve
L	(m)	Wheelbase

Glossary of Terms

SAS	Semi-Active Steering
LSRS	Low Stiffness Resilient Shaft
HPAS	Hydraulic Power Assisted Steering
EPAS	Electrical Power Assisted Steering
SBW	Steer-by-Wire
FBD	Free Body Diagram

Chapter 1

1. Introduction

1.1. Evolution of Steering Technologies in Road Vehicles

Road vehicles have undergone considerable evolution to improve safety performance since the invention of the car over 100 years ago. The braking system for example has evolved from the conventional human-operated pedal to the refined Antilock Braking System (ABS) which was invented to prevent wheel lock and subsequent skidding. Another advanced technology is Electronic Stability Control (ESC) which detects and prevents instability by braking individual wheels in order to control the yaw rates of road vehicles. In the suspension, fully active systems with a mechanical linkage attached to the chassis incorporating active springs and dampers have replaced the conventional springs and dampers in high performance cars. Semi-active suspension is a cheaper alternative to the fully active suspension system but it trades off ride comfort in order to meet safety requirements and cost targets. In this thesis, the area of research concentrates on active steering and safety in road vehicles.

Similarly, the steering system has also undergone a process of evolution and modern steering systems started with the invention of the steering wheel. The driver applied torque at the steering wheel which was transmitted by a rigid shaft to operate a gearing system or a linkage mechanism to generate steering motion at the front road wheels. The evolution of road vehicles has caused the torque required to steer a vehicle to increase due to the increase in vehicle size and weight (note: especially the weight on the front-steered-wheels in Front Wheel Drive (FWD) designs). The problem was solved with the introduction of power-assisted steering in the 1950s, and now this system has become standard (Yih, 2005). The current energy crisis has made hydraulic power-assisted steering to be considered inefficient because the hydraulic pump runs continuously even when the steering is not operating. The hydraulic fluid also poses environmental hazards from leakage and disposal. The introduction of electric power steering has provided a better alternative for power assistance; it is more efficient than hydraulic power-assisted steering because the motor only operates during operation and the absence of hydraulic fluid eliminates environmental hazards.

The introduction of active steering in the early days which control was performed with the presence of a rigid steering shaft has led modern steering systems to evolve into a new era where machine intervention or automatic steering can be performed during emergency. Although the technology could provide some benefits for safety and handling (Ackermann J. , 1998), the presence of a rigid steering shaft has raised concerns about the disadvantage in packaging and safety during front-end collisions ((Yih, 2005), (Oh, Chae, Yun, & Han, 2004).

The latest most crucial evolution in steering technology is the introduction of steer-by-wire (SBW) where an electronic system replaces the mechanical connection or steering shaft. "Fly-by-Wire" control technology has already been implemented on aircraft and has been proven to be reliable and effective (Yih, 2005). The concept of SBW technology could have many advantages in the automotive industry, as listed below ((Yih, 2005), (Cesiel, Gaunt, & Daugherty, 2006)):

- The absence of a steering column simplifies the design of car interiors.
- The steering wheel can be easily located on either side of the vehicle depending on requirements.
- The absence of a steering column prevents noise, vibration, and harshness from the road wheels from being transmitted to the driver through the steering wheel.

- The absence of the steering column prevents impact force from being transmitted to the driver through the steering wheel in the event of a frontal crash.
- Variable steering ratios can be introduced to the steering system as required.
- Active steer technology which is the ability to electronically augment the driver's steering input, can be performed without any limit of the corrective steer.

1.2. Problem Definition

Although a SBW system has many advantages if implemented on road passenger vehicles, the number of SBW systems which are fitted to cars in the main automotive markets is very small. The reason is mainly because of safety concerns in the event of system failures. Catastrophe will result if the moving vehicle can no longer be controlled. Therefore, SBW needs backup mechanical systems for safety reasons. However, including additional redundancy features or back-up systems means that the steering system may become bulky, complicated, and unsuitable due to the increase in cost, packaging space and weight. Moreover, having a back-up system or improving the back-up system by having several redundancies will not increase customers' confidence level because to most customers the back-up systems are simply the standby units which only operate when failure occurs. Customers' safety confidence level will greatly increase if they are told that the steering system they are operating does not have any backup systems but the conventional unit is readily available to take over in case of any active system failure.

1.3. Research Aim

The main aim of this research was to design and propose an improved active steering system technology for a road going passenger car which is similar to the concept of steer-by-wire (SBW) but possesses additional safety features and advanced control algorithms to enable active steering intervention. Innovative active steering system technology is defined in this research as 'Semi-Active Steering' (SAS) because the system configuration is similar to conventional electrical power-assisted steering but the rigid steering shaft is made active by replacing it with a low stiffness resilience shaft (LSRS). The flexibility of the low stiffness resilience shaft allows active steer to be performed by producing additional or less steer to the front steered road wheels relative to the steering wheel input angle. Such a system could switch to either being 'active' or 'conventional' depending on the running conditions of the vehicle; e.g. during normal driving conditions, the steering system behaves similarly to a power-assisted steering system, but under extreme conditions the control system may intervene in the vehicle driving control. A safe SAS will satisfy the following functional requirements of an effective steering system:

- To maintain advantages offered by SBW e.g. cost, packaging, and frontal collision safety.
- To revert to a safe system in case of system failure.
- To provide power-assisted steering with similar characteristics to those of a current hydraulic power-assisted steering system.
- To be capable of performing similar steering control as SBW.

1.4. Project Objectives

The objectives of the project are therefore given as follows:

- Review existing, and published work in the related fields to identify the state-of-art of the steering system technology.
- Develop mathematical models of a cornering vehicle to enhance knowledge on power-assisted steering systems, predict vehicle performance and select suitable parameters for system designs, and provide designers with a simplified approach

to initial design work. The formulae for the mathematical models will be programmed and solved using MATLAB/SIMULINK, and validated by experiment.

- Perform experiments on a real vehicle fitted with suitable flexible shaft stiffness in order to verify the feasibility of implementing an SAS system in the event of active system failure and validate the mathematical models.
- Present the concepts and design of an SAS system which includes the control algorithms comprising of power-assistance and active control systems.
- Develop a full vehicle software model fitted with an SAS system using ADAMS/car. A novel transformation from EPAS to HPAS will be utilized and a selected control strategy will be selected.
- Evaluate the performance of the SAS system by comparing the simulation results with the conventional steering system; and demonstrate the working concept of the SAS system in order to show its feasibility and practicality.

The detailed activities of the research are presented in the chapters of this thesis.

1.5. Thesis Outline

The outline of the thesis is as follows:

- Chapter 1 presents an introduction to the research field which includes the evolution of steering systems.
- Chapter 2 presents a literature review of previous and published work on steer-by-wire, active steering technology and power-assisted steering. The details of the project methodology are established.
- Chapter 3 presents the mathematical models which are required for knowledge enhancement, vehicle performance predictions and selection of flexible steering

shaft properties. The results for the mathematical models intended for knowledge enhancement is discussed in this chapter.

- Chapter 4 presents the experimental set-up, work and results. The preparation work before and during the experiments is explained and the method of vehicle testing used during the experiment and also the type of data acquisition systems which were utilised are discussed. Preliminary results which determine whether a low stiffness resilience shaft could provide stability and safety during system failure are presented.
- Chapter 5 presents the concepts of semi-active steering. The chapter discusses the main differences as well as advantages and disadvantages between SAS and SBW. The chapter also describes the embodiments and control algorithms of the semi-active steering system.
- Chapter 6 presents the modelling activities of electrical power-assistance and control of SAS. The chapter explains in details how the SAS full vehicle software models are built using ADAMS/car software and how the control algorithms are programmed within ADAMS/car templates.
- Chapter 7 presents the results and discussions on the SAS simulation results. The chapter analyzes the results and provides some discussions on the findings.
- Chapter 8 presents a summary of the SAS technology, conclusion and recommendations for future work.

Chapter 2

2. Literature Review and Discussions

This chapter introduces steering systems and reviews published research work in theories, designs, and inventions for different types of steering systems leading to the innovative ideas on semi-active steering presented in this thesis.

2.1. Introduction

The basic functional requirements and description of a steering system have been described in (Reimpell, Stoll, & Betzler, 2001). The main function of a steering system is to steer the front or rear wheels in response to the driver command inputs in order to provide overall directional control of the vehicle (Gillespie, 1992). The steering system must also convert the steering wheel angle to the steered front wheels on the vehicle and convey feedback about the vehicle's state of movement back to the steering wheel (Reimpell, Stoll, & Betzler, 2001). The relationship between the steering wheel angle and the change in the driving direction is not linear mainly due to the linkage design and steering ratio, the development of lateral tyre forces, and the alteration of driving direction. A driver must adjust a suitable steering wheel angle in order to account for deviation from the desired course due to irregularities of the road conditions or other situations which occur during driving, e.g. the roll of the vehicle body, the feeling of being held steady in the seat due under lateral acceleration and the self centring torque the driver feels through the steering wheel (Reimpell, Stoll, & Betzler, 2001).

2.2. Conventional Automotive Steering System

In general, a conventional automotive steering system can be broken down into two main designs; rack-and-pinion and steering gear types. In this research, only the rack-and-pinion system was considered for analysis since the majority of modern cars are fitted with this type of steering.

One of the main problems with the conventional steering system is that the overall steering ratio is approximately constant at any steering angle ((Gillespie, 1992), (Genta, 1997)). This is due to the rigid steering shaft as well as the design of the linkages. Depending on the driving conditions (forward speed, lateral acceleration, etc), a vehicle may experience understeer, neutral steer and oversteer (Pacejka, 2002). Understeer is where the ratio of the steering wheel angle gradient to the overall steering ratio is greater than the Ackerman steer angle gradient (Gillespie, 1992). In other words, the driver turns the steering wheel more than usual but the vehicle is steered less than expected. Neutral steer is where the ratio of the steering wheel angle gradient to the overall steering ratio equals the Ackerman steer angle gradient (Gillespie, 1992). Oversteer is where the ratio of the steering wheel angle gradient to the overall steering ratio is less than the Ackerman steer angle gradient (Gillespie, 1992). In this case, the driver turns the steering wheel less than usual but the vehicle is steered more than expected. This variety demonstrates how active steering could be beneficial for safety purposes by adjusting to the requirements based on driving conditions.

2.3. Active Steering with the Presence of a Rigid Steering Shaft

Active steering (with rigid shaft) is added to or modified from a conventional steering system in order to perform corrective steer based on the driving situation ((Aneke, Ackermann, Bünte, & Nijmeijer, 1999) and (Guldner, Sienel, Tan, Ackermann, Patwardhan, & Bünte, 1999)). It is a system which varies the degree to which the front wheels turn in relation to steering input from the driver (Kasselmann & Keranen, 1969). The first proposal for active steering was made about 40 years ago; Kasselmann, et al. (Kasselmann & Keranen, 1969) designed an active steering controller which used yaw rate signals as input. The system used proportional feedback to generate an additive steering input to the front wheels.

An active steering system offers several advantages such as follows:

- ***Ease of Manoeuvring during Parking and at Low Speed***

  During parking or low speed manoeuvring, the steering ratio should be decreased, to improve manoeuvrability and stability (Oh, Chae, Yun, & Han, 2004).

- ***Vehicle Stability Control at High Speed***

  When a vehicle is travelling at high speed, the steering ratio should be increased (Cesiel, Gaunt, & Daugherty, 2006). This is because the vehicle becomes more sensitive to high lateral forces and wind gusts which will affect its directional stability. Increasing the steering ratio will improve vehicle stability at high speeds because the yaw rate is reduced (Oh, Chae, Yun, & Han, 2004). This kind of vehicle behaviour is required especially when travelling downhill at high speed under strong winds. Increasing the steering ratio will decrease the output to the road wheels from the steering wheel input; this will make the vehicle become less sensitive.

- ***Improvement in Safety Aspects***

  An improvement in safety can be achieved by implementing 'Automatic Steering Control' ((Ackermann, Walter, & Bunte, 2004), (Ackermann J. , 1998)). Automatic Steering is a system that takes over driver control of the vehicle during undesired events. For example, in case of a tyre puncture or gusty winds, the electronic system will take over the driver control of the vehicle by ensuring that the vehicle is stabilized. Ackermann, et al (Ackermann & Bunte, 1997) stated that a driver needed at least 500 milliseconds before he/she can react to unexpected yaw motions when driving a conventional vehicle. It is impossible for such a driver to react because during this time the car may produce a dangerous yaw rate and side slip angle.

Ackermann ((Ackermann & Bunte, 1997), (Ackermann & Bünte, 1999)) also proposed a design of Automatic Steering Control for disturbance rejection which bridged over the driver's reaction time during emergency but then returned the full steering authority to the driver thereafter.

- ***More Efficient than Individual Wheel Braking for Vehicle Stability Control***

  It was demonstrated by (Ackermann, Bunte, & Odenthal, 1999) that an active steering system was more efficient than implementing individual wheel braking for vehicle stability. This system is referred as Electronic Stability Control (ESC) where the system is normally integrated with Antilock Braking System (ABS) (Yasui, Kodama, Momiyama, & Kato, 2006). Ackermann et al. (Ackermann, Bunte, & Odenthal, 1999) showed that active steering only required one quarter of the front wheel tyre force compared to asymmetric braking of the front wheels. Active steering also has an advantage for generating a corrective torque since it allows for a compensation of torques caused by asymmetric braking. Moreover, active steering can be implemented in continuous operation.

Other active steering technologies which are relevant to this research but belong to different fields can be found in ((Gjurkov, Danev, & Kosevski, 2005), (Hac, 2006), (Odenthal, Bünte, & Ackermann, 1999), (Li, Shen, & Yu, 2006), (George, Lendaris, Schultz, & Shannon, 2000) and (Riccardo, Stefano, & Fabio, 2006)).

2.3.1. Means of Implementing Active Steering on Vehicle

There are several means of how active steering can be implemented on passenger vehicles. BMW has developed an active steering system technology using the concept of planetary gears ((BMW, 2008) & (Kerr, 2003)). The system is added to the conventional steering system and controlled electronically by varying the steering ratios. This is achieved by varying the inputs and outputs of the sun and planetary gears depending on vehicle running conditions. For this technology, the steering wheel is connected to the pinion by means of a steering shaft (refer to Figure 2.1).

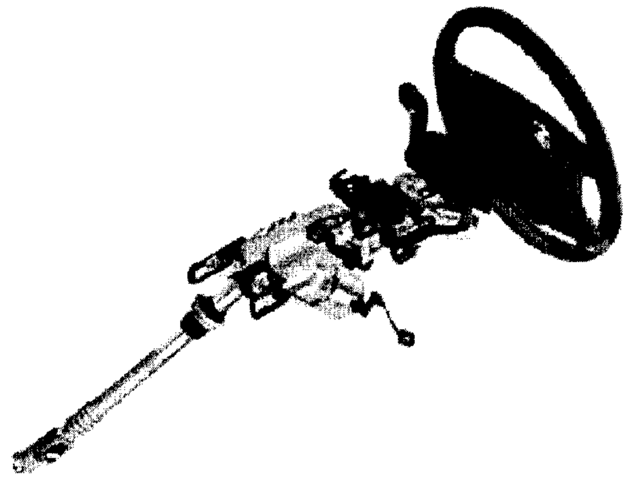

Figure 2.1: Steering Column with Actuator for Active Steering (Courtesy of BMW)

It was stated in (Ackermann, Bunte, & Odenthal, 1999) that TRW designed an active steering system by installing flexible rubber bearings (See Figure 2.2), which connect the steering gear housing to the car body. The bearings are flexible in the direction of the rack travel and stiff in the transverse direction, and are under the control of an actuator which may be either hydraulic or electrically powered.

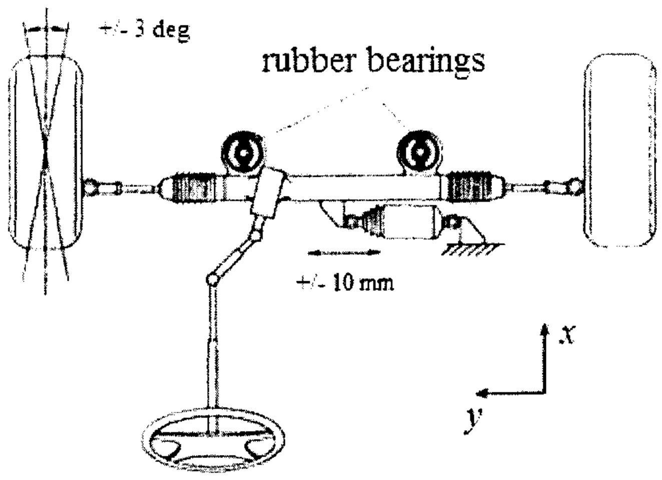

Figure 2.2: Example of An Additive Steering Actuator (courtesy of TRW)

There are several patents e.g. (Sawyer, 2008), (Mitsuhiro & Yoshiteru, 2001), (Augustine, 2006) on active steering systems which have been proposed by researchers but most of them are not yet fully commercialized. One of the latest inventions is an active steering system which provides variable assist to the driver (Augustine, 2006). The system includes a differential actuator having an input gear and an output gear. The differential actuator has a default relationship between the input gear and the output gear such that the magnitude of an output speed and an output torque is approximately equal to a magnitude of an input speed and an input torque with opposing directions. The invention, shown in Figure 2.3 is also capable of generating variable steering ratios.

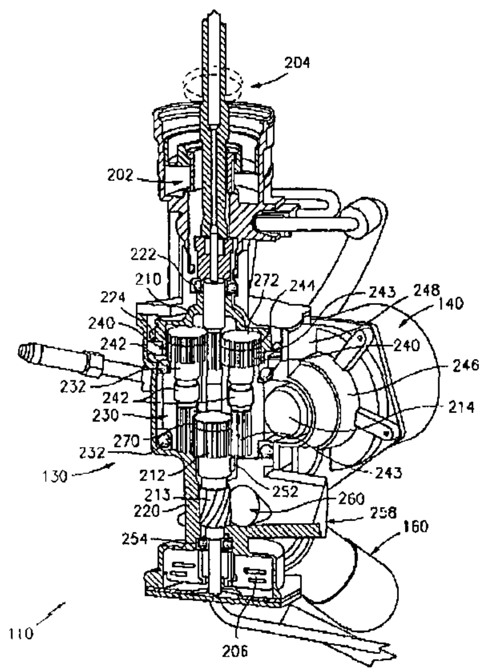

Figure 2.3: Mechanically Linked Active Steering System – US Patent 7063636

2.3.2. Control System for Active Steering

There are many kinds of control systems which can be used to implement active steering and a few examples are discussed in this section. Ackermann, et al. (Ackermann J. , 1994) derived robust feedback control laws which decoupled the lateral and yaw motions of a car, so the yaw rate could be used as feedback to the control system. The benefit of the control law was that it used a generalized decoupling control law for arbitrary vehicle mass distribution. The robust decoupling control law was used to perform automatic steering control [(Ackermann & Bunte, 1997), (Ackermann, Walter, & Bunte, 2004), (Ackermann, Bunte, & Odenthal, 1999), (Guldner, Sienel, Ackermann, & al, 1997) and (Ackermann & Bunte, 1996), (Ackermann, T. Bünte, Sienel, Jeebe, & Naab, 1996), (Ackermann & Bunte, 1996), (Ackermann & Bünte, 1998), (Bunte, Odenthal, & Aksun-Guvenc, 2002)]. The inputs to the controllers were yaw rates with sensors installed on the front, rear or both axles.

Huh, et al. (Huh, Seo, Kim, & Hong, 1999) designed a fuzzy logic controller based on the estimated tyre forces for automatic steering. A method was proposed for active steering or steer-by-wire such that vehicles on slippery roads were steered as if they were driven by experienced drivers. The estimated lateral forces acting on the steered tyres were compared with the reference values and the difference was compensated by the active steering method.

Rossetter, et al. (Rossetter & Gerdes, 2002) looked at the combined influence of decoupling lateral and yaw modes, preview distance, and controller damping on the stability and performance of lateral controllers. The outcomes of these characteristics were studied using an intuitive 'virtual' forces analogy where the control inputs were viewed as single forces acting on a vehicle.

Other researchers who worked in the area of automatic steering include ((You & Jeong, 2002), (Guldner, Sienel, Ackermann, & al, 1997)).

2.3.3. Discussion on Conventional Steering System and Active Steering

Based on the advantages offered by active steering, it was concluded that an active steering system would be more effective in terms of stability control and safety as compared to a conventional steering system. However, the presence of mechanical connections, viz. the rigid steering shaft, may consume some packaging space and in some cases may limit the amount of steering control that can be exercised on a vehicle and thus generate safety concerns. For the cases presented in (BMW, 2008) and (Augustine, 2006), the control capability were unlimited (using planetary gear concepts and clutches) but the systems were very complicated and bulky, while for the case of (Ackermann, Bunte, & Odenthal, 1999), the limitations of corrective steer arise from the limited flexibility of rubber bearings. During frontal collision, a rigid steering shaft may intrude and injure the driver as a result of transmitted force. Although articulated shaft and crush members now are implemented to minimize hazards, more packaging space is then required to compensate for the additional components added to existing steering systems.

Due to several disadvantages of the presence of a mechanical linkage in active steering, any designs improvement such as steer-by-wire system should be considered. All the control algorithms or strategies which can be implemented on active steering can also be implemented on a steer-by-wire system.

2.4. Steer-by-Wire (SBW) Steering

Steer-by-wire is a steering system which replaces the conventional mechanical linkages with electronic sensors, controllers and actuators (Cesiel, Gaunt, & Daugherty, 2006). There is no mechanical connection between the steering wheel and the steering mechanism, i.e. the vehicle's steering wheel is disengaged from the steering mechanism during normal operation (Yao, 2006). The idea of SBW may be new in the automotive industry but it is not new to the aeronautical industry (Yih, 2005). In the aeronautical industry, this technology is referred as fly-by-wire. Nowadays, many modern aeroplanes, both commercial and military, rely completely on fly-by-wire technology.

A SBW system offers several advantages as stated below:

i. Control Aspects

It should be noted again that all the control advantages provided by active steering also belong to SBW. The only difference is that due to the absence of any mechanical linkage, the amount of corrective adjustments, such as correcting the front steered wheel during undesired condition is unlimited or "free control" (Cesiel, Gaunt, & Daugherty, 2006). Among the several advantages in the control aspects offered by SBW are directional control and wheel synchronization, adjustable variable steering feel, adjustable steering wheel return capability, and variable steering ratio (Yao, 2006).

ii. Less Packaging Space and Interior Design Flexibility

The absence of any mechanical linkage simplifies the interior of the car design and the steering wheel can be placed on either side of the car as required (Yih & Gerdes, 2004). This is a packaging advantage which allows much better space utilisation in the engine compartment, and the entire steering mechanism can be designed and installed as a modular unit. Packaging flexibility can also be enhanced because steering gear location is not critical to obtain the desired Ackerman correction or tie-rod load gradient (Cesiel, Gaunt, & Daugherty, 2006).

iii. Energy Saving

The absence of any mechanical linkage and other accessories can reduce the weight of vehicle which can lead to energy savings (Oh, Chae, Yun, & Han, 2004). SBW technology makes use of electrical or electronic systems which consume less energy in comparison with conventional hydraulic power-assisted steering (Yao, 2006).

iv. Safety

During frontal collision, the danger of a driver being crushed by the steering wheel is eliminated since there is no steering column to transmit the force (Oh, Chae, Yun, & Han, 2004). Automatic steering could also be implemented effectively during an emergency in order to assist the driver in controlling the vehicle. By including lane following with SBW, it is estimated that, thousands of lives per year could be saved by maintaining lane position in the absence of driver steering commands ((Switkes, Rossetter, Coe, & Gerdes, 2004) & (O'Brien, Urban, & Iglesias, 1995)). According to the U.S. National Highway Administration, 55% of vehicle fatalities in 2004 were the result of unintended lane departure (Switkes, Rossetter, Coe, & Gerdes, 2004).

v. Vibration and Harshness (NVH)

With the absence of any mechanical connection between the steering wheel and the road wheels, noise, and vibration cannot be transmitted to the driver through the steering column (Yih, 2005). As a result, this will improve driving comfort.

2.4.1. Controls of Reaction Motor and Power Motor

In general, the controllers for SBW motors are divided into two main systems, viz. the steering wheel motor (reaction motor) controller and the front wheel motor (power motor) controller. Many types of approach in designing these controllers have been used e.g. (Coudon, Canudas-de-Wit, & Claeys, 2006) and (Gaspar, Szaszi, & Bokor, 2003) but most of them are derived from vehicle dynamics characteristics and relationships.

Other types of controllers proposed by researches include ((Yih, Ryu, & Gerdes, 2004), (Ueki, Kubo, Takayama, Kanari, & Uchiyama, 2004), (Sharp & Valtetsiotis, 2001), (Shutto & LeRoy, 2006), (Segawa, Nakano, Nishihara, & Kumamoto, 2001) and (Kader, 2006)).

2.4.1.1. Reaction Motor Controller (Steering Feel and Reactive Torque)

The basic purpose of the steering wheel motor control for SBW is to generate reactive torque when the driver steers (Oh, Chae, Yun, & Han, 2004). Oh, et al. (Oh, Chae, Yun, & Han, 2004) designed a PID-based steering wheel motor controller that makes steering 'easy' at low speeds or when parking and 'harder' at high speeds to improve steering feel by adjusting reactive torque. A torque map was proposed for the steering response since the steering wheel motor could not be controlled in real time using vehicle dynamics because the ECU capacity was insufficient (Oh, Chae, Yun, & Han, 2004). The control gain formula was derived for the steering reactive torque and the reactive torque was increased according to vehicle speed and steering wheel angle (Oh, Chae, Yun, & Han, 2004).

Segawa, et al. (Segawa, Kimura, Kada, & Nakano, 2002) found that the reactive steering torque was a function of vehicle speed, and designed a controller in which the steering wheel angle was used as input. Vehicle speed was introduced to the reactive torque control in order to stabilize vehicle behaviour at high speed similar to a conventional vehicle. With the introduction of reactive torque, the steering wheel returns to the centre position smoothly when the driver releases it.

A typical SBW system uses the steering wheel position signal in order to control the position of the road wheels (Amberkar, Bolourchi, Demerly, & Millsap, 2004). The forces from the road wheels are then measured and used to provide the feedback torque to the driver. Amberkar, et al. (Amberkar, Bolourchi, Demerly, & Millsap, 2004) proposed a steering wheel reactive torque controller which feeds steering wheel position information directly into the steering wheel motor command through an appropriate transfer function. By selecting the transfer function, the desired steering feel is obtained from the direct relationship between the steering wheel angle and the steering wheel torque.

2.4.1.2. Power Motor Controller

Oh, et al. (Oh, Chae, Yun, & Han, 2004) modelled a controller for the power motor using the bond graph method which relates to vehicle dynamics consisting of mechanical and electrical systems energy flow. The PID control was used to perform feed forward control to improve the vehicle's manoeuvrability and stability. The vehicle behaviour was controlled to provide an oversteer characteristic at low speeds for quick response, and understeer at high speed to prohibit rapid steering inputs.

Yih, et al. (Yih & Gerdes, 2004) presented an approach to estimating vehicle side slip angle using steering torque information which could be easily determined from the current drawn by the steering motor. An algorithm was devised to estimate the side slip with the inputs of yaw rate and steering angle. Feedback control was developed based on the estimated side slip to alter the handling characteristics of a vehicle through active steering intervention.

Yao, (Yao, 2006) designed a controller where the road wheel angle could track the steering wheel angle. A road wheel servo feedback control was developed to implement the tracking of the actual road wheel angle to the desired reference angle. The basic property of the servo control system was that the controlled output signal tracked a reference input signal through the rejection of external disturbance effects.

2.4.2. Safety Back-up Systems and Power Assistance

Due to the absence of the mechanical connection from the steering wheel to the road wheels, safety back-up systems are required to be installed on any SBW system. This is because in the event of SBW system failure, the vehicle will not be controllable and hence may lead to catastrophe! Several designs of backup systems have been suggested which can be found in the patent documents or manufacturers' websites. Selected designs of most relevance to this research will be discussed in this section.

Inventor (Wittmeijer, 2004) proposed a fully electric power assistance steering system with mechanical back-up device. The mechanical backup device is a rotatable connection between the steering wheel and the steering assembly. The inventor referred the rotatable connection as a back-up system because when fully power assistance is provided by the power motor, the steering shaft will not carry any twisting load and therefore it is in a state of stand-by. In case of failure, the back-up system is readily available. The proposed system was only an electric steering system and no control aspects were stated in the patent documents (refer to Figure 2.4).

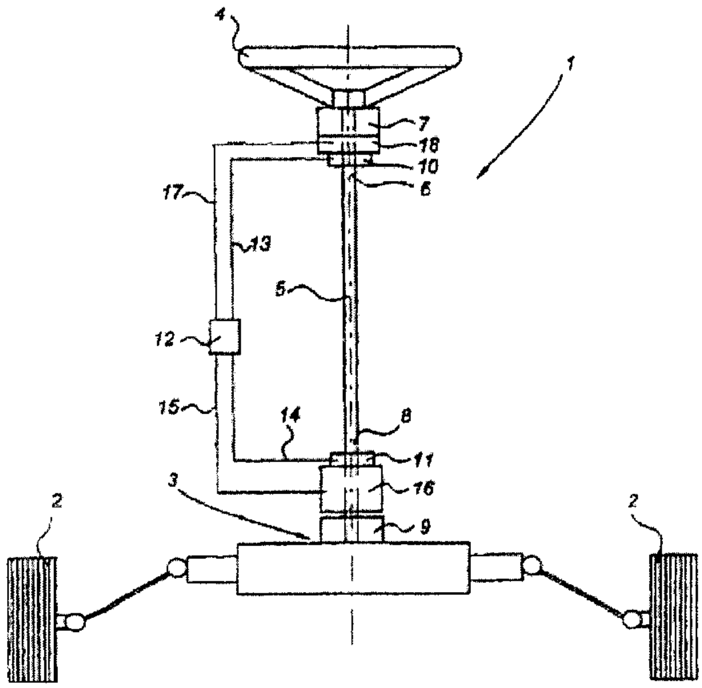

Figure 2.4: Electric Steering System with Mechanical Back-up Device, Patent Pub. No. US 2004/0007418 A1 [82]

Similar to the concepts proposed by (Wittmeijer, 2004), some inventors (Kanagawa & Saitama, 2005) proposed a steering system with a back-up (Figure 2.5) which is capable of allowing active control to be performed on the front wheels through a torsion bar. The reaction motor pinion gear is attached to the steering shaft through planetary gear configurations which allow the reduction of gear ratios. The torque applied at the steering wheel is measured through the deflection of the torsion bar. The amount of measured torque is then used to provide power assistance to the steering system. The yaw rate value is also measured in order to perform corrective steer through the torsion bar.

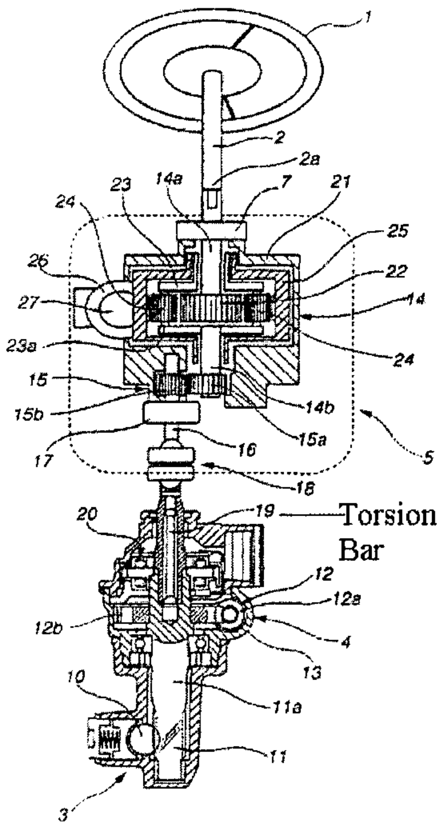

Figure 2.5: Steering Control System, Patent Pub. No. US 2005/0016791 A1
(Kanagawa & Saitama, 2005)

Other inventors (Husain, Daugherty, & Oynoian, 2004) proposed an invention comprising a steering system selectively operable in one of three modes, viz. SBW, electronic power assisted steering, and manual steering. Inter-changeability between modes is achieved using a clutch which engages or disengages a flexible shaft connecting the steering wheel to the road wheels; during SBW mode, the clutch is disengaged. During active system failure, the clutch is engaged so that a mechanical connection is available for electronic power assisted steering mode. In the event of system power cut-off or vehicle is not running, the system is operable in manual mode through clutches. Refer to Figure 2.6.

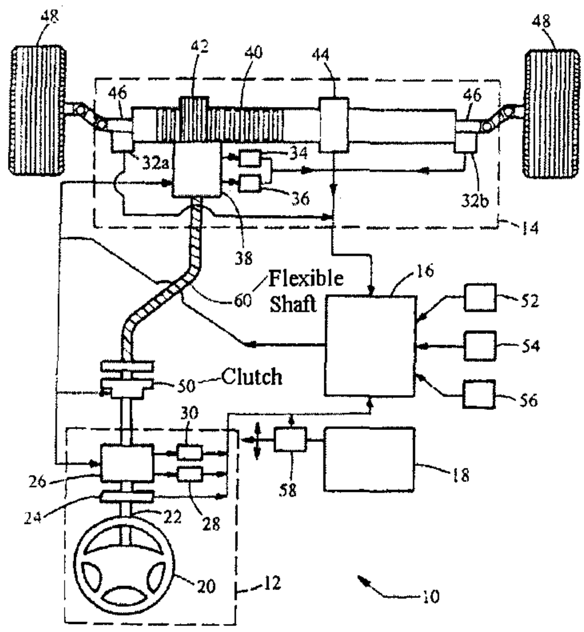

Figure 2.6: Motor Vehicle Steering System, Patent Pub. No. US 2004/0262073 A1 (Husain, Daugherty, & Oynoian, 2004)

There are many more designs which are similar to the invention in (Husain, Daugherty, & Oynoian, 2004) that make use of flexible shaft and clutches mechanisms. The differences are mainly the ways in which the clutches are activated e.g. by mechanical, electronic or hydraulic systems. Examples of these can be found in patent documents e.g. (Sherwin & DuCharme, 2003), (Itoh, 2006), and (Yoshiyuki, 2006).

The design of back-up systems not only involves the design of clutches but also includes the strategy for software configurations. Pimantel, (Pimentel J. , 2004) presented a hardware and software architecture suitable for a safety critical SBW system which supports component failures, software errors and human errors. Pimantel, (Pimentel J. R., 2006) further verified and validated of the safety critical aspects of steer-by-wire system using the DO-178B standard. Other safety aspects related to steer-by-wire can be found in the following literatures (i.e. (Song, Simonot-Lion, & Clement, 2001), (Krautstrunk & Mutschler, 2000) and (Rossetter, Switkes, & Gerdes, 2003)).

Gadda, et al. (Gadda, Yih, & Gerdes, 2004) stated that a probabilistic analysis of the failure rates of fly-by-wire systems using various forms of redundancy coupled with diagnostic techniques could be designed to have an overall reliability rate of 10^{-9} failures/hour. In an automotive SBW context, such reliability rate of failure is very small and the system may be implemental on passenger cars.

2.4.3. Discussion on Steer-by-Wire

The advantages of SBW indicate that it is a suitable steering system for modern cars. The major problem with SBW is safety issue. In the case of electronic system failure, a moving vehicle will face catastrophe if it cannot be controlled without a mechanical connection between the steering wheel and the road wheels. How reliable are SBW electronic systems?

Some researchers may claim that SBW system is reliable as the system has been proven to be successful in the aeronautical industries. Gadda, C. D., et al (Gadda, Yih, & Gerdes, 2004) argued that the diagnostics systems for aircraft are not the same as for ground vehicles as aircraft have certain design freedoms. For example, triply redundant sensors, actuators, and controllers which are common practice in fly-by-wire, but are prohibitive in automotive industries. Also, aircraft are typically tens of seconds or more from any possible source of collision.

In the report of the US National Science and Technology Council Committee on Technology, entitled “Review of Federal Programs for Wire-System Safety” (National Science and Technology Council Committee on Technology, Nov 2000), it was stated that the failures of by-wire systems are mainly due to the aging of wiring systems from the following causes:

- Chemical, including corrosion and moisture intrusion.
- Thermal, including fluctuations in thermal which cause embrittlement.
- Electrical discharges such as surges or arcs and partial discharges or transient.
- Mechanical such as vibration, chafing, overload and fatigue
- Radiological, which also causes embrittlement.

Whatever measures are taken to promote the life of SBW technology such as providing multiple wiring redundancies or utilising the best software architecture, the system is still subject to failures and questionable safety issues. The only measure that will increase customers' safety confidence level is a permanent mechanical connection between the steering wheel and the road wheels as found in the conventional steering system.

The proposal made by patent inventors (Wittmeijer, 2004) of a back-up system in the form of a permanent steering shaft connecting the steering wheels to the road wheel is a good choice. However, the technology is only an electrical power assisted steering system where no active steering aspects are considered. The proposal made by inventors (Kanagawa & Saitama, 2005) also includes a permanent steering shaft connecting the steering wheels to the road wheels but the connections are through gears. Active steering can also be performed on the front wheels of the system by using a torsion bar. The main problem with these two inventions is that the proposed steering shafts may be rigid longitudinally which is undesirable in the event of frontal collision. Moreover, the systems may require more packaging space.

Inventors (Husain, Daugherty, & Oynoian, 2004) solved the problems of the safety issues during frontal collision and the packaging benefits by introducing a flexible shaft that can be routed through any desired locations. This design is very useful and important because the proposed steering system will be able to maintain all the benefits offered by SBW. The main problem with the invention is that the flexible shaft connects the steering wheel to the road wheels through a clutch mechanism. No matter how good such a clutch system is designed, one can still argue that more failure modes are introduced with the clutch.

Based on the previous design concepts presented for active steering and steer-by-wire, a system which compromises both technologies that utilizes a special steering shaft is the most practical. It is therefore proposed that the special steering shaft of the system has a permanent mechanical connection between the steering wheel and the road wheels; and it is designed to have low stiffness so that it is flexible in the twist direction to allow steering intervention (active control), and resilience in the transverse direction to improve packaging and safety. The proposed steering shaft can be referred as low stiffness resilience shaft (LSRS).

It can be noted from the previous patent documents that the trends of current SBW or active steering designs are to segregate active control and power assisted steering systems [(Kanagawa & Saitama, 2005) and (Husain, Daugherty, & Oynoian, 2004)]. This is a good approach since the control algorithm would be much simpler. In this case, the theory and knowledge of power assisted steering designs and configurations must be considered in detail for optimisation purposes.

2.5. Power-Assisted Steering and Control

The need for power steering has increased and is widely used nowadays due to the increasing front axle loads of vehicles, and the requirement for fast action during steering (Davis, 1945). Manual steering systems are used as a basis for power steering systems because the mechanical connection can serve as a safety device and continue to operate with or without the help of the auxiliary power in case of failure. The main reasons why power steering is needed are to take the effort out of parking and low speed manoeuvring, and to reduce effort when completing a severe cornering or correction of a car's attitude at medium speeds (Adams, 1983). The additional characteristics that are required for a power steering system will be discussed later.

Power steering 'feel' is a system characteristic that will 'tell the driver' what forces are being used to steer the vehicle and provide him/her with steering characteristics that are as near as possible to, and as controllable as, a manual steering system (Adams, 1983). Baxter, (Baxter, 1988) derived a simplified mathematical formula to calculate the steering gear 'stiffness' as the change of the rack output force with respect to the change in the steering wheel angle, and the steering gear 'feel' as the change of the steering wheel torque with respect to the change in the rack output force. The performance of a hydraulic power assisted steering can be assessed from boost curves and steering design variables.

The types of power assisted steering that will be reviewed here are hydraulic power assisted steering and electrical power steering. The work done by previous researchers will be discussed and presented. The focus will be on the mathematical modelling, boost curve characteristics and control algorithms.

2.5.1. Hydraulic Power Assisted Steering System

This type of power steering system is the most widely used nowadays (Reimpell, Stoll, & Betzler, 2001). The principle of operation is very complicated but it is advantageous in term of cost, space and weight. The hydraulic rack and pinion steering system provides self-damping that reduces the effect of torsional impacts and torsional vibrations (Gillespie, 1992).

The basic working principle of hydraulic power assisted steering has been described in (Reimpell, Stoll, & Betzler, 2001). The vane pump which supplies the oil pressure is driven by the engine via a V-belt. The pressurized oil is routed to the steering valve which distributes the flow to either right or left pressure lines depending on the rotation of the steering wheel.

In some designs, the measurement of the steering wheel torque is achieved through the use of a torsion bar which connects the valve housing to the valve piston in a torsionally elastic way. When the driver turns the steering wheel, torque is generated in the torsion bar. The actuation of power assist depends on the characteristic curves (boost curves) which are functions of steering wheel torques or valve deflection angles. The valve characteristics which determine the power boost can be changed by changing the strength of the torsion bar alone or by changing valve sensitivity alone or by the combination of the two (Adams, 1983).

2.5.1.1. Mathematical Modelling of a Hydraulic Power Assisted Steering (HPAS)

Pfeffer et al. (Pfeffer, Harrer, Johnston, & Shinde, 2006) developed a complete simulation model starting from the steering valve in order to predict the steering wheel torque which is a key feature for steering feel. The model has five degrees of freedom and new advanced friction elements were included. The high order hydraulic system was also modelled with consideration of fluid inertia and compliance.

Post et al. (Post & Law, 1996) developed a method to characterize the inherent friction behaviour for a given steering gear. Experiments were conducted and the results showed that the friction level could depend on steering gear input shaft position, angular velocity and loading conditions.

Baharom et al. (Baharom, Hussain, & Day, 2006) developed a mathematical model of a cornering vehicle fitted with hydraulic power assisted steering (HPAS). The model had three degree-of-freedoms; lateral motion, yaw and roll, and an extra one degree-of-freedom from the HPAS assembly. The main intention of the modelling was to evaluate the HPAS system performance by measuring the steering gear 'stiffness' and 'feel'.

Wong, (Wong T. , 2001) presented a HPAS system design and optimisation using a software called 'Hydraulic Integrated Power Steering' (HIPS). The software provided a design and test environment for the integrated steering and suspension system subjected to disturbance forces, which may be induced by pump flow oscillation and tyre loads.

2.5.1.2. Ideal HPAS Boost Characteristic Curves

There are many types of power boost characteristics which are used by different manufacturers in the automotive industry for their HPAS systems. The differences among these characteristics are mainly due to the different designs of the hydraulic valves produced by different manufacturers. In this section, only the most ideal HPAS boost curve will be discussed. As suggested by Adams, (Adams, 1983), the most ideal boost curve for the HPAS is shown in Figure 2.7.

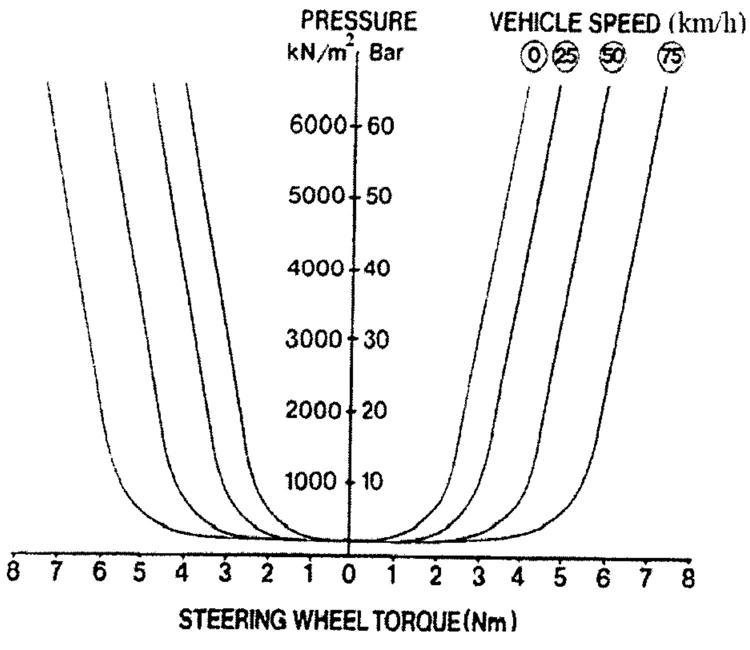

Figure 2.7: An Ideal Hydraulic Power-Assisted Steering Boost Curve (Adams, 1983)

The power boost curve shown in Figure 2.7 is considered to be an ideal one because it has the following advantages (Adams, 1983):

- At low vehicle speed or during parking, the driver needs to apply less steering wheel torque but the power assistance is high. This behaviour is very good since quick action is required during parking or manoeuvring at low vehicle speed.
- At high vehicle speed, the driver needs to apply higher steering wheel torque for steering assistance to take effect. For specific vehicle speeds, the power assistance will be activated only after the driver exceeds a certain amount of torque or deflection angle. This is to ensure that the driver will have sensitivity when handling a high-speed-vehicle and avoids any human error that might cause the vehicle to be difficult to control as a result of a small change in the steering wheel rotation.
- All the linear region curves have the same slope. This ensures that the driver's steering feel and power assistance are consistent.
- The linear curves increase in a specified pattern. This characteristic is desirable in order to make sure that the steering feel or steering wheel torque also increases based on the specified pattern. The intention is mainly to inform the driver that at higher vehicle speeds, the vehicle is more sensitive and the consequence of any accident is more serious.

2.5.2. Electrical/Electronics Power Assisted Steering (EPAS)

Electrical power assisted steering (EPAS) systems do not make use of any hydraulic circuit and the steering boost is activated through an electric motor (Reimpell, Stoll, & Betzler, 2001). The actuation of the servomotor corresponds to a specified design curve, determined by the steering wheel torque and the vehicle speed. Despite having several advantages as compared to the hydraulic power assisted steering, EPAS has limited power due to the maximum operating voltage of 12 V. Recently, some new designs have incorporated a voltage increase to 42V which makes the EPAS and other control tasks much easier (Reimpell, Stoll, & Betzler, 2001). The mathematical modelling of EPAS was discussed in (Badawy, Zuraski, Bolourchi, & Chandy, 1999). The advantages of EPAS as compared to hydraulic power assisted steering include (VISTEON):

- Improved fuel economy. Unlike hydraulic power assisted steering, the electric motors are not on all the time but only during cornering or parking.
- Reduced complexity to automotive manufacturers by simplifying the steering system package.
- Customised steering feel.
- No need for power steering fluid and hoses.

Selected work on the control and steering feel aspects is discussed in the following section.

2.5.2.1. Control and Steering Feel

MacCann (McCann, 2000) investigated a method for improving vehicle stability by incorporating feedback from a yaw rate sensor into EPAS. One of the reasons of the loss of vehicle control is the reduction in tactile feedback from the steering wheel when driving on wet or icy roads. The method improved vehicle stability by increasing the amount of tactile feedback when driving under adverse road conditions through variable effort steering.

Sugiyama et al. (Sugiyama, Kurishige, Hamada, & Kaifuku, 2006) presented a new control strategy for EPAS to reduce steering vibration associated with disturbance from road wheels. The controller was constructed based on damping for specified frequency using the motor angular velocity. The experimental result was proven successful without sacrificing road information generated by self-aligning torque.

Yasui et al. (Yasui, Kodama, Momiyama, & Kato, 2006) developed a control system which coordinated the electronic stability control (ESC) with EPAS. The system estimated a new vehicle state estimation from EPAS which provides the information on the steering torque and ESC which supplies the information on the handling characteristics of the vehicle.

A few examples of research in the steering feel for EPAS can be found in ((Switkes, Coe, & Gerdes, 2004), (Agebro, Nilsson, & Stensson Trigell, 2006), (Camuffo, Caviasso, Pascali, & Pesce, 2002), (Chai, 2004)). The research in modelling of EPAS and its control can be found in ((Pang, Jang, & Lee, 2005), and (Liao & Du, 2003)).

2.5.3. Discussion on Power-Assisted Steering and Control

Based on the advantages of EPAS as compared to HPAS, EPAS is definitely suitable for automotive use. However, the ideal boost curve of hydraulic power assisted steering fulfils almost every requirement of an effective steering system. Therefore, it is desirable that the proposed steering system can be designed to operate on an EPAS system while the power boost characteristics of EPAS can be made to follow the ideal characteristic curve of HPAS. Since the proposed steering system has similar concepts to active steering and steer-by-wire, any types of control implemental on the two should also be applicable to the system.

2.6. Chapter Summary

Chapter 2 presents published work on steering systems in theories, designs and inventions including the role of steering systems and their requirements. The types of steering systems based on chronological technology were presented and the advantages as well as the disadvantages of each system were discussed. The embodiments as well the implementation of control algorithms of each system were described.

The first illustrated topic was the conventional steering system. The main problem with the conventional steering system was that the overall steering ratio was almost constant due to the rigid shaft and linkage design. Depending on driving conditions, a road vehicle can experience situations such as understeer, neutral steer and oversteer, which might result in instability; hence active control was needed for safety reasons.

Active steering was a solution to the conventional steering system by improving the performance in terms of ease of manoeuvring, vehicle stability, safety aspects and efficiency; but the presence of a mechanical connection in active steering resulted in packaging and safety disadvantages, and in some cases limited the capability of performing control.

Steer-by-wire could provide similar advantages offered by active steering but the system offers additional features such as unlimited control capability, packaging advantage and safety aspects due to the absence of mechanical linkage. The main problem with steer-by-wire (SBW) is that back-up systems either in the form of mechanical connection (e.g. flexible resilience steering shaft) or redundancies (wiring and software architectures) are required because the vehicle would be uncontrollable in the case of system failure.

Any form of back-up system which relied on clutches might not increase customers' safety confidence level since clutches introduce more failure modes. The presence of a mechanical connection between the steering wheel and the road wheels was hoped to increase customers' safety confidence level.

Based on the previous findings, a steering system which implemented a low stiffness resilience shaft (LSRS) that combined the advantages offered by active-steering and steer-by-wire has been proposed. The LSRS is readily available in the event of system failure; and its flexibility allows steering intervention to be performed.

Based on previous published work, active control on vehicles could be performed either using a vehicle dynamics approach which was more complicated but efficient; or segregating the power assistance and control aspects which was simpler but might be less efficient. Due to simplicity, it was decided that control algorithm of the proposed steering system would follow the approach of the latter.

It was illustrated that an ideal Hydraulic Power-Assisted Steering (HPAS) boost curve could provide a road vehicle with advantages in providing steering feel and safety aspects during low and high speed manoeuvres. Also, it was found that Electrical Power-Assisted Steering (EPAS) could offer more advantages than HPAS in terms of energy saving, design simplicity and customized steering feel capability.

Based on the previous findings, it was concluded that the power assistance of the proposed steering system would be designed to operate on an EPAS system while its power boost characteristics would be made to follow the ideal characteristic curve of an HPAS. For the implementation of active control, any types of control strategies should be applicable to the proposed system.

2.7. Restatement of Research Methodology

As a result of the literature review, the research methodology was developed as follows. The first task is to increase knowledge in the field by developing a mathematical model of a full cornering vehicle fitted with hydraulic power-assisted steering and analysing the model in order to understand the relationships among steering characteristics such as steering feel, steering wheel torque and power boost forces. Then the most important aspect that needs to be verified is whether the low stiffness resilience shaft (LSRS) will be able to provide vehicle stability and safety in case of active system failure. For verification purposes, a mathematical model which predicts the behaviour of a vehicle fitted with a flexible shaft is required. Such a mathematical model can be developed by modifying the steering formula and approximating the remaining formula from the previously developed vehicle model of a cornering vehicle with hydraulic power assistance. The formula for all mathematical models will be developed and solved by using MATLAB/SIMULINK. The results from the mathematical model of a vehicle fitted with flexible shaft can then be used to estimate suitable range of lowest steering shaft stiffness to be used for the experiment. The mathematical model can also be used to predict vehicle characteristics under different driving conditions which are impossible to perform experiments.

Experiments on a real vehicle fitted with suitable flexible shaft stiffness will be conducted and the results will be used for the following purposes:

- To ensure that a vehicle fitted with suitable range of lowest steering shaft stiffness is safe and stable to be driven before proceeding with further work.
- To validate the mathematical model of a cornering vehicle fitted with flexible shaft so that the formula can be used for prediction purposes.

After conducting experiments and verifying that a vehicle fitted with suitable range of lowest steering shaft stiffness is stable and safe to be driven, the concepts, system designs and control algorithms of SAS will be presented. Also, after validating the mathematical model, the formula will be used to determine the exact suitable stiffness of low stiffness resilience shaft and basic parameters of SAS.

A full-vehicle software model of a selected car will be built and simulated by using ADAMS/car software in order to demonstrate the embodiment and implementation of SAS system. The process of developing the virtual model will begin with the construction of a full-vehicle software model fitted with conventional hydraulic power-assisted steering. This model can be validated by using the mathematical model of a cornering vehicle fitted with hydraulic power-assisted steering.

After validating the conventional vehicle model, the next task will be to create a new model equipped with the SAS system from the existing conventional model. This can be done by replacing the rigid steering shaft with the low stiffness resilience shaft. The development of control algorithms will be implemented in two stages. The first stage is to add electrical power assisted steering to the SAS system. The power-assistance characteristics are optimised and parameters are determined by using trial-and-error iteration techniques inside the ADAMS/car software. The next stage is to add the control features to the SAS system. An example of an open-loop control system will be selected for demonstration; converting the vehicle to behave either under-steer or over-steer depending on the vehicle forward speed.

Finally, the full vehicle software model with a complete SAS system will be simulated on a few selected cornering events and the results are compared with the conventional hydraulic power-assisted steering model. The detailed activities in all the tasks are presented in different chapters.

Chapter 3

3. Mathematical Models

This chapter presents three mathematical models which were developed mainly for the knowledge enhancement of power-assisted steering, performance predictions of a vehicle fitted with a flexible steering shaft, and selection criteria of flexible steering shaft properties. The first model was a three-dimensional (3D) full vehicle model while the remaining two were the simplified two-dimensional (2D) linear models.

Two passenger cars were used as the subjects of studies and experiments; a Jaguar X-Type 2.2L Diesel and a Ford Fiesta. A complete data set including vehicle geometric hard points was available for the Jaguar car. The manufacturer only provided basic data for the Ford Fiesta such as cornering stiffness, centre of gravity locations and moment of inertia. The Jaguar car was used for the modelling and simulation work while the Ford Fiesta was used for the experimental work.

3.1. Modelling of a Cornering Road Vehicle Fitted with Hydraulic Power-Assisted Steering

This section presents the mathematical modelling of a cornering car fitted with hydraulic power assisted steering, to enhance the knowledge of the cornering behaviour of such a vehicle and to validate a full-vehicle software model. The fundamental knowledge required to understand the relationships affecting steering characteristics includes steering feel, reactive torque, and steering wheel torque. A formula was also required to derive a mathematical model of a cornering vehicle fitted with a flexible steering shaft (LSRS) and also for the future design of SAS. The 3D full vehicle model was used also to validate the ADAMS/car software model which is used to simulate the embodiment and control algorithms of the SAS system presented in Chapter 6.

The Jaguar car under study had the actual dimensional data and design parameters shown in Appendix 1(a). The tyre data was taken from the file 'pac2002_195_65R15.tir' (Appendix 1(b)), which was accessible from the ADAMS 2005 software. The tyre file command was set to 'USE_MODE = 13', which implies that the software will compute F_x, F_y, M_x, M_y and M_z using uncombined (pure slip) force and moment calculation including tyre relaxation behaviour.

The mathematical formulae that were used in deriving the model were the same (or as close as possible to) those implemented in the commercial software depending on their level of complication. These formulae are in the forms of equations of motion and are programmed in MATLAB/SIMULINK to solve.

In deriving the complete mathematical formula, the 'cornering vehicle' and 'power-assisted steering' cases were initially separated. The formula for the cornering vehicle was derived from three equations, namely the summation of lateral forces, the summation of yaw moments and the summation of roll moments. The input to the equations of motions was the front-steered wheel angle.

The next task was to develop and add the power-assisted steering model to the cornering vehicle model. The mathematical modelling of the power-assisted steering could not be analyzed independently. This is because the system was dependent on the self-aligning moments generated at the front wheels and the yaw rate of the cornering vehicle. The formulae were derived from the summation of yaw moments from the free body diagram of the steering assembly which includes the steering wheel, steering column, rack and pinion, and front wheels. After the two models were assembled, the final required inputs to the system were the steering wheel angles and the power boost characteristics.

3.1.1. Mathematical Modelling of a Cornering Vehicle

The full mathematical modelling of a cornering vehicle was derived from four equations of motion, viz. the summation of longitudinal forces, lateral forces, and yaw moments as well as roll moments (Pacejka, 2002). For the case of a constant forward speed, the equations of motion involving the longitudinal forces were omitted. The load transfer through linkages which contribute to the roll angle inclination was assumed to be negligible. With small angle approximations and neglecting the non-linear terms, the equations of motions reduced to the following (Pacejka, 2002):

$$F_{xF}\delta + F_{yF} + F_{yR} = m_s h\ddot{\phi} + m(rV_x + \dot{V}_y) \tag{3.1}$$

$$aF_{xF}\delta + aF_{yF} - bF_{yR} + M_{zF} + M_{zR} = (I_{zz}\theta_r - I_{xz})\ddot{\phi} + I_{zz}\dot{r} \tag{3.2}$$

$$m_s h(\dot{V}_y + rV_x) + (I_{zz}\theta_r - I_{xz})\dot{r} + (C_{\phi F} + C_{\phi R})\dot{\phi} + (K_{\phi F} + K_{\phi R} - m_s gh)\phi + (I_{xx} + m_s h^2)\ddot{\phi} = 0$$

where $F_{xF} = F_{xLF} + F_{xRF}$; $F_{yF} = F_{yLF} + F_{yRF}$; $F_{yR} = F_{yLR} + F_{yRR}$

$$M_{zF} = M_{zLF} + M_{zRF} \; ; \; M_{zR} = M_{zLR} + M_{zRR} \tag{3.3}$$

Similar to the computational processes performed by ADAMS software, the interaction of forces and moments with individual wheels was calculated. In line with the selected tyre file for this analysis, the Magic Formula Tyre Model (PAC2002) was used to compute the lateral as well as the longitudinal forces and moments. The general form of the formula to calculate forces for given values of vertical load and camber angles reads (Pacejka, 2002):

$$f = D\sin[C\tan^{-1}\{Bx - E(Bx - \tan^{-1}(Bx))\}] \tag{3.4}$$

with $F(X) = f(x) + S_V$; $\quad x = X + S_H$

where F : Represents outputs for $F_{yj}(F_{zj}, \gamma_j, \alpha_j)$ or $F_{xj}(F_{zj}, \gamma_j, \kappa_j)$; X : Represents inputs of α_j or κ_j.

The general forms of the formulae for the moment calculations are as follows (Pacejka, 2002):

$$M_{zj}(F_{zj},\gamma_j,\alpha_j) = -t(F_{zj},\gamma_j,\alpha_{tj})\cdot F_{yj}(F_{zj},\gamma_j,\alpha_j) + M_{zrj}(F_{zj},\gamma_j,\alpha_{rj}) \qquad (3.5)$$

where $t(\alpha_t) = D_t \cos[C_t \tan^{-1}\{B_t\alpha_t - E_t(B_t\alpha_t - \tan^{-1}(B_t\alpha_t))\}]$; with $\alpha_t = \alpha_j + S_{Ht}$

$M_{zr}(\alpha_r) = D_r \cos[\tan^{-1}(B_r\alpha_r)]$; with $\alpha_r = \alpha_j + S_{Hf}$

Details of the calculation of the coefficients of equations (3.4) and (3.5) are provided in Appendix 1(c) (Pacejka, 2002). The remaining sub-coefficients and data for each of the above coefficients were readily specified in the tyre file complete with their descriptions. In this analysis, the contribution of 'turn slip' or 'path curvature' was neglected. Therefore, the factors ζ_i appearing in the previous equations were set to unity, $\zeta_i = 1$ $(i = 0,1,....,8)$ (Pacejka, 2002).

The input values for the calculation of forces and moments were $\alpha_j, F_{zj}, \gamma_j$ and κ_j. At time, $t = 0$ all of the input variables were equal to their initial values, except for the case of lateral slip angle where the initial value was equal to the initial toe angles, $\alpha_{j0} = \psi_{j0}$. The expression for the assumed small lateral slip angle reads [(Pacejka, 2002), (Dixon, 1996)]:

$$\alpha_{LF,RF} = \delta - \frac{V_y + ar - e\dot{\delta}}{V_x} \quad ; \qquad \alpha_{LR,RR} = -\frac{V_y - br}{V_x} \qquad (3.6)$$

In order to calculate the vertical tyre force for each wheel, F_z, the load transfers for the front and rear axles needed to be determined. In the commercial software, the computation of load transfers was performed rigorously by calculating the interaction of forces in every linkage of the suspension parts and the vehicle body. For approximation purposes, the calculation of load transfers could be simplified by determining the proportionality of the equivalent masses and stiffness for the front and rear, hence the approximate load transfers to/from the front and rear axles are as follows (Dixon, 1996):

$$\Delta F_{zF} = \frac{1}{T_F}\left[m_{uF}h_{uF} + m_{sF}h_F + (\frac{K_{\phi F}}{K_{\phi F} + K_{\phi R} - m_s g h}) m_s h \right] a_y \tag{3.7}$$
;

$$\Delta F_{zR} = \frac{1}{T_r}\left[m_{uR}h_{uR} + m_{sR}h_R + (\frac{K_{\phi R}}{K_{\phi F} + K_{\phi R} - m_s g h}) m_s h \right] a_y \tag{3.8}$$

where $m_{sF} = \dfrac{mb}{(a+b)} - m_{uF}$; $\quad m_{sR} = \dfrac{ma}{(a+b)} - m_{uR}$;

The tyre vertical forces for individual wheels were calculated from the formula:

$$F_{zj} = F_{zj0} \pm \Delta F_{zj} \tag{3.9}$$

When the vehicle is cornering to the left, the left inner wheel vertical load decreases while the right outer wheel vertical load increases. During steady state cornering, the vehicle roll angle is proportional to the camber angle for each individual wheel. Therefore, there exists a unique value of a constant, referred to as roll-camber-coefficient, $k_{\phi\gamma j}$ for each wheel. These values can be experimentally determined and the method is discussed in (Reimpell, Stoll, & Betzler, 2001). With the availability of these constants, the camber angle can be determined from the calculated roll angle (Gillespie, 1992),

$$\gamma_j = k_{\phi\gamma j}\phi \tag{3.10}$$

The last task was to calculate the longitudinal slip ratio where a variety of definitions are used worldwide (Milliken & Milliken, 1995). In ADAMS/car, the longitudinal slip ratio is calculated by considering the tyre relaxation length, and the theory is discussed in detail in (ADAMS, 2005). For simplicity of computation, a definition stated in (Milliken & Milliken, 1995) was selected:

$$\kappa = (\frac{\Omega R_e}{V_x \cos\alpha}) - 1 \tag{3.11}$$

In this case, the tyre equivalent radius, R_e needed to be determined but the procedure was not straight forward. The first step was to calculate individual tyre deflections, ρ as a result of load transfer for each wheel. With the provided values of vertical stiffness and damping in the tyre file, the tyre deflection can be determined from the following differential equation (ADAMS, 2005):

$$K_z \dot{\rho}_j + C_z \rho_j = F_{zj} \tag{3.12}$$

The contribution of the damping is much smaller compared to the stiffness, and therefore the damping term can be neglected. The individual tyre deflection can be estimated as $\rho_j = \frac{F_{zj}}{C_z}$. The tyre equivalent radius can then be determined from the following formula (ADAMS, 2005):

$$R_e = R_0 - \frac{F_{z0}}{C_z}\{D_{reff}\tan^{-1}(B_{reff} \cdot \frac{\rho C_z}{F_{z0}}) + F_{reff}\frac{\rho C_z}{F_{z0}}\} \tag{3.13}$$

All the above coefficients and constants were available in the tyre files complete with their descriptions. The wheel angular speed for individual wheels could be determined during the initial stage before cornering begins from the formula, $V_x = R_e\Omega$.

In brief, the computation (which was performed in SIMULINK) follows an iteration process. With the initial input values that compute the forces and moments, and all other outputs are initialized to zero, the first output of lateral velocity V_y can be obtained from equation (3.1); and then the lateral acceleration can be computed. The values obtained in (3.1) are then used to compute the angular velocity in equation (3.2) and so on. The outputs are then used to generate the next inputs to be fed into the calculation of forces and moments.

3.1.2. Full Vehicle Modelling with Improvement in Roll Angle Prediction

This section continues from Section 3.1.1 with developments in the mathematical modelling to improve the prediction of roll angles (equation (3.3)) should large deviations in computational results be observed. The main reasons for the deviation of roll angles from expectations could be mainly due to neglecting 'turn slip', and the contribution of lateral forces in causing the vehicle to roll. The improvement over neglecting the effect of 'turn slip' could not be verified here since the coefficients needed for computation were not available. The only improvement could be to modify the current roll formula by including the load transfer through suspension linkages which contributed to the vehicle roll angle.

The derivation of the improved roll formula for further verification was obtained from Figure 3.1 and Figure 3.2. The vehicle masses are segregated into three parts viz. the sprung mass, front unsprung mass and rear unsprung mass; the unsprung masses are assumed to be concentrated in the middle of the front and rear axles. Independent lateral forces act on each tyre. So during cornering, the vehicle was assumed to roll about its 'roll axis' which connects the front and the rear roll centres.

The Free Body Diagram (FBD) for the roll moment includes of the main parts; the unsprung mass, the front and rear axles, and the front and rear suspension geometries. The suspension geometries are represented as 'independent suspensions' for front and rear, comprising springs, dampers and independent joints. Each suspension was assumed to have a negligible moment of inertia. During cornering, the unsprung masses were assumed to be non-rolling. The derivation of the mathematical formulae is presented as follows.

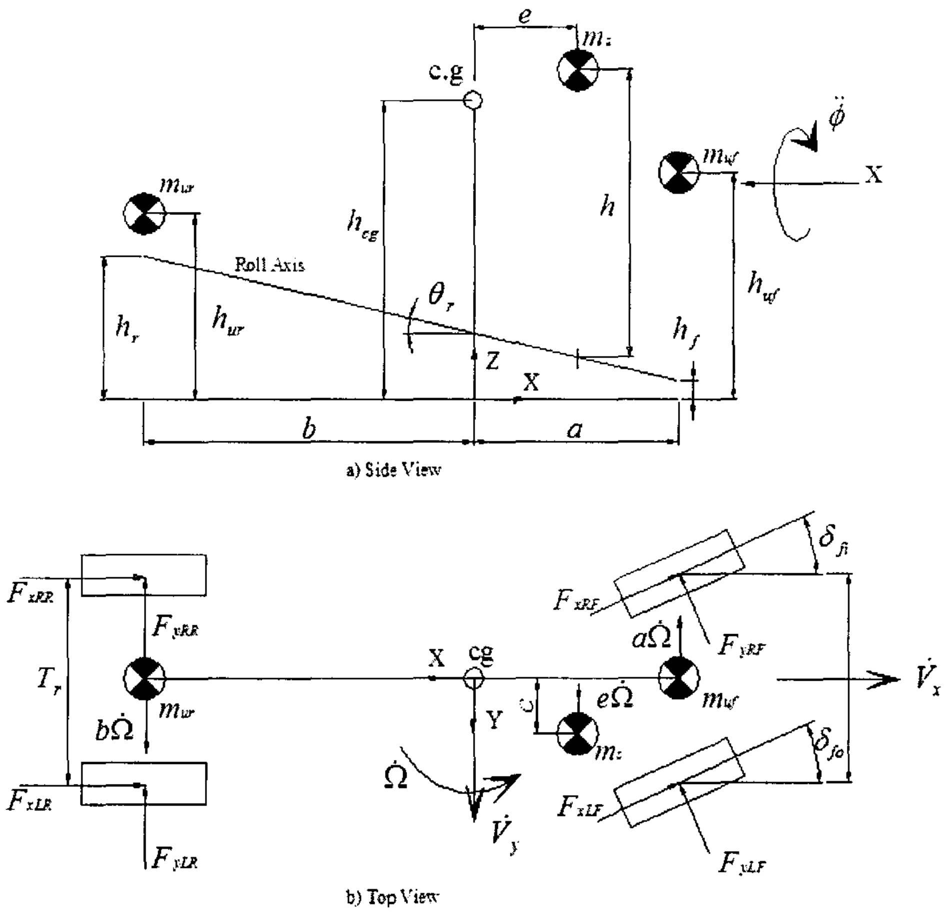

Figure 3.1: Side View and Top View of Free Body Diagrams (FBD)

Summation of Lateral Forces:

$$\Rightarrow (F_{yLF} + F_{yRF}) + (F_{yRF} + F_{yRR}) + (F_{xLF} + F_{xRF})\delta_f + m\Omega V_x + m_s(h\ddot{\phi} - h\Omega^2\phi) = -m\dot{V}_y$$

where $F_{xij} = f(F_{zi}, \kappa_{ij})$; $F_{yij} = f_F(F_{zi}, \psi_{0ij}, \alpha_{ij}, \gamma_{0ij}, \gamma_{ij})$; (3.14)

Summation of Yaw Moments:

$$a(F_{xLF} + F_{xRF})\delta_f + a(F_{yLF} + F_{yRF}) - b(F_{yRF} + F_{yRR}) + M_{zF} + M_{zR} - (I_{zz}\theta_r - I_{xz})\ddot{\phi} - m_s h\Omega V_y \phi = I_{zz}\dot{\Omega} \quad (3.15)$$

where $M_{zi} = M_{zr} - t_p \cdot f_M(F_{zi}, \psi_{0ij}, \alpha_{ij}, \gamma_{0ij}, \gamma_{ij})_{MF}$

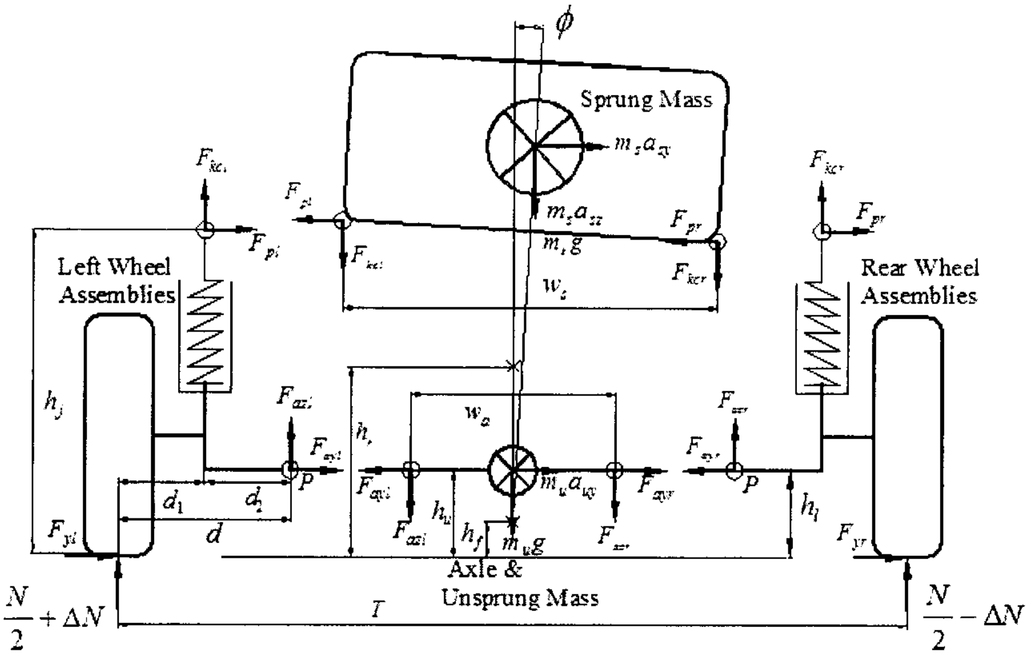

Figure 3.2: Front View of FBD

Summation of Roll Moments:

The derivation of the summation of roll moments was not as straightforward as the summation of lateral forces and yaw moments because the horizontal components which act on the sprung mass and suspension upper joints had first to be determined. The procedure will involved seven equations from FBDs in Figure 3.2.

The following equations were obtained from the FBD of each suspension: $\sum M_P = 0$

$$\Rightarrow F_{pfl} = \frac{1}{(h_{jf} - h_{lf})}(F_{yfl}h_{lf} - F_{kcfl}d_{2f} - (N_{fl} + \Delta N_{fl})d_f) \tag{3.16}$$

$$\Rightarrow F_{prl} = \frac{1}{(h_{jr} - h_{lr})}(F_{yrl}h_{lr} - F_{kcrl}d_{2r} - (N_{rl} + \Delta N_{rl})d_r) \tag{3.17}$$

$$\Rightarrow F_{pfr} = \frac{1}{(h_{jf} - h_{lf})}(F_{yfr}h_{lf} + F_{kcfr}d_{2f} + (N_{fr} - \Delta N_{fr})d_f) \tag{3.18}$$

$$\Rightarrow F_{prr} = \frac{1}{(h_{jr} - h_{lr})}(F_{yrr}h_{lr} + F_{kcrr}d_{2r} + (N_{rr} - \Delta N_{rr})d_r) \tag{3.19}$$

By combining the left and right suspension assembly with the corresponding axle, the following equations were derived:

$$\Rightarrow \Delta N_f T_f - F_{yf} h_f + (F_{kcfl} - F_{kcfr})(\frac{w_a}{2} + d_{2f}) + (F_{pfl} + F_{pfr})(h_{jf} - h_f) = m_{uf}(\dot{V}_y + V_x \Omega)(h_{uf} - h_f) \quad (3.20)$$

$$\Rightarrow \Delta N_r T_r - F_{yr} h_r + (F_{kcrl} - F_{kcrr})(\frac{w_{ar}}{2} + d_{2r}) + (F_{prl} + F_{prr})(h_{jr} - h_r) = m_{ur}(\dot{V}_y + V_x \Omega)(h_r - h_{ur}) \quad (3.21)$$

The last equation was derived from the FBD of the sprung mass, by summing the roll moment about the roll axis: $\sum M_{Roll} = I_{xx}\ddot{\phi}$

$$\therefore -(F_{pfl} + F_{pfr})(h_{jf} - h_f) - (F_{prl} + F_{prr})(h_{jr} - h_r) - (F_{kcfl} - F_{kcfr})\frac{w_{tf}}{2} - (F_{kcrl} - F_{kcrr})\frac{w_{tr}}{2} \quad (3.22)$$
$$+ m_s g h \phi = (I_{xx} + m_s h^2)\ddot{\phi} + (I_{zz}\theta_r - I_{xz})\dot{\Omega} + m_s(\dot{V}_y + V_x \Omega)h$$

The forces due to the springs and dampers were represented as follows:

$$(F_{kcfl} - F_{kcfr}) = k_f w_{tf} \phi + C_f w_{tf} \dot{\phi}; \qquad (F_{kcrl} - F_{kcrr}) = k_r w_{tr} \phi + C_r w_{tr} \dot{\phi} \quad (3.23)$$

By solving the above equations in terms of the desired variables, the general solution was shown to have the following form:

$$-F_{yf} L'_{Fyf} - F_{yr} L'_{Fyr} = (K_{fx} w_{sf} L'_{Fkcf} + K_{rx} w_{sr} L'_{Fkcr} - m_s g h)\phi + (C_{fx} w_{sf} L'_{Fkcf} + C_{rx} w_{sr} L'_{Fkcr})\dot{\phi} - \quad (3.24)$$
$$m_{ur}(\dot{V}_y + V_x \Omega) L_{mur} - m_{uf}(\dot{V}_y + V_x \Omega) L_{muf} + (I_{zz}\theta_r - I_{xz})\dot{\Omega} + m_s(\dot{V}_y + V_x \Omega)h + (I_{xx} + m_s h^2)\ddot{\phi}$$

where the equivalent lengths above were represented below:

$$L_{\Delta N_f} = (\frac{T_f}{2} - \frac{(h_{jf} - h_f)d_f}{(h_{jf} - h_{lf})}); L_{Fyf} = (h_f - \frac{(h_{jf} - h_f)h_{lf}}{(h_{jf} - h_{lf})}); L_{Fkcf} = ((\frac{w_{af}}{2} + d_{2f}) - \frac{(h_{jf} - h_f)d_{2f}}{(h_{jf} - h_{lf})});$$

$$L_{\Delta N_r} = (\frac{T_r}{2} - \frac{(h_{jr} - h_r)d_r}{(h_{jr} - h_{lr})}); \; L_{Fyr} = (h_r - \frac{(h_{jr} - h_r)h_{lr}}{(h_{jr} - h_{lr})}); \; L_{Fkcr} = ((\frac{w_{ar}}{2} + d_{2r}) - \frac{(h_{jr} - h_r)d_{2r}}{(h_{jr} - h_{lr})});$$

$$L'_{Fyf} = (h_{lf} - \frac{L_{Fyf} d_f}{L_{\Delta N_f}})\frac{(h_{jf} - h_f)}{(h_{jf} - h_{lf})}; \quad L'_{Fyr} = (h_{lr} - \frac{L_{Fyr} d_r}{L_{\Delta N_r}})\frac{(h_{jr} - h_r)}{(h_{jr} - h_{lr})};$$

$$L'_{Fkcf} = ([(d_{2f} - \frac{L_{Fkcf} d_f}{L_{\Delta N_f}})\frac{(h_{jf} - h_f)}{(h_{jf} - h_{lf})}] - \frac{w_{sf}}{2}); \; L'_{Fkcr} = ([(d_{2r} - \frac{L_{Fkcr} d_r}{L_{\Delta N_r}})\frac{(h_{jr} - h_r)}{(h_{jr} - h_{lr})}] - \frac{w_{sr}}{2});$$

$$L_{muf} = (\frac{(h_{uf} - h_f)d_f}{L_{\Delta N_f}})\frac{(h_{jf} - h_f)}{(h_{jf} - h_{lf})}; \quad L_{mur} = (\frac{(h_{ur} - h_r)d_r}{L_{\Delta N_r}})\frac{(h_{jr} - h_r)}{(h_{jr} - h_{lr})} \qquad (3.25)$$

The same computer program developed for Section 3.1.1 could be modified to cater for the improvement of roll angle predictions. The final formula derived from roll moments shown in equation 3.22 would replace equation 3.3 from Section 3.1.1. The equations for the summation of lateral forces and the summation of yaw moments would not change.

3.1.3. Modelling of a Hydraulic Power Assisted Steering

The steering system fitted to the vehicle under study was of the rack-and-pinion type. Figure 3.3 shows the basic configuration. Due to the complexity of calculation, several assumptions were made; the pinion was assumed to be very stiff and did not posses any damping and moment of inertia. The friction that exists in the steering and column assembly was assumed to be negligible.

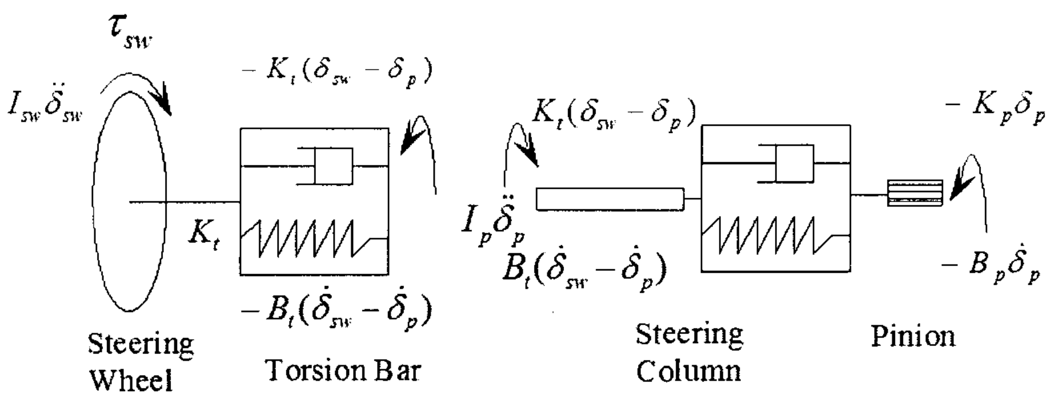

Figure 3.3: FBD of a Steering and Column Assembly

The following expressions were obtained from the separated free body diagrams (FBD) from Figure 3.3:

$$\tau_{sw} = I_{sw}\ddot{\delta}_{sw} = -K_t(\delta_{sw} - \delta_p) - B_t(\dot{\delta}_{sw} - \dot{\delta}_p) \tag{3.26}$$

$$\tau_p = I_r\ddot{\delta}_p = K_t(\delta_{sw} - \delta_p) + B_t(\dot{\delta}_{sw} - \dot{\delta}_p) - K_p\delta_p - B_p\dot{\delta}_p \tag{3.27}$$

The relationship between the pinion rotation angle with the front steered wheel angle is given by $\delta_p = G_{pfw}\delta$, where G_{pfw} is the pinion to front-wheel angle ratio, which is found through experiment. By using the principle of conservation of energy, it can be shown that the applied torque for the conventional rack-and-pinion steering system has the following relationship:

$$\tau_p \cdot \delta_p = \tau_{fw} \cdot \delta; \quad \Rightarrow \tau_{fw} = G_{pfw}\tau_p \tag{3.28}$$

Figure 3.4 shows the FBD of the hydraulic power-assisted steering assembly complete with the front wheels, with the column and pinion assembly attached to the system. With the presence of the assist torque from the hydraulic supply, the new relationship between the applied torque becomes

$$\tau_{fw} = G_{pfw}(\tau_p + \tau_a); \qquad \text{where } \tau_a = PA_p r_{eff} \tag{3.29}$$

The equation of motion relating the steering wheel angle to the front wheel steer angles can be obtained from Figure 3.4 from the summation of yaw moments:

$$I_{sa}(\ddot{\delta} + \dot{\Omega}) = \tau_{fw} - B_{sa}\dot{\delta} + M_{zF} \tag{3.30}$$

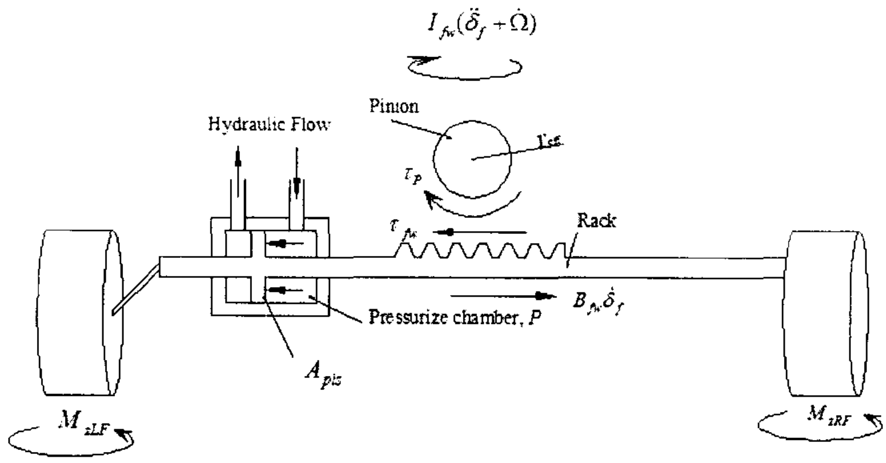

Figure 3.4: FBD of Front Steering Wheel Assembly

Substituting equations (3.27), (3.28) and (3.29) into (3.30), the equations of motion that relate to the variables of interest can be obtained:

$$I_{sa}(\ddot{\delta}+\dot{\Omega}) = G_{pfw}(K_t(\delta_{sw}-G_{pfw}\delta)+B_t(\dot{\delta}_{sw}-G_{pfw}\dot{\delta})+PA_{pis}r_{eff})-B_{sa}\dot{\delta}+M_{zF} \quad (3.31)$$

The term $P \cdot A_{pis}$ is referred to as the 'boost force'. The hydraulic pressure, P is actuated from a hydraulic pump in which flow is based on the valve deflection, i.e. the difference between the steering wheel angle and the pinion rotation angle, $(\delta_{sw}-\delta_p)$. The characteristics of the boost pressure as a function of valve deflection depend on the power steering design. An example of a hydraulic boost curve is shown in Figure 3.5.

Since the relationship between the boost pressure and the valve deflection angle is normally nonlinear, this parameter is represented as 'data input' in programming where interpolation methods are required. The front wheel steering assembly damping, B_{sa} consisted of several elements including the rack assembly, pinion and road wheels. In this analysis, the damping effect from the pinion and front wheels was neglected, leaving the rack damping only. It can be shown that the damping of the rack assembly B_{rack} can be expressed as follows: $\ell_r = r_{eff}\delta_p = r_{eff}G_{pfw}\delta$; $\Rightarrow B_{sa}\dot{\delta} = [B_{rack}r_{eff}G_{pfw}]\dot{\delta}$ (3.32)

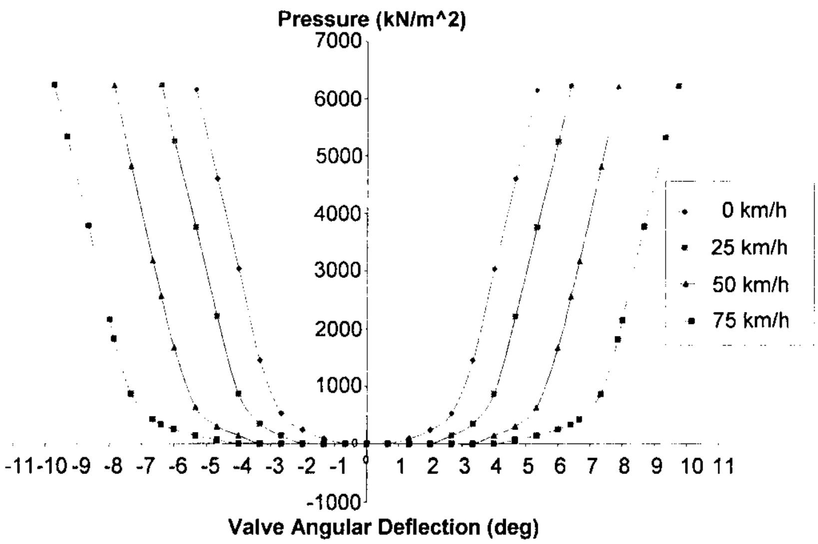

Figure 3.5: An Example of a Boost Curve of a Hydraulic Power Assisted Steering (Adams, 1983)

With the derived equations of motions and the values of constants and coefficients, the mathematical modelling of the hydraulic power-assisted steering was then added to that of the cornering vehicle. The final inputs to the systems were the steering wheel angle and the power boost curve.

3.1.4. Analysing the Performance of a Hydraulic Power Assisted Steering

In order to understand the characteristics of a hydraulic power-assisted steering, the performance of the system, i.e. the stiffness and feel, was selected for evaluation. The steering system under investigation belonged to the Jaguar car, which power boost characteristic curves were provided by the manufacturer. It was also intended to verify whether the power boost characteristic curves of the Jaguar car were as effective as the suggested curves discussed in Section 2.5.1.2.

There are several quantitative definitions of the terms 'stiffness' and 'feel' proposed by researchers (e.g. (Harrer, Pfeffer, & Johnston, 2006), (Rosth, 2007), (Zaremba, Liubakka, & Stuntz, 1998)) but the mathematical definitions of Baxter, (Baxter, 1988) were used in this analysis. Baxter derived a simplified mathematical formula to calculate the steering gear 'stiffness' as the change of the rack output force with respect to the change in the steering wheel angle, and the steering gear 'feel' as the change of the steering wheel torque with respect to the change in the rack output force. Baxter used data obtained from the boost curves and steering design variables to assess the performance of a hydraulic power assisted steering system. Among the graphical plots he produced were steering gear stiffness and feel versus the valve angles and the pressure boost rates. Although the idea is very useful for design engineers, it is very difficult to measure the actual performance of a hydraulic power assisted steering when the actual deflections of hydraulic valves vary depending on the actual torque applied at the steering wheel as well as the self-aligning moments generated at the front wheels. In this analysis, the performance of a hydraulic power-assisted steering is assessed by analyzing the graphical plots of steering gear stiffness and feel versus the lateral accelerations and yaw velocities under a selected steady state cornering event.

Baxter derived the steering gear stiffness and feel based on the condition of the steady state cornering of vehicles. He also assumed that the efficiency of the mechanical arrangement was 100%. The steering gear stiffness and feel he used are given by:

Steering Gear Stiffness, $$\frac{dF_{rack}}{d\delta_{sw}} = \frac{1}{r_{eff}} \cdot \frac{K_t K_r}{(K_t + K_r)} + \frac{dP}{d\alpha_V} \cdot \frac{A_p K_r}{(K_t + K_r)} \tag{3.33}$$

Steering Gear Feel, $$\frac{d\tau_{sw}}{dF_{rack}} = \frac{r_{eff} K_t}{(K_t + r_{eff} A_p \frac{dP}{d\alpha_V})} \tag{3.34}$$

These were compared with those from manual steering systems which are given by:

Manual Steering Gear Stiffness, $$\frac{dF_{rack}}{d\delta_{sw}} = \frac{K_r}{r_{eff}} \quad \text{for } K_t = \infty \text{ and } \frac{dP}{d\alpha_V} = 0 \tag{3.35}$$

Manual Steering Feel, $$\frac{d\tau_{sw}}{dF_{rack}} = r_{eff} \quad \text{for } K_t = \infty \text{ and } \frac{dP}{d\alpha_V} = 0 \tag{3.36}$$

Equations (3.1–3.3) and equation (3.31) were programmed and simulated using MATLAB/SIMULINK. The main data required to calculate the steering stiffness and feel namely $dP/d\alpha_V$, were computed from the boost curve at instantaneous values of deflection angles. A schematic block diagram for the computation is shown in Figure 3.6. The full program is attached in Appendix 1(d).

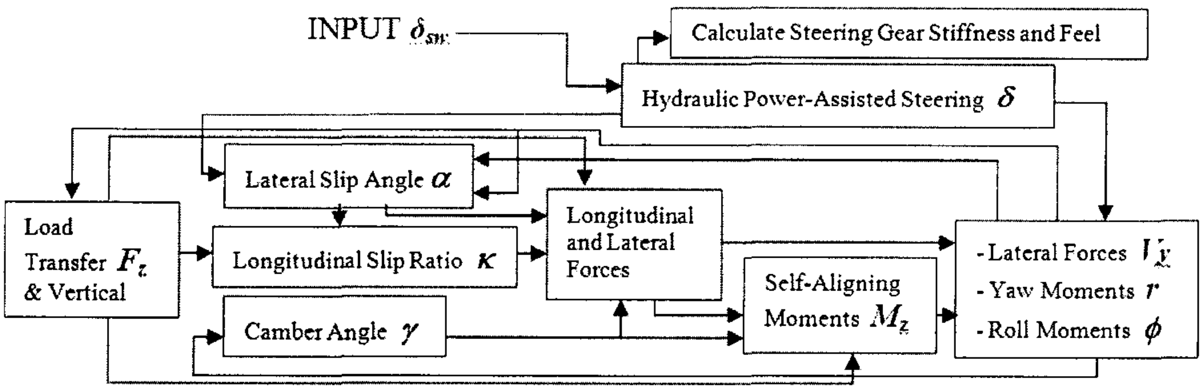

Figure 3.6: The Block Diagram

3.1.5. Results and Discussion on a Hydraulic Power-Assisted Steering Performance

The analyses to determine the performance of the hydraulic power-assisted steering fitted on the Jaguar car were performed for low and high vehicle cornering speeds of 30 km/h and 100 km/h respectively. Two power boost curves were selected, referred to as 'curve A' and 'curve B' respectively (Figure 3.7). For all cases, the steering wheel was gradually turned to the left under a defined sequence as shown in Figure 3.8.

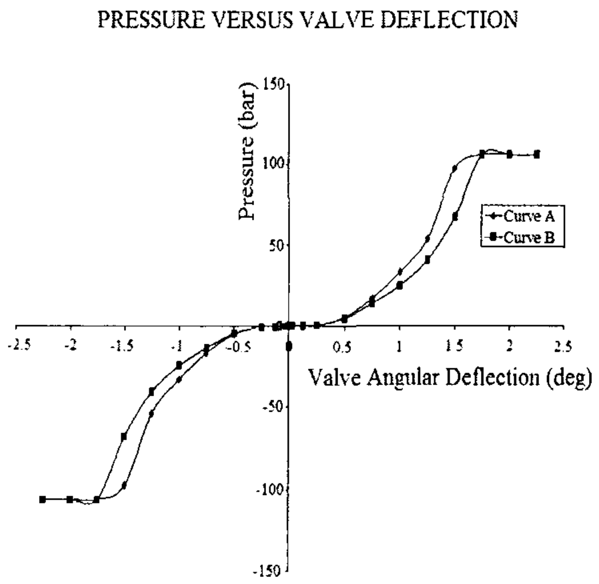

Figure 3.7

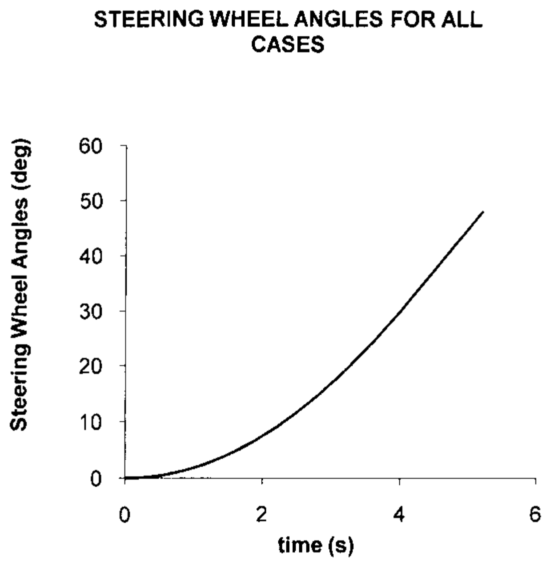

Figure 3.8

The main outputs from this analysis are namely the lateral acceleration, yaw velocity and the computation of steering gear stiffness and feel. The graphical plots of the steering gear stiffness versus vehicle lateral accelerations and yaw velocities are shown in Figure 3.9 and Figure 3.10. It can be seen that at low vehicle lateral acceleration, the steering gear stiffness is low; and vice versa for the case of high lateral acceleration. This indicates that the design of this steering system is good since at low lateral acceleration or stationary the low steering gear stiffness helps the driver to reduce steering effort during parking. At low speed cornering (low lateral acceleration) the friction forces interacting with road wheels are significant and the low steering gear stiffness can reduce the driver's effort. On the other hand, at high vehicle lateral acceleration, the car will be very sensitive so the driver must hold the steering wheel firmly in order to avoid the vehicle from moving away from the required path. Therefore, high steering gear stiffness is desirable during high vehicle lateral acceleration. It was also found that at low speed (30 km/h) and at high speed (100 km/h), the difference in the steering stiffness with lateral acceleration is very small and it is hard to tell whether the curves are speed dependant. For low lateral acceleration, curve B is preferable to curve A because it has lower stiffness. On the other hand, curve A is preferable to curve B at high lateral accelerations. A system that makes use of the two curves can be achieved by installing speed sensitive hydraulic valves [(Davis, 1945), (Adams, 1983)].

Similar characteristics are found for the plots of steering gear stiffness versus yaw velocity and the steering gear stiffness versus lateral acceleration. In general, the steering gear stiffness is lower at low yaw velocity and higher at high yaw velocity. Therefore, similar comments can be made for the performance of both cases as well as for the selection of power boost characteristic curves. The advantage of having the plot of steering gear stiffness versus yaw velocity is that it clearly shows how the stiffness of the hydraulic power assisted steering analysed in this study is in fact speed dependent. At low vehicle speed, the steering gear stiffness is also low and increases at a slower rate with the increase in yaw velocity. However, at high vehicle speed, the steering gear stiffness is high and increases at higher rate with the increase in yaw velocity.

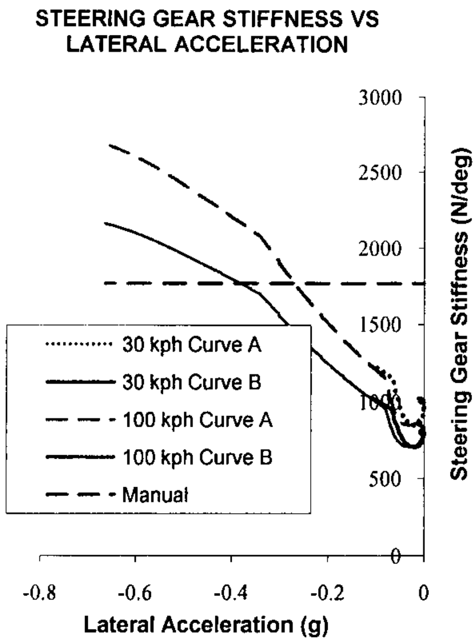

Figure 3.9

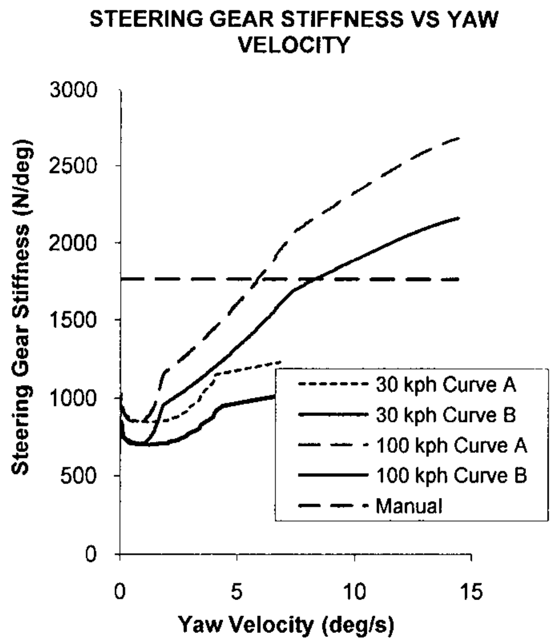

Figure 3.10

Figure 3.11 and Figure 3.12 show the steering gear feel versus vehicle lateral acceleration and yaw velocity respectively. Steering gear feel is higher at low lateral acceleration and yaw velocity; and lower at high lateral acceleration and yaw velocity, in opposite to the previous findings. This characteristic is desirable because at low lateral acceleration and yaw velocity, the irregularities at the road wheels are not transmitted to the steering wheel. Therefore, additional feel is required for the driver to have some understanding of what is happening at the road wheels. However, at high lateral acceleration or yaw velocity, any abnormalities experienced by the road wheels can be easily felt on the steering wheel. Therefore, low steering gear feel is required in order to ensure the ride comfort for the driver. The steering gear feel for the hydraulic power-assisted system analysed in this study was found to be about 20% compared with the manual system. The system will therefore prevent or minimize any shocks on the road wheels from transmitting to the steering wheel; however, it is a concern that such design may cause the driver to lose judgement of the forces acting at the road wheels.

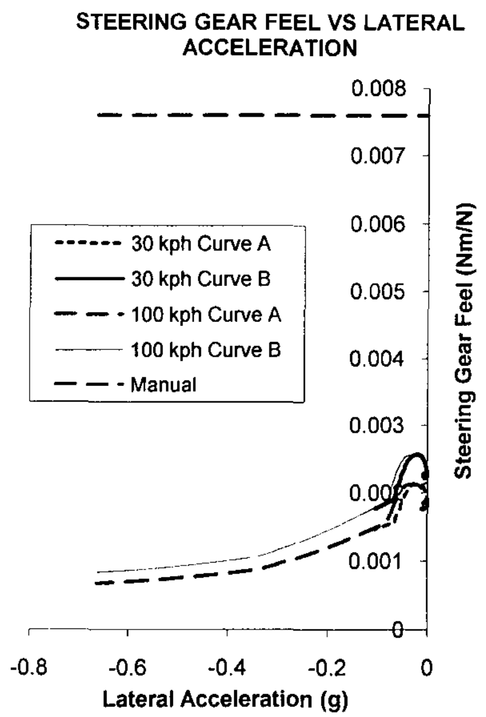

Figure 3.11

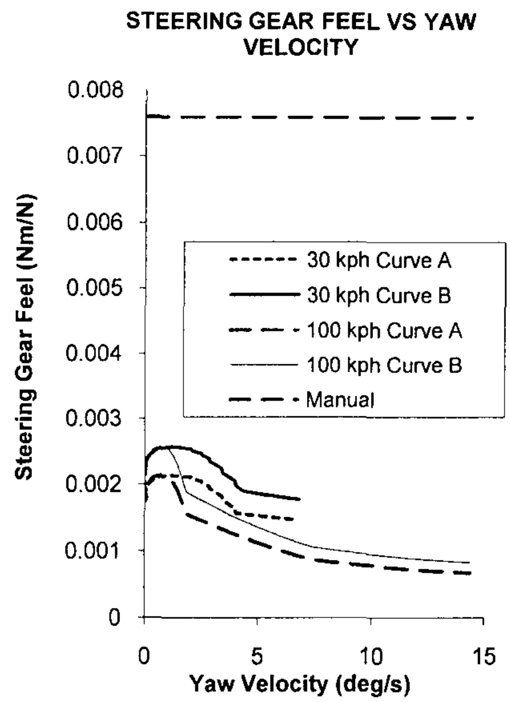

Figure 3.12

3.1.6. Conclusions on a Hydraulic Power-Assisted Steering Performance

The full mathematical modelling of a cornering vehicle fitted with hydraulic power-assisted steering system presented in this section has enabled the assessment of the hydraulic power-assisted steering performance in term of steering gear stiffness and feel. The graphs of steering gear stiffness and feel versus lateral acceleration and yaw velocity have enhanced understanding in analyzing the performance and characteristics of hydraulic power-assisted steering. The performance of the hydraulic power-assisted steering system fitted on the Jaguar car was found to assist the driver during parking, provide more steering gear stiffness at high lateral acceleration and yaw velocity, increase the driver's feel at the steering wheel during low speed manoeuvring, and prevent forces from being transmitted through the steering column at high lateral acceleration as well as yaw velocity. However, the design level of the steering gear feel may be very low that the driver may not have enough sensitivity to the actual conditions on the road wheels.

The analyses presented in this section have provided some general knowledge on how an effective steering system should be designed. For more meaningful interpretation of the results, the steering gear stiffness and steering gear feel had to be related to a driver interaction with a car. The steering gear stiffness was related to driver steering feel (steering wheel torque) while steering gear feel was related to the comfort of operating a steering system. Since vehicle forward speed is directly proportional to both lateral acceleration and yaw velocity, it can be concluded that the steering gear stiffness and steering gear feel also vary the same manner with vehicle forward speed.

Finally, it was concluded that the characteristics of the power boost curve of the Jaguar car had some similarities to the ideal hydraulic power assisted steering presented in Section 2.5.1.2. The only difference was that the curves were not as ideal as presented in the theory since it was generated using hydraulic valves and the slopes were not constant.

3.2. Detailed Modelling of a Cornering Vehicle Fitted with Flexible Shaft

This section presents the detailed modelling of a cornering vehicle fitted with a flexible steering column. The main objective of the simulation was to simulate the behaviour of Steer-by-Wire (SBW) as well as Semi-Active Steering (SAS) in the case of active system failure. It was intended to find out how the failed SBW or SAS behaves with different properties (stiffness and damping values) of the flexible steering column. The vehicle behaviour when fitted with different steering shafts at different speeds was investigated.

The vehicle studied was a Ford Fiesta which was used in the experimental work. The basic vehicle data is given in Appendix 1(e). Preliminary results from the theoretical formula were used to estimate the minimum range of required stiffness values in order to ensure vehicle stability for experimental work. The derived mathematical formula was also simulated under several cornering events to predict vehicle behaviours when fitted with different properties of steering shaft. The same formula would be validated in Chapter 4 using experimental results.

A mathematical model of a vehicle fitted with flexible shafts was constructed using Figure 3.14(a-c). The free-body diagram consists of the steering wheel assembly, feel motor gearing, and the actuator motor gearing which is attached to the vehicle front wheels assembly. The main equation of motion was derived by summing the moment of the steering wheel assembly about the z-axis. The input to the model is the steering wheel angle as a function of time.

Using Figure 3.14(b) and (c), the steering dynamic equations were derived and presented as follows (Baharom, Hussain, & Day, 2006):

$$G(B_l(\dot{\delta}_{sw}-\dot{\delta}_p)+K_l(\delta_{sw}-\delta_p))-B_{Fw}\dot{\delta}_F-\tau_f-M_{zF}=I_{Fw}(\ddot{\delta}_F+\dot{r}), \tag{3.37}$$

where $\tau_f = F_{cf}\,\mathrm{sgn}(\dot{\delta}_F)$; $M_{zF} \approx C_{M\alpha F}\alpha_F = C_{M\alpha F}(\delta_F - \beta - \frac{ar}{V_x})$; $\delta_p = G\delta_F$

Rearranging equation (3.37) gives:

$$G(B_l\dot{\delta}_{sw}+K_l\delta_{sw})=I_{Fw}\ddot{\delta}_F+(B_{Fw}+G^2B_l)\dot{\delta}_F+(C_{M\alpha F}+G^2K_l)\delta_F+F_{cf}\,\mathrm{sgn}(\dot{\delta}_F)-C_{M\alpha F}\beta-\frac{aC_{M\alpha F}}{V_x}r+I_{Fw}\dot{r} \tag{3.38}$$

A simplified vehicle dynamics model was used to test the steering dynamics (Gillespie, 1992) as shown in Figure 3.13, simulating side slip angle, β and yaw velocity, r. The resulting equation for the vehicle model is given by equation (3.39), the input being the calculated front steered wheel angle, δ_F.

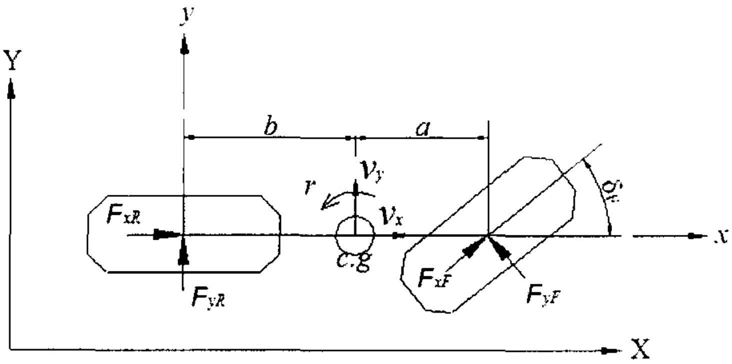

Figure 3.13: 2D Vehicle Model Representation

$$\begin{bmatrix} \dot{\beta} \\ \dot{r} \end{bmatrix} = \begin{bmatrix} -\frac{(C_{F\alpha F}+C_{F\alpha R})}{mV_x} & -1+\frac{bC_{F\alpha R}-aC_{F\alpha F}}{mV_x^2} \\ (\frac{bC_{F\alpha R}-aC_{F\alpha F}}{I_{zz}}) & -\frac{(a^2C_{F\alpha F}+b^2C_{F\alpha R})}{I_{zz}V_x} \end{bmatrix} \begin{bmatrix} \beta \\ r \end{bmatrix} + \begin{bmatrix} \frac{C_{F\alpha F}}{mV_x} \\ \frac{aC_{F\alpha F}}{I_{zz}} \end{bmatrix} [\delta_F] \tag{3.39}$$

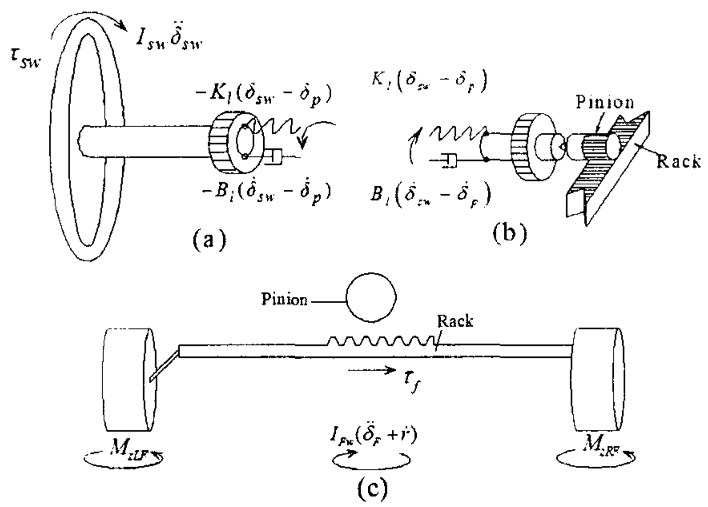

Figure 3.14: Detailed FBDs of Steer-by-Wire during System Failure (Baharom, Hussain, & Day, 2006)

Equation (3.38) can be simplified in order to obtain a relationship between the feel motor positional angles and the steered front-wheel angles. The variable $\dot{r}$ in (3.38) can be substituted with the expression found in (3.39) in order to obtain the formula as a function of β, r and δ_F. The Coulomb friction term F_{cf} was assumed to be negligible (A detailed study of this force in the steering system can be found in [(Pfeffer, Harrer, Johnston, & Shinde, 2006), (Post & Law, 1996), (Data, Pesce, & Reccia, 2004)]. The final expression for equation (3.38) can be simplified as follows:

$$G(B_l\dot{\delta}_{sw} + K_l\delta_{sw}) = Q_{\ddot{\delta}_F}\ddot{\delta}_F + Q_{\dot{\delta}_F}\dot{\delta}_F + Q_{\delta_F}\delta_F + Q_\beta\beta + Q_r r + F_{cf}\,sign(\dot{\delta}_F) \qquad (3.40)$$

where $Q_{\ddot{\delta}_F} = I_{Fw}$; $Q_{\dot{\delta}_F} = (B_{Fw} + G^2 B_l)$; $\quad Q_{\delta_F} = (C_{MaF} + G^2 K_l + \frac{aI_{Fw}C_{FaF}}{I_{zz}})$;

$Q_\beta = (\frac{I_{Fw}}{I_{zz}}(bC_{FaR} - aC_{FaF}) - C_{MaF})$; $\quad Q_r = -\frac{aC_{MaF}}{V_x} - \frac{I_{Fw}}{I_{zz}V_x}(a^2 C_{FaF} + b^2 C_{FaR})$

Using equation (3.40), a transfer function for the dynamic systems was derived (Baharom, Hussain, & Day, 2006). The input to the complete system is the steering wheel angle, δ_{sw} and the output is the front steered road-wheel, δ_F. The corresponding output δ_F was used as the input to the vehicle dynamics model. The outputs from the vehicle model, namely the yaw and the side-slip angles were then used as the external inputs to the transfer function by multiplying with their specific coefficients. The description of the computational processes is shown in Figure 3.15. The MATLAB/SIMULINK complete program is shown in Appendix 1(f). The output parameters of the model are the yaw velocity, r lateral acceleration defined by $a_y = \dot{\beta}V_x + rV_x$ and the front steered wheel angle, δ_F.

The amount of torque applied at the steering wheel by the driver can be represented by the following equation:

$$\tau_{sw} - K_l\left(\delta_{sw} - G\delta_F\right) - B_l\left(\dot{\delta}_{sw} - G\dot{\delta}_F\right) = I_{sw}\ddot{\delta}_{sw}$$

$$\Rightarrow \tau_{sw} = (I_{sw}\ddot{\delta}_{sw} + B_l\dot{\delta}_{sw} + K_l\delta_{sw}) - (GB_l\dot{\delta}_F + GK_l\delta_F) \qquad (3.41)$$

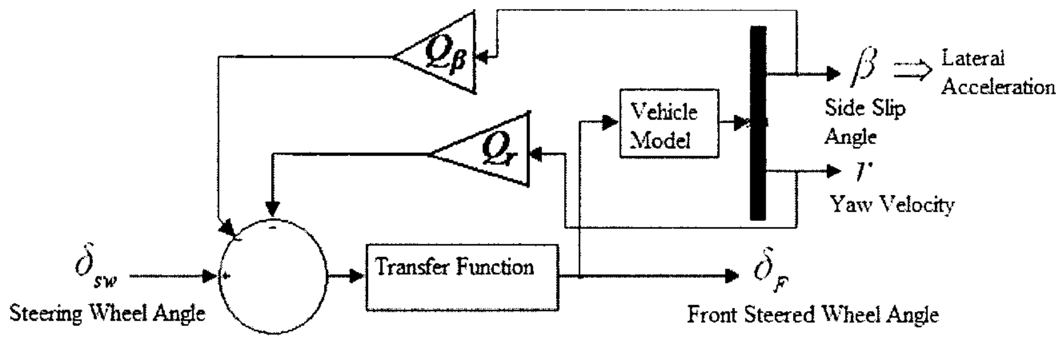

Figure 3.15: Block Diagrams of SIMULINK Program for Semi-Active Steering During System Failure

As the amount of torque applied on the steering wheel varies for each experiment, a mathematical formula to predict the relationship between the torque and the steering wheel velocity was derived as shown in equation 3.41. In this case, the torque applied at the steering wheel was chosen as input and the corresponding output was the steering wheel rotational velocity. Equations 3.40 and 3.41 are combined and the formula can be represented by the MATLAB/SIMULINK block diagrams shown in Figure 3.16. The program was then added to the block diagram of Figure 3.15.

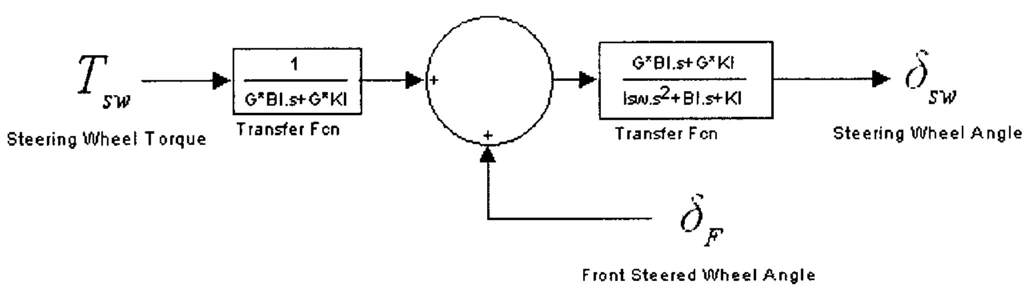

Figure 3.16: Block Diagrams of a SIMULINK Program That Uses Steering Wheel Torque as Input

3.2.1. Preliminary Results for Preparation of Experimental Work

Prior to conducting the experimental work, the stiffness values of flexible shafts fitted to the experimental car were determined. The predicted values had to be specified within a certain range because the theoretical formula had not yet been validated and the results were therefore uncertain. The selected steering wheel input angle for the experimental event is shown in Figure 3.17 which is also referred as 'step steer' analysis (BRITISH STANDARD, 2003). The analysis represents the worst case scenario during collision avoidance. The driver turns the steering wheel abruptly from the straight ahead position to a 90-degree position in 0.2 seconds.

The selected vehicle speed was 50 km/h (30 mph) because this was the maximum permissible speed for safety reasons. The detailed procedure for the experimental work is discussed in chapter 4. The output result for the analysis was a set of plots of the yaw velocity versus time, with each curve corresponding to a specific steering shaft stiffness ranging from 2 Nm/rad to 60 Nm/rad. The results for the conventional vehicle are also presented for comparisons. The graphs are shown in Figure 3.18.

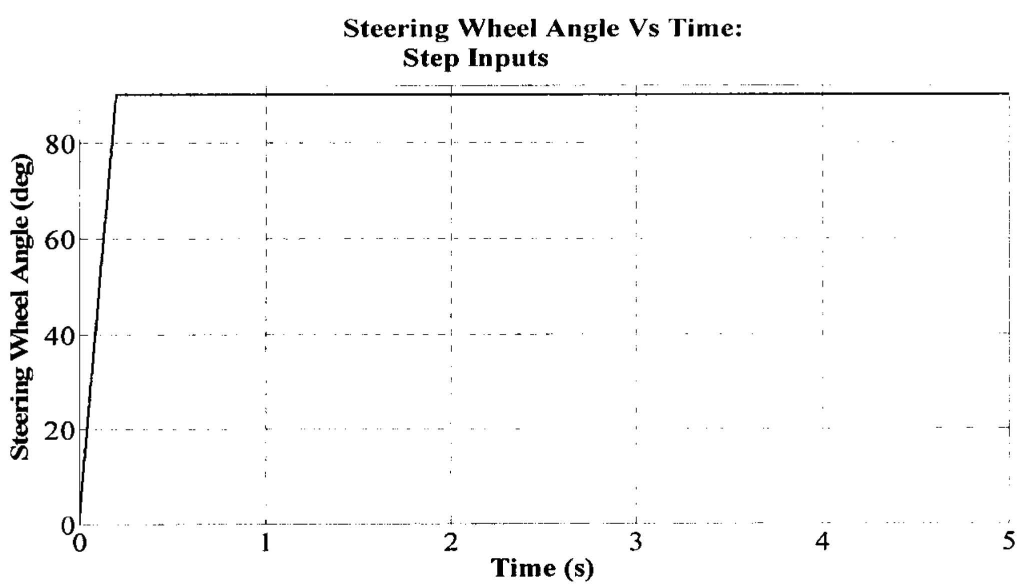

Figure 3.17

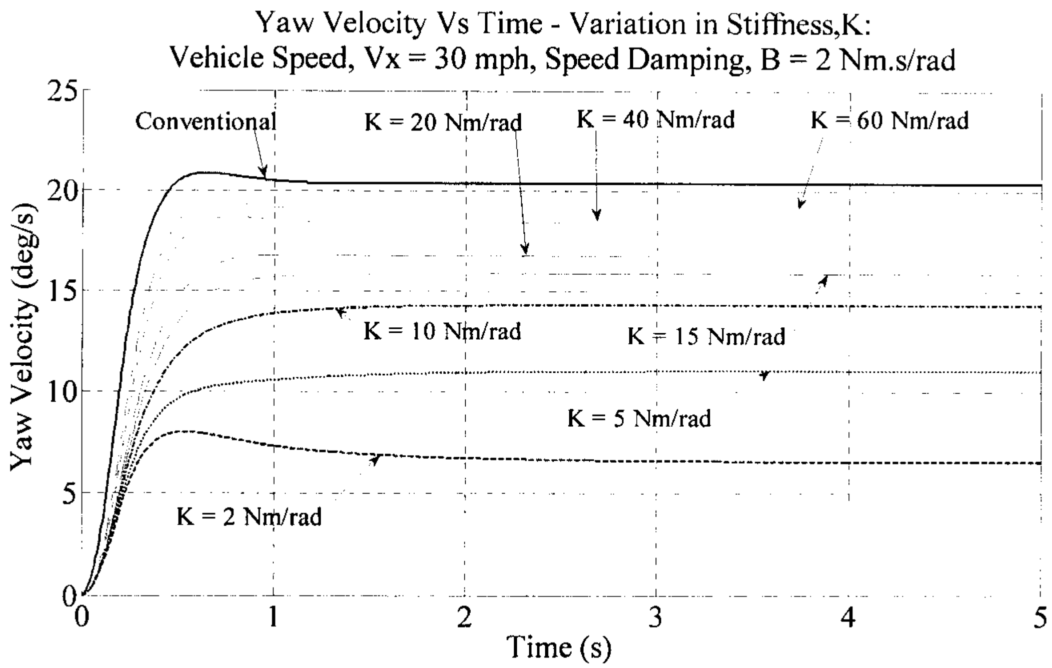

Figure 3.18

3.2.2. Discussion on Preliminary Results for Experimental Preparation

Based on Figure 3.18, it can be observed that overshoots in steering response increase as steering shaft stiffness changes. Overshooting behaviour is undesirable because such a characteristic can cause the vehicle to be unstable. For lower stiffness values, overshoots start to occur when the stiffness value is below 5 Nm/rad. For higher stiffness values, the overshoots start to develop when the stiffness values are above 15 Nm/rad. Based on these findings, the stiffness values of the steering shafts for experimental work were set within the range of 5 Nm/rad to 15 Nm/rad. Due to the complexity of fabricating flexible steering shafts, only three were fabricated for the experimental work, with stiffnesses of 5 Nm/rad, 10 Nm/rad and 15 Nm/rad respectively.

3.2.3. Conclusions on Preliminary Results for Experimental Preparation

The theoretical model presented in this chapter is useful for predicting a suitable stiffness of low stiffness resilience shaft which ensures vehicle stability and safe driving in the event of system failure. Preliminary predicted results of steering shaft stiffness were computed for experimental preparation purposes. The selected steering shaft stiffness for the experimental work was 5 Nm/rad, 10 Nm/rad and 15 Nm/rad respectively. These values were determined based on the range of overshoots from simulation results.

3.3. Simplified Modelling of a Cornering Vehicle Fitted with Flexible Shaft

The most important criteria that should be analysed and validated during the preliminary stage of designing a SAS are the selection of low stiffness resilience shaft (LSRS) and the behaviour of the vehicle when the chosen LSRS is fitted. The vehicle with the LSRS must meet minimum safety standards to ensure that the driver can bring the vehicle safely to rest in the event of failure. Although vehicle stability during failure is a concern, the LSRS should not be designed to be too stiff as this will require more power to be consumed by the motors. Therefore, the main objective of performing the simplified mathematical modelling was to quickly identify the range of LSRS stiffness in order to meet the safety criteria as well as to fulfil the functional requirements. The method simplifies computation and saves time during the preliminary design stage of the SAS.

The derivation of the formula is similar to section 3.2 which makes use of figure 3.14 (a-c). For simplicity of computation, several assumptions were made to equation 3.38. The friction in the steering assembly was assumed to be negligible; and the contribution of self-aligning moment was also neglected. The main objective of making these assumptions was to allow a linear solution which simplifies computation.

The following transfer function was derived from equation 3.38 after applying the assumptions:

$$GB_l\dot{\delta}_{sw} + GK_l\delta_{sw} = I_{Fw}\ddot{\delta}_F + (G^2B_l + B_{Fw})\dot{\delta}_F + (G^2K_l + C_{MzF})\delta_F$$

$$\Rightarrow \delta_{sw} \rightarrow \boxed{\frac{(GB_l.s + GK_l)}{[I_{Fw}.s^2 + (G^2B_l + B_{Fw}).s + (G^2K_l + C_{MzF})]}} \rightarrow \delta_F$$

The remainder of the computational steps are similar to those performed in section 3.2. The MATLAB/SIMULINK block diagram is shown in Figure 3.19.

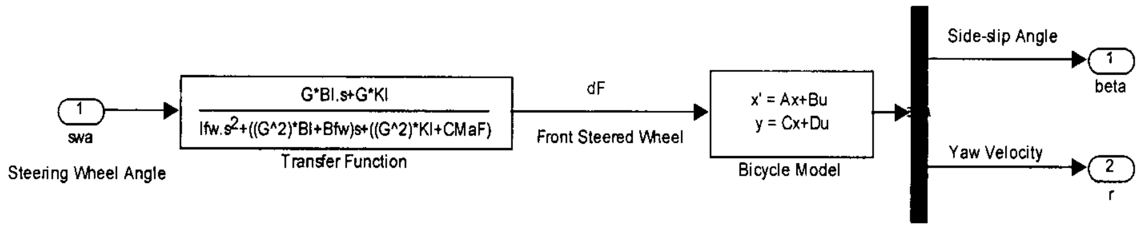

Figure 3.19: SIMULINK Program for SBW during System Failure

The simplified modelling presented in this section will be analysed in Section 3.3.1 and the output results will be compared with the results of the detailed modelling. The process is required in order to find out the accuracy of the formula and also to determine the corresponding range of parameters for accurate results.

3.3.1. Verification on Simplified Modelling of a Cornering Vehicle Fitted with Flexible Shaft

This section presents the verification processes of the simplified mathematical modelling of a cornering vehicle fitted with a flexible steering shaft as developed in this section. The main intention of verifying the theoretical formula was to determine the range of validity of parameters where the equations can be implemented. The derived mathematical formula was less complicated and can provide quick results when dealing with preliminary design work. The verification processes were done by comparing the results from the detailed modelling of a cornering vehicle fitted with flexible shaft which was developed in Section 3.2 with the simplified one.

3.3.2. Comparisons of Simulation Results

In order to compare the simulation results between the detailed and simplified modelling, a specific steering wheel angle characteristic shown in Figure 3.17 was selected as input to computer programmes. The reason for the selection was because the situation represents the worst scenario during collision avoidance. It was expected that when the worst scenarios were verified, more common events will also be satisfied. The computer program codes for the simplified formula can be found in Appendix 1(g). The main difference between the simplified model and the detailed model is neglecting the contribution of self-aligning moments which are a function of vehicle forward speed. Therefore, the simulation of the computer programs were performed under variable speeds namely 50 km/h (30 mph), 80 km/h (50 mph) and 110 km/h (70 mph). For all of the analyses, the stiffness of the flexible shaft is 5 Nm/rad and the corresponding damping is $2\ \mathrm{Nm \cdot s/rad}$. The output results for comparisons were the angular velocities and lateral accelerations as functions of time which are presented in Figure 3.20 (a)-(b). For each case of analysis, the plots of the results from the simplified models and the detailed models are overlaid for comparison.

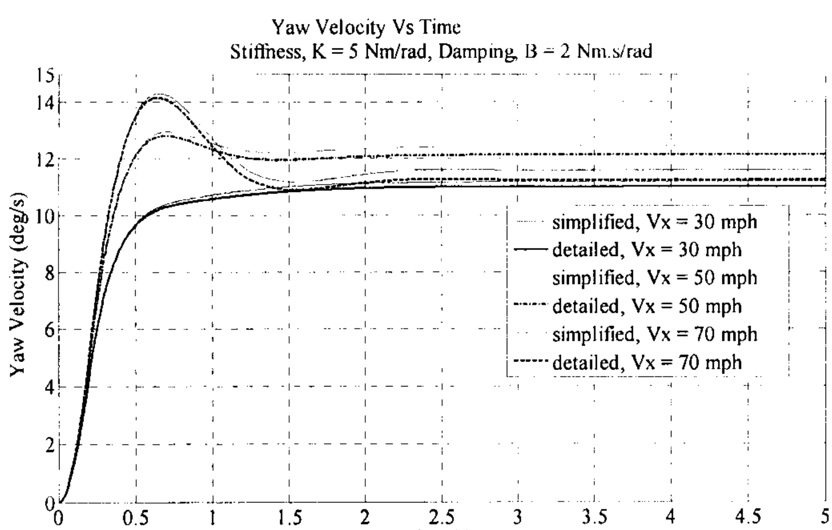

(a)

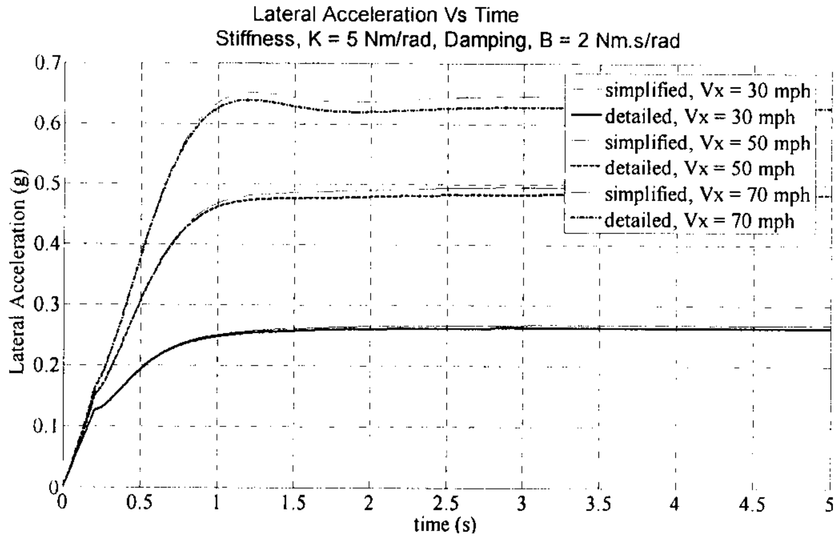

(b)

Figure 3.20: Comparison of Results between the Detailed Model and Simplified Model

3.3.3. Analysis of Comparison of Results

In order to compare the difference between the results of the detailed modelling and the simplified modelling, the final settling values during steady states of the two cases were compared. The values were compared by computing the absolute and relative errors. The absolute error was obtained by computing the difference between the results of the detailed modelling and the simplified modelling. The relative error was computed by using the following formula, $\frac{\text{(simplified - detailed)}}{\text{detailed}} \times 100\%$. The results are illustrated in Table 3.1.

Angular Velocity

Vx (mph)	Detailed (deg/s)	Simplified (deg/s)	Absolute Error	Relative Error (%)
30	11.013	11.224	0.211	1.92
50	12.142	12.448	0.306	2.52
70	11.274	11.604	0.330	2.93

(a)

Lateral Acceleration

Vx (mph)	Detailed (deg/s)	Simplified (deg/s)	Absolute Error	Relative Error (%)
30	0.2628	0.2678	0.0050	1.90
50	0.4829	0.4950	0.0121	2.51
70	0.6277	0.6460	0.0183	2.92

(b)

Table 3.1: Summary of Comparison of Results between the Detailed and Simplified Analysis

3.3.4. Discussion and Conclusion on Simplified Mathematical Modelling

It can be observed from Table 3.1 that as vehicle forward speed increases, the absolute error as well as the relative error increases. The results agree with the expectation because as vehicle speed increases, the self aligning moment also increases. The increments of the relative errors for yaw velocity and lateral acceleration are found to have similar trends.

From Figure 3.20(a), it can be noted that the settling value of the yaw velocity drops when vehicle forward speed reaches 110 km/h and the corresponding magnitude is lower than the settling value of yaw velocity at 80 km/h. The explanation of this phenomenon could be that the simulated models were in the verge of skidding. However, the increasing trend of errors is still similar to the results of the lateral accelerations. In order to predict the behaviour of errors with increasing vehicle speeds, a plot of errors versus vehicle speed is shown in Figure 3.21.

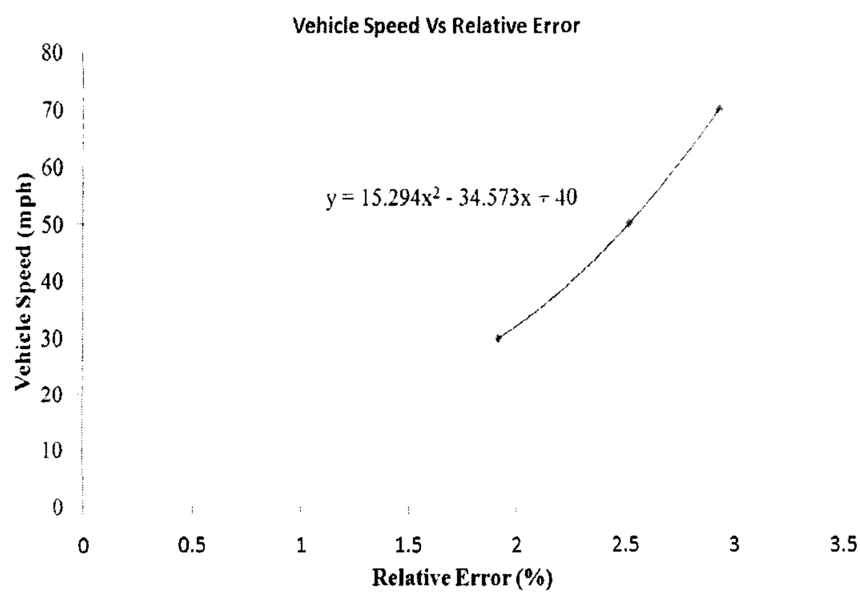

Figure 3.21: Prediction of Relative Errors

Based on the interpolation formula obtained from Figure 3.21, it was expected that as the error reaches about 5%, the corresponding vehicle speed would be about 385 km/h (240 mph) which is not very practical for a passenger car. It was therefore concluded that the simplified mathematical model of a cornering vehicle fitted with flexible shaft developed in Section 3.3 was accurate to be used to predict the behaviour of the selected vehicle in this research with less than 5% relative error.

It should be noted that the trend of error may be different for different vehicles due to the difference in parameters. However, based on the results obtained from this analysis, it can be concluded that the magnitude of error is very small and the same may apply to vehicle of different parameters. The derived simplified formula is convenient for use during preliminary design stage where quick results are expected.

3.4. Vehicle Performance Predictions under Variable Properties of Low Stiffness Resilience Shaft (LSRS)

This section presents predictions of vehicle performance when variable properties of the LSRS are installed. The properties of the LSRS are referred as its stiffness and damping values. The selected vehicle to be analysed was a Ford Fiesta. The computation was performed using the formulae and computer program developed in Section 3.3. The formulae used in the computation were validated using experimental results discussed in Chapter 4. Two types of analyses were presented using two different inputs, namely the steering wheel angle and the steering wheel torque.

3.4.1. Predictions Using Steering Wheel Angle as Inputs

In order to perform the analysis, two characteristics of steering wheel angles were selected. The first was a sinusoidal input which represented the driver's medium manoeuvring action when negotiating corners of a curvy road. The steering wheel angle function was represented by: $\delta_{sw} = \frac{\pi}{2}\sin(\omega t)$ where $\omega=2\pi f$, with $f = 0.25\ Hz$

The selected steering wheel angle characteristics had a physical interpretation. Starting from the straight ahead position, a driver turned the steering wheel clockwise to reach the maximum angle of 90^{0} on the right hand side and then turned the steering wheel counter-clockwise to reach the maximum angle of -90^{0} on the left hand side. Immediately after reaching this position, the driver turned the steering wheel clockwise back to the position of straight ahead.

The second steering wheel angle characteristics represented the driver's fast manoeuvring action when avoiding obstacles. The steering wheel angle function was represented by a step input, where the angle was ramped up linearly from the straight ahead position to 90^{0} in 0.2 seconds. The driver kept the steering wheel at this position for 5 seconds.

The two types of analyses were chosen because they represented the worst scenario that might happen during SBW failure before the vehicle came to a stop. If a shaft possessing selected properties is proven to be able to handle the two worst cases, it can be preliminarily concluded that the same shaft will be able to handle other manoeuvring tasks during normal driving.

The steering wheel angle characteristics for the two cases are shown in Figure 3.22. For all of the analyses, the road conditions were assumed to be smooth and level. Also, it was assumed that the driver is an expert, who is capable of generating the steering wheel angle with the required characteristics.

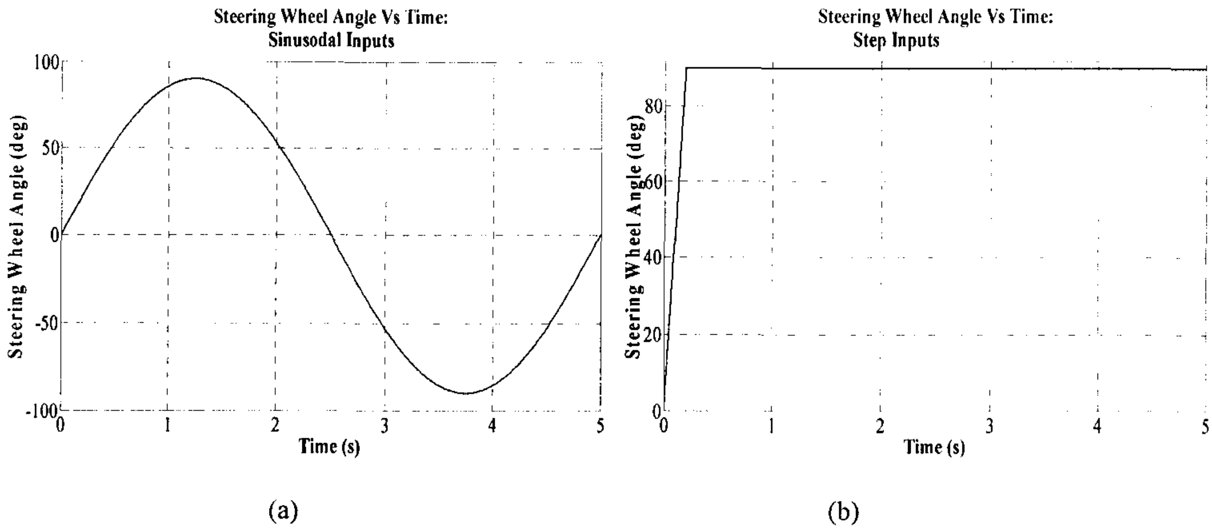

Figure 3.22: Steering Wheel Angle Characteristics used in all Analyses

Four analyses were performed using each of the steering wheel input characteristics. The first analysis was to determine the vehicle behaviour when the steering shaft stiffness was varied from $2\ \mathrm{Nm/rad}$ until the vehicle behaviour resembled the manual steering system, while its damping value was maintained at $2\ \mathrm{Nm \cdot s/rad}$. The vehicle speed was set at 50 km/h.

The second analysis was to study the effect of increasing damping constants while keeping the steering shaft stiffness at a specified value of $5\ \mathrm{Nm/rad}$. The vehicle speed for this analysis was also 50 km/h. The stiffness value of $5\ \mathrm{Nm/rad}$ was used in the analysis because the plots showed that the value was sufficient enough for stability and safety of the car used in the experiment. The highest feasible value of the damping constant was not exactly known as the design of such damper has not yet been considered or fabricated. For preliminary analysis, a certain upper limit value was chosen without considering the limitation of the actual system. A damper can be designed in a similar approach like the design of struts used in suspensions, but in this case rotational characteristics would be involved.

The third analysis was to observe vehicle behaviour when the vehicle speed was increased with the steering shaft stiffness and damping values set at lowest, $K = 5$ Nm/rad and $B = 2$ Nm · s/rad.

The last analysis was to determine the effect of increasing vehicle speed on the behaviour of a failed SBW system fitted with a low steering shaft stiffness, 5 Nm/rad and a high damping value, approximately 200 Nm·s/rad. For the third and fourth cases, the minimum vehicle speed was set at 15 km/h while the maximum speed was 80 km/h.

The output results for all the cases were the yaw velocities, which are plotted here against time for the two inputs of steering wheel angle characteristics. The yaw velocities were the only outputs selected for analysis because the behavioural trends found in the lateral accelerations and front steered wheel angles were similar to the behavioural trends found in the yaw velocities.

3.4.1.1. Results and Discussion on Vehicle Performance Prediction

The output results for the first analysis are shown in Figure 3.23(a)-(b), the second analyses in Figure 3.24(a)-(b), the third analyses in Figure 3.25(a)-(b) while the last analyses in Figure 3.26(a)-(b). The analyses of results and discussions are noted respectively.

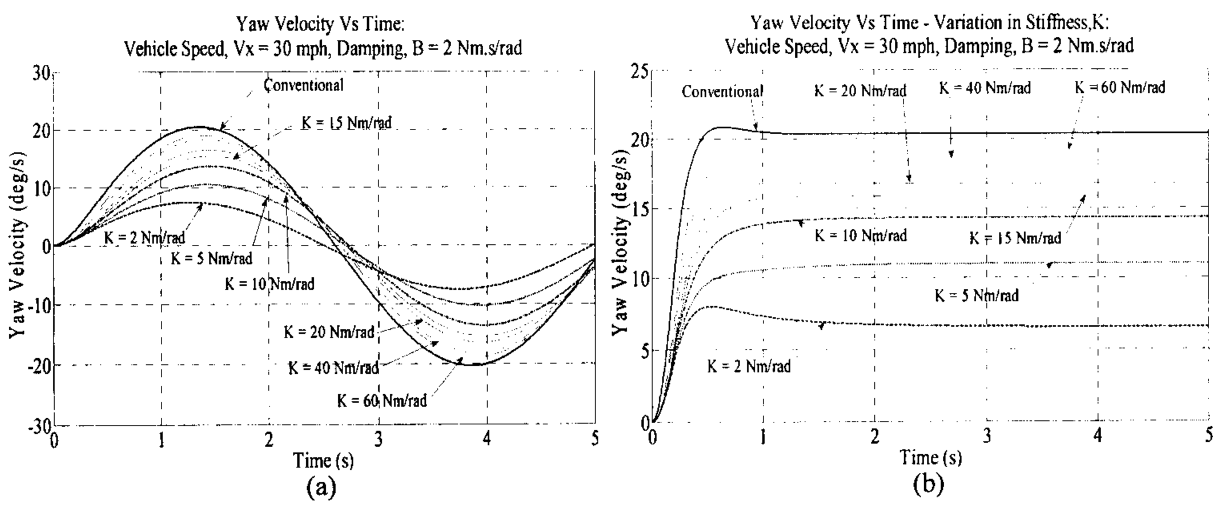

Figure 3.23: Variation of Stiffness at Specified Speed and Damping Value

Figure 3.23(a) and (b) show the yaw responses for both sinusoidal and ramp inputs. It can be observed that the higher the stiffness of the steering shaft, the higher are the peaks of the maximum yaw velocities. The incremental rate of the peak values however, decreases as the stiffness value increases. As the stiffness of steering shaft increases to infinitely rigid, the peak values approach to the expected results of the manual steering system. The steering ratios decrease with the increase in shaft stiffness. The incremental rate of the steering ratios increases as the stiffness value decreases.

For the sinusoidal input (Figure 3.23(a)), the curves become more symmetric like the shape of the conventional one when they approach either towards low stiffness or high stiffness values. The curves in between them are not symmetric and can be seen to have offsets with some delays. The non-symmetric and offset is due to the contribution of damping forces. Due to the elasticity of the steering shaft stiffness, it takes a longer time for energy to develop. Once sufficient angle of twist is reached, the turning speed of the front wheel steered angle increases, therefore the contribution from damping forces become higher. At high stiffness, the contribution of damping forces is small relative to other forces. At low stiffness, the forces due to stiffness and damping are almost similar.

For the step input (Figure 3.23(b)), overshoots are observed when the curves approach either low stiffness values or high stiffness values. Overshoot for the case of low stiffness values is undesirable because more turns and broader judgements are required to turn and control the steering wheel. The percentage of overshoot is also greater for the case of low stiffness which causes ride discomfort, and also takes longer time to settle. When the stiffness value is low, more angle of twist is required to achieve the required torque, and an increase in the required angle of twist will result in a delay of the response time. Such a delay in the response time will result in more energy being stored and the restoring of energy will increase the inertia of the system, and hence lead to overshoot.

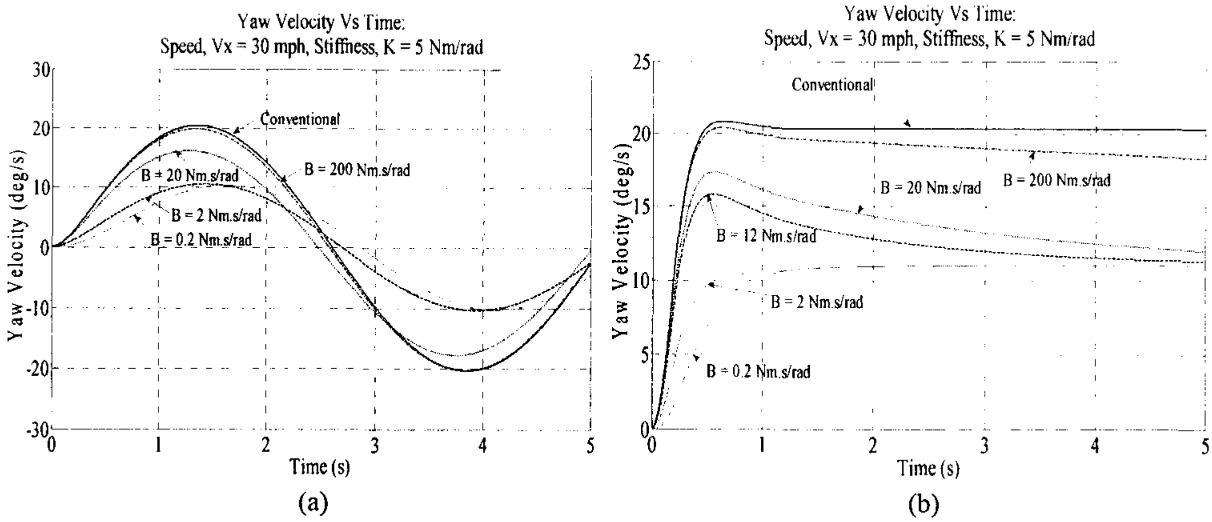

Figure 3.24: Variation of Damping Values at Specified Speed and Stiffness

It can be observed from Figure 3.24(a)-(b) that when the stiffness value is fixed while varying the damping values, the higher the damping of a steering shaft, the closer the yaw velocity approaches that of the manual steering system.

The incremental rate of the peak values decreases as the damping value increases for the case of sinusoidal input (Figure 3.24(a)). Due to the very low stiffness, the damping forces dominate other forces. However, at low damping values, the contribution of forces from the stiffness is significant and therefore contributes to the delays and offsets.

It can be observed from Figure 3.24(b) that as the damping decreases, the yaw velocity drops to approach the steady state value of the steering shaft with the lowest damping. The explanation of this relates to different characteristics of the steering wheel inputs. For the sinusoidal case, although the steering wheel velocity varies throughout the cycle, the process is continuous. On the other hand, for the step input, the steering wheel velocity is initially constant but then drops to zero. The presence of the steering wheel velocity contributes to the amount of damping force applied to the system. As the velocity becomes zero, there is no longer damping force to assist the motion. If the damping values are within the range of minimum acceptable and maximum achievable, the vehicle may be unstable during the step steer condition as shown in Figure 3.24(b) due to overshoot.

The other finding is that overshoot was found to be minimal at low damping. Damping values of 0.2 Nm·s/rad and 2 Nm·s/rad did not result in overshoot but the latter is preferable because the response time is faster. This is because as the damping values are small, the force contributed by the damping becomes negligible with respect to the stiffness forces.

It can be concluded that although steering shaft stiffness is low, good performance can be achieved by combining it with high damping values; but the steering wheel must be in continuous turning for better performance. For the case of step-steer analysis, low steering shaft stiffness will result in a reduction of yaw velocity. In order to maintain good operating conditions when performing the step-steer manoeuvre, the driver must always apply torque on the steering wheel continuously. Although this can be done, it may not be very desirable as it would be tiring while driving.

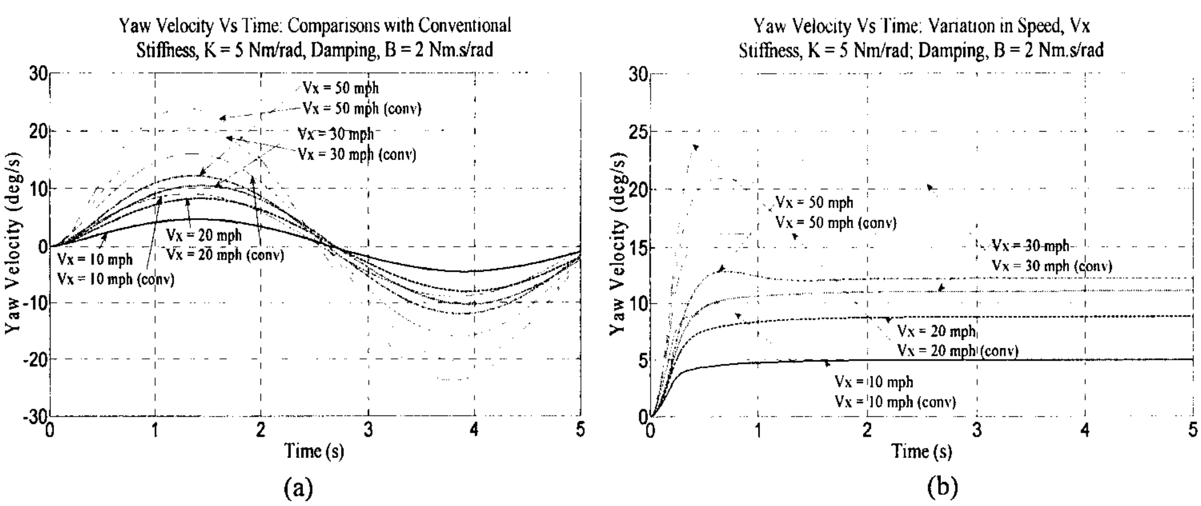

Figure 3.25: Variation of Vehicle Speed at a Specified Stiffness and a Low Speed Damping Value

Figure 3.25(a)-(b) indicate that for both conventional and non-conventional cases, as vehicle speeds increase the yaw velocities also increase. For the sinusoidal input case

(Figure 3.25 (a)), the ratio (approximately 2) of peak values between the yaw velocities of the conventional to non-conventional cases are maintained and not affected by the variation in vehicle speeds.

For the step input case (Figure 3.25(b)), the ratio of settling values of yaw velocities between the conventional and non-conventional cases are also maintained and not affected by variation in vehicle speed. However, overshoot is found to increase as vehicle speed increases.

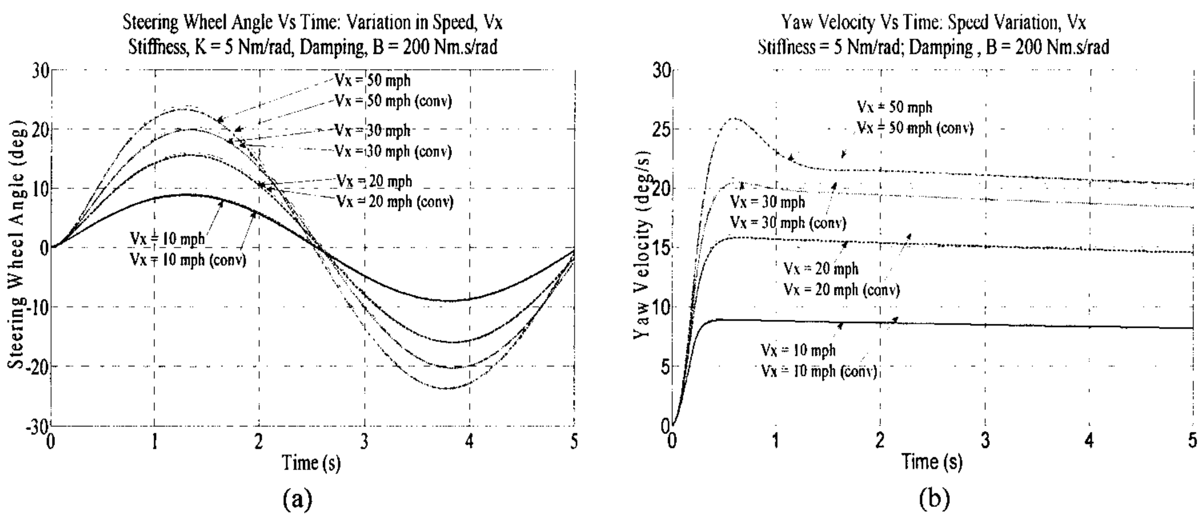

Figure 3.26: Variation of Vehicle Speed at a Specified Stiffness and a High Speed Damping Value

It can be concluded from Figure 3.26(a)-(b) that by having high damping values, vehicle behaviour during SBW failure can be almost similar to the conventional steering system. Although the reductions in yaw velocities increase as vehicle speeds increase for the case of step input, the effect can be considered as small.

3.4.1.2. Conclusion on Vehicle Performance Prediction

Based on the analysis performed in Section 3.4, several conclusions can be made about the selection of the best properties of steering shaft. The shaft with a minimum acceptable stiffness value which causes the vehicle to be stable without overshoot during SBW system failure was found to be the best of all. The main reason is because the flexibility of the shaft enables it to have packaging advantage. With minimum stiffness, it was found from the plots that the vehicle is more stable with minimal overshooting. The characteristics of the curves are also similar to the conventional vehicle but with different magnitudes.

As for the case of the damping properties, it was found from the previous plots that the best choice was either to have an acceptable minimum value of damping or to have a maximum acceptable value. Having high damping values clearly shows advantages as vehicle behaviour tends to follow the behaviour of the conventional vehicle during failure. Although having high damping values may be an advantage, the design of a system that produces such a high damping effect may sacrifice the packaging benefit. The decision on whether to use this option would rely on whether the design of dampers would lead to any added advantage.

The next choice would be to select the damping value from the minimum acceptable as shown in the previous plots. In most cases, a damper is not required to produce such small damping value since it is present naturally in the system. The natural damping values are functions of materials and design of the steering shaft.

Although having acceptable low stiffness and low damping values are preferable, the steering ratios are increased and this requires faster response time to control the steering wheel. For example, based on the previous analysis, the most preferable steering shaft stiffness is 5 Nm/rad but this value has doubled the system steering ratios. When the steering ratio increases, the driver needs to turn the steering wheel angle twice as much with a faster speed. It is questionable whether the driver will manage to handle the situation and this matter will be investigated in the following section.

3.4.2. Predictions Using Steering Wheel Torque as Inputs

Predictions using steering wheel torque as input to a mathematical model are important in order to understand its relationship with steering wheel velocity. The predictions are required because the experimental data could not provide sufficient information for a complete study. The formula and procedure for modelling the steering wheel torques as input were discussed previously in Section 3.2. For all the analyses, the torque applied at the steering wheel was assumed to be constant (10 Nm) as shown in Figure 3.27(a). The output results are the steering wheel velocity, angular velocity and lateral acceleration as functions of time, shown in Figure 3.27 (b)-(d).

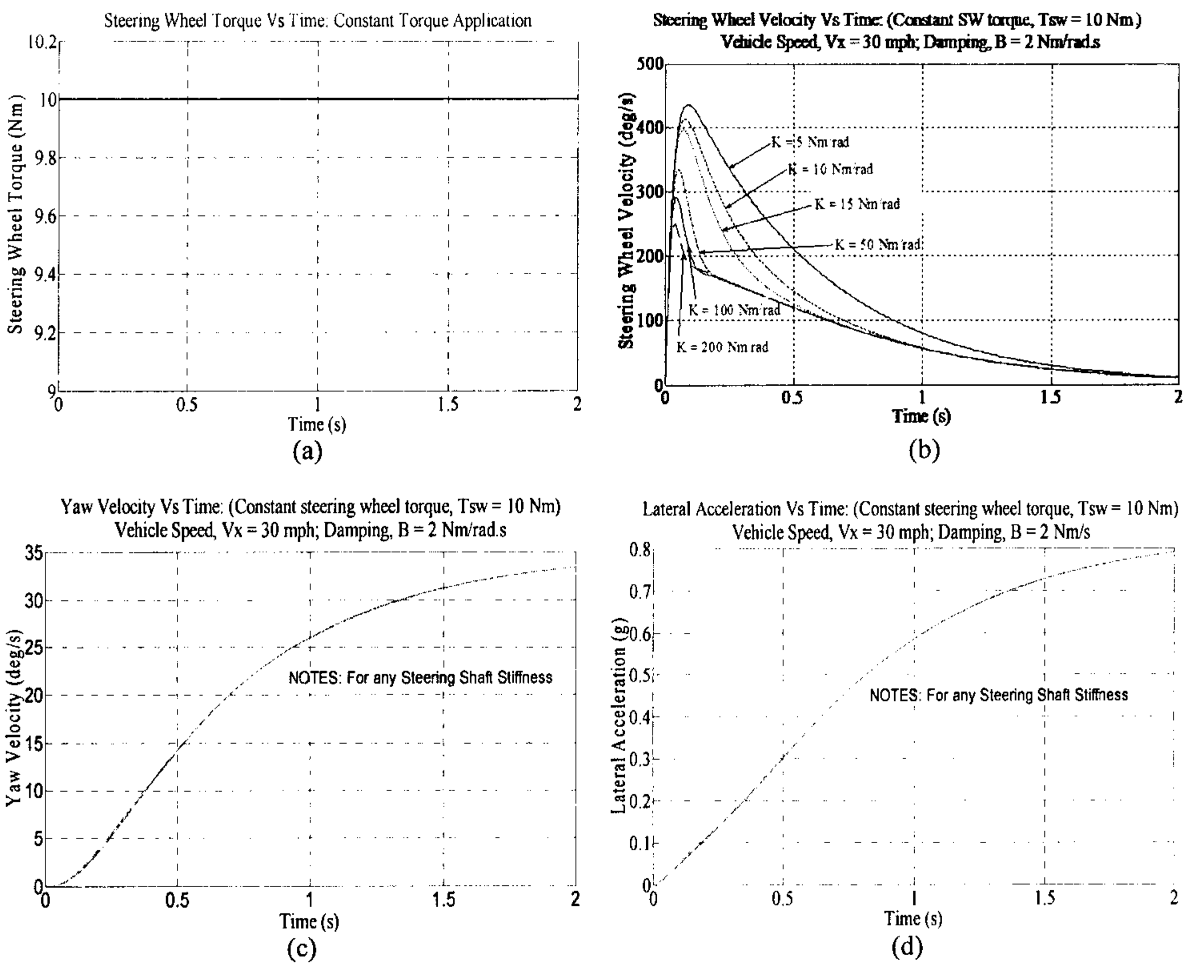

Figure 3.27: Output Results for Constant Steering Wheel Torque

3.4.2.1. Discussion on Predictions Using Steering Wheel Torque as Inputs

From Figure 3.27(b), different characteristics of steering wheel velocities can be observed for different steering shaft stiffness when subjected to an equal amount of steering torque. The lower the stiffness value of the steering shaft, the higher is the steering wheel velocity during the initial period. After a certain period of time, it can be shown that all the plots are approaching to the same trend of velocity behaviour. Due to the different stiffness values, different angles of twist are required for each case in order to achieve the final state condition and each will also require different time. The final velocity state is when the steering wheel acceleration becomes constant. Therefore, in this case it should be a straight line curve with a slope representing the acceleration value.

3.4.2.2. Conclusion on Predictions Using Steering Wheel Torque as Inputs

From this analysis, it can be concluded that applying the amount of torque required for a certain manoeuvre during emergency is more important than applying the required steering wheel velocity. This is because when a certain amount of torque is applied at the steering wheel, the resulting steering wheel velocity will vary automatically depending on the steering shaft stiffness.

3.4.3. Conclusion on Vehicle Performance Prediction

It can be concluded that the best stiffness value would be the minimum acceptable stiffness value that does not cause the vehicle to be unstable due to overshoots. The selected low stiffness is desirable because it contributes to packaging advantage. Also, the selected stiffness causes vehicle to be more stable and produce outputs with characteristics similar to the conventional system. The characteristics of vehicle behaviours such as yaw velocity and lateral acceleration were not affected by vehicle speeds.

It was found out from the analysis that the best choice of damping value was either the minimum acceptable value or the maximum allowable value. The choice of having the maximum allowable value is only kept as an option because it may lead to disadvantages in terms of design and packaging benefits. The minimum acceptable damping value may be found naturally in the steering shaft without any need of dampers. This is because the damping is a function of steering shaft design and material. Finally, the combination of the minimum acceptable steering shaft stiffness and the minimum acceptable damping value was found to be the best choice for the properties of steering shaft to be used for back-up system of SBW during system failure. With the minimum steering shaft stiffness, the steering ratio increases and this means that the driver needs to apply additional effort to increase the speed of the steering wheel. Based on further analysis, it was found out that this is not a problem as the steering wheel speed will adjust automatically depending on the torque applied at the steering wheel. If the stiffness is low, the turning of the steering wheel will be light and the steering wheel speed will increase. Based on the safety aspects, the car is definitely safe to be driven under this condition but the performance may be slightly under par as compared to the conventional system during failure.

3.5. Chapter Summary

Chapter 3 presents the development of three mathematical models of a cornering vehicle. The first model was a mathematical model of a full (3D) cornering vehicle fitted with hydraulic power-assisted steering. The aims of developing the model were to gain some knowledge and understanding of power-assisted steering characteristics and to use the developed formula to validate a full vehicle software model. The formula for an improvement to the roll angle prediction was also presented just in case the simulation results were not satisfactory.

The first mathematical model was programmed using MATLAB/SIMULINK. The computer program simulated the performance of a hydraulic power-assisted steering system fitted to a Jaguar passenger car. The characteristics of power assisted steering systems such as steering gear feel and stiffness were analysed. It was found that at low vehicle lateral acceleration and yaw velocity, the steering gear stiffness is low; and vice versa for the case of high lateral acceleration. In contrast, steering gear feel was higher at low lateral acceleration and yaw velocity; and lower at high lateral acceleration and yaw velocity. The steering gear stiffness and steering gear feel was found to be speed dependent. For more meaningful interpretation of the results, the steering gear stiffness and steering gear feel were related to a driver interaction with a car; i.e. driver steering feel (steering wheel torque) and driver steering comfort respectively.

The performance of the hydraulic power-assisted steering system fitted on the Jaguar car was found to assist the driver during parking, provide more driver steering feel at high vehicle speed, increase the driver's feel on what is happening at the road wheels during low speed manoeuvring, and prevent forces from being transmitted through the steering column at high vehicle speed. These characteristics were found to be similar to the behaviour offered by an ideal hydraulic power-assisted steering power boost curves presented in Section 2.5.1.2. The steering comfort for the hydraulic power-assisted system analysed in this study was found to be about 20% compared with the manual system. Such a design was comfortable but it might cause the driver to lose judgement of the forces acting at the road wheels.

The second mathematical model was of a 2D cornering vehicle fitted with a flexible steering shaft. The model represented a failed SBW or SAS system in the event of active system failure and the flexible shaft represented a back-up system. The model was developed in order to predict the lowest steering shaft stiffness that would ensure that the vehicle was safe to be driven, and was stable. It was found that overshoots started to occur when the stiffness values were either lower than 5 Nm/rad or higher than 15 Nm/rad. It was therefore concluded that range of the acceptable flexible shaft was between 5 Nm/rad to 15 Nm/rad. For experimental work, the shaft of stiffness 5 Nm/rad, 10 Nm/rad and 15 Nm/rad were fabricated.

The last mathematical model was a simplification of the second model. The main intention of introducing this model was to aid engineers in speeding up design work to determine the minimum stiffness values. The simplicity of the formula made it very useful to be used during the preliminary design stage. The accuracy of the formula was verified by comparing the simulation results of the simplified model with the detailed model. A cornering event representing the worst scenario of collision avoidance was selected and vehicle speed was varied for each case. The results showed that the difference of errors increased with the increase in vehicle speed but the results were accurate to within less than 5% for vehicle speed of less than 385 km/h.

The second mathematical model is revisited at the end of the chapter. Upon validation using experimental data performed in Chapter 4, the theoretical formula was used to predict vehicle characteristics when fitted with flexible steering shaft of different properties such as stiffness and damping. The main aim was to study vehicle characteristics when fitted with different properties of a steering shaft and also to determine the best steering shaft properties to be chosen.

When stiffness was varied while fixing vehicle speed and low damping, the results showed that the higher the stiffness of the steering shaft, the higher were the peaks of the maximum yaw velocities. The incremental rate of the peak values however, decreased as the stiffness value increased. As the stiffness of steering shaft increased to infinitely rigid, the peak values approached to the expected results of the manual steering system. The steering ratios increased with the decrease in shaft stiffness at an incremental rate. For the step input, overshoots are observed when the curves approach either low stiffness values or high stiffness values.

When damping was varied while fixing vehicle speed and low stiffness, the results showed that for sinusoidal input, the higher the damping of a steering shaft, the higher were the yaw velocity peak values but with the decrease in incremental rate. For the case of step input, when damping decreased, the yaw velocity dropped to approach the steady state value of the steering shaft with the lowest damping. Surprisingly, overshoot was minimal at low damping.

When vehicle speed was varied while fixing low stiffness and low damping, the results showed that the ratio of peaks of non-conventional to conventional was maintained and not affected by vehicle speed. However, overshoot was found to increase as vehicle speed increased.

Based on the previous results, it was concluded that the best stiffness value would be the minimum acceptable stiffness value that did not cause the vehicle to be unstable due to overshoots; and such stiffness could contribute to packaging advantage. The selected stiffness caused vehicle to be more stable and produced outputs with characteristics similar to the conventional system.

It was found out from the analysis that the best choice of damping value was either the minimum acceptable value or the maximum permissible value. The choice of having the highest permissible value was only kept as an option because it might lead to disadvantages in terms of design and packaging benefits.

Finally, the combination of the minimum acceptable steering shaft stiffness and the minimum acceptable damping value was found to be the best choice for the properties of steering shaft to be used for back-up system of SBW during system failure. The steering ratio increased when the steering shaft stiffness decreased; therefore the driver needed to apply additional effort to increase the speed of the steering wheel during cornering. Further analysis using torque as input showed that this was not a problem because steering wheel speed would adjust automatically depending on the torque applied at the steering wheel. When the stiffness was low, the turning of the steering wheel would be light and the steering wheel speed would increase.

Chapter 4

4. Experimental Work and Validation of Mathematical Models

This chapter presents the preparation, equipment setup, procedure, and data processing of the experimental work. Each section is arranged to be in chronological order and include explanations. The chapter ends with the presentation of preliminary results which were used to verify the proposal of implementing low stiffness resilience shaft (LSRS) for a backup system in the event of SAS failure. The experimental results were also used to validate mathematical models developed in Chapter 3. Computations of steering wheel speeds and steering wheel torque were also performed to verify theoretical predictions.

4.1. Experimental Vehicle

The selected experimental vehicle was a Ford Fiesta (2006) 5-door hatchback. Photographs of this vehicle can be found in Appendix 2(a).

The car was selected for experiment for the following reasons:

- ***It is a medium size car weighing about 1100 kg including the driver.*** A medium size car (class B) is preferable because most electrical power assisted steering systems are fitted on medium size cars and have been proven to be successful. This is mainly due to the limitations of power supply.
- ***The steering shaft is connected through splined connections which can be easily removed and reinstalled.*** Several different properties of flexible shafts will be tested during experiments. Since there was only one experimental car available, each shaft

was fitted in turn, for each specific experiment, so the steering shaft must be able to be removed and reinstalled as quickly as possible.

- ***The intermediate shaft is long enough to attach a flexible connection.*** Sufficient space must be available for the installation of a flexible connection which consumes some space based on initial design estimation.
- ***The steering assembly must be able to accommodate some room for the installation of apparatus for steering wheel angle measurement.*** The apparatus includes potentiometer, brackets and a gear set.
- ***The hydraulic power assisted steering system can be easily disabled by removing the power pump belt and draining the hydraulic fluid.***

Basic data on the car are documented in Appendix 1(e). A set of vehicle data which are sufficient for two-dimensional vehicle modelling was required for this research in order to validate the experimental results as well as for theoretical predictions. It was therefore necessary for this research to determine additional data through measurements, testing and experimental work.

The vertical reaction forces at each wheel were measured using a load cell. The casing as well as the moveable top cover for the load cell were designed and fabricated for measuring purposes. The values of these items are shown in Appendix 1(e). The location for the centre of gravity was calculated from the measured front and rear vertical forces (Figure 4.1). The data such as cornering stiffness, aligning moment stiffness and the moments of inertia were obtained from the manufacturer's data.

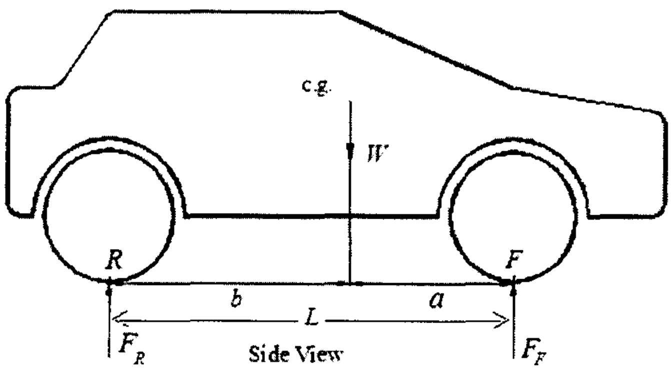

$$a = \frac{F_R L}{W} \; ; \quad b = \frac{F_F L}{W}$$

Figure 4.1: Calculation of Centre of Gravity Location

The remaining data such as the steering ratio and the number of turns for steering lock-to-lock were determined by experiment; measuring the steering wheel angles and the corresponding front steered wheel angles. The measurement of the steering wheel angles was recorded by using a potentiometer while the front steered wheel angles were measured by using a protractor and ruler. The results for these measurements are shown in Appendix 2(b). The reason for determining the number of turns for steering lock-to-lock was for the selection of a potentiometer; the maximum allowable number of turns of the steering wheel in a specific direction during the experiments must not exceed the limit of the number of turns of the potentiometer. The relationship between the steering wheel angle and the turning angle of the potentiometer also depends on the gear ratio. The gear ratio for the whole experiment was selected to be 2:1. Therefore, the specification of the potentiometer was four times more than the maximum allowable steering wheel turn in a specific direction, and a 10-turn potentiometer was selected. The mounting of the potentiometer to the steering shaft is shown in Figure 4.2.

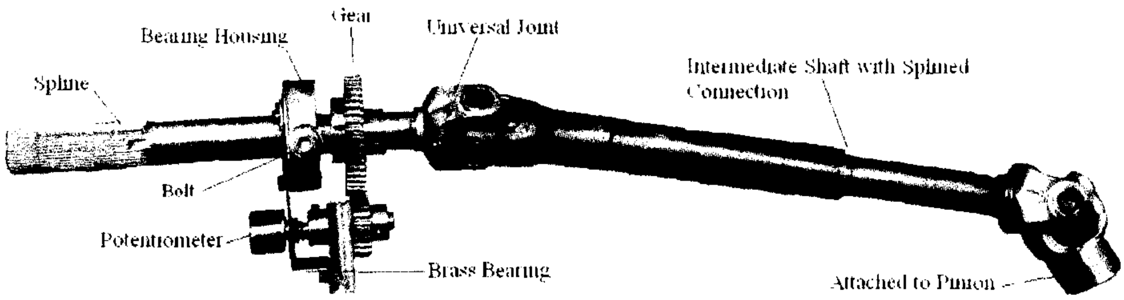

Figure 4.2: Conventional Steering Shaft with Installed Potentiometer

Prior to the installation of the potentiometer, the conventional steering shaft was first removed from the vehicle as explained in Section 4.2 below.

4.2. Removal and Reinstallation of Conventional Steering Shaft

The most important safety aspect prior to the removal of the steering shaft was to disconnect the battery cables and wait for at least 15 minutes before starting any work. By disconnecting the battery cables, the air-bag system is automatically disabled. The 15-minute waiting time is required in order to ensure that the stored current in the air-bag electronic system has been fully discharged. Other safety matters were documented in approved 'Permit to Work' form.

Prior to the removal work, the dimensions of the intermediate steering shaft were measured and the orientations of every part were marked in order to ensure that they could be reinstalled correctly. The removal of the steering shaft started with dismantling and detaching the connection to the pinion. The intermediate shaft was then shortened to the limit, using the inner and the outer shaft where a spline connection allows them to move in translational motion with respect to each other. The final step was to pull out the steering shaft assembly from the steering column. These two parts were also joined through a spline connection.

A new set of steering shaft was purchased for the experimental work (Appendix 2(c)). The new steering shaft assembly was required because the intermediate steering shaft had to be cut in order to install the flexible connections. The cut was between the upper and lower universal joints.

4.3. Design and Fabrication of Flexible Shafts

The next preparation work was to design, fabricate and attach a flexible connection to the spare rigid intermediate steering shaft. It was preferable to replace the rigid shaft with a flexible steering shaft due to its packaging benefits as well as to demonstrate how the proposed system works. However, due to the time constraints, flexible connections which can be produced easily were preferable, and it was expected that the substitutes would also produce the same experimental results.

A schematic representation of the proposed flexible connection is shown in Figure 4.3. The main parts of the flexible connection include the double torsion spring of equal stiffness K on the left and right sides, the input and output shafts, the shaft sleeve and the hollow tube. The shaft sleeve has a long slot which holds the double spring in place.

When the assembly is held at both shaft ends and twisted in the clockwise direction, the right hand spring will tend to expand while the left hand spring will elongate and wind up around the left shaft. The hollow tube inner diameter is made equal to the spring outer diameter, and this will then prevent the right hand spring from expanding. As a result, the right hand shaft assembly will become rigid since the shaft will lock to the hollow tube, while twisting is only permitted on the left hand shaft assembly which spring winds up around the shaft. The same concept will apply to the counter clockwise twist in vice-versa. The design of the flexible connection will ensure that equal stiffness value K can be obtained when the shaft is either twisted in the clockwise or anti-clockwise direction. The flexible spool was then attached to the end connections of the cut intermediate steering shaft, while maintaining the overall length. The connections between the flexible spool and the intermediate steering shaft were made by drilling holes through them and inserting bolts through the holes to stop them from rotating with respect to each other.

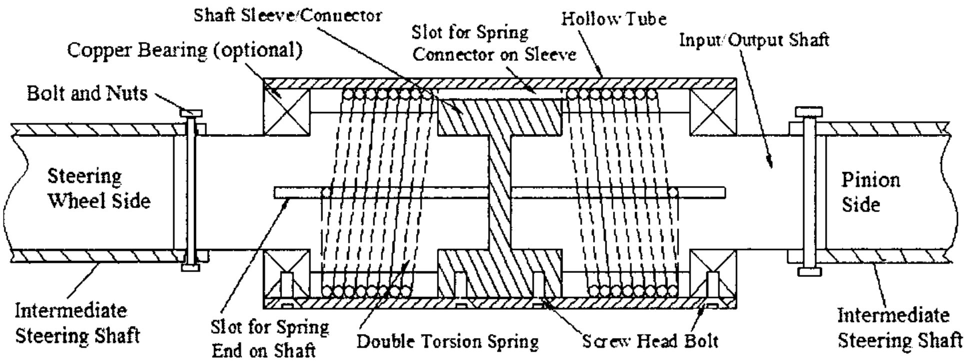

Figure 4.3: Schematic Diagram of a Flexible Connection

The detailed design of the above schematic representation was not a straightforward task. This is because the design had several major constraints as follows:

- The diameter of the flexible shaft must not exceed the surrounding allowable room.
- During removal, the flexible shaft must be removed first. In this case, it must be able to slide along the hollow intermediate steering shaft for removal. Therefore, the length of the flexible shaft is bounded by this procedure.
- The spring's deformation is only allowed to be within 10% of its nominal diameter.
- Springs are subjected to premature fatigue failure if they are operated in unwinding mode. The weakest points are at bends as shown in Figure 4.4.

Based on the previous constraints, it was decided that the dimensional requirements for all the parts other than the springs would be fixed. The detailed drawings for all major parts are shown in appendix 2(d). The designs of springs were considered separately and had to follow the dimensional requirements of other major parts. The schematic drawing for the double springs is shown in Figure 4.4.

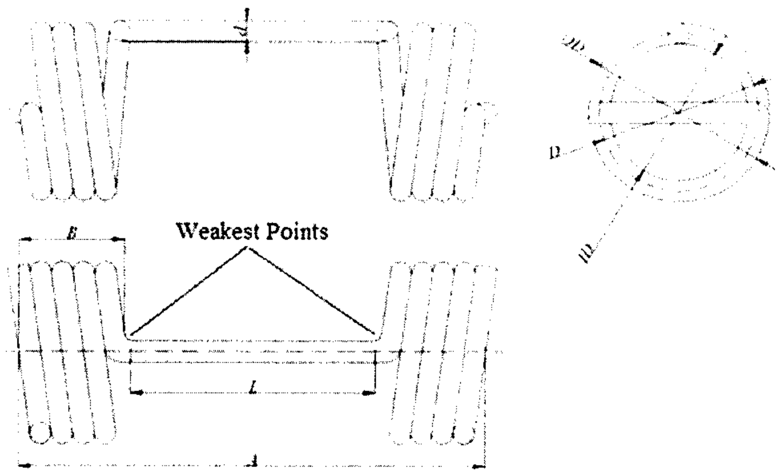

Figure 4.4: Schematic Drawing of a Double Spring

The stiffness value of the left and right springs, K can be calculated by using the following relationship:

$$K \approx (\frac{1}{2\pi})\frac{d^4 E}{10.8 D N_b} \, Nm/rad$$

, where

$d \equiv$ Wire Diameter
$D \equiv$ Spring Coil Mean Diameter
$N_b \equiv$ Number of Spring Body Turns
$E \equiv$ Modulus of Elasticity

Three categories of springs were selected based on the results obtained from chapter 3 and each to possess average values of 5 *Nm/rad*, 10 *Nm/rad* and 15 Nm/rad respectively. The selected material for the springs was chrome carbon steel. The number of body turns for all the springs was 4 and the length of each spring was specified. The desired pin diameter or the diameter of the shaft on which the springs wound was specified. The specifications for the pin diameters were selected based on trial-and-error because the corresponding calculated wire diameters had to follow the standard wire dimensions. Based on all of the available specifications, the final task was to calculate the diameter of the wire to make the springs.

The computation to find suitable wire diameters involved an iteration process. A computer program using MATLAB codes was developed to perform the calculations (refer to

Appendix 2(e)). The examples of hand calculations to verify the results are shown in Appendix 2(f). When the specifications of the complete sets of double springs were decided, they were sent for vendors' quotations (Appendix 2(g)). The pictures of the fabricated springs and the assembly of the flexible shafts are shown in Figure 4.5.

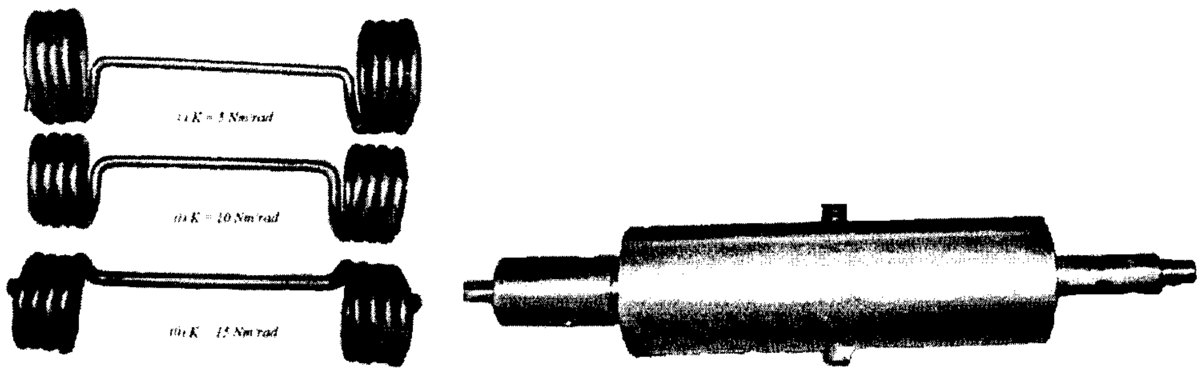

i) Custom Made Double Springs ii) Fabricated Flexible Shaft

Figure 4.5: Double Springs and Fabricated Flexible Shafts

Prior to site installation and experiments, the flexible shaft assemblies had to be tested to determine the actual stiffness in both left and right twist directions. A torsion test jig was designed and fabricated for testing purposes (refer to Figure 4.6 for details). The detailed drawing of the test jig is shown in Appendix 2(h). The test jig was secured to a test bench by using G-clamps. A specimen was held by drill bit holders (clamps) on both ends, attached to two solid blocks. One of the blocks was fixed while the other one was moveable so that it could accommodate variable sizes of specimens. One of the drill bit holders was welded to the sliding block. The other drill bit holder was designed to rotate and axially slide on the fixed block. This was done in order to twist the specimen and to allow it to elongate axially. The specimen was not allowed to shorten as a result of buckling. A moment arm and a needle were attached to the rotating and sliding drill bit holder for testing purposes. The needle and the moment arm were placed perpendicular to one another. A protractor was used to measure the twist angle when the needle moved due to the applied test weight.

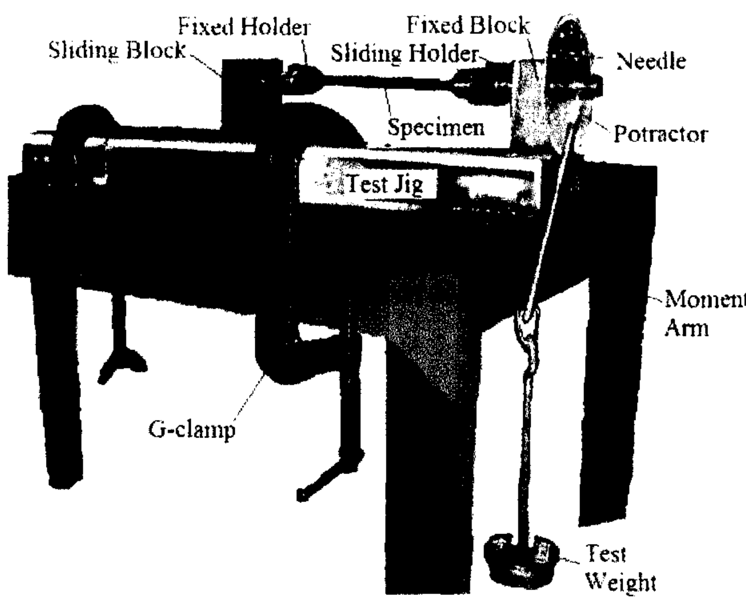

Figure 4.6: Details of Torsion Test Jig

For each specimen, the measurements of twist angles and the corresponding loads were recorded during gradual loading and unloading of test weights, and the procedure was repeated twice. The stiffness values were computed by plotting the torques applied on the specimen versus the specimen twist angles. The torques was computed by multiplying the test weights by the effective moment arm (horizontal component). The results are presented in Appendix 2(i). The summary of the calculated and measurement results is presented in Table 4.1 below.

No.	Category/Class	Calculation	Measurement
1	5 Nm/rad	5.5 Nm/rad	5.2 Nm/rad
2	10 Nm/rad	10.7 Nm/rad	9.5 Nm/rad
3	15 Nm/rad	16.4 Nm/rad	15.3 Nm/rad

Table 4.1: Summary of Results of Flexible Shaft Stiffness

When all the stiffness measurements had been carried out on each flexible spool, one of the flexible connections was then fitted to the intermediate steering shaft assembly without installing the bolt and nut connecting the spool to the constant velocity (CV) joint on the steering wheel side. The top side of the immediate shaft assembly was attached to the steering column through splint connection; the bottom side was connected to the pinion, while the overall length of the intermediate shaft was shortened by sliding the flexible spool along the shaft. The bolt and nuts which prevented the flexible shaft from rotating and sliding about the intermediate shaft assembly were the last ones to be installed. This is shown in Figure 4.7 .

The removal process of the complete assembly was the opposite of the installation process. When replacing a different flexible spool for different experiment, the task was to remove and reinstall the bolts and nuts which connected the flexible shaft to the intermediate steering shaft assembly on both sides.

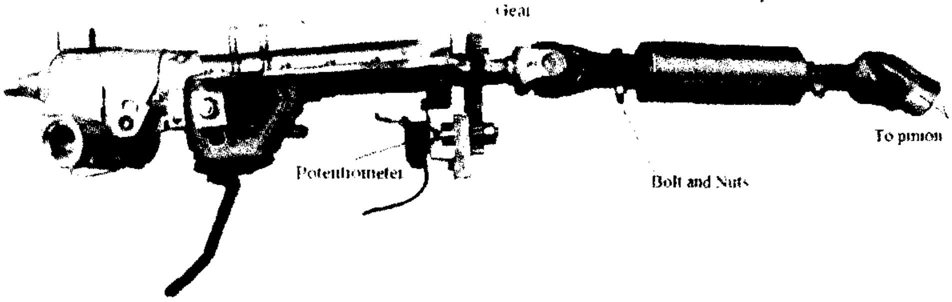

Figure 4.7: Flexible Shaft Assembly which was fitted to the Steering Column

4.4. Vehicle Preparation

Prior to performing the experiment, preparation work was conducted on the vehicle. The required preparations included basic safety checks, draining out steering hydraulic fluid completely from the reservoir and finally installing measuring apparatus as well as the data logger.

The first preparation was to perform basic safety checks such as lighting signals, brakes, tyres and vehicle integrity. Since the proposed SAS was powered by electricity, steering hydraulic fluid from the test car had to be drained out completely. This is very important since the presence of the fluid in the system, especially in the piston chambers, could cause the rotation of steering wheel to become heavier due to fluid damping. If the hydraulic fluid draining was not carried out, the experimental results may not match theoretical predictions.

The most important final task was to equip the test vehicle with apparatus and instrumentation for data collection during the experiments. A data logger (DL1 purchased from 'Race Technology') was used. The apparatus is a compact 'black box' which has a built-in high accuracy GPS system and accelerometer. The device, powered by a 12V cigarette-lighter socket, was installed on a flat surface and secured in the middle of the test vehicle. The DL1 was also capable of storing data from external sources, so the steering wheel angle was measured by using a potentiometer, powered by the DL1, and its output signal was logged on the DL1. An additional accelerometer (IMU06), also powered by DL1, was installed in order to verify the logged data obtained from the built-in devices in DL1. An antenna with a magnetic base which received signals from the GPS satellites was mounted on the roof of the test car. The data logger was capable of acquiring data by itself without the need of a portable computer, and the data were stored on a memory card. Photography of all the equipment installed for data acquisition can be found in Appendix 2(j). A close look at the DL1 data logger is shown in Figure 4.8. Among the default data logged by DL1 are the time, acceleration/deceleration, vehicle speed, distances, positions, power output, yaw velocity, cornering radius, and many others. The sampling time interval for all the experiments was set to be 0.01 s.

Figure 4.8: DL1 Data Logger

4.5. Experimental Procedure

All the experimental work involving vehicle testing was conducted on a two-way single lane test track belonging to TMD Friction Ltd., Sherburn in Elmet, UK. A plan of the track is shown in Appendix 2(k). The experiments which were carried out are classified into two main types; the first type was driving along a constant curve with an average radius of curvature of about 100m while the second type was performing a single lane change to the point of skidding. The detailed procedure of vehicle testing can be found in Appendix 2(l).

For the first type of testing, the situation represented a normal condition of driving when negotiating moderate corners. For the second type of testing, the situation represented a situation where a driver suddenly noticed an obstacle in front of him and tried to avoid it. For both cases, the test vehicle was initially driven from rest until it reached a specified constant speed before manoeuvring.

The main objective of conducting the first type of experiment was to find out whether the test vehicle was driveable and stable when fitted with the selected values of steering shaft stiffness. It was also important to know whether the lowest permissible value could be designed to be lower than 5 Nm/rad, or within the selected range, or higher than 15 Nm/rad.

The behaviour of test vehicle when fitted with a selected steering shaft stiffness value and driven at variable speeds would also be investigated.

There were two main objectives of conducting the second type of experiments. The first was to obtain accurate experimental results and use them to validate theoretical formula, required for the prediction and selection of LSRS and also to understand vehicle behaviour at high speeds or during extreme conditions. The second objective was to measure the steering wheel velocity or the rate of turning of the steering wheel by a driver during quick action manoeuvre or 'panic' situation. The subject of interest was to find out the effect of steering shaft stiffness at variable vehicle speeds on driver's reaction time when turning the steering wheel to avoid obstacles.

The experiments can be classified into three tests. The first was for the same test vehicle fitted with an average steering shaft stiffness of 5 Nm/rad, the second was for 10 Nm/rad while the third was for 15 Nm/rad. For each test, the experimental vehicle undertook both types of experiment; each was further divided into three average speed classes, namely 15 km/h, 25 km/h and 30 km/h. Therefore, the total number of experiments was eighteen. Each experiment was repeated at least three times and the average or the best one was selected for analyses.

There were several factors which could lead to some deviations in actual experimental results. For safety reasons, the maximum permitted speed for both types was limited to 30 km/h. Therefore, the behaviour of the test vehicle if driven at higher speeds could only be predicted using validated theoretical formula. As vehicle instability or undesired response might only occur at higher vehicle speeds, it would be very hard to predict such behaviour when the theoretical formula is only based on fundamental equations. A constant speed condition was not possible because the test vehicle was not equipped with 'cruise control' while manoeuvring during a certain experiment. This means that vehicle 'speed class' is only referred as the average vehicle speed based on the driver's judgement. The actual speed may fluctuate either higher or lower compared to the specified 'speed class'. The driver's effort when turning the steering wheel during experiment was also based on a single driver and his performance might also have been affected by tiredness, level of mind concentration, consistencies, etc.

4.6. Data Processing

After performing all of the experiments, the next task was to study and analyze the data obtained from the experiments and stored in a memory card. Two sets of experimental data were obtained; both were logged by the DL1. The first set was acquired by the DL1 through its satellite navigation while the second one used an independent accelerometer. The data obtained by using an accelerometer were not processed due to excessive noises. The data acquired by the accelerator were only used as a comparison to the overall graphical trends with the data acquired from the DL1.

The experimental data logged by the DL1 were uploaded into a computer and processed by using software provided by the hardware manufacturer named 'Race Technology V6'. The software was capable of generating plots of selected variables. One of the unique features of the software is that it was capable of dividing data into track markers, lap markers and sections. This means that a portion of the entire run could be chosen for analysis and the time domain as well as initial conditions can be shifted.

Although the DL1 software was capable of performing data processing and linking with MATLAB, the raw data were temporarily exported into EXCEL, and then to MATLAB for further analysis such as filtering. In MATLAB, the processed raw data was reprocessed by using a Butterworth filter in order to smooth the plots and eliminate noise. Since a portion of the data from each of the entire run was selected for analysis, the first data represented the initial condition, e.g. t = 0. The total time taken for each analysis varied depending on the number of selected data points.

4.7. Preliminary Results to Verify the SAS Concepts and Discussion

As previously stated, the proposal to implement LSRS for the safety backup system of SAS in the event of active system failure first had to be verified prior to proceeding with further development work. The first type of vehicle testing as explained in section 4.5 would provide the information for the validation work. The experimental results, namely the steering wheel angle, vehicle speed, lateral acceleration and yaw velocity with each as a function of time, are presented in Figure 4.9 – Figure 4.11 under each speed class. For each graph, the characteristics of parameters with varying shaft stiffness values are plotted.

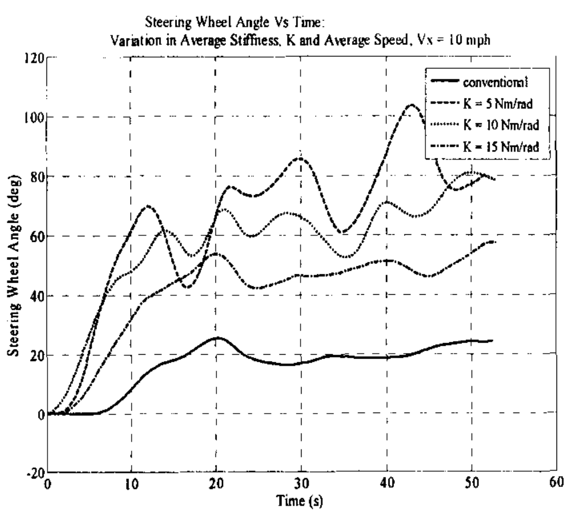

(a)

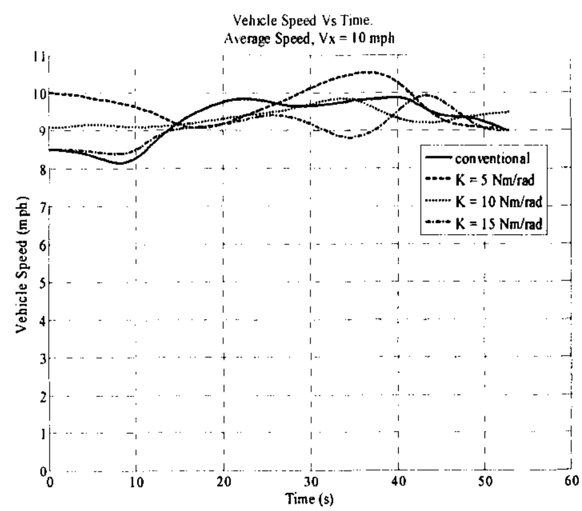

(b)

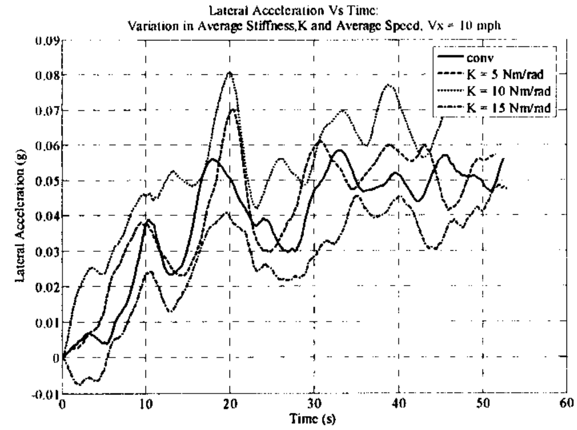

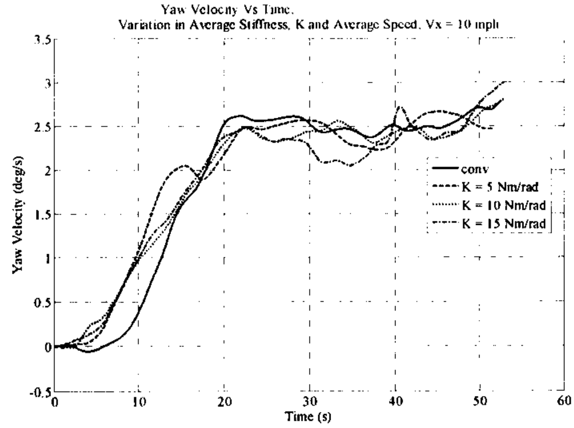

(c) (d)

Figure 4.9: Vehicle Characteristics at Variable Stiffness, K and Average Speed, V_x = 15 km/h

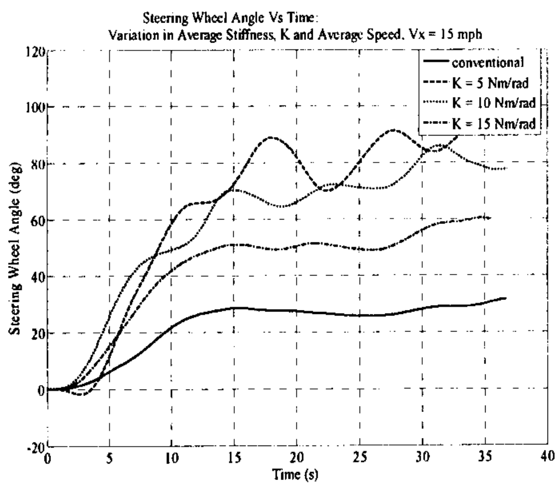

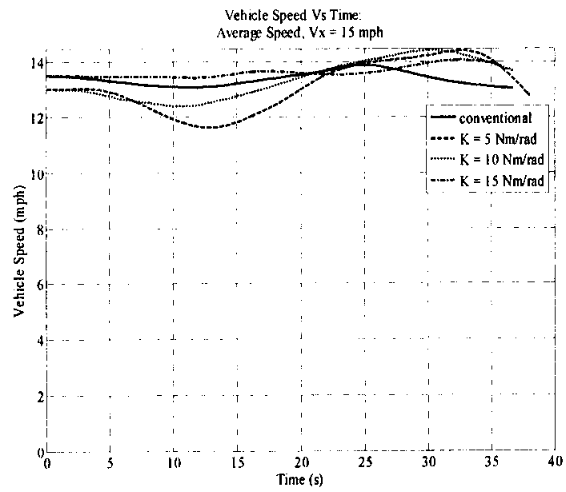

(a) (b)

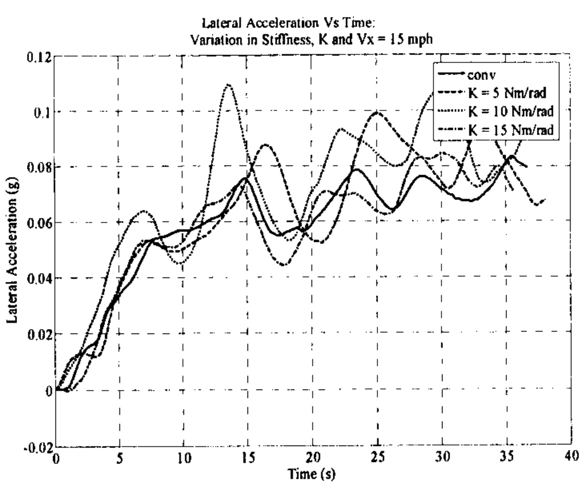

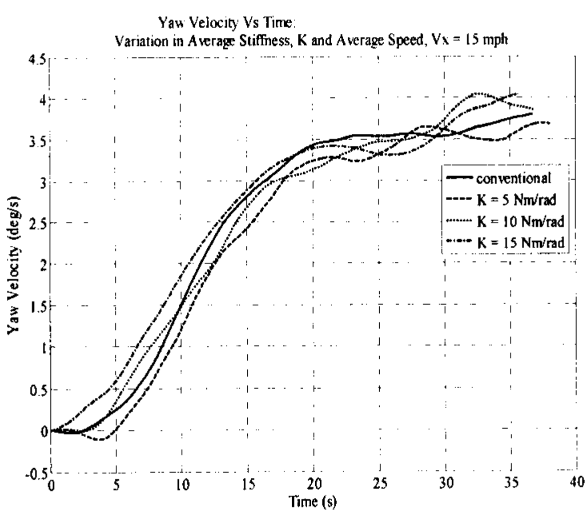

(c) (d)

Figure 4.10: Vehicle Characteristics at Variable Stiffness, K and Average Speed, V_x = 25 km/h

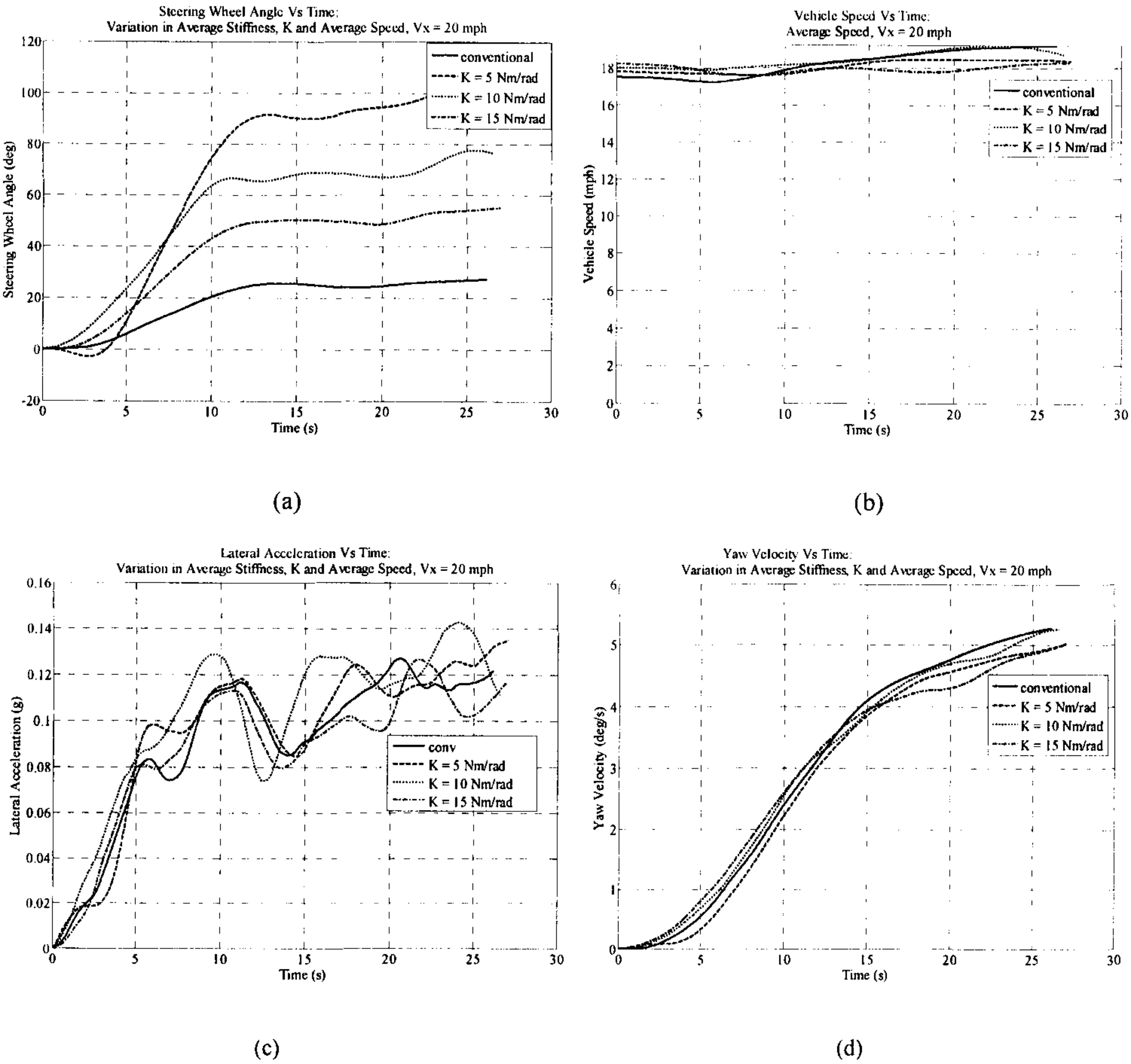

Figure 4.11: Vehicle Characteristics at Variable Stiffness, K and Average Speed, V_x = 30 km/h

In general, the test vehicle was found to be stable and safe to be driven during every experiment. For all the lateral accelerations and yaw velocities under each speed class, it was found that the experimental vehicle fitted with steering shaft of stiffness 5 Nm/rad behaved similar to the test car with the conventional steering system as observed from the graphical trends of the output graphs. This was also true for the same test car fitted with a steering shaft of stiffness of 10 Nm/rad and 15 Nm/rad. The magnitudes of lateral acceleration and yaw velocity were also found to increase with an increase in vehicle speed. Although slight fluctuations and variations were observed under each speed class, these factors were negligible because the vehicle speed for each test under the same speed class was not constant. Therefore, the experimental results confirmed that the steering shaft stiffness of 5 Nm/rad is the lowest among all the selected stiffness within the minimum acceptable range required by the test car for its stability and safety in case of SBW system break down. Better results for vehicle stability could be obtained with the stiffness values higher than 5 Nm/rad.

From all the graphs of steering wheel angle versus time under each speed class, it can be observed that the lower the steering shaft stiffness, the higher is its steering wheel angle. This is due to the flexibility of the steering shaft; more angle of twist is required to develop the required torque for turning.

It can also be seen that the lower the vehicle speed, the more fluctuations can be observed in the steering wheel angle characteristics. This is because at low speed, the self aligning moment is also very low. When the self aligning moment is low, the moving vehicle will tend to be unstable and try to deviate from a straight-line path. As a result, the driver needs to turn and control the steering wheel in order to ensure a straight path is maintained.

With the increase in flexibility, more steering adjustments are required from the low steering shaft stiffness compared to the more rigid ones. This situation can be improved at higher vehicle speeds where the self-aligning moment is high enough to maintain a vehicle in a straight path. These phenomenon can be confirmed where the lateral accelerations and yaw velocities are more consistent for all categories in speed class 30 km/h as compared to the characteristics found in speed class 15 km/h. From this finding, it can also be concluded that it is not necessary for the experiment to be conducted at higher speeds. This is because at higher speeds, moving vehicle tends to be more stable when moving in a straight line. Moreover, any accident that occurs at high speed will be more dangerous.

4.7.1. Conclusions on Verification of SAS Concept

The preliminary experimental results have shown that an experimental vehicle fitted with a flexible shaft of stiffness as low as 5 Nm/rad could provide stability and be safe to drive during cornering tests. The results have verified the proposal of using LSRS for a backup system of SAS in case of system failure. It should be noted that the expected results would vary depending on the size and design of cars.

The experimental results have shown that although vehicle stability could be achieved by installing a steering shaft of minimum stiffness, other contributing factors have also been found. For example, the lower the steering shaft stiffness, the higher the fluctuations in the steering wheel angle. When the steering shaft stiffness is low, the driver needs faster speed to turn the steering wheel to avoid obstacles. Because of this reason, it should be noted that the performance of vehicle in the event of SBW system failure will be lower in comparison to a conventional steering system. However, it was proven from the experiments that the vehicle was stable, drivable and safe to be driven to safety after SBW or SAS failure. It is therefore concluded that further development work of SAS system could be continued.

4.8. Validation of Mathematical Models

The details of the experiments which were conducted to validate the theoretical formula were discussed in Section 4.5; single lane change to the point of skidding manoeuvre tests were conducted.

Although many tests were carried out during the experiments, only some data could be used for analysis because there were cases where the experimental vehicle road/tyre adhesion was exceeded during the manoeuvres. The behaviour of a vehicle in these conditions does not match theoretical predictions because its tyres are sliding on the ground. The main parameters which contribute to loss of adhesion were found to be vehicle speed, steering wheel speed and steering shaft stiffness. The experimental results are shown in Figure 4.12 - Figure 4.13, all cases can be found in Appendix 4(a)-(c). The selected parameters for analysis are yaw velocities and lateral accelerations as functions of time and for each experimental case, the steering wheel velocity and the actual vehicle forward speed are also presented. The predicted computational results and the experimental results are overlaid for comparison. The theoretical results were computed by using the formula and computer program developed in Section 3.2. For better accuracy of the predicted results, the real-time or actual vehicle speed was used in the computations. The actual steering wheel angle was used as input to the computer programme simulating the theoretical vehicle model. All of the plots were generated by using MATLAB/SIMULINK software.

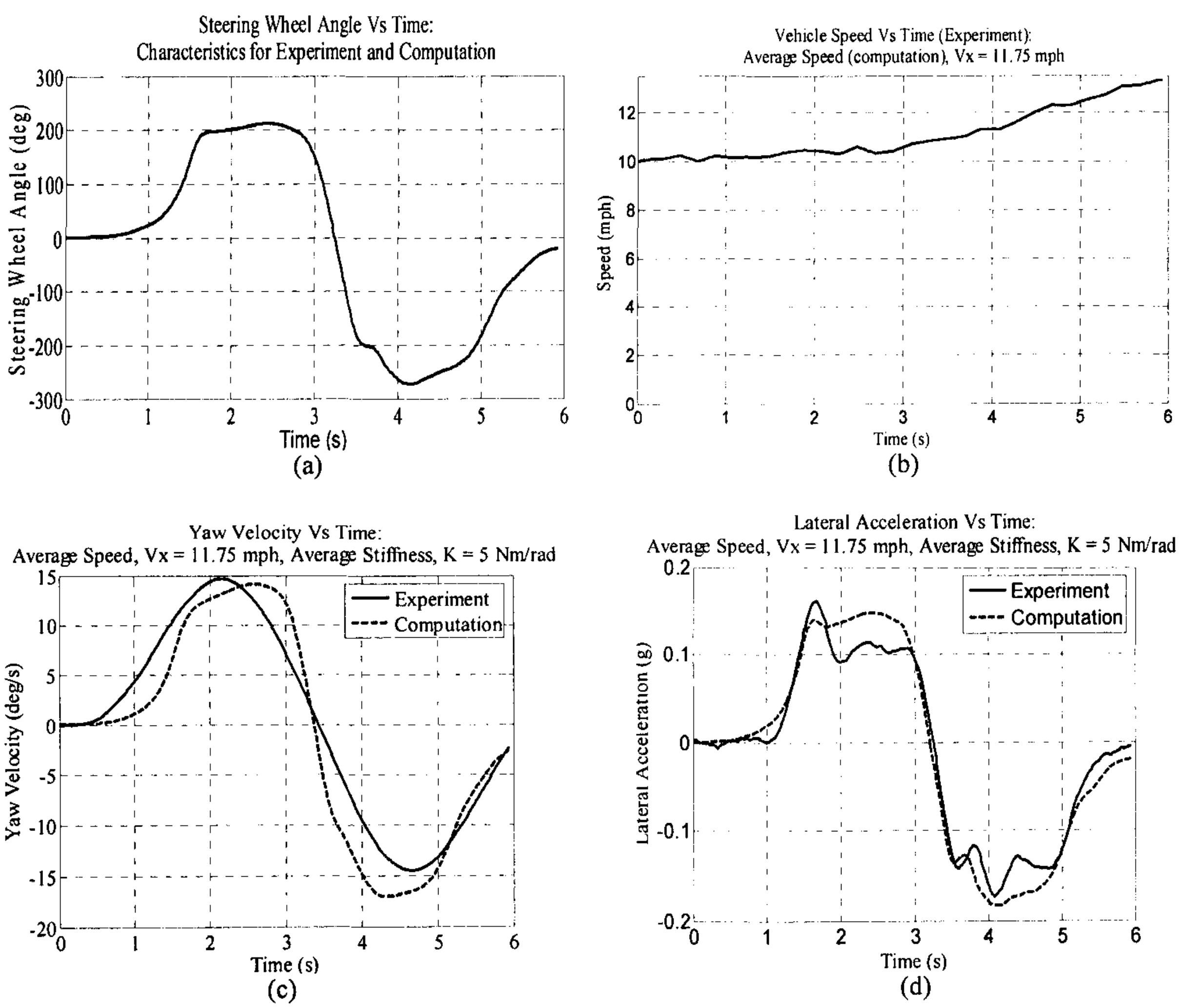

Figure 4.12: Output Results for Average Stiffness, K = 5 Nm/rad and Average Speed, $V_x = 19$ km/h.

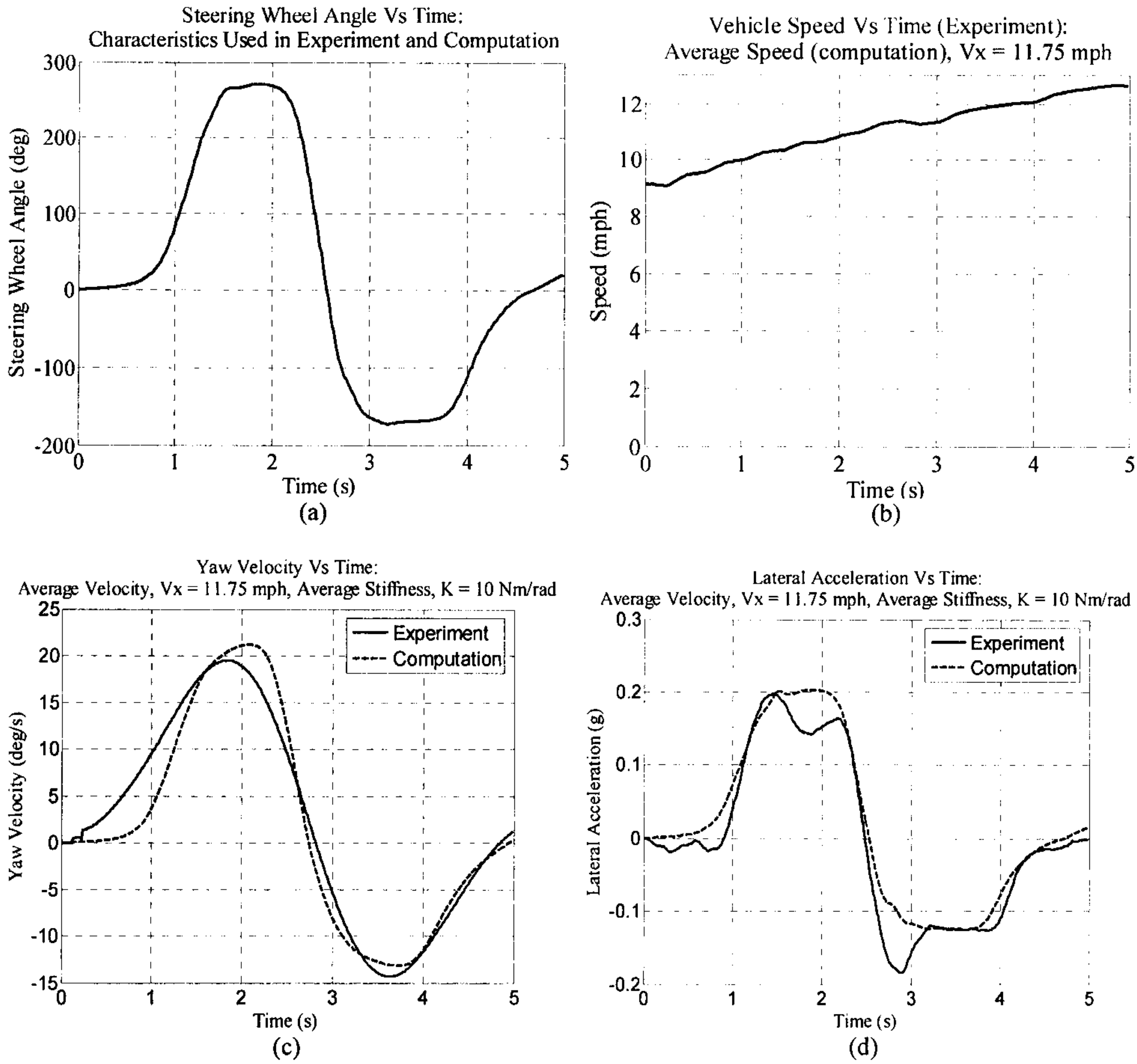

Figure 4.13: Output Results for Average Stiffness, K = 10 Nm/rad and Average Speed, $V_x = 19$ km/h.

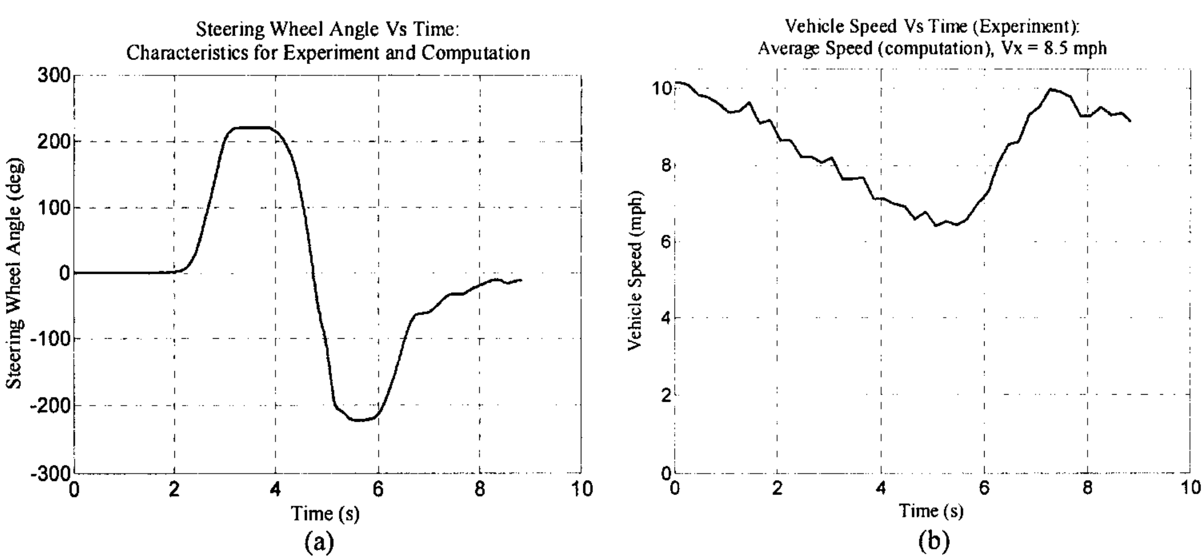

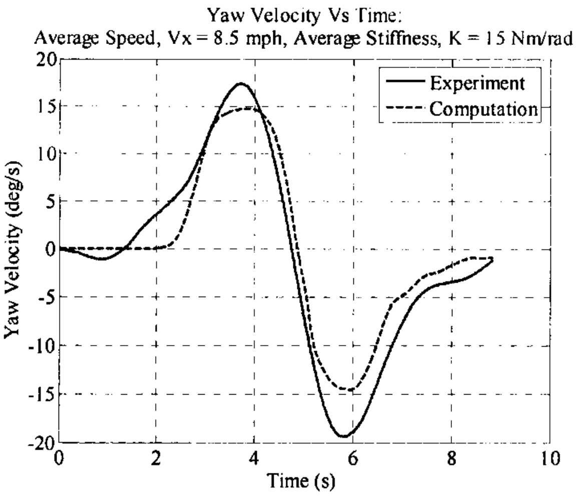

(c)

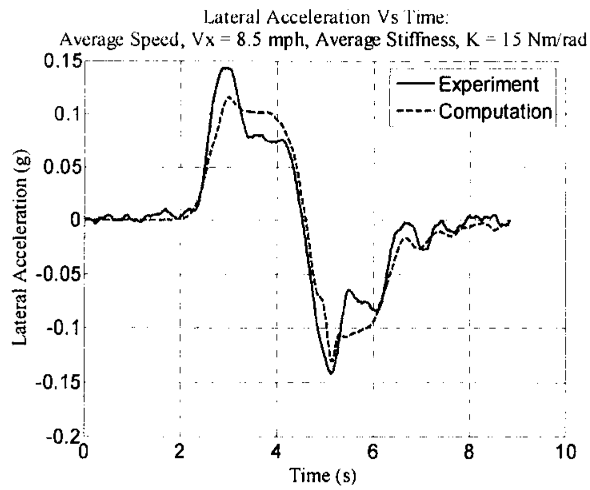

(d)

Figure 4.14: Output Results for Average Stiffness, K = 15 Nm/rad and Average Speed, $V_x = 14$ km/h.

4.8.1. Discussion on Validation of Theoretical Formula

Based on general observations from Figure 4.12 - Figure 4.13, results from the theoretical formula agree with the experimental results; although some deviations can be observed, they are explainable. For example, from Figure 4.12(c) with an average stiffness of 5 Nm/rad, the yaw velocity for the experimental results was observed to be higher during the clockwise turning of the steering wheel while they lagged behind during counter-clockwise turning. This result could be explained because the steering shaft of average stiffness of 5 Nm/rad had different values of stiffness for clockwise and counter-clockwise turning (see Appendix 2(i)). In this case, the clockwise value is higher than the counter-clockwise value while the computation only uses the average values. Also, due to the 'sticking' effect, additional torque is required during the initial turning of the steering shaft. From Appendix 2(i), the plots do not pass through the origin. In general, accuracies should not be much expected as the derivation of most formula also involves some simplifications, assumptions and approximations. One of the examples is the derivation of the 'bicycle model' itself (Pacejka, 2002).

4.8.2. Conclusion on Validation of Mathematical Model

Based on the previous findings and discussion, it can be concluded that the derived mathematical formula are correct and valid for predictions in order to obtain better understanding of vehicle behaviour during SBW failure when fitted with different properties of steering shaft. The computed lowest natural frequency of the experimental car was about 285 rad/s which was much higher than the frequency of the steering wheel motion during the experiments; and therefore resonance would not occur. The theoretical formula can also be used to predict vehicle performance at extreme conditions where it is impossible or impractical to perform experiments. The results can be used to predict the best properties of LSRS which provide good vehicle stabilities, safety and minimum power consumption. The results for the prediction of vehicle performance when fitted with different properties of steering shaft had been presented in Chapter 3, Section 3.4.

4.9. Calculation of Steering Wheel Speed and Torque

This section presents the calculation of steering wheel speeds and torques using the experimental data. The calculation of steering wheel speed was performed by using the experimental data used to validate the mathematical model. The computation was done by measuring the slope of 'steering wheel angle versus time' of the plots shown in Appendices 4(a)-(c). The main purpose of measuring the steering wheel speed was to determine the maximum steering wheel speed achievable during fast action manoeuvring while driving a class B vehicle. It is also required to find out the effect of steering shaft stiffness on the driver's reaction to turn the steering wheel. It was stated in (Yih, 2005) that during an emergency manoeuvre, the steering rate target is two full turns of the steering wheel per second (720 deg/s) or a road wheel slew rate of 45 deg/s. The results are presented in Table 4.2. In order to compare the results shown in Table 4.2, two cases from speed class 15 km/h were chosen. The selected cases are the experimental vehicle fitted with steering shaft stiffness of 15 Nm/rad and with the conventional steering shaft. These cases were chosen because they had the same average vehicle speed and also almost the same amount of maximum steering wheel angle as well as the maximum yaw velocity. Although the two cases posses similar characteristics, the experimental vehicle fitted with a flexible shaft of 15 Nm/rad could deliver much higher (almost double) steering wheel speed as compared to the conventional one. Any two samples from the same speed class could be chosen for comparison as long as the samples have similar characteristics.

Speed Class 10 mph	SW Speed (deg/s)	Max SWA (deg) (p-p)	Max Yaw (deg/s) (p&p)	Average Vx (mph)	Status (Stable/Skidded)
S10_K5	660.84	483	15/-15	11.75	Stable
S10_K10	763.89	449	20/-15	11.75	Stable
S10_K15	924.23	443	17.5/-20	8.5	Stable
S10_conv	466.02	426	19/-22	8.5	Stable
Speed Class 15 mph	**SW Speed (deg/s)**	**Max SWA (deg) (p-p)**	**Max Yaw (deg/s) (p&p)**	**Average Vx (mph)**	**Status (Stable/Skidded)**
S15_K5	773.49	494	20/-10	14	Skidded
S15_K10	555.09	419	13/-13	14.5	Skidded
S15_K15	447.41	402	13/-15	14.5	Skidded
S15_conv	444.26	320	10/-22	14	Skidded
Speed Class 20 mph	**SW Speed (deg/s)**	**Max SWA (deg) (p-p)**	**Max Yaw (deg/s) (p&p)**	**Average Vx (mph)**	**Status (Stable/Skidded)**
S20_K5	535.08	463	11/-13	18	Skidded
S20_K10	447.17	381	16/-16.5	16	Skidded
S20_K15	453.92	369	14/-12.5	18.5	Skidded
S20_conv	219.27	300	17.5/-16.5	18	Skidded

Table 4.2: Summary of Steering Wheel Speeds and Other Characteristics

Based on the previous findings, it would be very interesting to find out how much torque the driver had applied to the steering wheel and how this torque affects the steering wheel speed. The formula and procedure for calculating the torque applied on the steering wheel during the experiments were described previously in Section 3.2. The results are shown in Figure 4.15(a)-(c) for speed class 15 km/h.

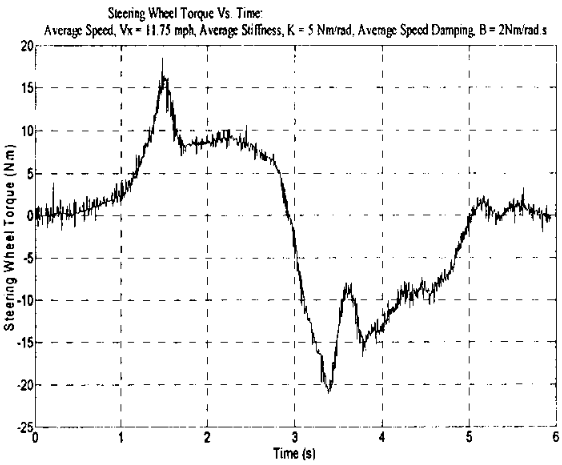

(a)

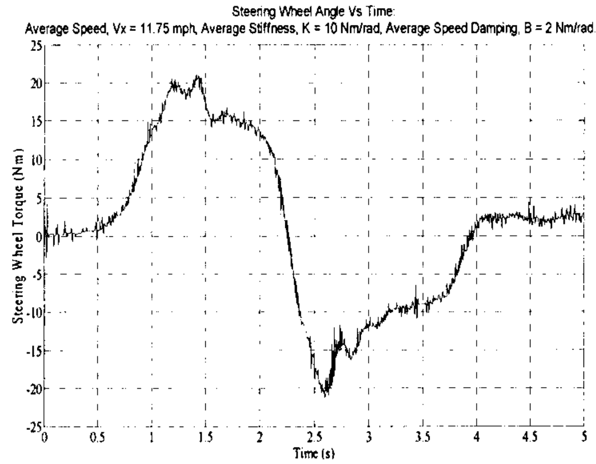

(b)

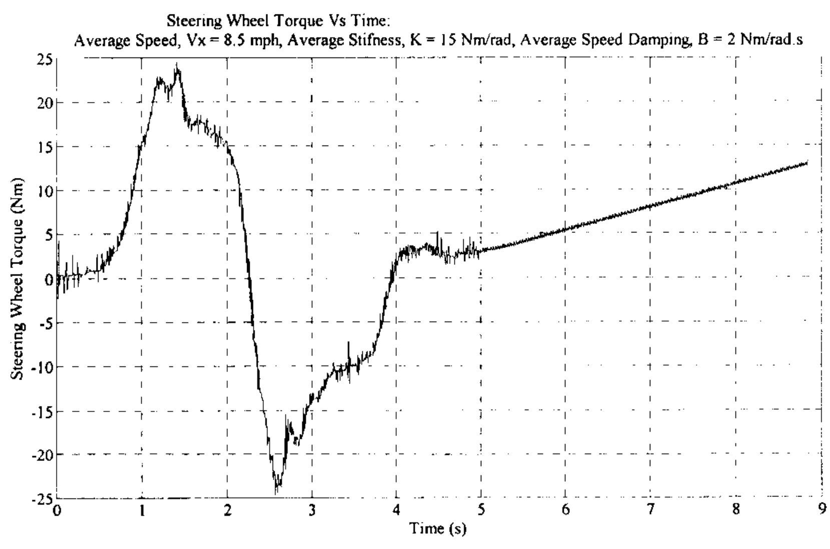

(c)

Figure 4.15: Applied Torque at Steering Wheel for Speed Class 10 mph

From the graphs, it can be concluded that the driver applied a similar trend of torque on the steering wheel but the magnitudes were not similar. Therefore it was difficult to make a clear relationship between the applied torque and the steering wheel speed. It can be seen that the amount of applied torque at the steering wheel for the case in Figure 4.15(b) is higher than for the case in Figure 4.15(a). As a result, the vehicle fitted with steering shaft of 10 Nm/rad possessed higher peaks of yaw rate as compared to the 5 Nm/rad one. The relationships between steering wheel speed and torques was discussed in Section 3.4.2.

4.10. Chapter Summary

This chapter illustrates the experimental preparation work such equipment setup, experimental procedure, and data processing; and the validation of mathematical models developed in Chapter 3 using the experimental data. Each section was presented in sequence with the first topic about the selection of a test vehicle and how required parameters were measured. In this research, a medium size car of class B was selected. The car was selected based on a few criteria such as simplicity in removal and reinstallation of the steering shaft, and safety related matters. The removal and reinstallation procedures of the steering shaft were illustrated in detail. The design, fabrication and the installation methods of the flexible shaft were also presented, and when the flexible shafts were ready, vehicle preparation work such as safety checks, draining of hydraulic fluid and the installation of the data acquisition system were explained. Due to the time constraint and cost, the fabricated flexible shaft was not resilient in the same way as a cable but it was expected that the experimental results would be the same.

An experiment of driving a research vehicle fitted with a selected stiffness of flexible shaft along a medium cornering curve was conducted to verify the proposal of implementing low stiffness resilience shaft (LSRS) in providing stability and safety to a vehicle during active system failure. The experimental results showed that an experimental vehicle fitted with a flexible shaft of stiffness as low as 5 Nm/rad provided stability and safe to drive during cornering tests based on the graphical trends of the output results viz. lateral accelerations and yaw velocities which behaved similarly to the same test car fitted with the conventional steering system. The test car became more stable when higher stiffness values were implemented. Slight fluctuations and variations were observed in the results with the decrease in stiffness values. Since steering ratio increased with the decrease in shaft stiffness, the lower the steering shaft stiffness the higher was the required steering wheel angle. It was seen that the lower the vehicle speed, the more fluctuations were observed in the steering wheel angle characteristics. The test vehicle was found to be more stable when driving at higher speeds for every case of stiffness value. However, it was not exactly known how the actual behaviour would be at much higher speeds and hence further testing would be required for verification.

Hence, the results had verified the proposal of using LSRS for a backup system of SAS in case of system failure. Although it was proven that LSRS could deliver the required tasks, the performance of the system was found to be under par compared to the conventional steering system; but safe to control and bring a failed vehicle to a stop in the event of system failure. It was therefore concluded that the proposal was feasible and practical; and further development work of SAS system could be continued.

The experimental results of single lane change to the point of skidding manoeuvre tests were used to validate the mathematical models developed in Chapter 3. These mathematical models were required to predict vehicle behaviour when fitted with different stiffness of flexible shafts in the event of system failures. Based on general observations, the theoretical formula agreed with the experimental results with slight deviations but the reasons were acceptable. For a selected case, the yaw velocity for the experimental results was observed to be higher during the clockwise turning of the steering wheel while they lagged behind during counter-clockwise turning. Further investigation revealed that the fabricated steering shaft had different values of stiffness for clockwise and counter-clockwise turning; whereas it was assumed that they were equal in computation. Slight deviations were also attributed to the 'sticking effect' of double springs to the wound shaft.

Based on the previous explanations, it was then concluded that the derived mathematical formula were correct and valid for predictions in order to obtain better understanding of vehicle behaviour during SBW failure when fitted with different properties of steering shaft. The theoretical formula could also be used to predict vehicle performance at extreme conditions where it was impossible or impractical to perform experiments.

The same experimental data used to validate the mathematical models were also used to compute the maximum steering wheel speed and the steering wheel torque. The main aim of computing the maximum steering wheel velocity was to determine the performance during fast action manoeuvring in order to find out the effect of steering shaft stiffness on the driver's reaction to turn the steering wheel. The computation of steering wheel torque was performed in order to find out how the torque varied with the steering wheel velocity.

It was found out that the generated steering wheel speed depended on the amount of torque applied at the steering wheel and the stiffness of the steering shaft. When applying the same amount of torque, higher steering wheel velocity could be generated with lower steering shaft stiffness. This finding validated the results presented in section 3.4.2. When a driver supplied sufficient torque to turn the steering wheel of his vehicle to avoid obstacle, the vehicle should respond accordingly based on the amount of steering wheel torque. For lower steering shaft stiffness, higher steering wheel speed could be generated and vice versa.

Chapter 5

5. Concepts of Semi-Active Steering

This chapter presents the concepts of SAS starting with a review of the advantages of SAS and describing the major parts and their function. The proposed installation and the SAS control algorithms are then explained, and the overall working principles of the SAS system are described.

5.1. Introduction

The system configuration of semi-active steering is similar to conventional electrical power-assisted steering but the rigid steering shaft is made active by replacing it with a low stiffness resilience shaft (LSRS). The innovative technology is referred as 'Semi-Active Steering' (SAS) because the steering system automatically switches to either being 'conventional' or 'active' depending on the driving conditions.

During the steady state normal running condition, the steering system behaves similar to a conventional electrical power-assisted steering. The electric motor provides power assistance based on the deflection angles between the steering wheel and the pinion as a result of deflection of a torsion link. The deflection angles are normally designed to be very small and therefore the LSRS will be in the minimal state of being twisted during operation.

On the other hands, during undesired conditions such as oversteer or understeer, the steering system will behave similar to an active steering or steer-by-wire (SBW) system. Since the LSRS is flexible in twisting, the steering system can be made active during undesired conditions by applying additional or less steer relative to the steering wheel input angle in order to turn the front wheels in a controlled fashion.

The additional components of SAS other than those used in the conventional steering systems are the LSRS, the reaction motor, the power motor, the sensors and the controller. These are described next.

The selection of the LSRS is described in Section 3.2. One of the alternatives is that LSRS may be a series of small torsion bars, or springs with coils of different orientations. The LSRS acts like a flexible shaft that is resilient to a twist induced along its length. The stiffness increases constantly with increased angle of twist but becomes extremely high when the maximum angle of twist is reached. The stiffness value should be properly selected so that in the event of active system failure, the vehicle should be controllable to meet the minimum requirement of the safety standard. The flexibility of LSRS allows the SAS to perform a similar control strategy as that implemented in the SBW system. The control strategy includes slight modification from the original control formula, but the control capability may be bounded with some limitations due to the presence of the LSRS. The advantages of SBW systems in control aspects have been discussed in Section 2.4.

The reaction motor is the motor that is installed closest to the steering wheel. This motor is referred to as the 'feel motor' or 'steering wheel motor'. The name 'reaction motor' is used here mainly because it serves two main functions unlike the motors used in other designs. The first function is to track the motion of the steering wheel angles or the deflection angles while providing variable torque to the driver in order to generate variable steering wheel effort and feel during power assist operation. The second function is to minimize disturbance at the steering wheel and also to allow acceptable disturbance to be felt at the steering wheel to alert the driver to what is happening at the road wheels.

The power motor is the motor that is used to drive the rack and hence the front wheels. This motor is normally referred as the 'actuator' motor. Similar to the reaction motor, the power motor also provides two main functions. The first is to deliver power assist in order to reduce the driver's effort during parking and manoeuvring, while the second is to steer the front wheels in the event of undesired conditions. These concepts are the same as SBW where the two functions are performed under a specific control algorithm.

The functions or tasks performed by both reaction motor and power motor are the torques produced by these motors as a result of a controlled electrical power input. For the case of the reaction motor, the total torque felt by the driver at the steering wheel is the sum of the torques intended for driver's feel during power assistance and the allowable torque from the road wheels transmitted through LSRS. While for the case of the power motor, in order to vary the front road wheel steer angle relative to the steering wheel input angle, the control system will supply the sum of either increasing or decreasing current to the power motor which also represents the sum of torques required for assistance and control.

A schematic diagram of the SAS is shown in Figure 5.1, and a brief description of each part and its function is presented in the subsequent section.

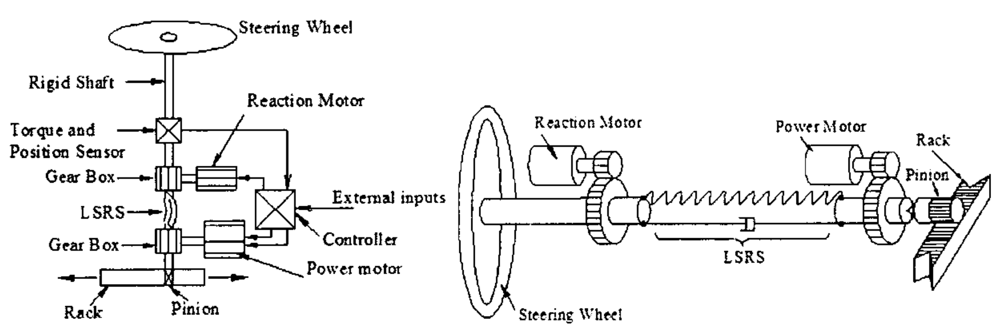

Figure 5.1: An Example of a Semi-Active Steering System Schematic and Detailed Configuration

The preliminary results discussed in Section 4.7 verified that the LSRS would ensure that a vehicle could be safely manoeuvred in the event of active system failure. It was found that a failed SBW system vehicle was stable and safe to be driven as long as the back-up steering shaft fitted on the vehicle possessed the minimum acceptable stiffness and damping values. Based on the experimental results, a proposal for the design of the SAS will be presented and then verified using commercial software, viz. i.e. ADAMS/car (Chapter 6). The verification work will involve computer simulation activities because the concepts of SAS are similar to the SBW and active steering, where most research has previously implemented and validated through experimental work.

Based on general analyses, the SAS is found to offer more advantages in terms of safety, vehicle handling and control, confidence level, and packaging as compared to conventional steering systems. These issues will be discussed later.

5.2. Safety Aspects

The most important safety aspect relating to SAS is that the system has a permanent mechanical connection (LSRS) between the steering wheels and the road wheels. In the SAS, the LSRS is always an integral part of the steering system, and is readily available to take over from the active system by switching to the mechanical steering system in case of system failure. The components are attached in the form of permanent connections and not in the form of meshing gears, as a geared system might create doubts for some customers. The system will behave almost the same as a conventional steering system in the event of active system failure. In a conventional steering system, component failures such as broken CV joints, shearing of main shaft, etc, are usually very remote since these components are very reliable.

In the event of active system failure, SBW makes use of mechanical linkages for safety backup. These mechanical linkages are not part of the controlled system. They are left idle and are only activated using mechanical, hydraulic, electrical or electronic clutches during control system failure. When the active system fails, the system relies on the actuation of clutches to connect to the safety backup components. The question is, how reliable are these clutches? When encountered with this type of question during emergency, customers may well say that the conventional steering system is preferable. Some manufacturers may claim that their clutch designs are superior and are not subject to failure. However, whatever the claims are, it is not an easy task to convince the customers. The SAS provides an effective solution.

In Chapter 2 (sections 2.3.3 and 2.4.3), it was explained that some researchers were attempting to design apparatus for active steering systems which has a permanent connection between the steering wheel and the road wheels because the system had better safety than SBW. On the other hand, SBW researchers insisted that active steering would results in additional package space and unsafe in the event of front-end collisions. Both researchers may promote each other's inventions but none has the absolute answer, which is the SAS system. The permanent mechanical linkage (LSRS) satisfies the advantage offered by the active steering system and the LSRS can be selected and designed to be flexible enough so that active control can be performed effectively in the event of even the poorest road conditions. However, in achieving this, some design compromise may be required as the selected stiffness value of the LSRS must ensure vehicle stability in the event of SBW failure. Hence, the advantage offered by the SBW can also be satisfied although not to the full scale levels.

5.3. Consumers' Confidence Level

One of the most important criteria for a vehicle system to be successfully commercialized is that it must provide consumers with a safety confidence level as high as possible. Obtaining the confidence level is time-consuming and past statistical data are needed. For example, fly-by-wire can be commercially accepted by most aeroplane passengers because accidents or incidents involving aeroplanes are rare since the system was invented. There were accidents involving aeroplanes in the past but after investigations it turned out that the problems originated from other sources. Moreover, most people travelling by aeroplane are in fact passengers, and most of them do not even know what fly-by-wire is all about.

It is very difficult for a SBW system on a car to be commercially accepted by most consumers because most people who travel by car are in fact drivers themselves. Therefore, most people may be very sceptical to find out that the vehicle they are driving does not have any mechanical connection between the steering wheel and the steered road wheels. Although mechanical back-ups are available, people may still be worried about the reliability of the clutches used to activate them. With the presence of the LSRS as part of the system, SAS is hoped to have advantages in terms of gaining consumers' confidence. The system may be accepted in the same way that ABS and ESC systems are being accepted worldwide.

SBW may be accepted worldwide for most passenger cars only if the system can be proven to be effective and reliable after a long period of time. However, the system cannot be successfully commercialised yet because most customers still do not have much confidence in it. In this case, the implementation of SAS may become a stepping stone in order to test the durability and reliability of wiring and electronic systems. If the wiring or electronic systems of SAS is proven to be effective and failures are rare after a long period of time, then the SBW concept can be proven to be effective as well. In this case, the concept of SAS with LSRS may not be necessary any more.

5.4. Packaging

SBW simplifies packaging as previously discussed in Chapter 2 (Section 2.4). Although not to the same standard as SBW due to the presence of the LSRS, SAS can also perform similar tasks and offer similar advantages to SBW. LSRS is much lighter compared to the rigid conventional shaft used in conventional steering systems. Hence the system can also lead to energy system effectiveness from a decrease in weight. Due to the flexibility of the LSRS, the steering wheel can be placed either on the left or right side of the car depending on requirements; the LSRS will also buckle during a front-end collision and this will prevent the driver from injury.

5.5. Fatigue Life

One of the major concerns about the SAS is the life of the LSRS. Frequent twisting of the LSRS may lead to material fatigue which will result in system failure after a certain number of life cycles. For this reason, the SAS system is suitable for fitment on common passenger cars where normal driving is mostly involved because during normal driving, the steering wheel angular displacement and speed is the same as to the pinion. Therefore, the LSRS is not in a state of being twisted all the time and the fatigue life of the LSRS should not be a major issue.

5.6. Design of Low Stiffness Resilience Shaft (LSRS)

For a shaft to be flexible in the transverse as well as elastic in the twist directions, it must possess certain characteristics. The first criterion is that the shaft must not transmit large bending moments. Negligible bending is acceptable as support bearings can be installed between the flexible shaft and its outer cover. The second criterion is that the shaft must be able to transmit torsion twists from one element to another up to the point of application.

An example of an LSRS is the flexible drill cable shown in Figure 5.2. The flexible shaft consists of several coils which are wound alternately in different directions. Support bearings are installed to prevent the shaft from bending. However, the commercial flexible drill cable is not suitable for the design of LSRS because the cable is normally designed to be stiff in one direction and less stiff in the opposite direction.

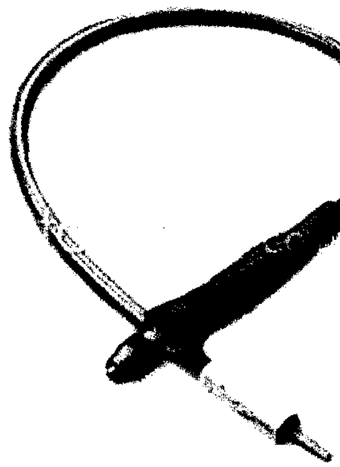

Figure 5.2: A Flexible Shaft used For Drilling [www.toolspot.co.uk]

In order to make use of a similar concept to the flexible drilling shaft for the LSRS, modification to the system is required having two sections of springs wound in opposite directions as shown in Figure 5.3. This type of spring configuration is referred as 'double spring' which has the same stiffness in both twist directions.

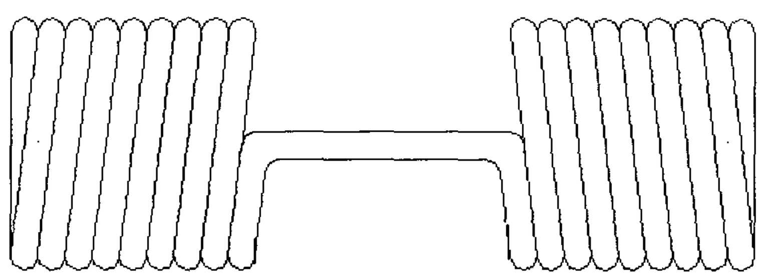

Figure 5.3: Double Spring

An alternative to using coiled springs would be to attach short pieces of torsion bars connected in series. An example of such a design is shown in Figure 5.4. Each element may possess high stiffness but when connected in series the overall stiffness will be lower. Also, when connected in series, each torsion bar will only experience a small deflection because the total deflection is the sum of each deflection of each torsion bar. This characteristic can prolong the fatigue life of the flexible shaft. The torsion bar must be designed to be attached to one another and transmit torque.

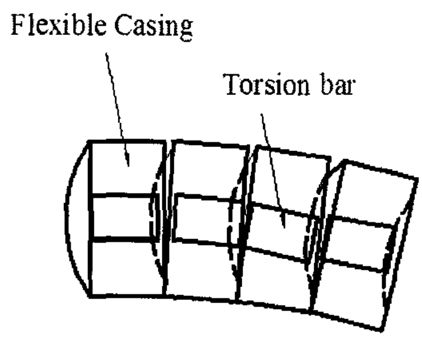

Figure 5.4: Flexible Shaft with Series of Torsion Bars

Any control strategy that is implemented on SBW can also be implemented in SAS, but the control in SAS is bounded. These limitations are due to the fact that the LSRS has a maximum angle of twist, which is a function of the number of turns of springs, the length and diameter of the LSRS, and the material. When LSRS reaches the maximum angle of twist, its stiffness becomes significantly high. The general representation of this behaviour is shown in Figure 5.5. The behaviour of a sudden increase in stiffness of LSRS after the maximum angle of twist is reached is also important as this will ensure that the vehicle is manoeuvrable or controllable during failure, especially at low speed.

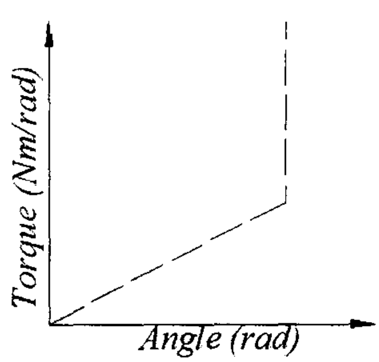

Figure 5.5: Graphical Representation of LSRS Stiffness

5.7. Design of Semi-Active Steering

In this research, there are two proposals which are presented for the design of semi-active steering. Each one has its own advantages in terms of design simplicity and control. The main differences between the two are mainly due to the way the signals of the deflection angles are obtained and the reactive torques as well as the steering feel are generated.

The first design proposal is shown in Figure 5.6(a), and is a simple design. Its main system configuration consists only of the steering wheel with a rigid shaft, the flexible shaft (LSRS), and the two motors. The configuration of the system without the reaction motor is similar to conventional hydraulic power assisted steering. The LSRS is analogous to the torsion bar while the section of the shaft from the power motor onward to the pinion is analogous to the rigid steering shaft. Since the stiffness of the LSRS is low, the reaction motor is used to manipulate or enhance the driver's feel at the steering wheel by applying artificial counter torque. Because of the simple configuration, the information of the steering wheel torque signal can simply be obtained from the reaction motor. The deflection angles are obtained from the difference between the rotational angles of the steering wheel and the pinion $\left(\delta_{sw}-\delta_{p}\right)$.

The second design proposal is shown in Figure 5.6(b). This design has the advantage in terms of control that it simulates the reactive torque to be as close as possible to the conventional steering system behaviour. The system is more complicated because it has an additional part, viz. the torsion bar. The system configuration is also similar to the hydraulic power assisted steering but the rigid shaft is made flexible. When the steering wheel is turned, the reaction motor will ensure that the flexible shaft (LSRS) is only minimally twisted by applying a counter torque. When the LSRS behaves like a rigid shaft, the end result is similar to the working principle of hydraulic power assisted steering. The steering wheel torque and the deflection angles $\left(\delta_{sw}-\delta_{pm}\right)$ can be obtained from the deflection of the torsion bar. The stiffness of the torsion bar is higher than the stiffness of LSRS, and the steering feel can be adjusted by selecting a suitable value of stiffness of the torsion bar.

The second design may be limited in operation because during steady state cornering where a specified angle is selected and there is no more turn from the steering wheel, the reaction motor will fail to activate because there is no deflection angle. The controller can recognise this situation by measuring the steering wheel speed. In order to solve the problem during this situation, the new deflection angle can be measured from the difference between the steering wheel angle and the pinion rotation angle, $(\delta_{sw} - \delta_p)$. The system during this situation behaves like the first design proposal. The reaction motor is then programmed to provide artificial torque to the steering wheel for driver's steering feel purposes. The torque must be applied directly to the steering wheel through a rigid shaft bypassing the torsion bar.

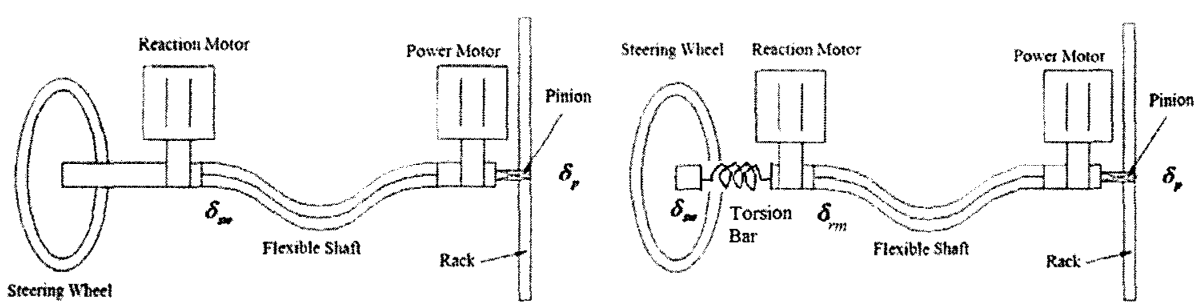

(a) (b)

Figure 5.6: Examples of Design of Semi-Active Steering (SAS)

5.8. Reactive Moment and Steering Feel

The SAS system does not require any motor to assist the steering wheel to become self-centring when the driver's hands are off the steering wheel. The task is achieved by deactivating all the motors whenever there is no torque applied at the steering wheel which overcomes the self aligning moment. Once all the motors are deactivated, the steering system is switched to conventional steering mode. The direct mechanical linkage will then automatically ensure that the steering wheel be self-centring.

Although the above technique can be implemented successfully, the reaction motor may still be required to provide some kind of force feedback to the steering wheel for lane keeping assistance (Switkes, Rossetter, Coe, & Gerdes, 2004). The reaction motor can provide such force feedback by tracking the motion of the steering wheel during the lane keeping process, while at the same time, generating and amplifying suitable torques to the steering wheel for lane keeping assistance. Also, if desired, any kinds of controls which are implemented on SBW should be able to be implemented on SAS as well by simply programming into the reaction motor.

Due to the availability of mechanical connection from the steering wheel to the road wheels in the SAS, the driver can feel directly on what is happening at the road wheels. The task is performed by the reaction motor by allowing acceptable disturbance to be felt at the steering wheel for the driver's steering feel purposes.

The force or torque information at the road wheels between the tyre-road contacts is important for the SAS system because it provides the steering feel and determines realistic road feedback to the driver. The basic principles of steering feel for both of the proposed designs are similar to a hydraulic power assisted steering system. However, if desired, active control on variable feel as implemented on SBW can be added to these systems.

For the first design proposal, all power assistance is provided by the controller. The steering wheel torque acting at the steering wheel is produced by the reaction motor, using he formula represented as follows:

$$\tau_{feel} = -K_f\left(\delta_{sw} - \delta_p\right) \tag{5.1}$$

he constant K_f was chosen so that the value of steering wheel torque can be calibrated to natch the conventional system (Hydraulic Power Assisted) at 50 km/h. Desired steering feel is generated by selecting a suitable constant value of K_f. The steering wheel torque can be made to vary with steering wheel speed by the following modification:

$$\tau_{feel} = -K_f\left(\delta_{sw} - \delta_p\right)\left(\frac{C}{C + \dot{\delta}_{sw}}\right) \tag{5.2}$$

The above modification helps to improve response during emergency cases where the driver needs to turn the steering wheel as fast as possible. The faster the steering wheel is turned, the lighter the steering wheel torque will be.

For the second design proposal, the reaction motor applies reactive torque also given by, $-K_r\left(\delta_{sw} - \delta_p\right)$ which acts as if to stiffen the flexible steering shaft. Similarly, a suitable value of K_r is chosen so that the reactive torque matches the conventional steering system at 50 km/h. The torque becomes the resistance to the steering wheel. When a steering wheel torque is applied at the steering wheel, the torsion bar will deflect. The desired steering feel can be adjusted by selecting a suitable stiffness of the torsion bar.

5.9. Disturbance Rejection

With the LSRS, the operation of the power motor cannot be assured without considering its effect on other system components because the power motor is directly connected to the steering wheel via the LSRS. When the power motor rotates at different speed from the steering wheel, a disturbance can be felt at the steering wheel. Therefore, a reaction motor is required to prevent such a disturbance from being felt by the driver.

The reaction motor can reject the disturbance by applying an equal and opposite torque to the source. Information on the magnitude of the disturbance torque can be obtained from the deflection of the LSRS as well as the power motor. The disturbance rejection task is discussed in Chapter 6.

5.10. Power-Assisted Steering

The power assistance system for the SAS was developed based on the ideal power boost characteristics of a hydraulic power assisted steering system as discussed in Chapter 2 (Section 2.5.1.2). The hydraulic valve characteristic curve is manipulated and converted so that it can be implemented in electrical power assisted steering. The process is performed by making each characteristic that corresponds to its specific vehicle speed to be linear; these are required for smooth and simplified operations of electrical motors. All the linear characteristics are assigned to have the same slope. For design simplicity, the horizontal distance between each linear characteristic is made to increase in a specific pattern, the choice of which is subjective and depends on the designer's choice since no conclusive research has been done in this area. The modified characteristics are obtained from Figure 2.7 as shown in Figure 5.7.

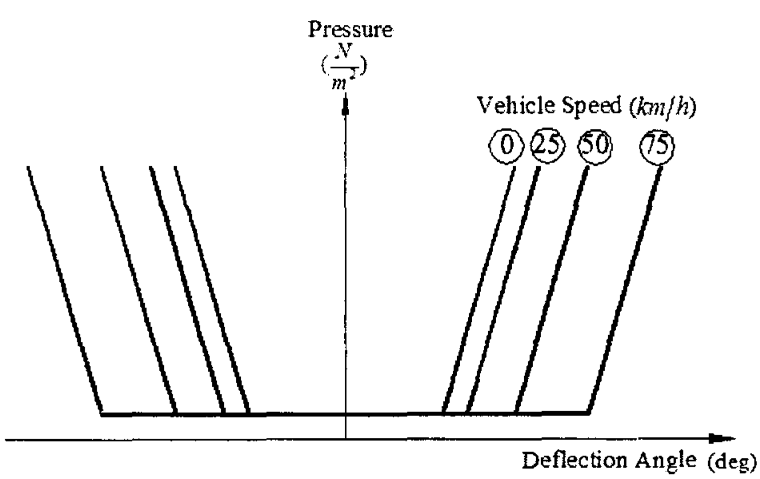

Figure 5.7: Modified Hydraulic Power Boost Curve

The vertical axis is the hydraulic system assist pressure, which can be converted to 'torque' by multiplying by piston areas and pinion effective radius obtained from the hydraulic power assisted system. The horizontal axis is the 'deflection angle' which is the difference between two rotational angles. These angles are selected based on the SAS power steering design and are discussed in Chapter 6.

5.11. Vehicle Control

All control strategies proposed for use in a SBW can also be implemented on the SAS with some modification to the control formula. However, the control that can be performed on the SAS is limited by the maximum angle of twist of the LSRS. A modification of the control formula is required in order to make a correction to the amount of torque required to operate the power motor as well as the reaction motor owing to the presence of the LSRS. Also, in the SAS, an additional control for disturbance rejection is required in order to prevent the irregular inputs from the road wheels from being transmitted to the steering wheel.

The control algorithms of SAS can be broken down into two main divisions. The first division is on power assisted steering while the second division is on active steer. The development of the control aspects will be carried out in sequence. For example, the first task will be to design and optimize the power assisted steering and the second task will be to add control aspects to the system.

The proposed control system for SAS power assistance in this research is formulated from a PD control formula ((Dorf & Bishop, 2005)). For the first design proposal, the desired value is the steering wheel angle while the actual value is the pinion rotation angle. For the second design proposal, the desired value is the steering wheel angle while the actual value is the reaction motor angle. The schematic diagrams for the control of both of the proposed designs are shown in Figure 5.8(a)-(b).

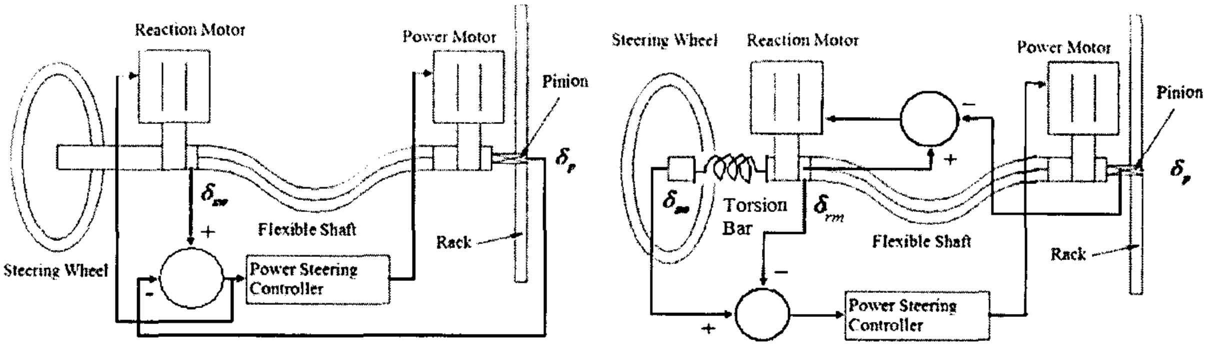

(a) (b)

Figure 5.8: Schematic Diagrams for Power Assistance Basic Control of SAS

The block diagrams for the control of the power assistance for the first and the second proposed designs are shown in Figure 5.9(a)-(b). It is noted that the form of control for the two designs, if simplified, follows the basic closed loop control diagram with feedback. Such form of control is the basic knowledge in the control system field and has been proven to be successful in most applications. Although the two proposed designs have a similar form of controls, the latter is more complicated due to the dependency between the torsion bar and the LSRS. This means that any deflection imposed on the LSRS will also be felt by the torsion bar. In this case, the reaction motor needs to be programmed to eliminate the transmission of force from the LSRS to the torsion bar.

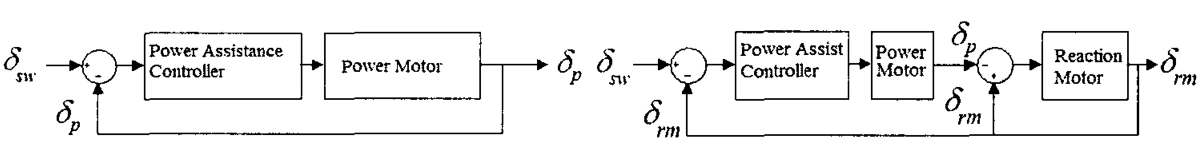

(a) (b)

Figure 5.9: Control Block Diagrams for the Proposed Designs

A software model using ADAMS/car was built for the first design proposal where the system is referred as "Electrical Power Assisted Steering" since no active control aspects were embedded into the system at this stage. The details of the modelling processes are discussed in Chapter 6. The model will be optimized to determine the best parameters for power-assisted steering characteristics. Due to the complexities in the control aspects, the modelling work for the second design proposal was not carried out in this research. The concept has its own unique advantages as previously discussed and could be considered for future research work.

The next task was to add active steer control algorithms to the SAS electrical power-assisted steering model. The control aspects can be introduced to the block diagram shown in Figure 5.9(a) by multiplying the feedback signal with the reciprocal of the ratio between the desired and the actual steer angles, $R = \frac{\delta_{desired}}{\delta_{actual}}$. The external input signals to the system can include the vehicle forward speed, yaw rate, and lateral acceleration depending on the selected control techniques. The input signals must first be multiplied by distinctive transfer functions in order to transform the system into functions of R. The block diagram for the processes is shown in Figure 5.10. The main intention of performing this type of control is to alter the front steered wheel angles based on vehicle stability and safety requirements with respect to the steering wheel angle.

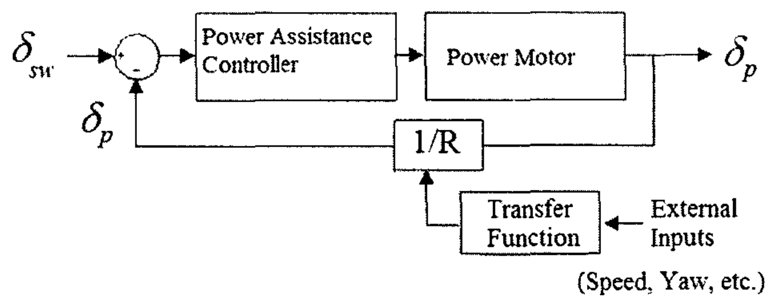

Figure 5.10: Block Diagrams for Active Control on SAS

forward speed of the vehicle, the higher the amount of resistance torque generated at the steering wheel. However, as the driver turns the steering wheel at a higher speed during collision avoidance, the amount of resistance torque at the steering wheel will become lower.

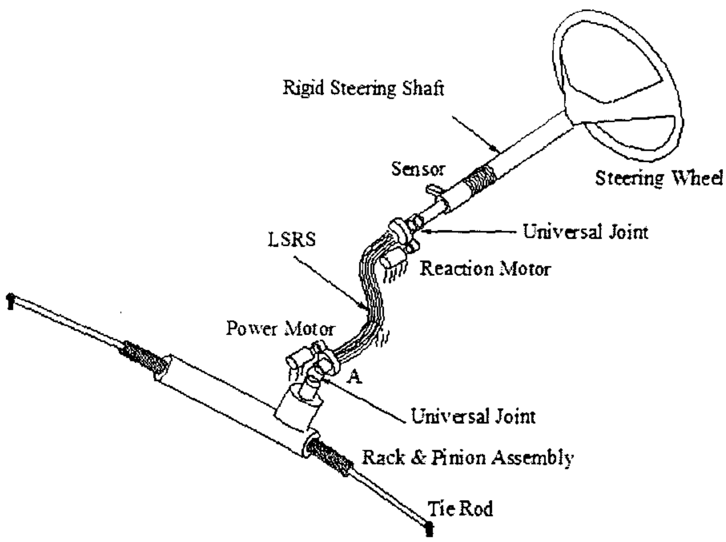

Figure 5.12: 3D representation of SAS

During normal driving where undesired events such as understeer or oversteer are not present, the system behaves the same way as a conventional electrical power assisted steering system. As the power assistance controller receives a signal representing the deflection angle, it will then operate the power motor to rotate the pinion to drive the rack either to the left or right. In this case, the steering wheel rotation angle is almost the same as the power motor rotation angle since the deflection of LSRS can be considered to be extremely small. The SAS system is designed such that the power motor provides all the assistance torque during cornering operation while the reaction motor provides artificial reactive torque to the driver for steering feel purposes. Any jolts or abnormalities from the road wheels can be felt directly by the driver at reduced magnitudes since there is a mechanical linkage between the steering wheel and the road wheels; and the driver's feel can be adjusted by modifying the power assistance characteristics.

In the event of understeer or oversteer, the power motor will rotate at different speeds in order to ensure that the overall steering ratio is varied for controlled steering. The LSRS provides the flexibility so that active steering can be performed either to provide additional or less rotation of the pinion with respect to the steering wheel input angle. The difference in speed between the steering wheel and the pinion causes the driver to feel some disturbance at the steering wheel either being assisted or resisted. In order to eliminate the disturbance from being felt at the steering wheel, the controller will receive the signal representing the rotation angle of the power motor and then operates the reaction motor to produce equal and opposite counter torque to cancel out the generated disturbance torque. A certain amount of disturbance is allowed to be felt at the steering wheel to inform the driver that an undesired condition is happening at the road wheels. The reaction motor should be equipped with suitable damping for smoothness of operation.

The system should be designed such that the failure of any subsystem will cause the whole system to fail in order to avoid any inconveniences. Therefore, when SAS system fails, the vehicle is left with the conventional system which may demonstrate degraded steering performance but is sufficient to meet the minimum safety standard. In order to ensure that the minimum safety standard is achieved, the stiffness of the LSRS should be selected so that it can provide safe vehicle manoeuvring during active system failure and minimal power is required to operate the power motor.

5.13. Chapter Summary

This chapter illustrates the concepts of the SAS system which include the safety aspects, general requirements, and system designs. The concepts of SAS were explained by analysing the advantages of the SAS system compared to the conventional system in terms of the customer's confidence level, packaging benefits, and fatigue life.

The most important safety aspect belonging to SAS was that the system had a permanent mechanical connection (LSRS) between the steering wheel and the road wheels. The LSRS was an integral part of the steering system, and readily available to revert to conventional mode in the event of system failure.

The presence of a permanent backup system not in the form of clutches was hoped to increase customers' safety confidence level to use the SAS system. The system might be accepted in the same way that ABS and ESC systems are being accepted worldwide. The SAS could be implemented as a stepping stone in order to test the durability and reliability of wiring and electronic systems of SBW; however the process might take a very long time.

SAS simplified packaging and offered similar advantages to SBW. The LSRS could lead to energy system effectiveness and buckle during a front-end collision to prevent the driver from injury.

Material fatigue was one of the major concerns about the SAS due to frequent twisting of LSRS. Therefore, the system is suitable for fitment on common passenger cars where normal driving is involved.

The LSRS could be designed using coiled springs alternately wound in different orientations or short pieces of torsion bars connected in series. The latter had the advantage of overcoming fatigue life since each element might have high stiffness but when connected in series the overall stiffness would be lower.

Two design proposals of SAS embodiments were presented. The first system only consisted of the steering wheel, LSRS, reaction motor, and power motor. The second system had similar configurations but possessed an additional component, i.e. the torsion bar. The configuration of both systems was similar to the conventional hydraulic or electrical power-assisted steering systems. Both systems were proposed to provide fully power assistance which received the signals based on the difference between steering wheel angle and pinion rotation angle. Due to design simplicity, the former was selected for further development work.

The steering wheel self-centring of SAS was achieved by deactivating all the motors to switch to conventional steering mode. Although this could be done, the reaction motor could be programmed to provide force feedback for lane keeping assistance.

Since the power-assistance was fully provided by the system, the steering feel was generated at the steering wheel by applying artificial reactive torque which triggered based on the signals of the difference between steering wheel angle and pinion rotation angle. The performance of the steering feel during special needs could be achieved by manipulating the input signals.

The presence of LSRS caused some disturbance to be felt at the steering wheel during active control. Therefore, a reaction motor was required to prevent such a disturbance from being felt by the driver by applying an equal and opposite torque to the disturbance source. Some disturbance could be allowed to be felt by the driver in order to alert the driver on the driving conditions.

The control algorithms of SAS were divided into two categories, viz. power assistance and active steer; each category was developed separately in sequence. The power assistance of SAS was proposed to be developed based on an ideal power boost characteristics of a hydraulic power assisted steering. For the case of active steer, all control strategy which could be implemented on SBW would be applicable for SAS with some modifications in the control formula. For demonstration purposes, a basic closed loop PID-control was proposed.

Chapter 6

6. Modelling of Semi-Active Steering System

This chapter presents research work in the modelling of a Semi-Active System (SAS) mainly relating to power steering assistance and active steer or control technology. The first topic related to the development of a full vehicle model developed in ADAMS/car. The same model was then modified to become an SAS system. This chapter then illustrates the techniques and approaches in optimising the power-assisted steering system. The final topic is about the introduction and implementation of control on the SAS system.

6.1. Objective

The main objective of developing a full vehicle software model complete with the control algorithms for simulation was to demonstrate the working concepts of the SAS system and to show how the system performance can meet the requirements of a robust steering system. The control algorithms implemented here are common practice in the SBW or active steering fields which have been previously implemented and proven to be successful. Therefore, the simulation results for the control of the SAS full vehicle software model did not need to be validated through experimental results.

6.2. Real Vehicle Model

The Jaguar car was selected for vehicle modelling work using ADAMS/car software because a complete data set including vehicle geometric hard points was provided by the manufacturer. This vehicle was on loan to the University of Bradford and no modifications were allowed, so no experimental work could be carried out on this car.

6.3. ADAMS/car Software Modelling

The selected software for full vehicle modelling work was ADAMS/car version 2005 (ADAMS, 2005). This software is a specialized environment for modelling real vehicles on virtual prototypes ((ADAMS, 2005) and (Yamakawa, Sakai, Yamamoto, Barber, & Wakabayashi, 2002)); the virtual vehicles can be built and analyzed like physical prototypes to understand their performance and behaviour.

The first approach to modelling work is to create subsystems such as front and rear suspensions, steering gears, anti-roll bars, and bodies. For common types of subsystems such as McPherson suspensions, rack-and-pinion steering systems, and tyres, ADAMS/car software already has built-in templates. In this case, users can make use of the templates and only need to change the properties as well as the geometry hard points of the subsystems. If built-in templates are not available, users can create their own templates by modifying from the existing built-in templates in order to save time. When the subsystems are ready, they are then grouped into an assembly of a full car in ADAMS. In assembly mode, the full vehicle model can be tested for vehicle performance using analysis such as step steer, double lane change, and constant radius cornering. During testing, changes to the vehicle parameters can be made in order to view how the design changes affect vehicle performance.

In this research, a full vehicle model was created using ADAMS and tested for its performance mainly for the following reasons:

i. The amount of available time for the fabrication of a physical prototype was very limited.

ii. The performance of software model could be explored and refined before building and testing a physical prototype if it is available in the future.

iii. The performance of a vehicle which is subjected to design changes can be analyzed at much faster and lower cost than physical prototype testing would require.

iv. Many types of analyses can be varied faster in the case of changes in testing procedures.

v. Safety from dangers associated with natural or unnatural phenomena which may lead to road accidents.

6.4. Planning and Creating Full Vehicle Model

Prior to creating a full vehicle model in template-based software, planning work was required in order to ensure that the least time was consumed. The planning work could be conducted by preparing a table on subsystems and making a checklist on what were needed to be done and what were already available in the software in the forms of templates. For this research, the planning work for the subsystems of the Jaguar car is presented in Table 6.1.

No.	Subsystem	Template Available? Name (if 'yes')	Template to modify from? (if 'no')	Remarks
1	Front Suspension	Yes, McPherson	-	Small modifications
2	Rear Suspension	No	Double Wishbone	Major modifications
3	Steering System	Yes, rack and pinion	-	Change properties
4	Chassis	Yes, rigid chassis	-	Change properties
5	Tyres	Yes, tyres	-	Change properties
6	Antiroll Bars	Yes, antiroll bars	-	Small modifications
7	Engine	Yes, powertrain	-	Change properties
8	Braking System	Yes, Brakes	-	Not required

Table 6.1: Details of Subsystem and Planning Activities

'he modelling of each subsystem is presented in the following sub-sections. The detailed vork such as changing hard points, creating parts, mounts, etc. can be found in the ιDAMS/car help file (ADAMS, 2005). Only the modelling techniques with explanations are lustrated in the following sub-sections. For effective explanations, the diagrams of original ·mplates and the modified templates are illustrated side by side for most cases.

6.4.1. Front Suspension Subsystem

The front suspension of the Jaguar car was of the McPherson type. The details of the suspensions are given in Appendix 3(a) as provided by the manufacturer. Since this type of suspension is very common, ADAMS/car software has the template of the suspension available. Due to this availability, the main tasks of creating the front suspension subsystem were only to change properties of parts and the geometries of hard points. The graphical representations were improved by changing the dimensions of parts; e.g. the diameters of bushings, springs and dampers were enlarged. The orientations of some bushings were also changed depending on their specified properties, and only a small modification was made to the template. A part that represented the lower strut with a specified mass was added to the new subsystem for detailed analysis. The differences between the original template and the new modified template are illustrated in Figure 6.1.

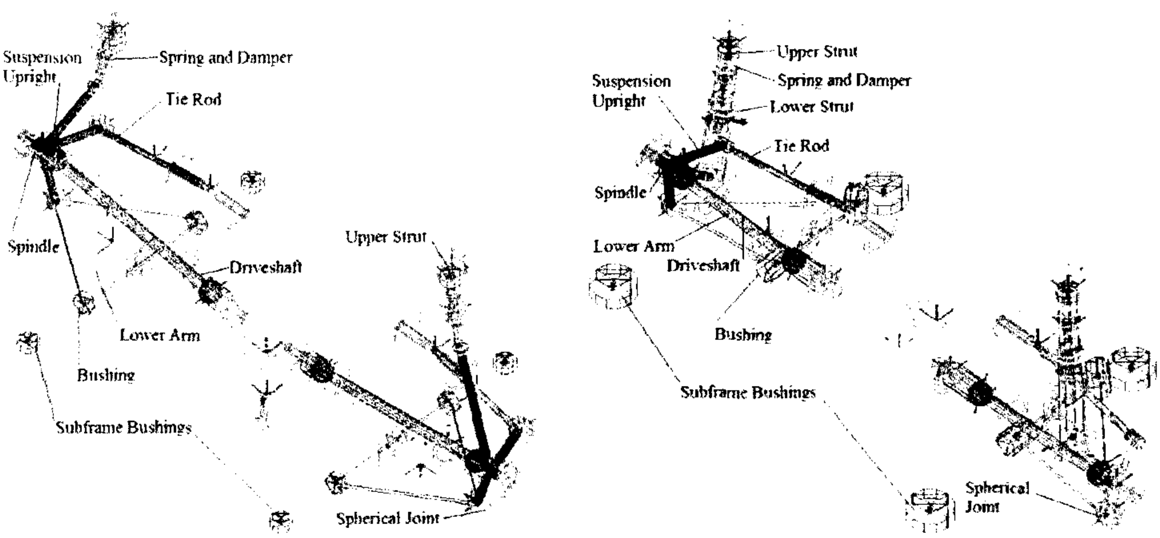

i) Original template ii) Modified template

Figure 6.1: McPherson Templates

6.4.2. Rear Suspension Subsystem

The rear suspension of the Jaguar car was of the short-long arm (SLA) trailing arm type suspension. Details of this suspension are given in Appendix 3(b). This type of suspension is not very common and it was specifically designed by the Jaguar Company. The choice of which available template in ADAMS/car subsystem to modify from depends on the least amount of required additional work. Creating a completely new suspension system was not recommended due to the extra time required. Some templates possess parameterization variables which are difficult to understand but are crucial for the functionality of the templates. For example, the driveshaft was parameterized to be either active or inactive depending on the users' choice.

Among the available templates relevant to the research are the Trailing Arm and Double Wishbone suspensions. The trailing arm suspension template has the trailing arm part but most of the other parts are either different or not available. On the other hand, the Double Wishbone suspension templates do not have the trailing arms but do have most of the other parts such as the upper and lower control arms, and require only minor modification. For these reasons, the Double Wishbone suspension template was selected for modification, and the original and modified templates are shown in Figure 6.2.

The spindle was modified to replace the suspension upright to which the control arms, driveshaft and trailing arms are attached. The lower control arm suspension was modified to form the front lower control arm of the SLA suspension. An additional part (the rear lower control arm) was added to the modified template. The upper control arm of the Double Wishbone suspension with two bushings was modified to become the upper control arm of the SLA suspension with a single bushing. The hard points for the spring were attached to the rear lower control arm while the hard points for the damper were connected to the spindle. The driveshaft was deactivated and was treated as the rear axle in the simulation. New mount locations were created in order to attach the suspension to other parts such as the chassis, sub-frames and wheels.

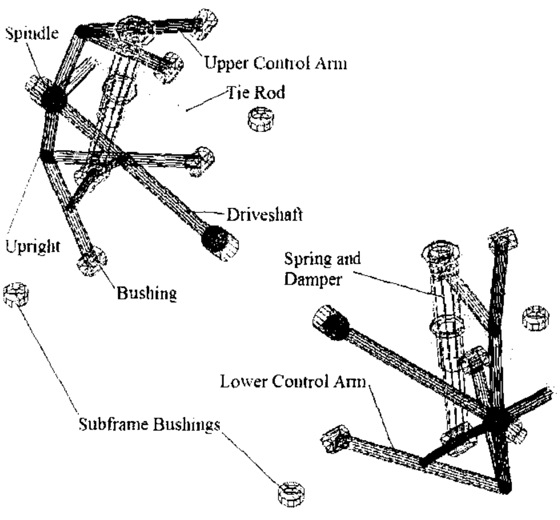

i) Original template

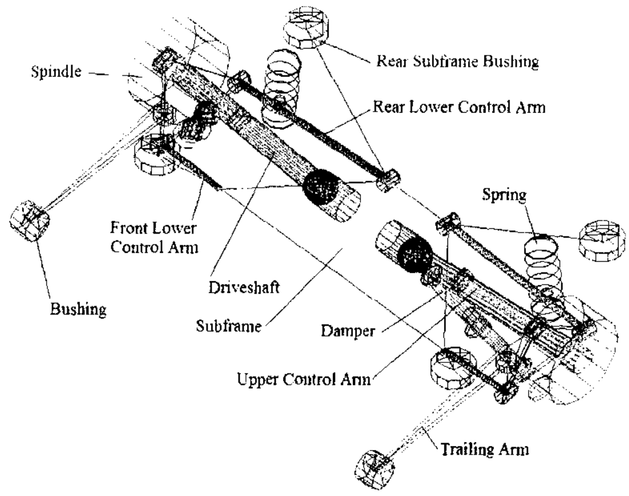

ii) Modified template

Figure 6.2: Rear Suspension Subsystem Templates

6.4.3. Rack-and-Pinion Steering Subsystem

The main changes made to the original template for the rack-and-pinion steering subsystem were the location of the torsion bushing and the method of power assistance. In the original template, the torsion bushing was a connector between the pinion and the steering shaft. A torsion bar was installed in the steering column to serve this purpose for the Jaguar steering system.

The modification to the original template to change the location of the torsion bushing was completed by deleting the bushing and applying a lock between the steering shaft and the pinion. The steering column was divided into two equal sections, viz. upper and lower part, joined by a revolute joint to allow relative displacement. A torsion bushing with a specified stiffness in the twist direction was attached to the revolute joint. In the original template, the steering power assistance was input by applying a vector force acting on the rack. The power assistance for the new template was created by applying a torque which acted on the steering shaft. Both techniques served the same purposes but the latter was found to be useful when the system was changed to electrical power-assisted steering.

The data for the rack and pinion steering system used for this research is shown in Appendix 3(c). Hydraulic power assisted steering was implemented on the steering system with the power boost characteristics as provided by the manufacturer are shown in Appendix 3(d).

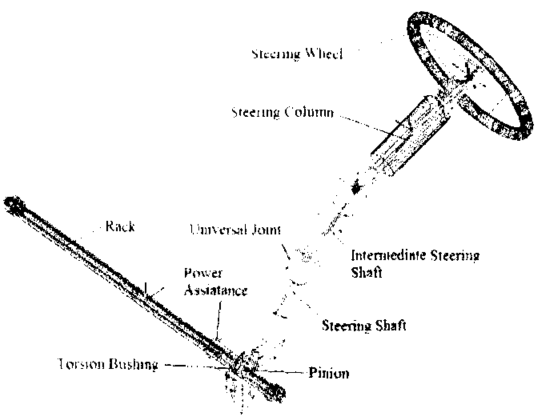

i) Original template

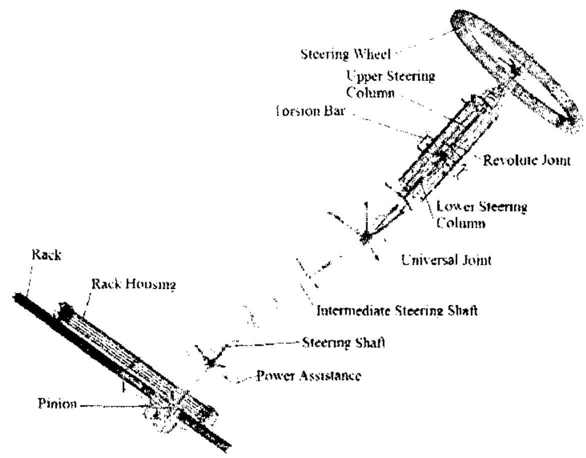

ii) Modified template

Figure 6.3: Rear Suspension Subsystem Templates

6.4.4. Rigid Chassis and Wheel Subsystems

No major modification was required for the rigid chassis and tyre subsystem templates, only differences in properties and geometries. The representation of the body shell and wheels of the templates were only for graphical purposes and did not contribute to any of the results from the simulation. The properties for the rigid chassis and wheel subsystems are in Appendix 3(e) and 3(f).

For the rigid chassis template, the aggregate mass was the vehicle sprung mass not including the driver. It was represented as a point mass with moments of inertia about the 3 orthogonal axes. The chassis was assumed to behave as a rigid body. For the wheel subsystem templates, the type properties were defined using 'Magic Formula 2002' (ADAMS, 2005). This enabled the computation of the reaction forces and moments between the wheels and the ground; non-combined slip analysis was used.

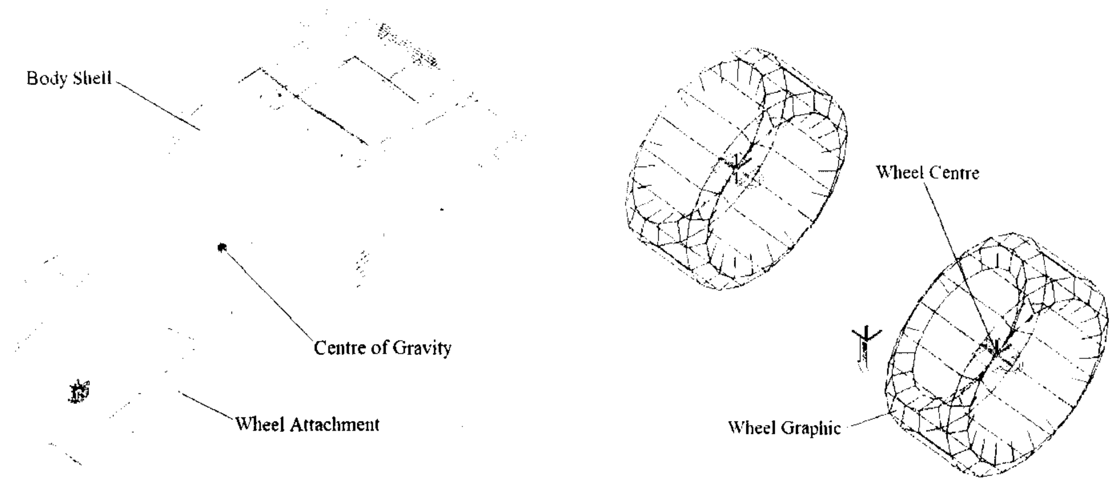

i) Rigid Chassis template ii) Wheels template

Figure 6.4: Rigid Chassis and Wheel Subsystem Templates

6.4.5. Anti-roll Bar Subsystem

For reasons of simplicity, the anti-roll bar was modelled with linear characteristics in the original template (refer to Appendix 3(g) for details). The linear analysis assumed that the anti-roll bar possessed a specific stiffness where the torsion torque varied linearly with twist angle. The anti-roll bar was split into two portions connected by a revolute joint with a specific torsional stiffness. For the Jaguar model, the anti-roll bar was attached to the suspension linkages, and was supported by two bushings attached to the subframe. A non-linear model of the anti-roll bar could be modelled using ADAMS flex but the process would involve more memory in computation, and was not pursued for this reason.

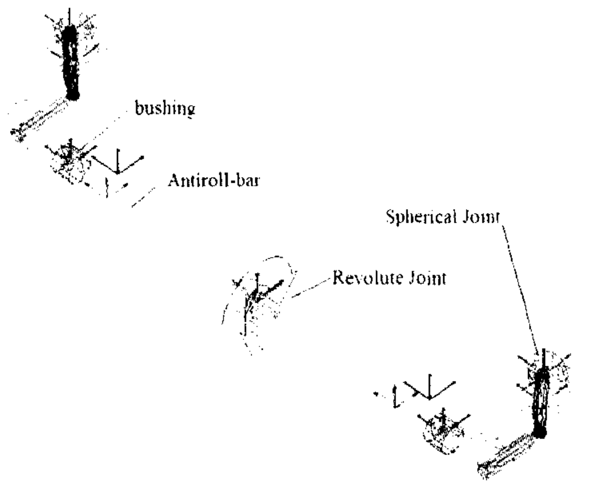

i) Original anti-roll bar template

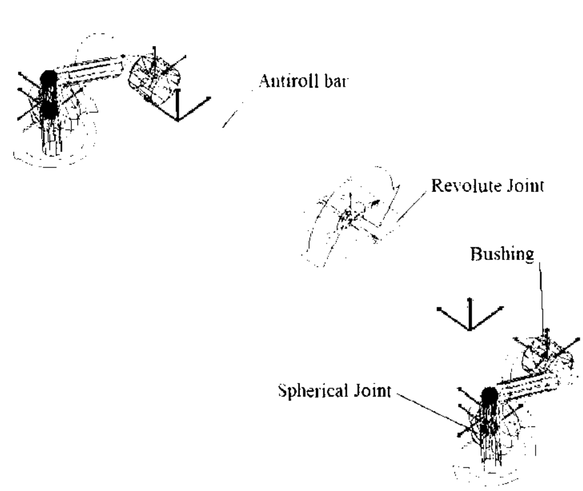

ii) Modified anti-roll bar template

Figure 6.5: Anti-roll Bar Templates

6.4.6. Power-train Subsystem

Property values in the engine model template were set to model the Jaguar, other changes made to the template included reorienting the engine graphics, relocating the engine mounts and adding a roll-restrictor. The engine graphics were reoriented because the original template was intended for an 'inline' engine layout; the Jaguar was 'transverse'. In order to prevent the engine from rolling, a roll restrictor was attached to the engine and the chassis, as specified by the manufacturer. Refer to Appendix 3(h) for the power-train data.

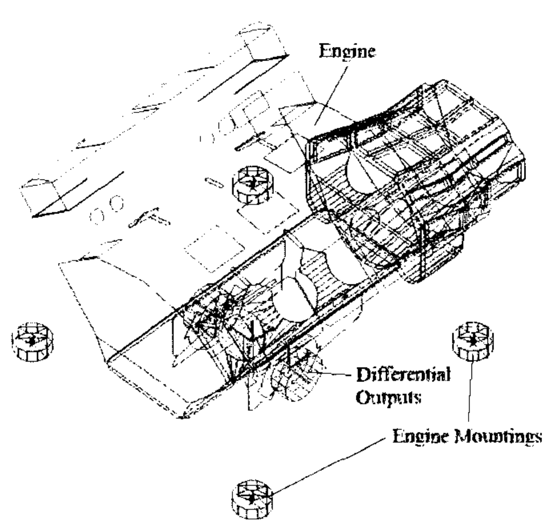

i) Original Powertrain Template

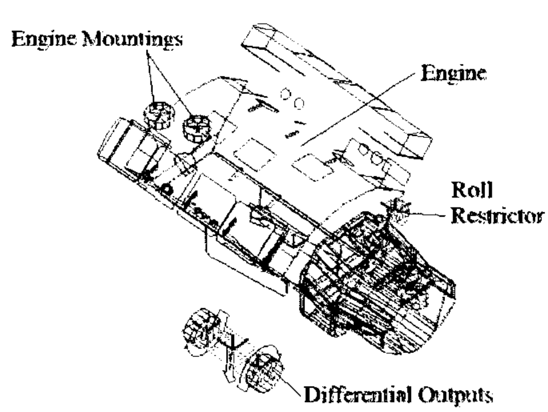

ii) Modified Powertain Template

Figure 6.6: Engine Templates

6.4.7. Brakes Subsystem

The brakes subsystem was not included in the full vehicle software model because the field of work in this research only involved vehicle steering analysis.

6.5. Creating an Assembly Vehicle

After all the required subsystems were created, they were combined into a full vehicle assembly, representing a collection of subsystems and a test jig which could be analyzed using ADAMS/Solver software. In ADAMS/car, the subsystems are assembled based on user specified 'communicators', which are the key elements in template-based products that enable the exchange of information between subsystems, templates, and the test rig. The full software model vehicle assembly for the Jaguar car is shown in Figure 6.7.

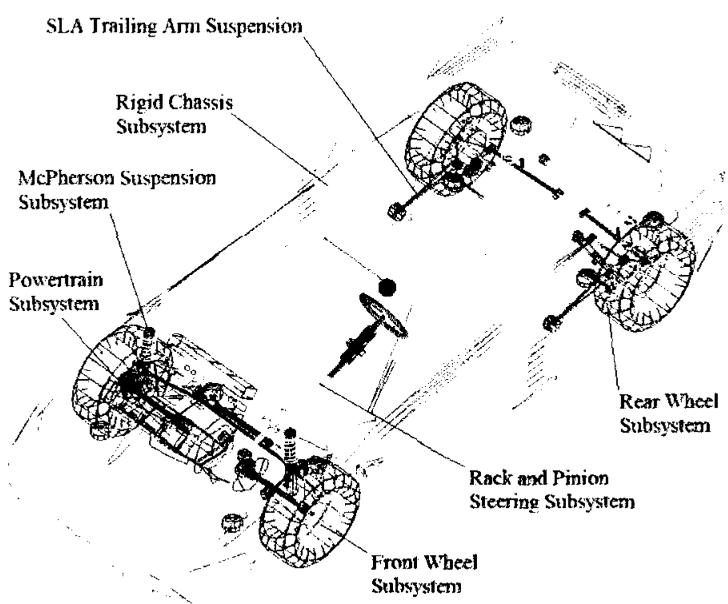

Figure 6.7: Full Vehicle Software Model Created in ADAMS/car

6.6. Development of Full Vehicle Software Model for Semi-Active Steering

In order to implement semi-active steering system on the full vehicle software model, some modifications were made to the rack and pinion steering template. The main modifications were to replace the rigid shaft with the LSRS, remove the torsion shaft attached to the steering column and create gearing systems for the motors. The developments of the software model are illustrated based on the original and modified templates. The original template in this case was the template that was modified in section 6.3.3 for the steering system of the full vehicle software conventional vehicle.

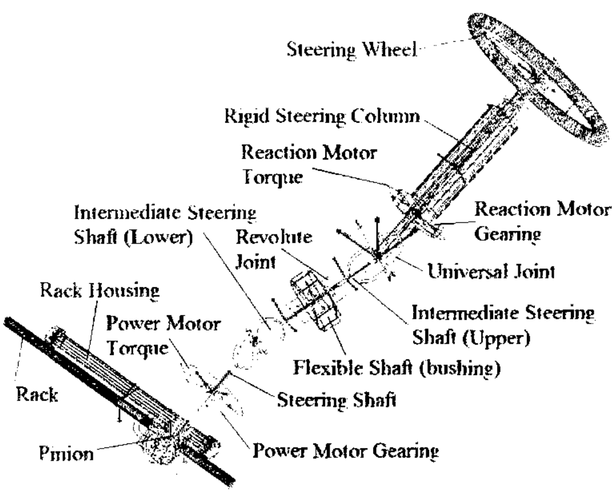

Figure 6.8: Steering System Templates

In order to replace the rigid steering shaft with a flexible shaft, the intermediate steering shaft was divided into two equal sections, namely the upper and the lower part, and the two pieces were joined by a revolute joint to allow relative displacement. A torsion bushing which represented the LSRS was attached to the location of the revolute joint.

The semi-active steering system did not require a torsion bar, so it was deleted on the original template. The upper and the lower steering column were also deleted and a single rigid steering column was created. A marker was created at the bottom portion of the steering column and a reaction motor gear was created on the marker. The gearing systems were created for graphics purposes only as they did not contribute any effect to the simulation results. The torque provided by the reaction motor was applied at the reaction gear marker while the torque supplied by the power motor replaced the existing torque by hydraulic power-assistance.

After modifying the steering system template to cater for the implementation of the SAS, the full vehicle software model assembly was ready to be assembled. The next steps were to fit control algorithms to the model along with power assistance systems. The full vehicle ADAMS/car model needed for the implementation of SAS system is shown in Figure 6.9.

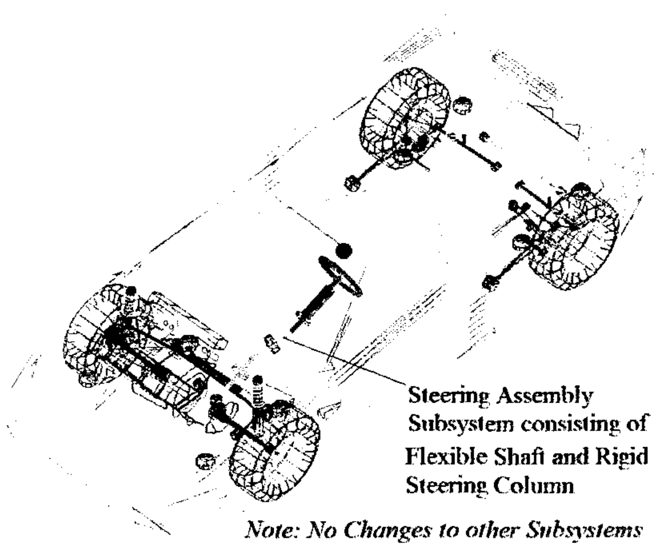

Figure 6.9: Full Vehicle ADAMS/car Model for SAS Simulation

6.7. Modelling the Characteristics of Power Assistance

The initial design stage of the SAS control system began with the development and optimisation of power-assisted steering and then active-steering was introduced through the use of a flexible resilient shaft. As discussed in Chapter 5, an ideal power boost characteristic for a hydraulic power assisted steering system (Figure 5.7) was selected, and its characteristics were converted to be implemented on electrical power-assisted steering. From the literatures studied, the characteristics of the power boost characteristic curve were not defined; e.g. the horizontal distance between each curve at a single speed was not specified.

For the best performance of power assistance system, the curves for power boost characteristics had to be mathematically modelled in order to perform design optimisation. The original curve shown in Figure 5.7 was redrawn to represent its details and characteristics, as shown in Figure 6.10.

Based on Figure 6.10, the slopes of the characteristics curve were the same for any vehicle speed. However, the distance between each curve was sequentially spaced from one another. The choice of selecting the distance between each curve depends on the designers themselves, because the research area is new and little is known about the advantages of having specific sequences. For this research, it was proposed that the distance between each curve should increase linearly as shown in Figure 6.10. Instead of using the summation of an arithmetic term, other alternatives were logarithmic or exponential functions. The choice of functions was expected to affect the characteristics of steering feel; and so this behaviour would be investigated in the future. It was also desired to have the steering feel to behave under specific characteristics with vehicle speeds.

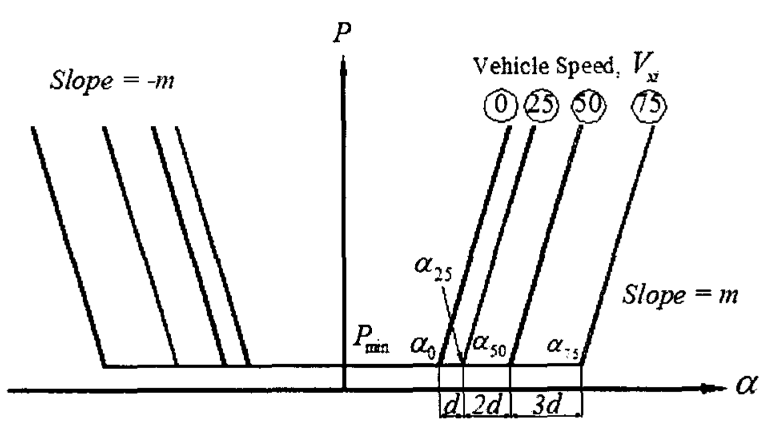

Figure 6.10: Mathematical Representation of Boost Curve in Electrical Power Steering

A mathematical formula is required in order to predict α_i at a given speed, V_{xi}. Two transformations were required for this derivation. First, the relationship between the speed and the index of counting n must be made linear, so that given a speed V_{xi}, the linear value of n could be calculated. Then the linear value of n was transformed to obtain the actual value of α_i. The linear relationship was derived from the following figures:

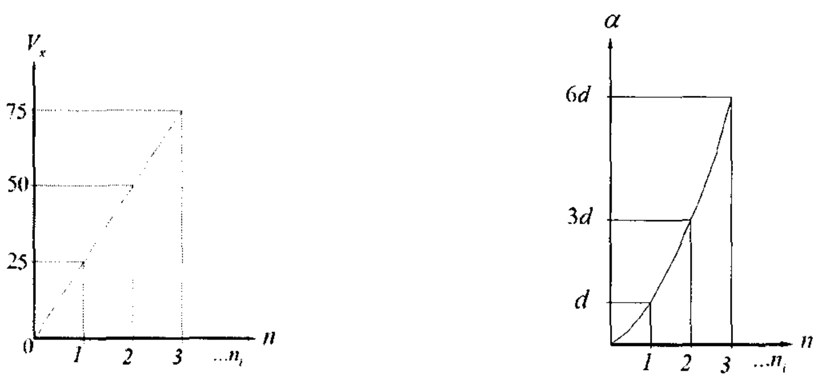

a) Calculate n at a specified value of V_x b) Compute α at calculated n

Figure 6.11: Representation of Transformations

From Figure 6.11(a): $V_x = 25n \qquad \Rightarrow n_i = \dfrac{V_{xi}}{25}$ (6.1)

It can be noted that $n_0 = 0, n_{25} = 1, n_{50} = 2, n_{75} = 3, \ldots$

The corresponding sequence can be represented as an arithmetic summation series below:

$$\alpha_i = \frac{n_i(n_i+1)d}{2} \qquad \Rightarrow \alpha_i = \frac{1}{2}\left(\frac{V_{xi}}{25}\right)\left(\frac{V_{xi}}{25}+1\right)d + \alpha_0 \tag{6.2}$$

at $\alpha = \alpha_i$, the corresponding pressure is , $P = P_{\min}$, therefore the linear equation passing through these points can be represented by:

$P - P_{\min} = \pm m(\alpha \mp \alpha_i)$; $\qquad \Rightarrow P = m\alpha + C$ {right side}; $\Rightarrow P = -m\alpha + C$ {left side}

where $C = P_{\min} - m\alpha_i$

The graphical representation of the previous derivations is presented in Figure 6.12.

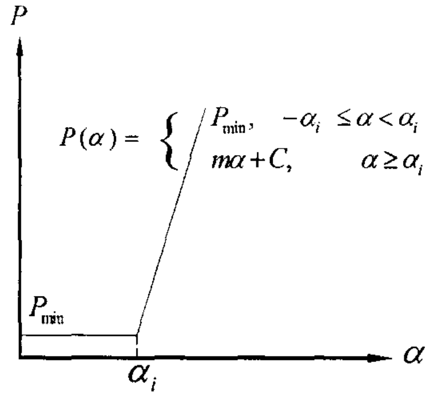

Figure 6.12: Mathematical Representation of the Boost Curve

The formula relating the deflection angle to the boost pressure which was previously derived can be programmed in a programmable motor. The operation of motors would be expected to be efficient due to the linearity of the boost curves.

6.8. Modelling Electrical Power Assisted Steering

When the characteristics of power assistance were defined, the next task was to implement the system for the modelling of electrical power assisted steering. The schematic diagram of the selected system from Figure 5.8(a) and its corresponding control block diagram from Figure 5.9(a) were reproduced and presented side by side (Figure 6.13) for better illustration.

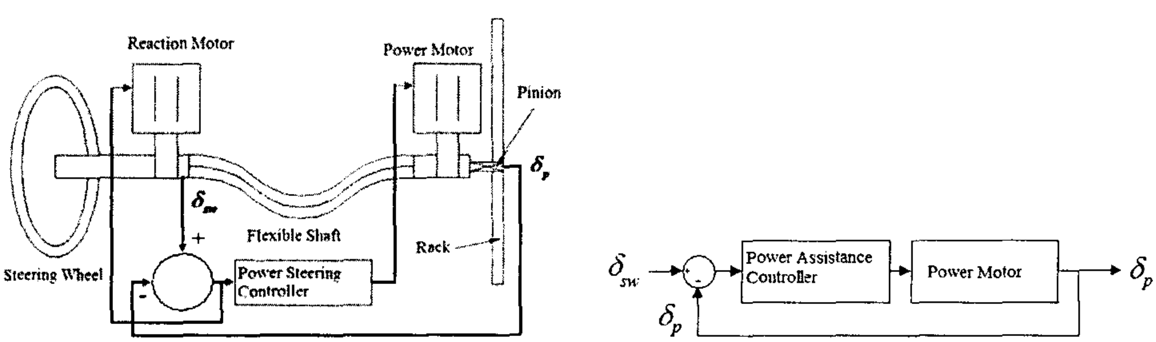

Figure 6.13: Schematic and Control Block Diagrams of Electrical Power Steering

For effectiveness and simplicity of modelling control in ADAMS/car, all the tasks were performed within the steering system template. When modelling control within such a template, ADAMS/control aspects were not required and information could be passed through local variables.

The signals of the steering wheel angles and pinion rotational angles were obtained by creating state variables. Two markers were created on the same location; one on the part and the other one on the ground. The command 'AZ' computed the displacement of angle in the z-direction from the part marker to the ground marker using the form, AZ (part marker, ground marker). The state variable for vehicle longitudinal speed was created by using the command 'VX' which measured the longitudinal speed of a marker on the steering mounted to the chassis with respect to the ground. The measurement has the form, -VX(part marker mounted to chassis, 0, part marker mounted to chassis, 0). The negative sign was used due to the axis orientation. After the state variables were created, they were referred as VARVAL(variable name), for example Steering Wheel Angle = VARVAL(δ_{sw}).

The torque representing the power motor was modelled by using a 'step function' to represent the power steering controller which provided the assistance based on power boost characteristic curves. For each unique curve which corresponded to a specific speed, the step function had the general form STEP($\alpha, \alpha_{0i}, \tau_{\min}, \alpha_{fi}, \tau_{\max}$). The graphical representation of the function is illustrated in Figure 6.14.

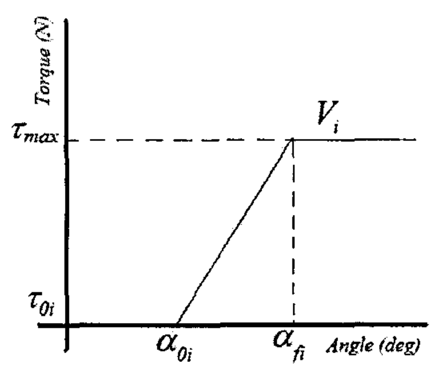

Figure 6.14: Step Function Representation in ADAMS/car

For ease of computation, it was assumed that the minimum torque τ_{0i} was approximately zero. The deflection angle α_{0i} represented the intercept along the horizontal axis and it was computed using equation (6.2). The deflection angle α_{fi} represented the minimum saturation value and was computed as $\alpha_{fi} = \frac{\tau_{\max}}{m} + \alpha_{0i}$. A condition was made such that if the deflection angle was greater than α_{fi}, the corresponding value of torque would be $\tau_{\max}$. In ADAMS/car, the command for the whole process was:

$$\mathrm{IF}\left(\alpha\text{-}\alpha_{fi} : \mathrm{STEP}\left(\alpha, \alpha_{0i}, \tau_{\min}, \alpha_{fi}, \tau_{\max}\right), \mathrm{STEP}\left(\alpha, \alpha_{0i}, \tau_{\min}, \alpha_{fi}, \tau_{\max}\right), \tau_{\max}\right)$$

It should be noted that for any speed, the solver would generate a specific curve and used the curve for interpolation.

The torque representing the reaction motor for steering feel was modelled using the common mathematical function,

$$\tau_{feel} = -K_f(\delta_{sw} - \delta_p) \tag{6.3}$$

The value of K_f was selected when vehicle speed was about 50 km/h. Upon completion of the power assisted steering modelling, the full vehicle software model was simulated for optimisation. The process involved trial-and-error tasks until an optimized power boost characteristics curve was obtained.

6.9. Modelling of Active-Steer

Once the optimisation of the power assisted steering had been performed, the next step was the extension of active-steering to the SAS. The active-steering technology was made possible through the use of a flexible resilient shaft. The schematic and the control block diagram are presented in Figure 6.15.

The term $\left(\frac{L}{L+KV_x^2}\right)$ can be regarded as the ratio between the desired and the actual steer angle defined by $\delta_c = R\delta_p$. If the following speed dependent understeer gradient is desired for a passenger vehicle:

30 km/h ← 50 km/h	← → 60 km/h	→ 80 km/h
($\delta_d = 1.33\delta_p$)		($\delta_d = 0.75\delta_p$)
Oversteer	Neutral Steer	Understeer

where $\delta_d \equiv$ desired pinion rotation and $\delta_p \equiv$ actual pinion rotation

when the vehicle speed is between 50 km/h to 60 km/h, the vehicle is required to be in neutral-steer gradient where there are no changes to the steering ratio. When vehicle speed exceeds 60 km/h, the vehicle is required to be in understeer gradient which ratio R decreases with increasing speed. It is expected that at vehicle speed $V_x = 60$ km/h, the ratio R=1 and at vehicle speed $V_x = 80$ km/h, the ratio R = 0.75. On the other hand, when vehicle speed drops below 50 km/h, the vehicle is required to be in oversteer gradient which ratio R increases with decreasing speed. It is expected that at a vehicle speed $V_x = 50$ km/h the ratio would be R = 1, and at a vehicle speed $V_x = 30$ km/h, the ratio would be R = 1.33. Based on the selected cases, the following relationships between the ratio R and vehicle forward speed could be obtained:

$$R = \frac{140 - V_x}{80} \textit{ (Understeer)}; \quad R = 1 \textit{ (Neutral Steer)}; \text{ and } R = \frac{110 - V_x}{60} \textit{ (Oversteer)} \qquad (6.6)$$

Besides providing some resistance at the steering wheel for steering feel, the reaction motor is also required to provide counter torque for steering comfort purposes. The presence of the flexible resilience shaft causes some disturbance to be felt at the steering wheel, and this is discussed next.

For ease of computation, it was assumed that the damping of LSRS is negligible and does not affect simulation results. During any condition, the reactive torque is given by

$$\tau_{feel} = -(K_f + K_{LSRS})\left(\delta_{sw} - \delta_{pm}\right) \tag{6.7}$$

It should be noted that the stiffness of the LSRS, K_{LSRS} was taken into consideration here for accuracy of results. This stiffness is much smaller than K_f and was neglected in the presentation of past formula. During active control, the disturbance torque is represented by

$$\tau_{disturbance} = (K_f + K_{LSRS})\left(1 - \frac{1}{R}\right)\delta_{pm} \tag{6.8}$$

Therefore, in order to eliminate the disturbance torque, the reaction motor should provide equal and opposite counter torque to the disturbance torque.

$$\tau_{counter} = -(K_f + K_{LSRS})\left(1 - \frac{1}{R}\right)\delta_{pm} \tag{6.9}$$

The total torque to be provided by the reaction motor is therefore

$$\tau_{rm} = -(K_f + K_{LSRS})\left(\delta_{sw} - \delta_{pm}\right) - (K_f + K_{LSRS})\left(1 - \frac{1}{R}\right)\delta_{pm} = -(K_f + K_{LSRS})\left(\delta_{sw} - \frac{1}{R}\delta_{pm}\right) \tag{6.10}$$

It can be noted from equations 6.8 and 6.9 that the amount of counter torque determines whether the reaction motor needs to increase or decrease its torque in order to maintain the steering feel. The decisions depend on the factor $\left(1 - \frac{1}{R}\right)$ which are illustrated below:

Understeer: $R < 1 \Rightarrow \left(1 - \frac{1}{R}\right) < 0$ (Decrease)

Neutral-steer: $R = 1 \Rightarrow \left(1 - \frac{1}{R}\right) = 0$ (None)

Oversteer: $R > 1 \Rightarrow \left(1 - \frac{1}{R}\right) > 0$ (Increase)

During understeer, the amount of torque to be provided by the reaction motor for steering feel is reduced due to the increase in steering ratio. On the other hand, the opposite will occur during oversteer, and no changes will occur during neutral-steer.

The modelling of control in ADAMS/car for active steer was adhered using the derived formula in this section and programming the formula to follow specified situations. Equation 6.10 was used to represent the torque provided by the reaction motor for steering feel. The 'IF' command, (similar to section 6.8) was used to assign the conditions stated in equations 6.6 based on vehicle forward speed. In ADAMS/car, the general format for the condition is

IF(*Conditions of vehicle speed: over-steer, neutral-steer, under-steer*)

6.10. Chapter Summary

Chapter 6 presents the full vehicle software modelling work complete with control algorithms using ADAMS/car. The main objective of developing a full vehicle software model complete with the control algorithms was to demonstrate the working concepts of the SAS system and to show how the system performance could meet the requirements of a robust steering system. The selected vehicle model for modelling work was the Jaguar car since a complete data set was available.

The ADAMS/car software was selected for simulation work because the software was a specialized environment for modelling real vehicles like physical prototypes to understand their performance and behaviour. The first approach was to plan activities by preparing a :able on subsystems and making a checklist on what were needed to be done and what were ılready available in the software in the forms of templates. The front suspension (McPherson) ınd anti-roll bars were created using available templates by changing properties with small nodifications. The rear suspension (SLA Trailing Arm) was created by modifying from a)ouble Wishbone Suspension with major modifications. The remaining subsystems such as ıe steering system, chassis, tyres and engine were created by changing properties of the riginal templates. The brake system was not included in the analysis. The steering system ır SAS model was modified for implementation of control using LSRS.

The modelling development of the SAS system was carried out in stages. The first stage was to model and optimize the power assistance system while the second stage was to add the control aspect to the system. The first step in modelling the power assistance system was to develop the power boost characteristic curve; i.e. conversion from HPAS to EPAS. The curve was mathematically modelled by assigning a variable for each parameter, viz. minimum saturation angle α_0, distance from the first and second curve *d,* and slope of the curve *m* for optimisation purposes. The distance between each two curves was modelled to increase like an arithmetic summation series. In order to predict the value of a deflection angle at a specified speed, the selected curve behaviour function (i.e. arithmetic summation series) was used.

The next task in modelling the power assistance system was to implement the power boost model on EPAS. The selected control block diagram was based on a PID controller. When the system received a signal, α representing the difference between the steering wheel angle and the pinion rotation angle, the controller then used the signal to compute the required power assistance, which task was performed by the power motor. The control activities in the vehicle model were performed within the steering system template where information could be passed through local variables. The computation of power boost curve by the controller was modelled using 'step' functions with programming conditions. The steering reactive torque or steering feel was modelled by multiplying a constant K_f with the signal α. The constant were determined by calibrating the EPAS with a conventional system at 50 km/h.

The second stage of the SAS system was to add active-steering technology to the EPAS system. The active-steering technology was made possible through the use of a flexible resilient shaft. In general, any control which could be implemented on SBW could also be performed on SAS system with some modification. A closed loop control was selected for this research by adding a transfer function to the feedback loop. The transfer function represented the ratio of the desired pinion rotation to the input steering wheel angle.

The selected control strategy was to vary the understeer gradient of a car depending on its forward speed. At low vehicle speed, the vehicle was required to be in oversteer for quick response during parking. At common driving speed, neutral steer was preferable. While at high speed, the vehicle was required to be understeer to eliminate driving sensitivity.

The presence of the flexible resilience shaft (LSRS) caused some disturbance to be felt at the steering wheel during control. Therefore, besides providing some resistance at the steering wheel for steering feel, the reaction motor was also required to provide counter torque to cancel out the disturbance forces. The total torque provided by the reaction motor was therefore the sum of the feel torque and the counter torque.

The control algorithms of all the strategies were programmed within ADAMS/car steering template. The driving conditions were distinguished using the condition 'IF' in order to implement the selected active control. The results are presented and discussed in Chapter 7.

Chapter 7

7. Results and Discussion on Simulation of Semi-Active Steering Models

This chapter presents and discusses the simulation results of the full vehicle software model presented in Chapter 6, by comparing the performance of the SAS system with the conventional system.

7.1. Validation of the Full Vehicle Software Model

Before the full vehicle software model developed in Chapter 6 could be used for simulation it needed to be validated by comparing the experimental results with the simulation results. However, before any such experimental work could be performed on the Jaguar, the car had to be returned to the company. An alternative validation method was sought and this was to use of the theoretical formula.

The mathematical formula and MATLAB/SIMULINK program for the cornering vehicle fitted with hydraulic power-assisted steering developed in Section 3.1.1 were used to validate the full vehicle software model presented in this section. In order to compare the two simulation results, a specific event of vehicle cornering was selected and illustrated in the following paragraph.

In the analysis of the specific event of vehicle cornering, the vehicle with hydraulic power steering was maintained with a constant speed of 100 km/h while the steering wheel was gradually turned to the left under specified conditions until the lateral acceleration of the vehicle reached 0.6 g. The main outputs for this analysis were the lateral acceleration, yaw velocity, roll angle, slip angle and lateral forces as functions of time. For both simulations, the input characteristics of the steering wheel angles were the same. The steering wheel angle characteristics used as input is shown in Figure 7.1.

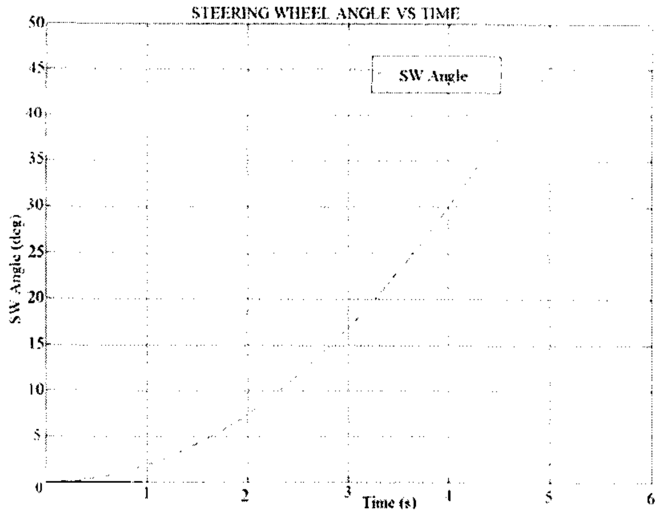

Figure 7.1: Steering Wheel Angle Characteristic Used for Input

7.1.1. Discussion of Results on Software Model Validation

The simulation results for the yaw velocity, angular acceleration and roll angle are shown in Figure 7.2(a)-(c).

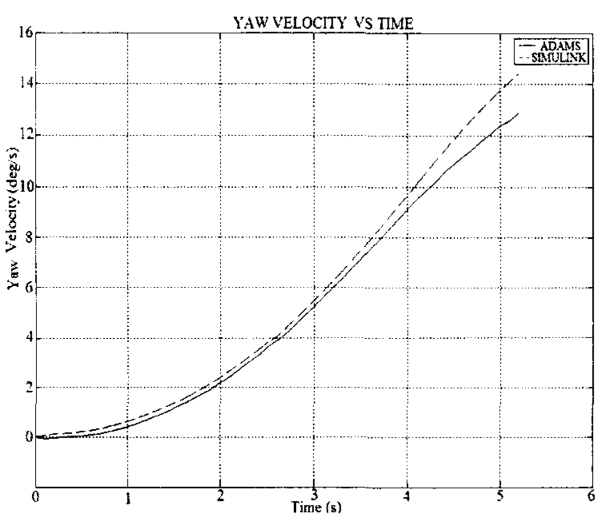

(a) Yaw Velocity

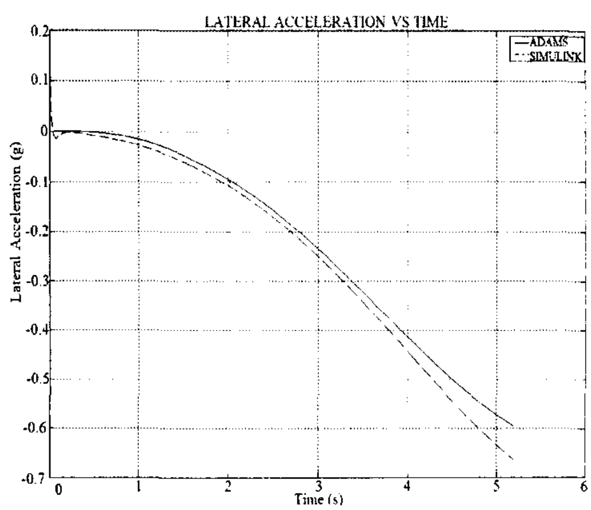

(b) Lateral Acceleration

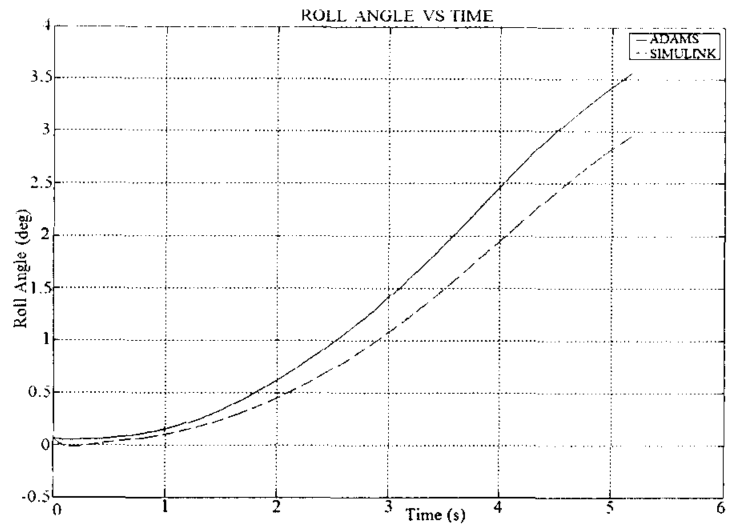

(c) Roll Angle

Figure 7.2: Comparisons of Yaw Velocity, Lateral Acceleration and Roll Angle

The MATLAB/SIMULINK results for the yaw velocity and angular acceleration agree overall with the ADAMS/car results. There are slight differences which occur towards the end of the simulation time. Although there are similar graphical trends, the roll angle predictions (Figure 7.2 (c)) vary by about 17% maximum.

The larger difference for the case of the roll angle may be due to the assumptions made in using equation 3.3 which assumed that lateral forces did not contribute any effect to the vehicle roll angle and the only contributions were from the sprung mass inertial forces and the stored energy from the suspension springs and dampers. The ADAMS/car simulation results are expected to be accurate since the software is capable of performing the calculation of the transfer of forces through suspension linkages, which also contributes to the vehicle body roll.

The comparisons for the output results of slip angle, lateral and longitudinal forces are shown in Figure 7.3(a)-(b).

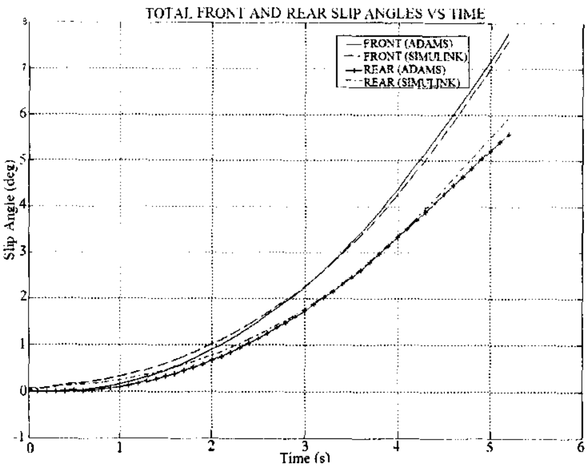

(a) Slip Angles

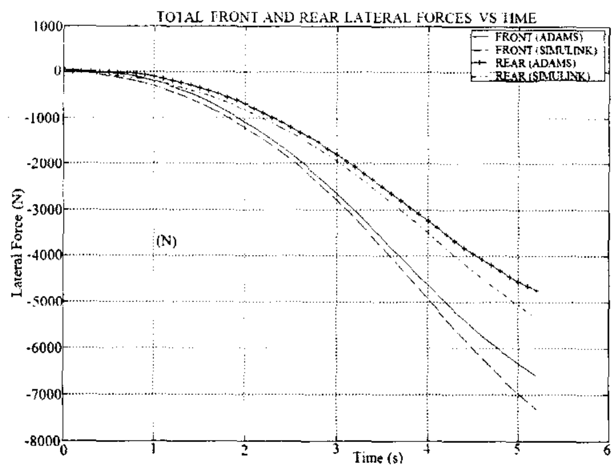

(b) Lateral Forces

Figure 7.3: Comparisons of Slip Angles, Lateral Forces and Longitudinal Forces

The slip angle results (Figure 7.3(a)) agree overall with the ADAMS/car results with minor differences, indicating that the small angle approximation ($\tan\alpha \approx \alpha$) yielded acceptable results for this analysis. Referring to the plots of lateral forces (Figure 7.3(b)), it can be observed that the MATLAB/SIMULINK calculated forces tend to differ from the ADAMS/car predicted results towards the end of the simulation time. Such behaviour is similar to the output results for the yaw velocity and angular acceleration.

The explanation to the variation of forces could be that the 'turn slip' or 'path curvature' has been neglected. The effect of turn slip takes into consideration the turning radius and the normalized change in vertical load, $df_z = \dfrac{F_z - F_{z0}}{F_{z0}}$. When the steering wheel is increasingly turned until vehicle acceleration reaches 0.6g, the front wheel steer angle increases and hence the turning radius decreases. Similarly, when a large change in vertical load occurs due to the load transfer, the normalized change in vertical load value could be very significant. The theoretical formula of 'turn slip' is discussed in (Pacejka, 2002). Although ADAMS takes 'turn slip' into consideration in computation, the sub-coefficients required to calculate the turn slip coefficients are not available in the tyre files used in this analysis.

The maximum deviation for the output of lateral forces occurred at the end of simulation time with the error found to be about 10%; which could be considered acceptable based on the previous explanations. It was expected that the magnitude of errors would improve if the 'turn slip' had been taken into consideration. The main concern was the results of the roll angle predictions where large errors were observed; an alternative for further improvement of the results is discussed in Section 7.1.2.

7.1.2. Improvement on Roll Angle Prediction

In order to improve the roll angle prediction results, the same MATLAB/SIMULINK program used in Section 7.1.1 was modified by replacing the roll angle formula represented by equation 3.1 with equation 3.24 (Section 3.1.2). The final results indicated that the outputs of yaw velocity, lateral acceleration and lateral forces have improved but did not show any significant changes as a result of replacing the roll angle formula. Hence, the results for such variables were not included for verification except for the case of roll angle prediction (Figure 7.4).

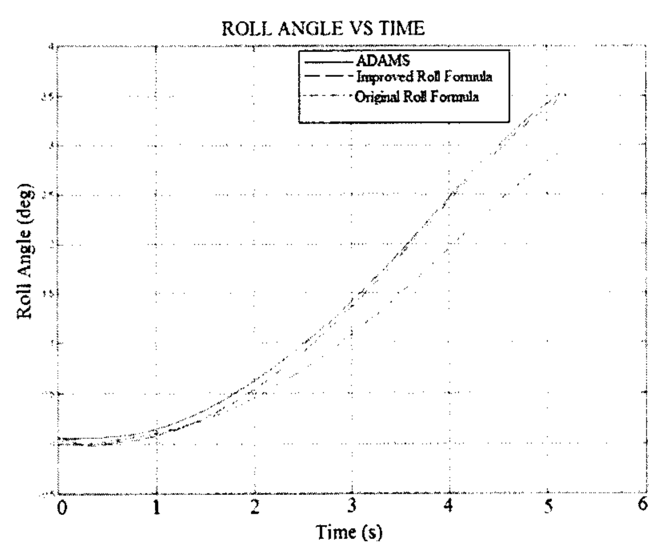

Figure 7.4: Improvement on Roll Angle Plots Comparisons

7.1.3. Discussion and Conclusion for the Validation of Full Vehicle Software Model

From Figure 7.4, it can be observed that the ADAMS simulation results are in close agreement with the MATLAB/SIMULINK program computational results using the improved roll angle prediction formula.

It was concluded that the full vehicle software model created using ADAMS/car was validated using the MATLAB/SIMULINK model. The model was therefore used to represent the Jaguar car.

7.2. Selection of parameters for Power Assistance Characteristic Curves

This section illustrates the selection of power assistance characteristics by finding suitable parameters to be used for power boost curves. The computations were performed by simulating a full conventional vehicle software model fitted with hydraulic power assisted-steering developed in ADAMS/car. The selections of parameters were based on those that could produce optimum or suitable results for intended applications. A specific event was selected for all the analyses and the results are plotted. The main variables for analysis are the steering wheel and power-assisted steering torques.

7.2.1. Parameters for Optimizations

The first task that had to be done prior to simulating the model was to determine the required parameters for optimisation. In this case, the power boost characteristic which was illustrated in Figure 6.10 is required. Due to its frequent reference, Figure 6.10 is shown again in this Section as Figure 7.5.

7.2.2. Results and Discussion on Selections of Parameters

The selected event for most of the analysis was a vehicle cornering course with the steering wheel angle characteristic as shown in Figure 7.6. In this case, a vehicle started from a straight line and began cornering after 1 second from a straight ahead position to 90^0 steering wheel angles. The cornering process took 5 seconds to complete, at a forward speed of 50 km/h. This vehicle forward speed was selected because the speed represented a common driving limit for most countries. The starting estimate guess for the value of *d* was 0.125^0 which was within the range of the original data supplied by the manufacturer. In the iteration process, the value of α_0 started from 0.2^0 which was also within the range of the original supplied data. Its incremental value was 0.15^0.

The output results from the simulation were the power assisted torque and steering wheel torque which were plotted versus time (Figure 7.7 and Figure 7.8).

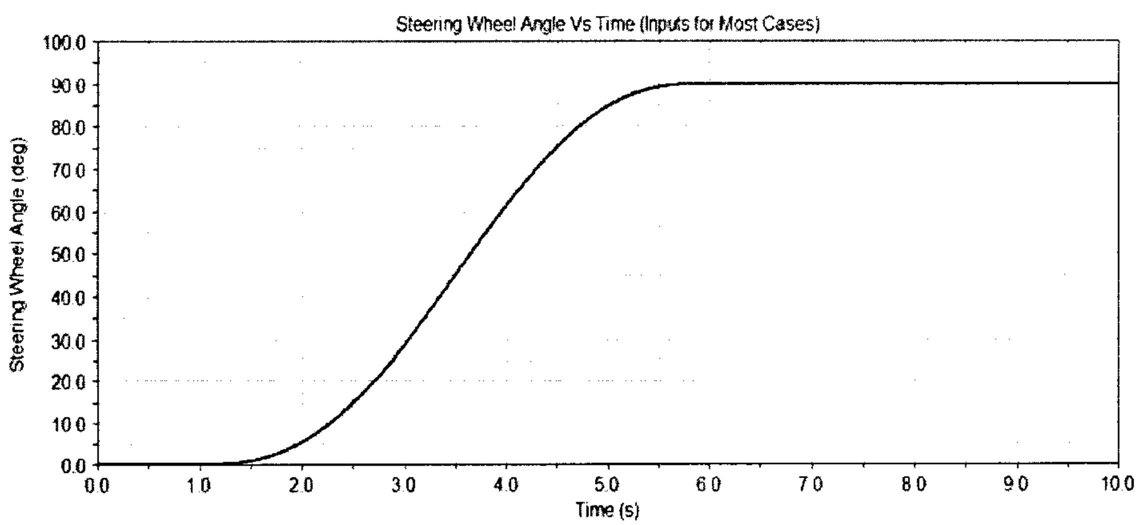

Figure 7.6: Characteristic of Steering Wheel Angle Used as Inputs for Most Analysis

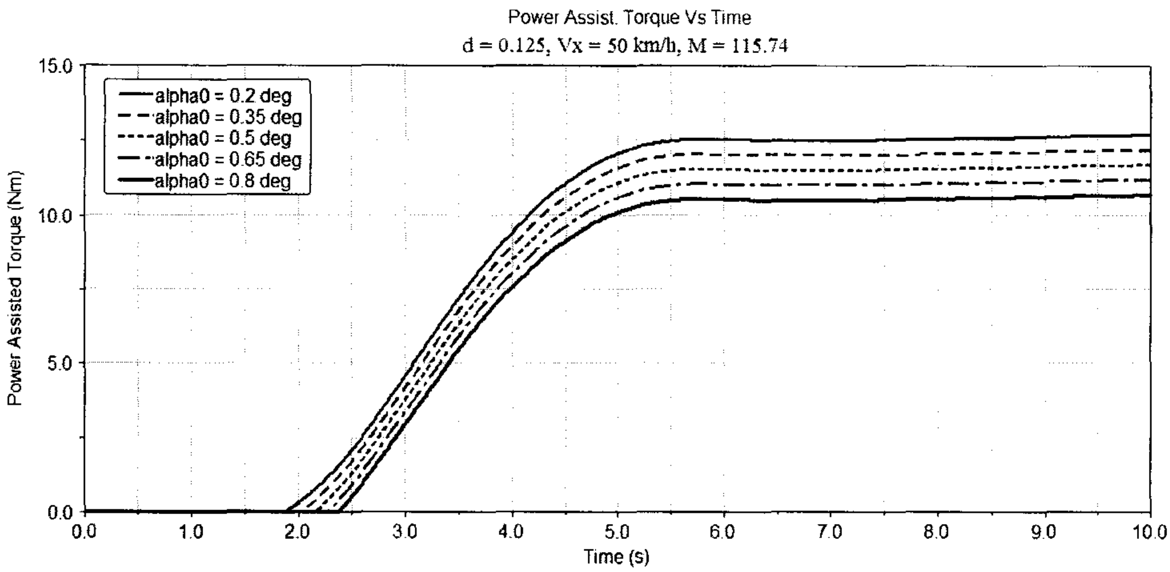

Figure 7.7: Characteristics of Power Assisted Torque under Variation of α_0

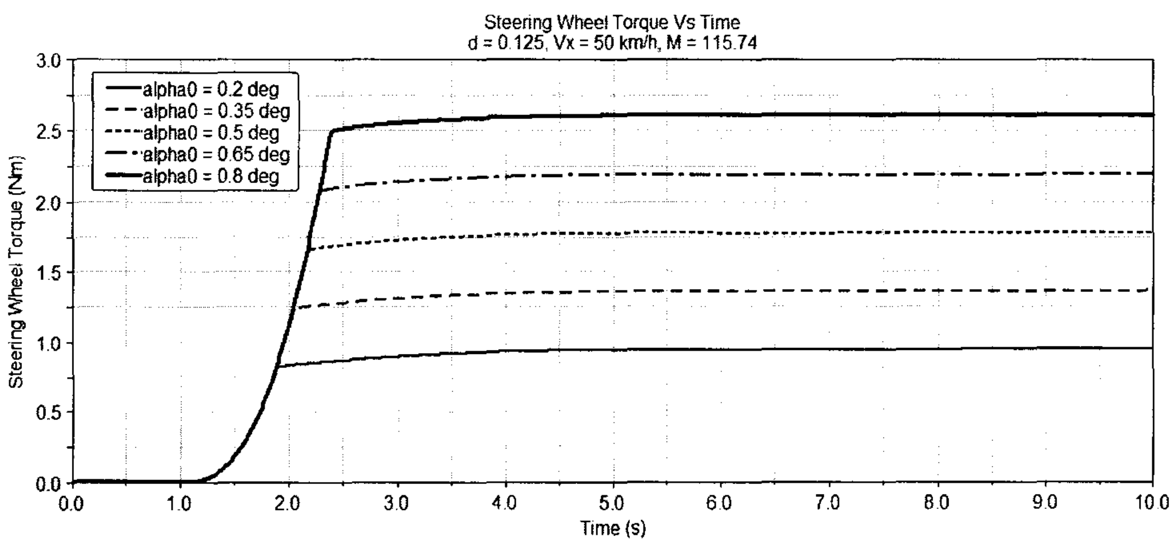

Figure 7.8: Characteristics of Steering Wheel Torque under Variation of α_0

Figure 7.7 indicates that as α_0 increases, the power-assisted steering torque decreases. On the other hand, the increase in α_0 causes the steering wheel torque to increase. This is expected because the total torque required to turn the front wheel assembly is equal to the sum of the power-assisted torque and steering wheel torque. The power-assisted torque was the energy provided by the machine while the steering wheel torque was the work done by the human driver.

In order to determine the trends of the increase and decrease of the steering wheel torque and steering wheel angle, graphs were drawn of a set of data during steady state conditions obtained at time, t = 7 seconds. The data was taken at the selected time because the steady state values were observed to have settled. The corresponding data at the specified time were then plotted against the corresponding values of the horizontal intercept of the initial curve, α_0. The summation of the steering wheel torque and the power-assisted steering torque was computed in order to determine whether the total torque required by the system is constant. The results for all the analyses are summarized in Figure 7.9(a)-(c).

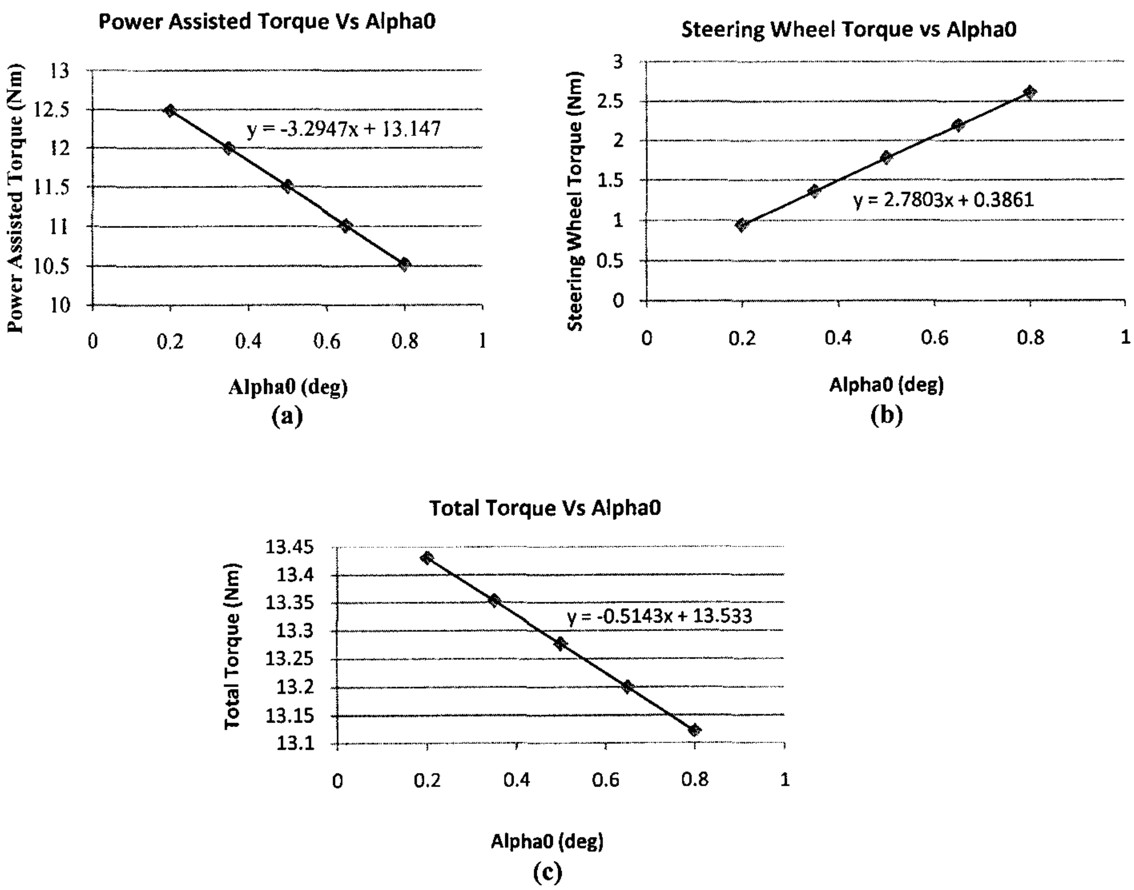

Figure 7.9: Analysis of Trends under Variation of α_0

From Figure 7.9(a)-(c), the power-assisted torque decreases linearly with α_0 while the steering wheel torque increases linearly with α_0. The total torque, which is the summation of power-assisted torque and steering wheel torque, was found to decrease with α_0. This result was very surprising because it was initially thought that the total torque must be constant as the required energy to turn the front wheels is conserved. Based on the finding, it can be said that the system is more efficient with the increase in α_0, or when the driver does more work. However, such a characteristic is not desired because it defeats the purpose of having power assisted steering. There is a possibility that the value of the slope m was not properly optimised which led to such characteristic. If the complete system was optimized, the plot in Figure 7.9(a) may approach to a zero-slope.

The current findings have still not provided sufficient information on the best selection of α_0. Yih (Yih, 2005) stated that the required steering wheel torque for normal driving should not be more that 2 Nm. Based on this information, it could be deduced from Figure 7.9 that the best value for α_0 was 0.5^0. This is because the corresponding steering wheel torque at $\alpha_0 = 0.5^0$ is less than but the closest to 2 Nm. The next parameter that needed to be determined was the value of d.

The simulation procedure and the analysis of results to determine the optimised value of d were performed in a similar way to the case of determining the value of α_0. The output results are presented in Figure 7.10 and Figure 7.11.

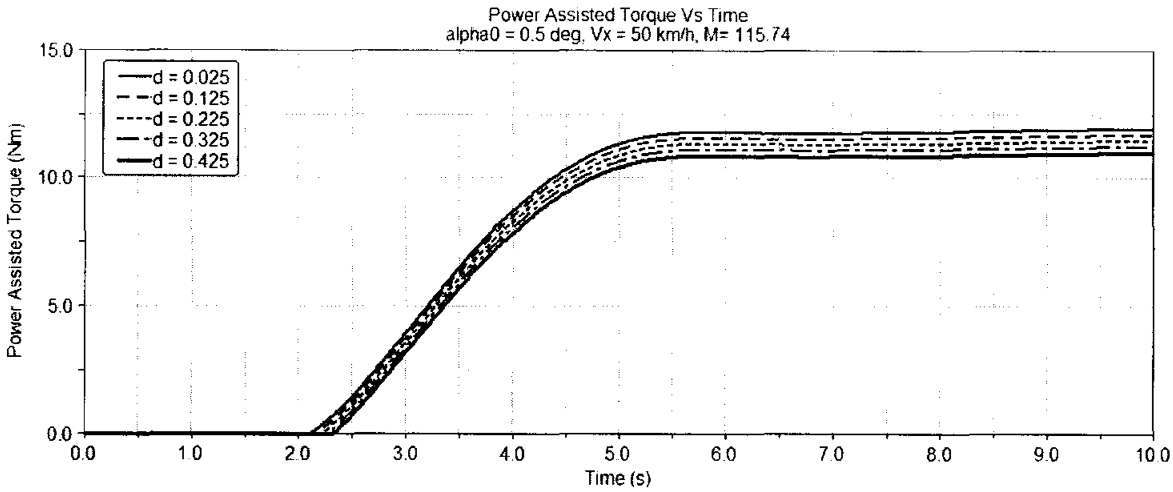

Figure 7.10: Characteristics of Power Assisted Torque under Variation of *d*

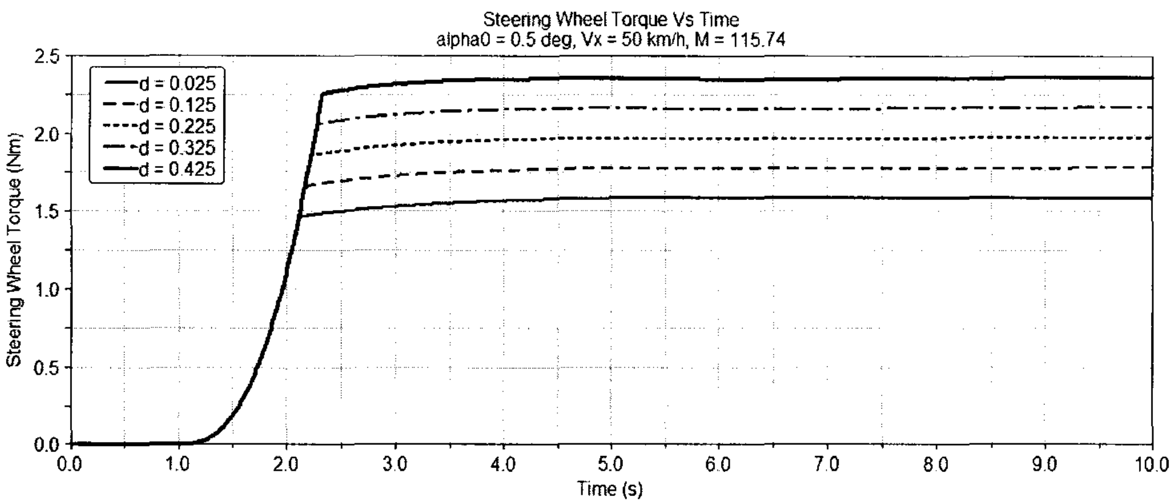

Figure 7.11: Characteristics of Steering Wheel Torque under Variation of *d*

From Figure Figure 7.10, the power-assisted torque decreases when the value of *d* increases. In contrast, the steering wheel torque increases when value of *d* increases as shown in Figure 7.11. The detailed plots are shown in Figure 7.12.

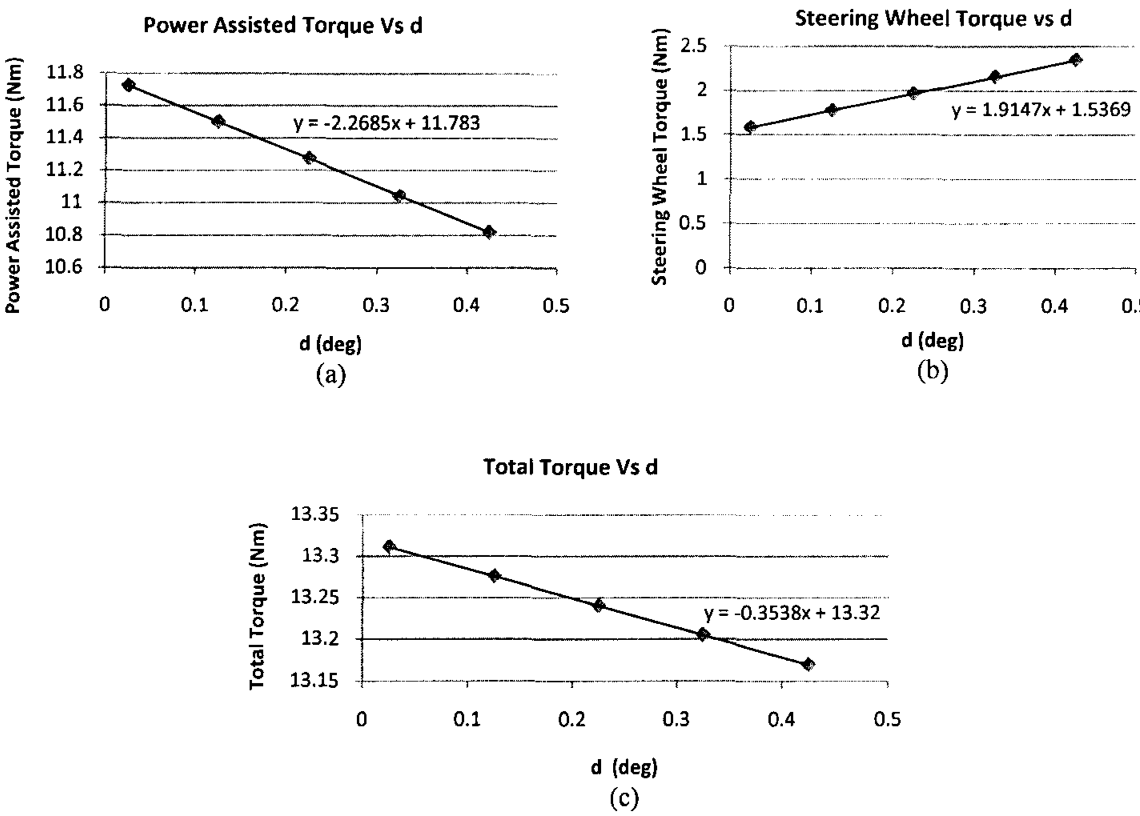

Figure 7.12: Analysis of Trends under Variation of *d*

From Figure 7.12, the power-assisted torque decreases linearly with *d* while the steering wheel torque increases linearly with *d*. The summation of the power assisted torque and the steering wheel torque decreases with *d*. The trends of characteristics of varying *d* and α_0 are found to be similar. The complete system may be optimized by iteration techniques with a constraint that the sum of power-assisted torque and steering wheel torque becomes a constant.

Similar to the earlier analysis, the suitable value of *d* can be determined based on the requirement of power-assisted torque during normal driving. From figure 7.19, the values of *d* which are close to 2 Nm are 0.225^0 and 0.125^0. When $d = 0.225^0$, the corresponding value of steering wheel torque is too close to 2 Nm. This is not very practical because when vehicle speed exceeds 50 km/h, the steering wheel torque can easily exceed 2 Nm and this would cause the vehicle steering to be too heavy. Therefore the most suitable value for d was found to be 0.125^0.

7.2.3. Conclusion on Selection of Parameters

Based on the previous analysis to determine suitable parameters for the optimisation of power boost characteristic curves, it was concluded that a suitable value for α_0 was 0.5^0 while the suitable value for d was 0.125^0. These values were used in all subsequent analyses.

The selected values were determined based on the required values of steering wheel torque during normal driving. The power-assisted torque was found to decrease linearly with both parameters while the steering wheel torque was observed to increase linearly with both parameters. For both cases, the sum of power-assisted torque and steering wheel torque was found to decrease with the increase in both α_0 and d. The complete system may be able to be optimized by considering the slope m as one of the parameters and adding a constraint that the sum of power-assisted torque and steering wheel torque should be constant.

7.3. Optimization and Performance of SAS Electrical Power-Assisted Steering (EPAS)

This section introduces the SAS system by firstly illustrating the differences between the conventional hydraulic power-assisted steering and SAS electrical power-assisted steering (EPAS). The technique and procedure for generating reactive torque for steering feel by calibrating the SAS EPAS properties to HPAS at vehicle speed of 50 km/h are discussed. The performance of SAS EPAS was evaluated based on its effectiveness in implementing reactive torque for steering feel and its capability of manipulating steering feel during emergency cases. The performance of SAS EPAS power-assisted torque was also compared to conventional HPAS system.

7.3.1. Main Differences between Conventional Hydraulic Power-Assisted Steering and SAS Electrical Power-Assisted Steering

Prior to introducing the SAS electrical power-assisted steering model, the differences between the SAS EPAS and the convectional power-assisted steering model were illustrated to give a clear view of the concepts. In general the main differences are:

i. The input to the conventional hydraulic power-assisted steering (HPAS) comes from the deflection of a torsion bar whereas the input to the SAS electrical power-assisted steering (EPAS) is the difference between the steering wheel angle and the rotation of the pinion angle.

ii. For the conventional HPAS, a driver needs to apply some torque to deflect a torsion bar and the same torque also contributes to a portion of work required to turn the front wheels. For SAS EPAS, the driver does not contribute any work to turn the front wheels. The EPAS system receives a signal from the difference of steering wheel angle and the pinion rotation angle, and then provides full power assistance to turn the front road wheels based on the input signal.

iii. For the conventional HPAS, the reactive torque or the steering feel can be felt by the driver through a torsion bar. The level of feel can be selected based on the stiffness of the torsion bar. For SAS EPAS, the driver will not have any steering feel because full power assistance is provided by the system. Therefore, the reactive torque is introduced to the system through an artificial means. When a driver turns the steering wheel, a reaction motor supplies opposite or resistive torque to the steering wheel motion for driver's steering feel. The steering feel can be adjusted by changing the properties of the reaction motor.

7.3.2. Reactive Torque for SAS Electrical Power Assisted Steering (EPAS)

The steering reactive torque for SAS EPAS was not the real steering feel but was artificially generated by the reaction motor in order to inform the driver about what is happening at the road wheels. In order to generate steering wheel torque based on general driving requirements, the intended values of steering wheel torque must be calibrated with the conventional HPAS at a certain common driving conditions. In this research, the calibration of SAS EPAS to HPAS was chosen at a vehicle speed of 50 km/h.

The reactive torque was represented by the formula $\tau_{feel} = -K_f(\delta_{sw} - \delta_p)$. The main task was to determine a suitable value of the constant K_f so that the reactive torque value of SAS EPAS was equal to the value of EPAS reactive torque at 50 km/h. The process was performed by simulating the software model of SAS EPAS and varying the values of K_f until the desired value was found. The final result is presented in Figure 7.13.

The torsion bar of the HPAS system has a stiffness of 120 Nm/rad and a damping of 0.2 Nm.s/rad. The calibrated value of K_f at 50 km/h was found to be 106 Nm/rad and this value was used by the full-vehicle software model to represent reactive torque for all applications.

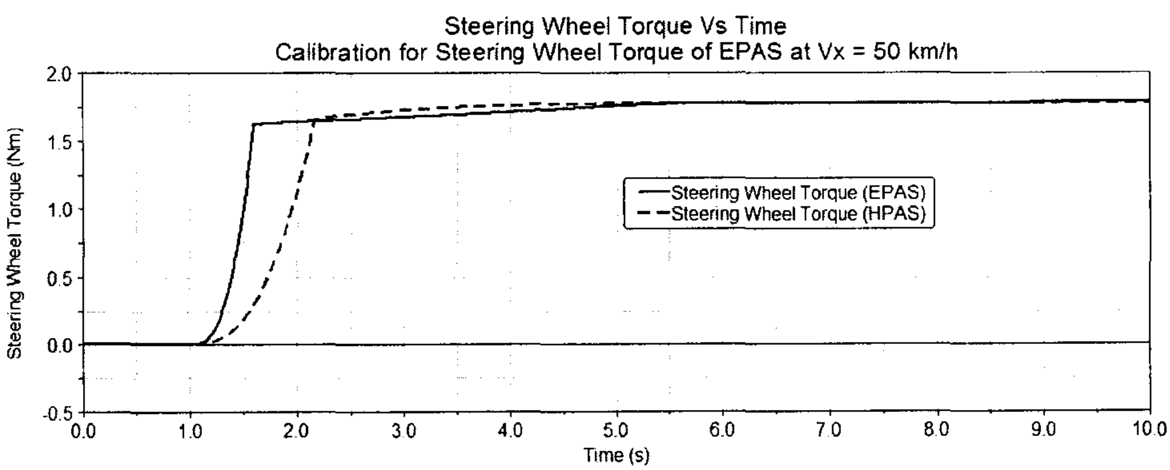

Figure 7.13: Reactive Torque Calibration for SAS Electrical Power Assisted Steering (EPAS)

It can be noted from Figure 7.13 that the steering wheel torque of the hydraulic power assisted steering lagged behind as compared to the steering wheel torque of the SAS EPAS. This was because when the torsion bar deflects during steering wheel turning, the steering wheel assembly also moves due to the developed torque and this causes the delay in reaching the steady state torsion bar deflection. When there is a difference in steering wheel and pinion rotation, the reaction motor immediately applies reactive torque and this causes an abrupt rise of the steady state torque.

7.3.3. Performance of SAS EPAS Power-Assisted Torque and Reactive Torque

The performance of SAS EPAS reactive torque based on the calibrated value found in section 7.3.2 was evaluated by comparing it to the reactive torque of HPAS. The comparisons were performed by comparing the simulation results of software models of the conventional HPAS and SAS EPAS. The software model of each system was simulated under several different speeds starting from 25 km/h until 75 km/h with an incremental value of 12.5 km/h. The output results for comparisons were the power-assisted torque and the steering wheel torque. The results of the power assisted torques are shown in Figure 7.14(a)-(b) and the results for the steering wheel torques are illustrated in Figure 7.15(a)-(b). The results for each criterion are discussed in sequence.

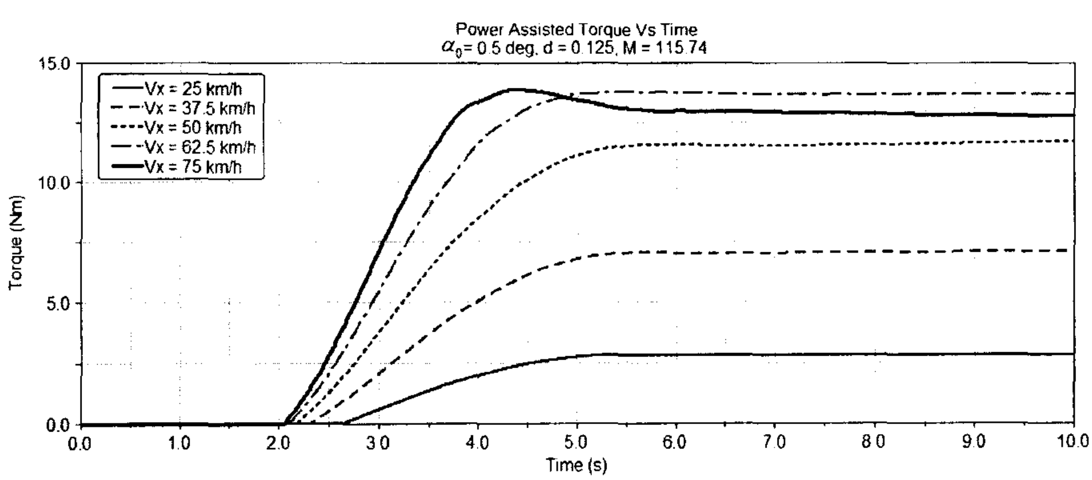

(a): Power-Assisted Torque For HPAS

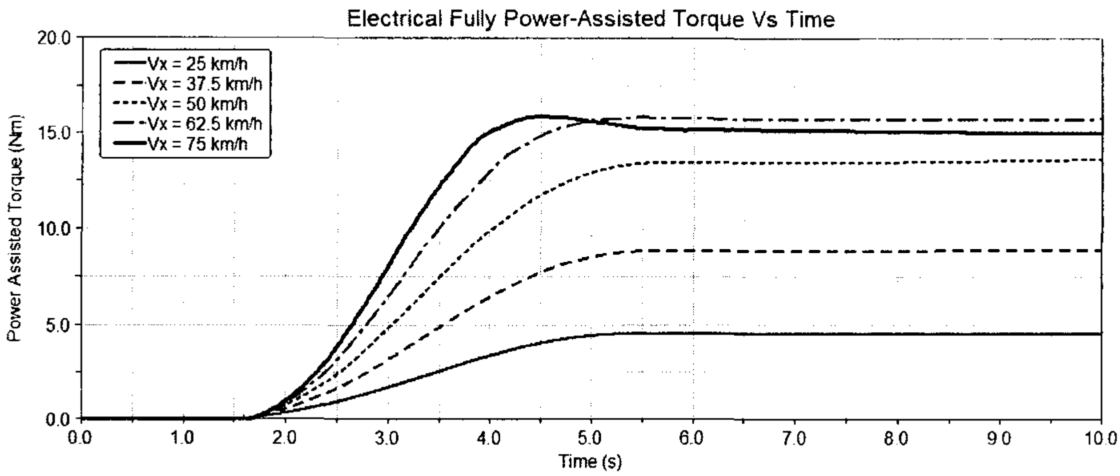

(b): Power-Assisted Torque for SAS EPAS

Figure 7.14: Comparisons for Power-Assisted Torques

It can be observed from Figure 7.14(a)-(b) that the activation of power assistance for HPAS of each case of vehicle speed occurs at a later time compared to the SAS EPAS system. As vehicle speed increases, the activation time for the power assistance decreases. On the other hand, the activation of power assistance of SAS EPAS occurs at the same time for all of the cases. The explanation of this phenomenon relate to the design of the power boost curve and the total torque of the HPAS system, which is the sum of its power-assisted torque and steering wheel torque. Based on the design of the power boost curve, power assistance for each of specific vehicle speed would only be activated after deflection angle exceeds a certain value. Prior to exceeding the specific deflection angle, the required torque to turn the front wheel was provided by the driver through the steering wheel torque. As previously discussed, it takes some time for the torsion bar to reach the required deflection for power assistance since the front road wheels also move during the time when the steering wheel is turned. However, as the vehicle speed increases, the self-aligning moment also increases. As a result, more resistance is generated at the road wheels to resist the steering wheel torque. Therefore, as the vehicle speed increases, the development of the required deflection angle for power activation must also increase.

Since both systems make use of the same power boost curve, the activation of power assistance for SAS EPAS system also occurs when the difference between steering wheel angle and pinion rotation angle exceeds a certain value. Before reaching the specified difference in angle, the steering wheel is being turned by the driver and the driver also feels the reactive torque at the steering wheel, but the front road wheels do not move. The time taken to reach the specified difference in angle for each vehicle speed is the same for all cases because all of them make use of the same steering wheel input.

In order to verify that the total torque which is required to turn the front road wheels is almost the same for both cases, the following analyses will make use of Figure 7.15(a)-(b) and Figure 7.16. The plots in Figure 7.15(a)-(b) illustrates the comparisons of the torque provided by SAS EPAS and HPAS in order to turn the front road wheels. The plot in Figure 7.16 shows the corresponding angular velocity versus time as a result of power-assistance provided by both systems.

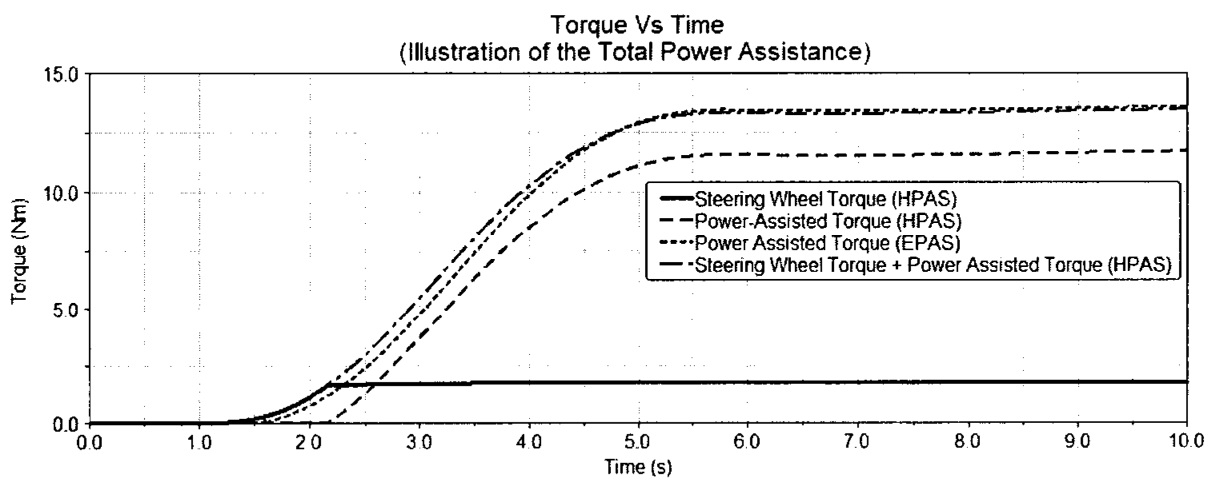

a) Comparison of Total Torque Required to Turn Front Road Wheels at Vx = 50 km/h

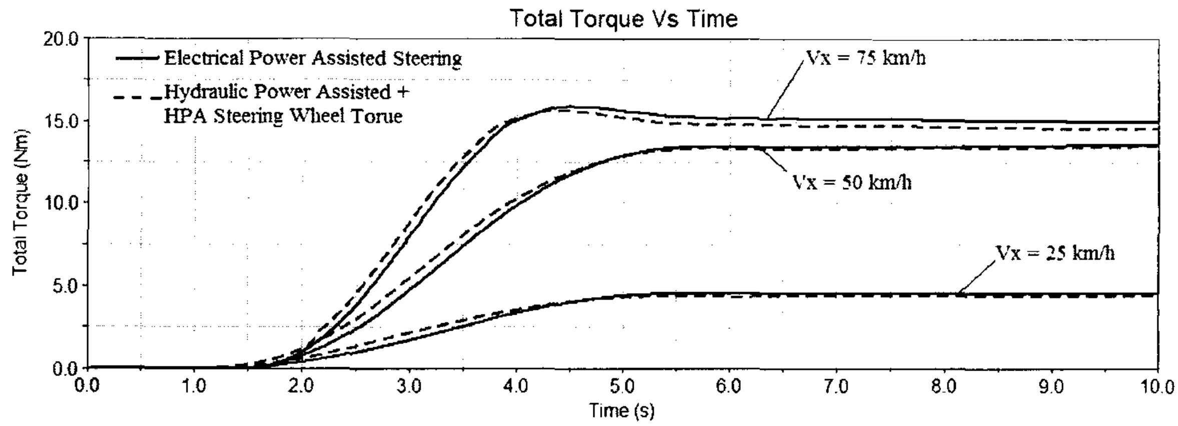

b) Comparison of Total Torque Required to Turn Front Road Wheels at Several Vehicle Speeds

Figure 7.15: Comparisons of Torque for SAS Electrical Power-Assisted Steering (EPAS) and HPAS Systems

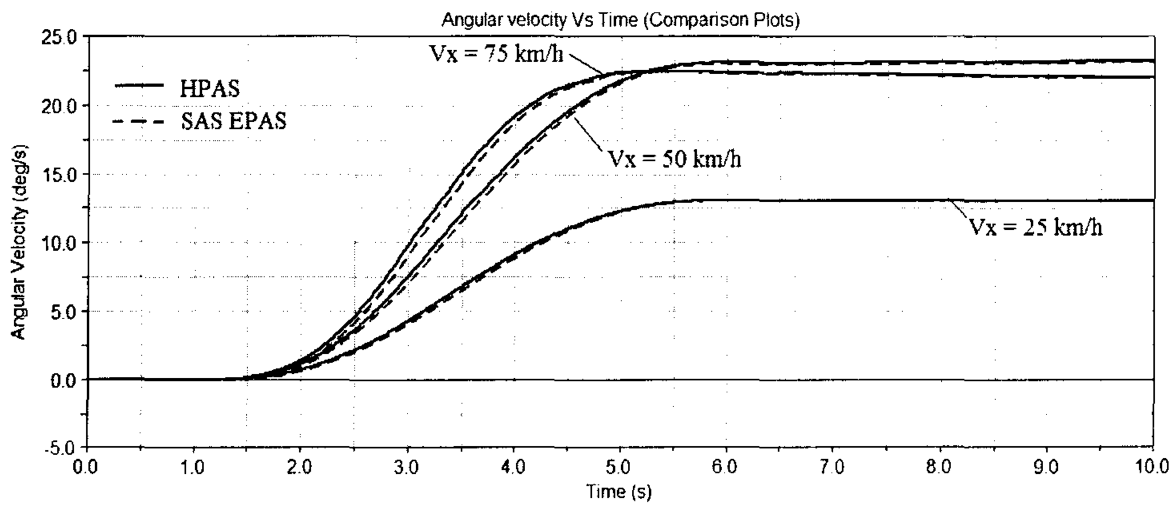

Figure 7.16: Comparisons of Angular Velocities as a Result of Different Characteristics of Total Torque provided by SAS EPAS and HPAS

From Figure 7.15(a), the overlaid plots of power-assisted torque provided by SAS EPAS and the sum of the power-assisted torque and steering wheel torque of the HPAS were almost identical but with slight differences during the cornering event. These were mainly due to the modelling of each system (Section 7.3.2). For the case of HPAS, the torsion bar was modelled to possess damping properties, while for the case of SAS EPAS, the flexible shaft (LSRS) was modelled to have negligible damping properties. When the damping properties were introduced, more steering wheel torque was required to overcome the damping forces. This explains why the total required torque for HPAS was higher than SAS EPAS; during steady state, both systems would approach the same value.

In this research, the damping property of the torsion bar was modelled in order to determine the influence of the damping forces. Moreover, the system also represents the real condition of the vehicle under study. Figure 7.16 shows that the differences of the corresponding yaw velocity plots for both cases due to variable torques were minimal. Hence, it could be concluded that the total torque provided by both systems in order to turn the front road wheels were identical. Figure 7.15(b) illustrates more examples for comparison purposes.

Based on the previous analyses, it can be concluded that the power assistance characteristics provided by SAS EPAS is similar to the HPAS system. This means that all power-assistance advantages belonging to HPAS can also be offered by SAS EPAS system. These advantages are mainly associated with the design of the power assistance curve and were discussed in Chapter 2 (Section 2.5.1.2).

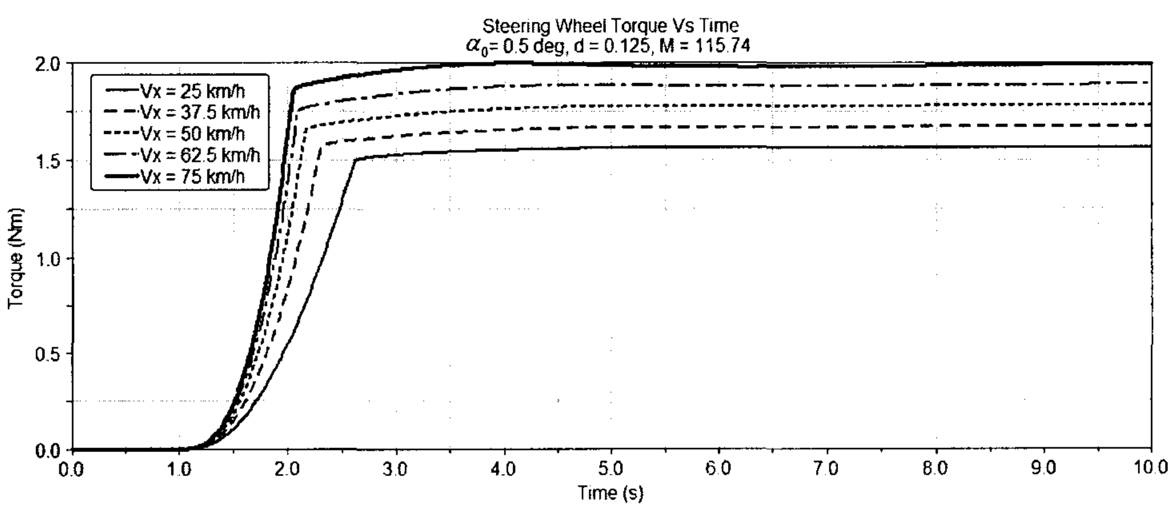

a) Steering Wheel Torque for HPAS

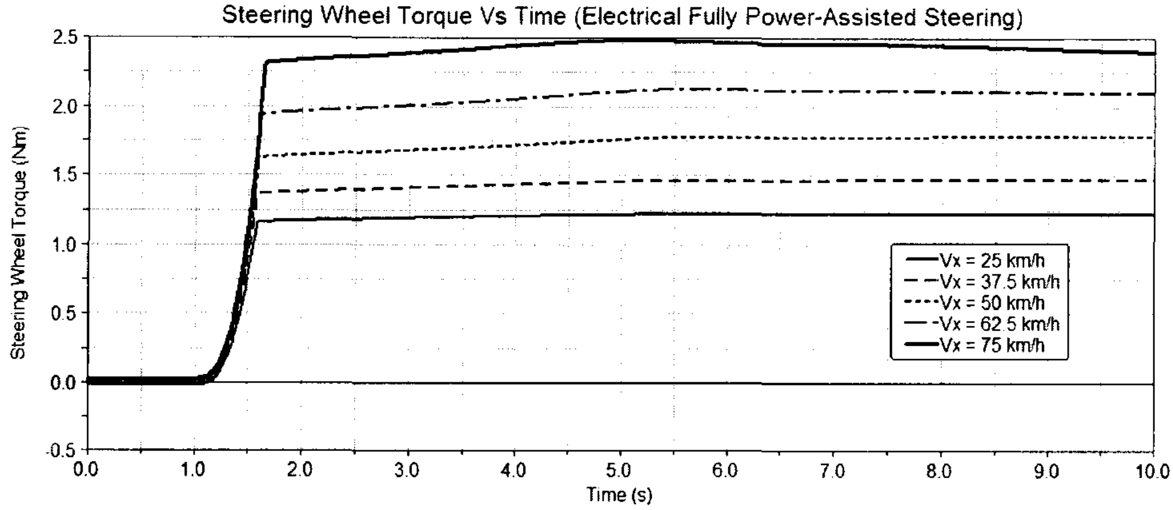

a) Steering Wheel Torque for SAS EPAS System

Figure 7.17: Comparisons of Steering Wheel Torque for SAS EPAS and HPAS Systems

The steering wheel torque for HPAS from Figure 7.17(a) can be observed to originate from a single point while the duration time for each case to reach specific steady state varies depending on vehicle speed. As the speed increases, the time taken to reach steady state decreases. Similarly, the starting point for SAS EPAS was also from a single point but the time taken to reach steady state value started almost immediately for all the cases.

The steering wheel torque for HPAS originated from a single point is explained by the fact that all analyses make use of the same steering wheel input. The time taken for the steering wheel torque of the HPAS system to reach steady state varies depending on the vehicle speed and has the same explanation why its power-assisted torque starts at different times. This is because it takes some time for the torsion bar to reach the required deflection for power assistance since the front road wheels also move during the time when the steering wheel is turned. The increase in self aligning moment due to the increase in vehicle speed causes more resistance for the road-wheels to turn and hence leads to more deflection of the torsion bar.

The reason that the starting point of steering wheel torque of SAS EPAS comes from the same point is because all analyses were performed using the same steering wheel input. The steady state value for each case started almost immediately because the reaction motor immediately applied reactive torque due to the difference in steering wheel and pinion rotation, and this caused an abrupt rise of the steady state steering wheel torque. The delay for each case of vehicle speed was due to the time taken to reach specific deflection angle. Since the deflection angles were very small, the response time difference for each case was also small.

In order to understand the characteristics of power-assisted torque and steering wheel torque with variation in vehicle forward speeds, detailed plots were obtained from Figure 7.14 and Figure 7.17. The data for all the plots were taken at simulation time, t = 7 s where steady state values started to settle down. The results are shown in Figure 7.18(a)-(b).

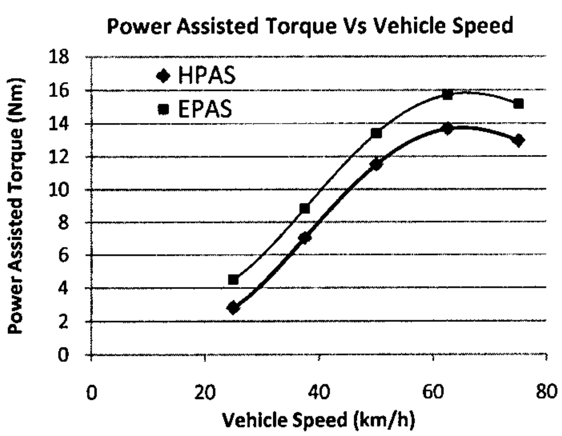

(a)

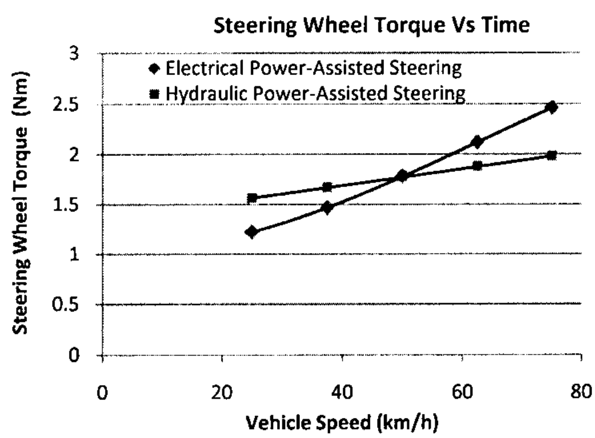

(b)

Figure 7.18: Characteristic Plots of Power-Assisted Torque and SW Torque as Functions of Speed

From Figure 7.18(a), it can be observed for both cases that initially the power-assisted torque increases at an increasing rate until vehicle speed reaches about 50 km/h. The increasing rate then decreases until vehicle speed reaches about 65 km/h. The power-assisted torque then starts to decrease at an increasing rate until vehicle speed reaches 75 km/h.

The explanation of the first portion of the graphs could be that the region is within the linear range of the cornering stiffness. As vehicle speed increases, the cornering stiffness also increases and therefore the vehicle demands more power-assistance. The second portion of the graphs is where non-linearity of the cornering stiffness starts to occur. Within this portion, the contact between tyre and the ground starts to deteriorate as vehicle speed increases. The last portion of the graphs is where slip starts to occur; as the tyre loses grip to the road, less power assistance is required due to the decrease in resistance.

It can be noted from Figure 7.18(a) that the amount of power-assistance provided by SAS EPAS was more than HPAS. This is because some of the required torque for HPAS was provided by the driver, unlike the SAS EPAS which provides all power assistance for operation. Based on these explanations, it can be argued that SAS EPAS was less economical than HPAS since it consumes more power. This argument may be correct, but in the long run, the SAS EPAS is more economical than HPAS because the HPAS system is always in operation when a vehicle is running. The SAS EPAS system only operates during cornering, which frequency of operation depends on road conditions.

From Figure 7.18(b), it can be observed that the steering wheel torque for SAS EPAS increases at an increasing rate while the steering wheel torque for HPAS increases linearly. The two graphs intercept at vehicle speed of 50 km/h. The steering wheel torque for SAS EPAS was lower than HPAS when vehicle speeds were below 50 km/h and the value was higher when vehicle speeds were above 50 km/h.

The steering wheel torque for SAS EPAS increases at an increasing rate with vehicle speed due to the design of power boost characteristic curve. The increasing trend is similar to the characteristic of an arithmetic function which was used to construct the power-boost curve. The steering wheel torque for HPAS increased linearly with vehicle speed because vehicle speed varied linearly with self-aligning moment within a certain range. The linear increase in self-aligning moment also caused the increase in reactive torque in a linear fashion. The two graphs intercept at a vehicle speed of 50 km/h because that was the point where the SAS EPAS reactive torque was calibrated.

Based on Figure 7.18(b), the performance of the SAS EPAS is better than HPAS because the system provides nonlinear variable steering wheel torque based on vehicle speed. At low vehicle speeds, the driver's response to steering wheel input should be fast especially during parking. At high vehicle speeds, the vehicle is very sensitive to steering wheel input, therefore, the steering wheel reactive torque should be high in order to avoid any mistakes by the driver.

7.3.4. Performance Enhancement on Reactive Torque

Performance enhancement of reactive torque can be achieved by adding active control. Since SAS power-assisted steering uses electrical motors for operation, it is much easier to implement active control on the reactive torque than the conventional hydraulic power-assisted steering. Active control on reactive torque of electrical motors can be implemented by manipulating the input current. The reactive torque for HPAS can be varied by changing the properties of torsion bars, which are normally constant for specific material and design.

Active control of reactive torque is required to enhance the performance of a steering system during extreme conditions or acquiring specific needs. A few cases are illustrated as follows:

- During emergency or collision avoidance, it is desirable that the steering wheel torque to be lighter even though our vehicle is moving at high speed.
- During lane change manoeuvre, it is desirable to turn the steering wheel as fast as possible in some cases.

- During parking or moving off, it is sometimes desirable to turn the steering wheel as fast as possible.
- When a vehicle is yawing or skidding, it is desirable to have a correct feel on what is happening on the road wheels depending on situations.

It can be noted that depending on situations, it is desired that the steering wheel torque to vary with steering wheel speed, yaw velocity and lateral acceleration. In order to vary the steering wheel torque depending on situations, the reactive torque can be varied with some modifications to the original formula:

$$\tau_{feel} = -K_f(\delta_{sw} - \delta_p) \cdot f(\dot{\delta}_{sw}, r, a_y) \tag{7.1}$$

An example of the cases previously presented was analysed in detail. When a driver spots an obstacle in front while driving at high speed car, it is necessary to avoid the obstacle as quickly as possible. However, at high vehicle speed, it is recommended that the steering wheel torque be high to provide the safety related to vehicle sensitivity. These two cases conflict with each other because one cannot steer the vehicle quickly enough in order to avoid an obstacle if the steering wheel reactive torque is very heavy.

It is possible to solve this conflict by implementing active control in the reactive torque of the SAS system. Such active control could be performed by adding a term to the existing reactive torque which is a function of steering wheel velocity as follows:

$$\tau_{feel} = -K_f(\delta_{sw} - \delta_{rm})\left(\frac{C}{C \pm \dot{\delta}_{sw}}\right) \tag{7.2}$$

This formula was implemented on the software model and the simulation results were compared with the conventional HPAS vehicle. The input angle characteristic is similar to Figure 7.6 but the time taken for manoeuvring is 1 second, which represents a collision avoidance event. The output results are presented in Figure 7.19. The constant C was obtained by using an iteration technique to obtain desired characteristics.

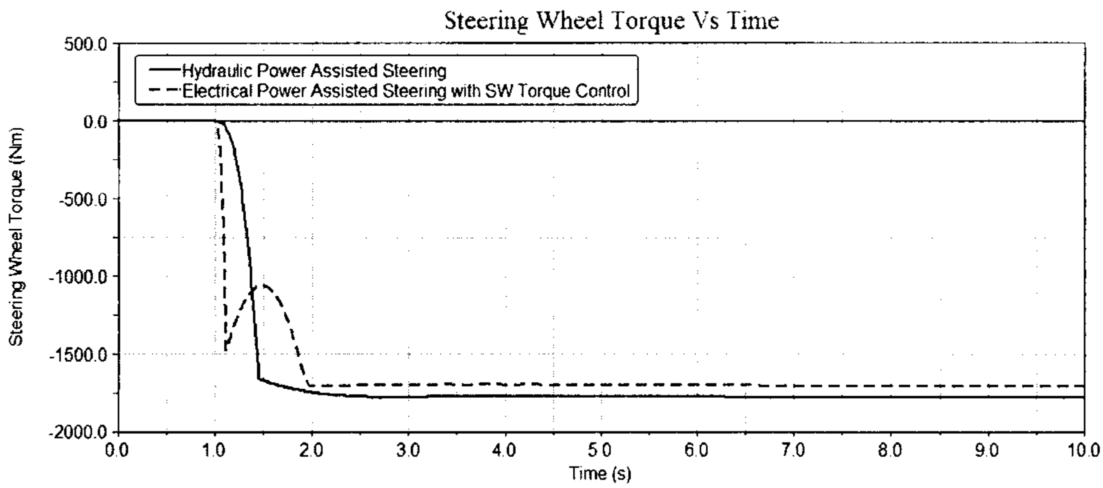

Figure 7.19: Active Control of Reactive Torque during Emergency

From Figure 7.19, at an early cornering period, the reactive torque for SAS EPAS is higher. However, as a driver applies more effort to turn the steering wheel (based on input angle characteristic), the reactive torque for SAS EPAS is lower than HPAS in order to allow fast cornering action. The characteristic can be obtained because the added term is a function of steering wheel velocity. As steering wheel velocity increases, the term approaches to a value much less than 1. At low vehicle speed, the term value becomes approximately equal to 1.

7.3.5. Conclusion on Optimisation and Performance of SAS EPAS

It was concluded that the performance of SAS EPAS was better than the conventional HPAS not only because the SAS EPAS behaves similar to HPAS, but its reactive torque has a better characteristic in terms of steering requirements and the reactive torque can also be improved by adding active control. The total torque required by the SAS EPAS was slightly higher than HPAS because some portion of the torque provided by HPAS was provided by the driver. Although this is the case, SAS EPAS can still offer energy saving advantages because additional power is only required during cornering. HPAS requires its hydraulic pump to be running all the time when a vehicle is being driven.

7.4. Active Control on Semi-Active Steering (SAS)

This section illustrates the implementation of active control in order to complete the design of the SAS system. With the implementation of the control aspects, the design of SAS system was considered to be complete and referred to as 'SAS complete' (or just 'SAS'). The first analysis was to assess the performance of the Jaguar car by simulating the software model and determining its under-steer gradient characteristics. An example of a control strategy stated in Chapter 6 (Section 6.9) was implemented on SAS ADAMS/car software vehicle model. The model was simulated and the results were obtained for presentation.

7.4.1. Performance Assessment of Research Vehicle

In order to assess the performance of the Jaguar car, an under-steer gradient characteristic test was performed on the ADAMS/car full vehicle software model; a constant radius cornering manoeuvre. Starting from rest, the vehicle accelerated and started cornering along a curve of radius 50m. Vehicle speed was gradually increased until the acceleration of the model reached a maximum of 0.9g or until the simulation failed due to loss of tyre/road grip or rollover. The output plot of the steering wheel angle versus lateral acceleration is presented in Figure 7.20.

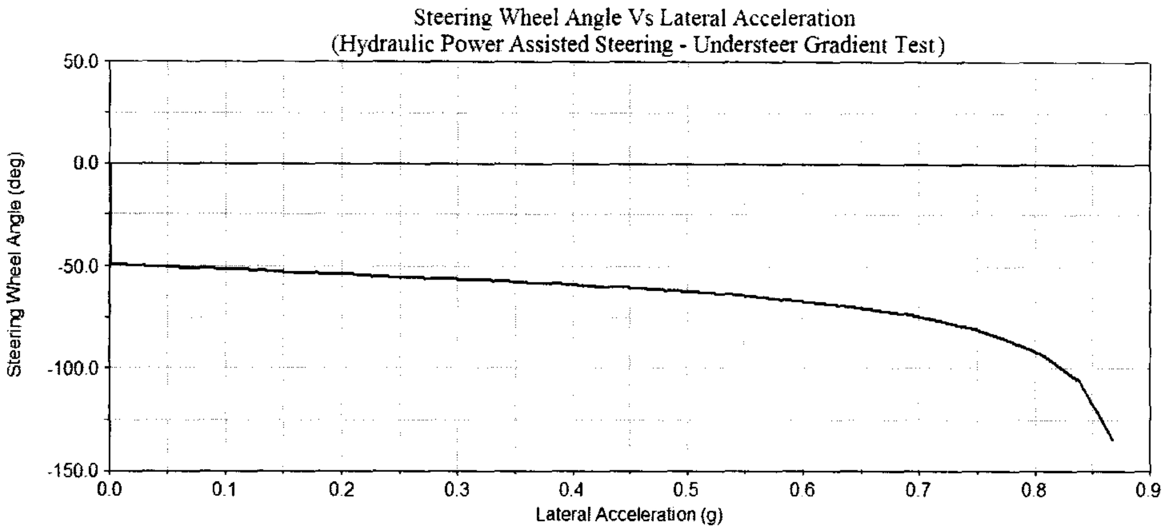

Figure 7.20: Expected Performance of Vehicle under Study

In Figure 7.20, the slope of the graph is constant with negative value until lateral acceleration reaches about 0.5g. This characteristic implies that the vehicle possesses a constant negative understeer gradient at both low speed and medium speed (state of oversteer). The steering wheel angle increases non-linearly at an increasing rate when lateral acceleration exceeds 0.5g, resulting in negative understeer gradient (oversteer) which increases nonlinearly at high vehicle speed.

It is desired to convert the Jaguar car to be over-steer at low vehicle speed, neutral steer during normal speed, and understeer characteristic at high speed. In order to control the under-steer gradient of a car, variable steering ratios are required. The analysis in the following section will demonstrate how steering ratios can be varied based on vehicle forward speed.

7.4.2. Implementing a Selected Active Control

Any kind of control that is implemented on SBW could also be implemented on an SAS system with some modification in the control formula. In this section, an example of an active control case is described to demonstrate how it could be implemented on SAS system. The selected control aims to control the under-steer gradient of a car to be speed dependent with the characteristic are follows:

30 km/h ← 50 km/h ↔ 60 km/h → 80 km/h

$(\delta_d = 1.33\delta_p)$ Oversteer	Neutral Steer	$(\delta_d = 0.75\delta_p)$ Understeer

The detailed description of the active control was presented in Chapter 6 (Section 6.9), and the control strategy was implemented on the full vehicle ADAMS/car software model of SAS EPAS. The new model was then referred as the complete system of SAS.

7.4.3. Results and Discussion on Implementing a Selected Active Control

The results from the vehicle software model with the control implementation were analysed. The selected steering wheel input to the model is shown in Figure 7.6. The analysis was divided into three criteria namely over-steer, neutral-steer and under-steer cases, each case corresponds to a vehicle speed of 30 km/h, 55 km/h and 80 km/h. The results are presented in Figure 7.21 - Figure 7.29 respectively.

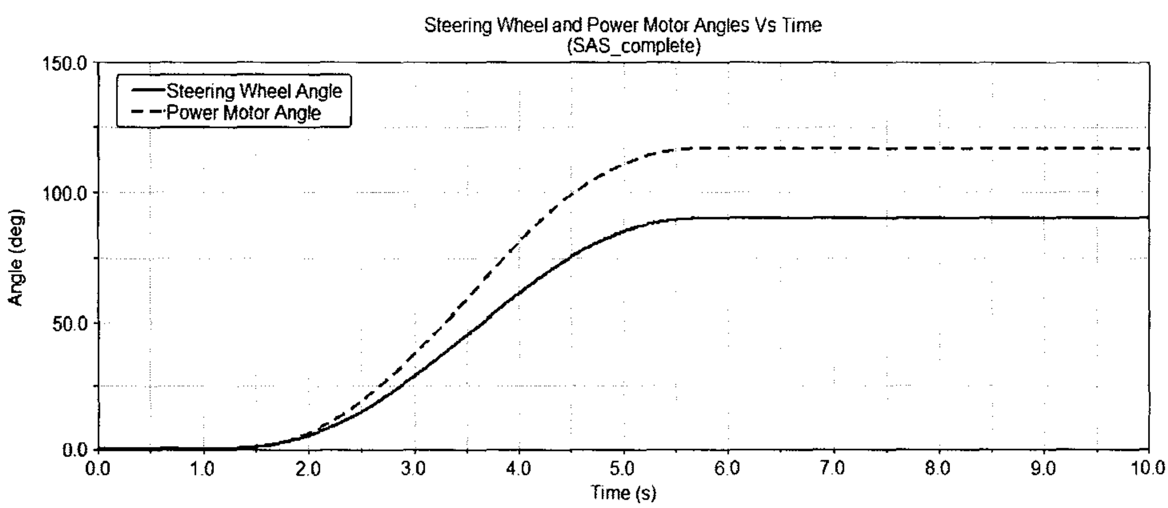

Figure 7.21: The difference of Reaction and Power Motor Angles for Over-steer Case

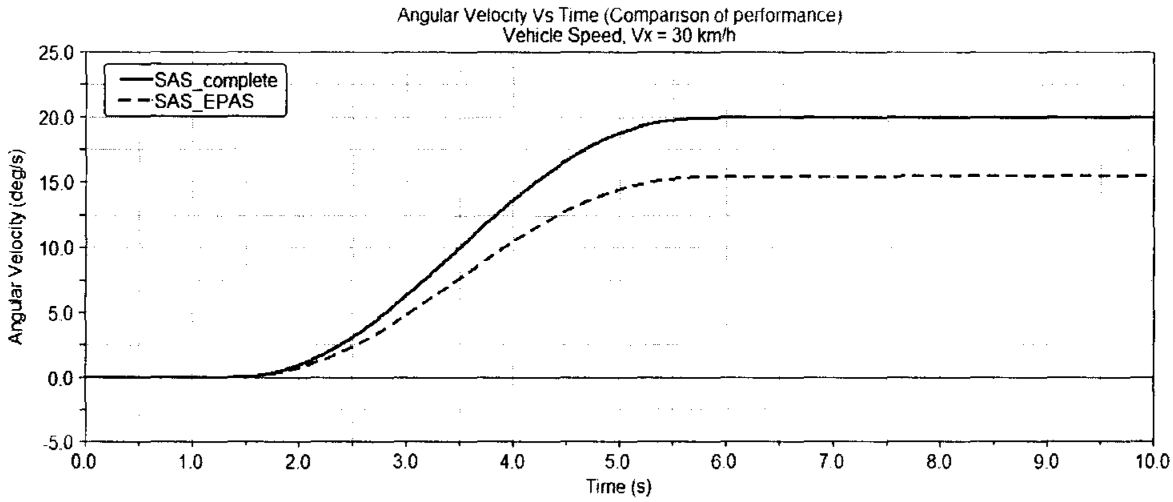

Figure 7.22: The difference of Yaw Velocities for Over-steer Case

Figure 7.21 illustrates how an over-steer case could be created on a vehicle, by varying the pinion rotational angle to be higher than the steering wheel angle. At steady state, the steering wheel angle settles at 90° while the pinion or the power motor angle settles at 116.8°, a difference of 26.8°. Figure 7.22 shows the comparison plots of angular velocities for the over-steer and neutral-steer cases; the yaw velocity for the neutral-steer case is 15 deg/s while for the over-steer case is 20 deg/s, a difference of 5 deg/s. The over-steer characteristic was generated for low speed by adjusting the amount of power-assisted torque applied at the front road wheels. The details of the process are presented through the results below.

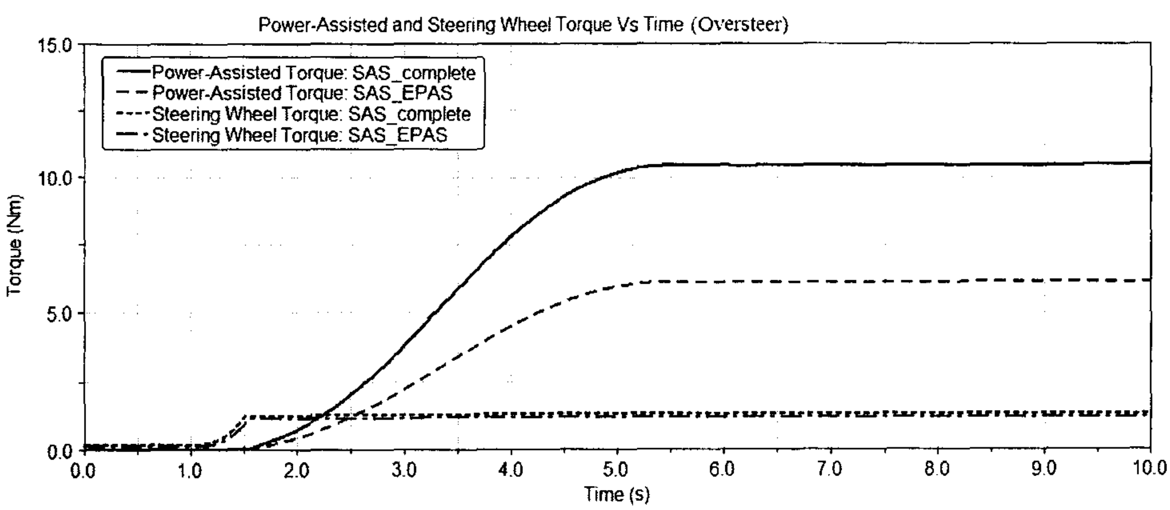

Figure 7.23: Illustrations for Power-Assisted and Steering Wheel Torques for Over-steer and Neutral-steer Cases

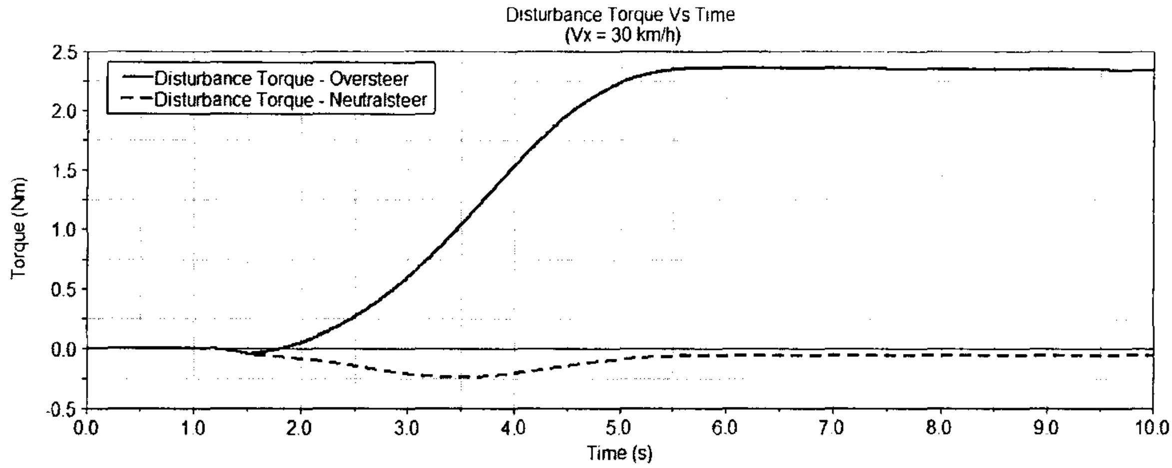

Figure 7.24: Illustrations for Disturbance Torques for Over-steer and Neutral-steer Cases

Figure 7.23 shows the amount of power assistance that would be required to produce over-steer characteristic in the Jaguar car at a speed of 30 km/h. The results for the normal case without any control were obtained from the SAS EPAS software vehicle simulation model. The required power assisted torque for the normal operation was 6.1 Nm while for the over-steer case it was 10.5 Nm. For both cases, the magnitudes of steering wheel torques were about the same; although some disturbance torque was present when the over-steer condition was created, it could not be felt at the steering wheel because the reaction motor for the SAS system applied equal and opposite torque to the disturbance torque to eliminate it. The characteristic of the disturbance torque which was rejected is shown in Figure 7.24. The disturbance torque for the neutral-steer case was very small and could be neglected. The maximum disturbance torque for the simulated results was 2.3 Nm, which means that the reaction motor needed to apply a counter torque of 2.3 Nm. The total torque to be provided by the reaction motor is the sum of reactive torque and counter torque, therefore, the reaction motor needed to produce more torque for over-steer cases.

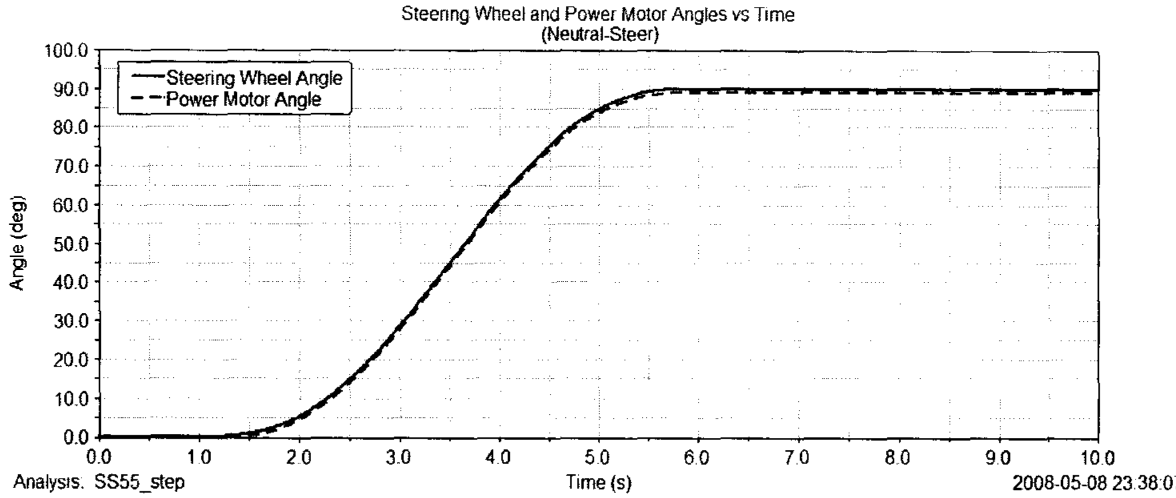

Figure 7.25: Illustration of Neutral-Steer Case when Vehicle Speed is 55km/h

Figure 7.25 shows the illustration of a neutral case for the selected control at vehicle speed of 55 km/h. The plot shows that the power motor rotational angle is almost similar to the steering wheel angle but has a lag of an amount defined as the deflection angle, α. The corresponding characteristics of this case can be referred to the previous analysis.

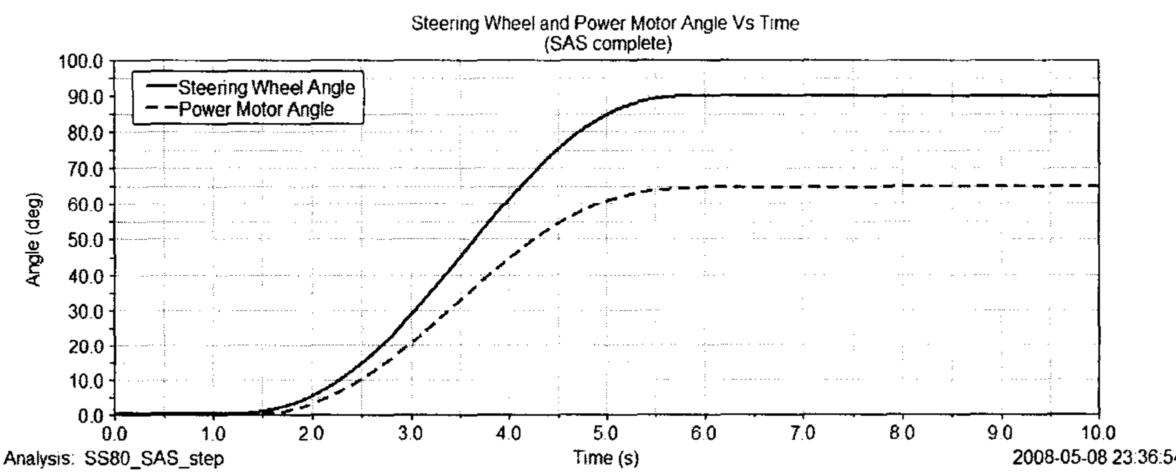

Figure 7.26: The difference of Reaction and Power Motor Angles for Under-steer Case

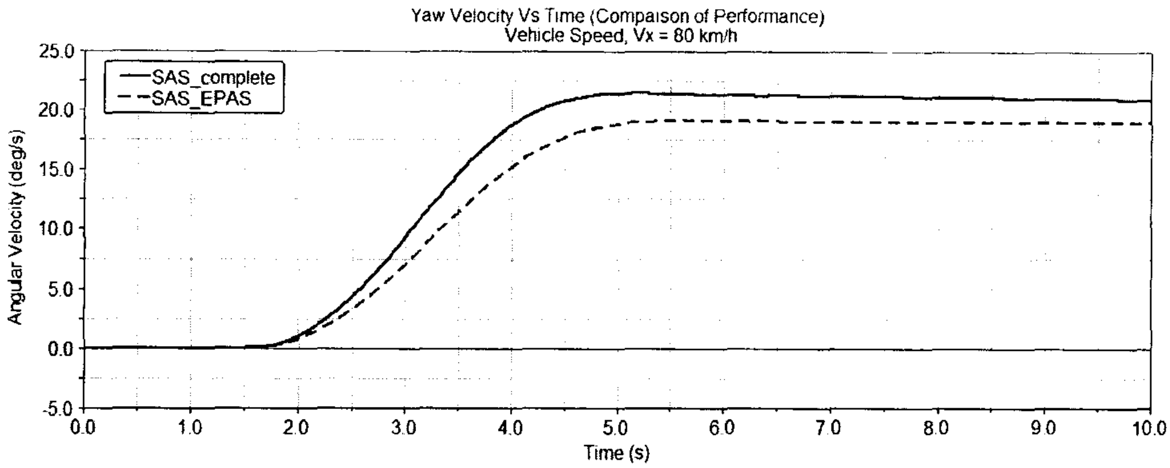

Figure 7.27: The difference of Yaw Velocities for Under-steer Case

Figure 7.26 illustrates how an under-steer case could be created by varying the pinion rotational angle to be lower than the steering wheel angle. At steady state, the steering wheel angle settles at 90° while the pinion or the power motor angle settles at 65.2°, a difference of 24.8°. Figure 7.27 shows the comparison plots of angular velocities for the controlled under-steer and non-controlled (SAS EPAS) cases. The yaw velocity for the SAS EPAS case is 20.9 deg/s while for the controlled under-steer case is 19 deg/s, a difference of 1.9 deg/s. It is interesting to note that although the difference between the steering wheel angle and the power motor angle is almost the same for the oversteer and understeer cases, the corresponding change of angular velocity with respect to the neutral steer cases is different. The oversteer case is higher than the understeer case by about 2.5 times. This phenomenon can be explained from the fact that the vehicle is originally in the state of oversteer based on the results presented in section 7.4.1.

The under-steer characteristic can be generated for a high speed vehicle by decreasing the amount of power-assisted torque applied at the front road wheels, as shown in the results below (Figure 7.28).

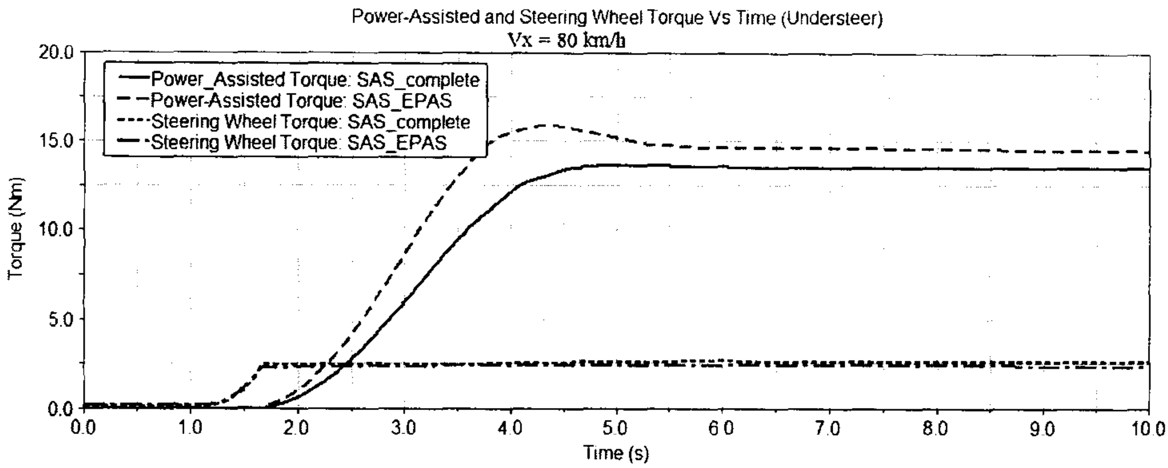

Figure 7.28: Illustrations for Power-Assisted and Steering Wheel Torques for Under-steer and Neutral-steer Cases

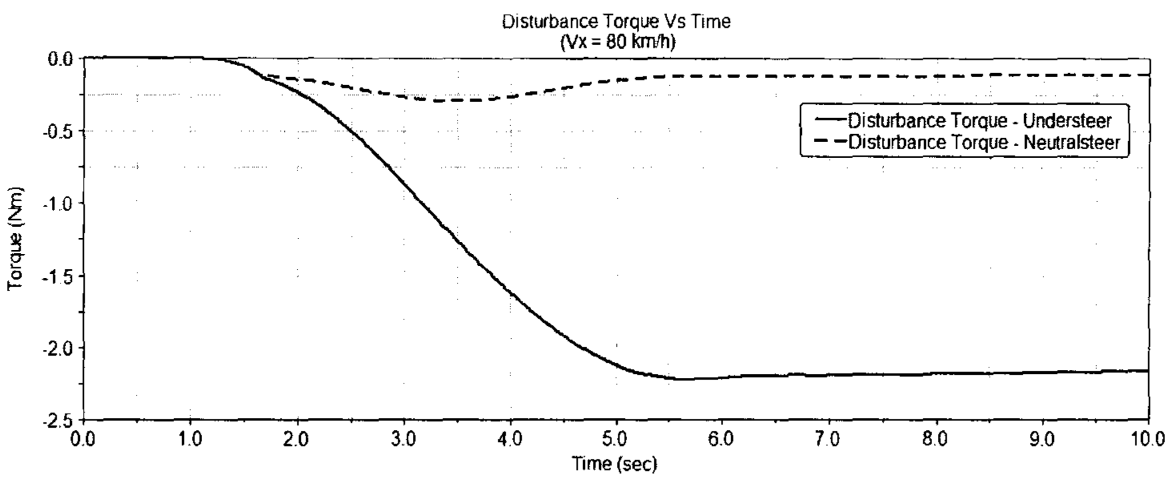

Figure 7.29: Illustrations for Disturbance Torques for Under-steer and Neutral-steer Cases

Figure 7.28 shows the amount of power assistance that was required to produce under-steer characteristic of the research vehicle at a speed of 80 km/h. The results for the normal case (under-steer) without any control were obtained from the simulation of the SAS EPAS software vehicle model. The required power assisted torque for the normal operation was 14.5 Nm while for the over-steer case it was 13.5 Nm. For both cases, the magnitude of steering wheel torques was about the same. Although some disturbance torque was present when over-steer condition was created, it could not be felt at the steering wheel because the reaction motor for SAS system applied equal and opposite torque to the disturbance torque to eliminate it. The characteristic of the disturbance torque which was rejected is shown in Figure 7.29. The disturbance torque for the neutral-steer case was very small and can be neglected. The maximum disturbance torque for the simulated results was -2.16 Nm. This means that the reaction motor needs to apply a counter torque of 2.16 Nm. The total torque to be provided by the reaction motor is the sum of reactive torque and counter torque, therefore, the reaction motor needed to produce less torque for under-steer cases.

The analysis described here could be used to determine the maximum allowable angle of twist for a specified selected control. The procedure is very subjective depending on the desired vehicle characteristics.

7.4.4. Steering Feel Enhancement during Active Control

During extreme conditions, the SAS system performs active control on a vehicle by applying corrective steer to the front road wheels. It is desirable to alert the driver on what is happening at the road wheels during active control so that the driver can take necessary actions to reduce risks. For example, if a driver is driving too fast while cornering, it is advisable to alert him/her to slow down. This can be done by adjusting the disturbance rejection torque so that some amount of disturbance can be felt by the driver. The reaction motor torque can be manipulated as follows:

$$\tau_{rm} = \left(\tau_{feel} + \tau_{counter}\right) \cdot (\text{manipulator function}) \tag{7.3}$$

The easiest manipulator function is a constant of value less than 1, e.g. 0.95. This means that 95% of the disturbance is rejected while the driver can feel 5% of the total disturbance magnitude. Other alternatives include the sine or cosine functions.

7.4.5. Conclusion on Implementing a Selected Active Control

The simulation results have shown that a selected control implemented on the SAS full vehicle software model could change the original vehicle characteristics to desired vehicle characteristics. The original vehicle which had an understeer characteristic at low speed and medium speed could be changed to be over-steer and neutral steer by applying additional power-assisted torque to turn the front steered wheels. Likewise, an under-steer characteristic at high vehicle speed could be achieved by applying less power assistance to turn the front road wheels. During active control, disturbance torque was eliminated by the reaction motor which applied equal and opposite torque to the disturbance source. During active control, the reaction motor applied the sum of reactive torque and counter-disturbance torque; it would provide more torque during over-steer than during under-steer. During active control, the steering feel can be enhanced by allowing some amount of disturbance to be felt by the driver.

7.5. Chapter Summary

This chapter analyzes the main results which were obtained from the simulation of full vehicle software models. Prior to simulation, the software model was validated using the mathematical models developed in Chapter 3. The simulation activities consisted of the selection of power-boost curve parameters, the development of SAS power assistance, the performance assessment of a research vehicle and finally the implementation of active control.

The validation of the software model was performed by comparing the simulation results of MATLAB/SIMULINK (mathematical models) with the simulation results of ADAMS/car vehicle model. A selected cornering event for both cases was driving a car at a constant speed while gradually turned the steering wheel under a certain characteristic angle until the final acceleration reaches 0.6g. The output results for comparisons were yaw velocity, lateral acceleration, roll angle, slip angle and lateral forces.

The output results of MATLAB/SIMULINK for yaw velocity, lateral acceleration and slip angle were found to agree overall with the ADAMS/car simulation results. The calculated lateral forces were found to differ from ADAMS/car simulation results toward the end of simulation time by about 10%. It was later discovered that this could be due to neglecting the effect of 'turn slip'; but further improvement in the computation could not be performed due to unavailability of required constants. The simulation results of the MATLAB/SIMULINK for the roll angle prediction was found to deviate with the ADAMS/car simulation results by maximum of 17% towards the end of the simulation time. In general, the main reasons for the deviation in roll angle results were due to neglecting the transfer of forces through linkages during cornering.

The MATLAB/SIMULINK computer program was modified by replacing the original roll formula with the modified roll formula illustrated in Section 3.1.2; while the remaining formula were still used. The final simulation results from MATLAB/SIMULINK and ADAMS/car showed that the roll angle prediction was then in agreement overall with each other.

The selection of parameters for the power boost characteristic curve were identified by simulating the full vehicle ADAMS/car software model fitted with conventional hydraulic power assisted steering (HPAS) and using the iteration technique. The parameters to be selected and optimized were the starting curve corresponding to vehicle zero-speed, α_o and the distance between each individual curve, d; the remaining variables followed manufacturer's recommendation. The analysis showed that suitable values were $\alpha_o = 0.5^o$ and $d = 0.125^0$; these were determined based on the output reactive torques which during normal driving should be about 2 Nm.

The first step in developing SAS EPAS was to calibrate the reactive torque of the system with the conventional HPAS. This was done by determining the constant K_f which corresponding reactive torque equalled the conventional HPAS at 50 km/h. The torsion bar of the HPAS system has a stiffness of 120 Nm/rad and a damping of 0.2 Nm.s/rad. The calibrated value of K_f at 50 km/h was found to be 106 Nm/rad.

After the calibration was conducted, the SAS EPAS software model was simulated and the results were compared with simulation results of the conventional HPAS for assessment of performance. It was found that the activation of power assistance for HPAS of each case of vehicle speed occurred at a later time and the behaviour was inversely proportional to speed; while for SAS EPAS system it occurred at the same time for all the cases. Similar characteristics were also observed for the steering wheel torque where the activation was found to delay with the increase in speed for the HPAS case. The explanation to these phenomena was owing to the configuration of each system. For the HPAS, the required energy for operation was provided by both the driver and the system; while for the case of SAS EPAS, all the energy was provided by the system.

The performance of SAS EPAS was found to be better than the conventional HPAS because not only did SAS EPAS behave similarly to HPAS, but also its reactive torque had a better characteristic in terms of steering requirements and could also be improved by adding active control. The reactive torque for SAS EPAS was low at low vehicle speed and high at high vehicle speed, with a non-linear relationship; and the HPAS reactive torque had a linear relationship. The total torque required by the SAS EPAS was found to be slightly higher than HPAS because the driver provided some portion of the total torque required to steer. SAS EPAS can still offer energy saving advantages in the long run because such additional energy is only required during cornering, unlike HPAS which requires its hydraulic pump to be running all the time when a vehicle is running.

The last task which completed the design of SAS was the addition of active control to the system. An example of a control to change vehicle under-steer gradient based on vehicle speed was selected. The simulation results showed that the selected control which was implemented on the SAS full vehicle model could change the original vehicle characteristics to the desired characteristics. The characteristics of the original vehicle could be changed to either being over-steer or under-steer by applying additional power-assisted torque or applying less power assistance to steer the front road wheels. The disturbance torque due to the presence of LSRS was eliminated by the reaction motor which applied equal and opposite torque to the disturbance source. During active control, the reaction motor applied torque which consisted of reactive torque and counter-disturbance torque. The reaction motor provided more torque during over-steer than during under-steer. The steering feel can be enhanced during active control by allowing some amount of disturbance to be felt by the driver.

Chapter 8

8. Summary, Conclusion, and Recommendations for Future Work

This section presents the final summary of the results and findings, conclusions of the research presented here on the design of a semi-active steering system for a passenger car, and then provides recommendations for future work in the field.

8.1. Summary

This research presented a proposal for the design of a semi-active system for a passenger car. The design concept of semi-active steering was derived from previous work in the field as a result of the literature review.

The main problem with a conventional steering system is that the overall steering ratio is almost constant due to the rigid shaft and linkage design. Depending on driving conditions, road vehicles experience situations such as understeer, neutral steer and oversteer cases which might result in instability; hence active control is needed for safety reasons. Active steering can be the solution to the conventional steering system by improving the performance in terms of ease of manoeuvring, vehicle stability, safety aspects and efficiency; but the presence of a rigid steering shaft causes disadvantages in packaging and safety concerns during front-end collisions.

Steer-by-wire could provide similar advantages offered by active steering but the system can offer additional features such as unlimited control capability, packaging advantage and safety aspects due to the absence of mechanical linkage. The main problem with steer-by-wire (SBW) is that back-up systems either in the form of mechanical connection (e.g. flexible resilience steering shaft) or redundancies (wiring and software architectures) are required because the vehicle would be uncontrollable in case of system failure.

Any forms of back-up systems which rely on clutches may not increase customers' safety confidence level since clutches introduce more failure modes. The presence of a mechanical connection between the steering wheel and the road wheels is hoped to increase customers' safety confidence level.

Based on these findings, a steering system which implemented a low stiffness resilience shaft (LSRS) that combined the advantages offered by active-steering and steer-by-wire was proposed. The LSRS was readily available in the event of system failure; and its flexibility allowed steering intervention to be performed.

Based on previous published work, active control on vehicles could be performed either using a vehicle dynamics approach which was more complicated but efficient; or by segregating the power assistance and control aspects which was simpler but might be less efficient. Due to simplicity, it was decided that control algorithm of the proposed steering system would follow the approach of the latter.

It was illustrated that an ideal Hydraulic Power-Assisted Steering (HPAS) boost curve could provide road vehicle with advantages in providing steering feel and safety aspects during low and high speed manoeuvres. Also, it was found that Electrical Power-Assisted Steering (EPAS) could offer more advantages than HPAS in terms of energy saving, design simplicity and customized steering feel capability.

Based on the previous findings, it was decided that the power assistance of the proposed steering system would be designed to operate on EPAS system while its power boost characteristics would be made to follow the ideal characteristic curve of HPAS. For the implementation of active control, any types of control strategies should be applicable to the proposed system. Finally, the proposed steering system was referred as 'Semi-Active Steering System' (SAS); the detailed description of the design would be described later.

Prior to detailed design work, the development of three mathematical models of a cornering vehicle was presented. The first model was a mathematical model of a full (3D) cornering vehicle fitted with hydraulic power-assisted steering with the aims of gaining some knowledge and understanding of power-assisted steering characteristics and to use the developed formula to validate a full vehicle software model. The formula for an improvement to the roll angle prediction was also presented.

The model was programmed using MATLAB/SIMULINK which simulated the performance of a hydraulic power-assisted steering system fitted to a Jaguar passenger car. The characteristics of power assisted steering systems such as steering gear feel and stiffness were analysed. It was found that at low vehicle lateral acceleration and yaw velocity, the steering gear stiffness was low; and vice versa for the case of high lateral acceleration. In contrast, steering gear feel was higher at low lateral acceleration and yaw velocity; and lower at high lateral acceleration and yaw velocity. The steering gear stiffness and steering gear feel was found to be speed dependent. For more meaningful interpretation of the results, the steering gear stiffness and steering gear feel were related to a driver interaction with a car; i.e. driver steering feel (steering wheel torque) and driver steering comfort respectively.

The performance of the hydraulic power-assisted steering system fitted on the Jaguar car was found to assist the driver during parking, provide more driver steering feel at high vehicle speed, increase the driver's feel on what is happening at the road wheels during low speed manoeuvring, and prevent forces from being transmitted through the steering column at high vehicle speed. These characteristics were found to be similar to the behaviour offered by an ideal hydraulic power-assisted steering power boost curves presented in Section 2.5.1.2. The steering comfort for the hydraulic power-assisted system analysed in this study was found to be about 20% compared with the manual system. Such design was comfortable but it might cause the driver to lose judgement of the forces acting at the road wheels.

The second mathematical model was of a 2D cornering vehicle fitted with a flexible steering shaft. The model represented a failed SBW or SAS system in the event of active system failure and the flexible shaft represented a back-up system. The model was developed in order to predict the lowest steering shaft stiffness that would ensure that the vehicle was safe to be driven, and was stable. It was found that overshoots started to occur when the stiffness values were either lower than 5 Nm/rad or higher than 15 Nm/rad. It was therefore concluded that range of the acceptable flexible shaft was between 5 Nm/rad to 15 Nm/rad. For experimental work, the shaft of stiffness 5 Nm/rad, 10 Nm/rad and 15 Nm/rad were fabricated.

The last mathematical model was a simplification of the second model. The main intention of introducing this model was to aid engineers in speeding up design work to determine the minimum stiffness values. The simplicity of the formula made it very useful during the preliminary design stage. The accuracy of the formula was verified by comparing the simulation results of the simplified model with the detailed model. A cornering event representing the worst scenario of collision avoidance was selected and vehicle speed was varied for each case. The results showed that the difference of errors increased with the increase in vehicle speed but the results were accurate to within less than 5% for vehicle speed of less than 385 km/h.

The second mathematical model was revisited for vehicle behavioural investigation during failure. The validation of the developed formula was performed in Chapter 4. The theoretical formula was then used to predict vehicle characteristics when fitted with flexible steering shaft of different properties such as stiffness and damping. The main aim was to study vehicle characteristics and also to determine the best steering shaft properties to be chosen.

When stiffness was varied while fixing the vehicle speed and low damping value, the results showed that the higher the stiffness of the steering shaft, the higher were the peaks of the maximum yaw velocities. The incremental rate of the peak values however, decreased as the stiffness value increased. As the stiffness of steering shaft increased to infinitely rigid, the peak values approached to the expected results of the manual steering system. The steering ratios increased with the decrease in shaft stiffness at an incremental rate. For the step input, overshoots are observed when the curves approach either low stiffness values or high stiffness values.

When damping was varied while fixing vehicle speed and low stiffness, the results showed that for sinusoidal input, the higher the damping of a steering shaft, the higher were the yaw velocity peak values but with the decrease in incremental rate. For the case of step input, when damping decreased, the yaw velocity dropped to approach the steady state value of the steering shaft with the lowest damping. Surprisingly, overshoot was minimal at low damping.

When vehicle speed was varied while fixing low stiffness and low damping, the results showed that the ratio of peaks of non-conventional to conventional was maintained and not affected by vehicle speed. However, overshoot was found to increase as vehicle speed increased.

Based on the previous results, it was decided that best stiffness value would be the minimum acceptable stiffness value that did not cause the vehicle to be unstable due to overshoots; and such stiffness could contribute to packaging advantage. The selected stiffness caused vehicle to be more stable and produced outputs with characteristics similar to the conventional system.

It was found from the analysis that the best choice of damping value was either the minimum acceptable value or the highest permissible value. The choice of having the highest permissible value was only kept as an option because it might lead to disadvantages in terms of design and packaging benefits.

The combination of the minimum acceptable steering shaft stiffness and the minimum acceptable damping value was found to be the best choice for the properties of steering shaft to be used for back-up system of SBW during system failure. The steering ratio increased when the steering shaft stiffness decreased; therefore the driver needed to apply additional effort to increase the speed of the steering wheel during cornering. Further analysis using torque as input showed that this was not a problem because steering wheel speed would adjust automatically depending on the torque applied at the steering wheel. When the stiffness was low, the turning of the steering wheel would be light and the steering wheel speed would increase.

After introducing mathematical models for experimental preparation and vehicle performance prediction, the very next step was to perform experiments to validate the theoretical formula and also to verify on main concepts. In this research, a medium size car of class B was selected. The car was selected based on a few criteria such as simplicity in removal and reinstallation of steering shaft and safety related matters. The removal and reinstallation procedures of a steering shaft were illustrated in detail. The design, fabrication and the installation methods of the flexible shaft were also presented, and when the flexible shafts were ready, vehicle preparation work such as safety checks, draining of hydraulic fluid and the installation of the data acquisition system were explained. Due to the time constraint and cost, the fabricated flexible shaft was not resilience but it was expected that the experimental results would be the same. The experimental procedures and how the data were processed were presented.

An experiment of driving a research vehicle fitted with a selected stiffness of flexible shaft along a medium cornering curve was conducted to verify the proposal of implementing low stiffness resilience shaft (LSRS) in providing stability and safety to a vehicle during active system failure. The experimental results had shown that an experimental vehicle fitted with a flexible shaft of stiffness as low as 5 Nm/rad provided stability and safe to drive during cornering tests based on the graphical trends of the output results viz. lateral accelerations and yaw velocities which behaved similarly to the same test car fitted with the conventional steering system. The test car became more stable when higher stiffness values were implemented. Slight fluctuations and variations were observed in the results with the decrease in stiffness values. Since steering ratio increased with the decrease in shaft stiffness, the lower the steering shaft stiffness the higher was the required steering wheel angle. It was seen that the lower the vehicle speed, the more fluctuations were observed in the steering wheel angle characteristics. The test vehicle was found to be more stable when driving at higher speeds for every case of stiffness value. Further investigation on this finding would be required as the vehicle test speeds during the experiments were only limited to 30 km/h.

The results had verified the proposal of using LSRS for a backup system of SAS in case of system failure. Although it was proven that LSRS could deliver the required tasks, the performance of the system was found to be under par compared to the conventional steering system; but safe to control and bring a failed vehicle to a stop in the event of system failure.

The experimental results of single lane change to the point of skidding manoeuvre tests were used to validate the mathematical models of a cornering vehicle fitted with flexible shaft. These mathematical models were required to predict vehicle behaviours when fitted with different stiffness of flexible shafts in the event of system failures. Based on general observations, the theoretical formula agreed with the experimental results with slight deviations but the reasons were acceptable. For a selected case, the yaw velocity for the experimental results was observed to be higher during the clockwise turning of the steering wheel while they lagged behind during counter-clockwise turning. Further investigation revealed that the fabricated steering shaft had different values of stiffness for clockwise and counter-clockwise turning; whereas it was assumed that they were equal in computation. Slight deviations were also attributed to the 'sticking effect' of double springs to the wound shaft.

The same experimental data used to validate the mathematical models were also used to compute the maximum steering wheel speed and the steering wheel torque. The main aim of computing the maximum steering wheel velocity was to determine the performance during fast action manoeuvring in order to find out the effect of steering shaft stiffness on the driver's reaction to turn the steering wheel. The computation of steering wheel torque was performed in order to find out how the torque varied with the steering wheel velocity.

It was found out that the generated steering wheel speed depended on the amount of torque applied at the steering wheel and the stiffness of the steering shaft. When applying the same amount of torque, higher steering wheel velocity could be generated with lower steering shaft stiffness. When a driver supplied sufficient torque to turn the steering wheel of his vehicle to avoid obstacle, the vehicle should respond accordingly based on the amount of steering wheel torque. For lower steering shaft stiffness, higher steering wheel speed could be generated and vice versa.

Once the concept of implementing LSRS during active system failure was verified, the detailed proposal of the SAS system design could proceed safely. The complete design aspects of SAS include the safety, general requirements, and system designs. The concepts of SAS were explained by analysing the advantages of the SAS system compared to the conventional system in terms of the customer's confidence level, packaging benefits, and fatigue life.

The most important safety aspect belonging to SAS was that the system had a permanent mechanical connection (LSRS) between the steering wheel and the road wheels. The LSRS was an integral part of the steering system, and readily available to revert to conventional mode in the event of system failure.

The presence of a permanent backup system not in the form of clutches was hoped to increase customer's safety confidence level to use the SAS system. The system might be accepted in the same way that ABS and ESC systems were being accepted worldwide. The SAS could be implemented as a stepping stone in order to test the durability and reliability of wiring and electronic systems of SBW; the process might take a very long time.

SAS simplified packaging and offered similar advantages to SBW. The LSRS could lead to energy system effectiveness and buckle during a front-end collision to prevent the driver from injury.

Material fatigue was one of the major concerns about the SAS due to frequent twisting of LSRS. Therefore, the system was suitable for fitment on common passenger cars where normal driving were involved.

The LSRS could be designed using coiled springs alternately wound in different orientations or short pieces of torsion bars connected in series. The latter had the advantage of overcoming fatigue life since each element might have high stiffness but when connected in series the overall stiffness would be lower.

The steering wheel self-centring of SAS was achieved by deactivating all the motors to switch to conventional steering mode. Although this could be done, the reaction motor could be programmed to provide force feedback for lane keeping assistance.

Since the power-assistance was fully provided by the system, the steering feel was generated at the steering wheel by applying artificial reactive torque which triggered based on the signals of the difference between steering wheel angle and pinion rotation angle. The performance of the steering feel during special needs could be achieved by manipulating the input signals.

The presence of LSRS caused some disturbance to be felt at the steering wheel during active control. Therefore, a reaction motor was required to prevent such a disturbance from being felt by the driver by applying an equal and opposite torque to the disturbance source. Some disturbance could be allowed to be felt by the driver in order to alert the driver on the driving conditions.

The control algorithms of SAS were divided into two categories, viz. power assistance and active steer; each category was developed separately in sequence. The power assistance of SAS was proposed to be developed based on an ideal power boost characteristics of a hydraulic power assisted steering. For the case of active steer, all control strategy which could be implemented on SBW would be applicable for SAS with some modifications in the control formula. For demonstration purposes, a basic closed loop PID-control was proposed.

The next step was to model the SAS system complete with control algorithms using ADAMS/car. The main objective was to demonstrate the working concepts of the SAS system and to show how the system performance could meet the requirements of a robust steering system. The selected vehicle model for modelling work was the Jaguar car since a complete data set was available.

The modelling development of the SAS system was carried out in stages. The first stage was to model and optimize the power assistance system while the second stage was to add the control aspect to the system. The first step in modelling the power assistance system was to develop the power boost characteristic curve; i.e. conversion from HPAS to EPAS. The curve was mathematically modelled by assigning a variable for each parameter, viz. minimum saturation angle α_0, distance from the first and second curve *d,* and slope of the curve *m* for optimisation purposes. The distance between each two curves was modelled to increase like an arithmetic summation series. In order to predict the value of a deflection angle at a specified speed, the selected curve behaviour function (i.e. arithmetic summation series) was used.

The following task in modelling the power assistance system was to implement the power boost model on EPAS. The selected control block diagram was based on a PID controller. When the system received a signal, α representing the difference between the steering wheel angle and the pinion rotation angle, the controller then used the signal to compute the required power assistance, which task was performed by the power motor. The control activities in the vehicle model were performed within the steering system template where information could be passed through local variables. The computation of power boost curve by the controller was modelled using 'step' functions with programming conditions. The steering reactive torque or steering feel was modelled by multiplying a constant K_f with the signal α. The constant were determined by calibrating the EPAS with a conventional system at 50 km/h.

The second stage of the SAS system was to add active-steering technology to the EPAS system. The active-steering technology was made possible through the use of a flexible resilient shaft. In general, any control which could be implemented on SBW could also be performed on SAS system with some modification. A selected closed loop control was selected for this research by adding a transfer function to the feedback loop. The transfer function represented the ratio of the desired pinion rotation to the input steering wheel angle.

The selected control strategy was to vary the understeer gradient of a car depending on its forward speed. At low vehicle speed, the vehicle was required to oversteer for quick response during parking. At common driving speed, neutral steer was preferable. While at high speed, the vehicle was required to understeer to eliminate driving sensitivity.

The presence of the flexible resilient shaft (LSRS) caused some disturbance to be felt at the steering wheel during control. Therefore, besides providing some resistance at the steering wheel for steering feel, the reaction motor was also required to provide counter torque to cancel out the disturbance forces. The total torque provided by the reaction motor was therefore the sum of the feel torque and the counter torque.

The control algorithms of all the strategies were programmed within ADAMS/car steering template. The driving conditions were distinguished using the condition 'IF' in order to implement the selected active control.

The last tasks were to simulate the ADAMS/car full vehicle software models and to analyze the results. Prior to simulation, the software model was validated using the mathematical models developed in Chapter 3. The validation of the software model was performed by comparing the simulation results of MATLAB/SIMULINK (mathematical models) with the simulation results of ADAMS/car vehicle model. A selected cornering event for both cases was driving a car at a constant speed while gradually turned the steering wheel under a certain characteristic angle until the final acceleration reaches 0.6g. The output results for comparisons were yaw velocity, lateral acceleration, roll angle, slip angle and lateral forces.

The output results of MATLAB/SIMULINK for yaw velocity, lateral acceleration and slip angle were found to agree overall with the ADAMS/car simulation results. The calculated lateral forces were found to differ from ADAMS/car simulation results toward the end of simulation time by about 10%. It was later discovered that this could be due to neglecting the effect of 'turn slip'; but further improvement in the computation could not be performed due to unavailability of required constants. The simulation results of the MATLAB/SIMULINK for the roll angle prediction was found to deviate with the ADAMS/car simulation results by maximum of 17% towards the end of the simulation time. In general, the main reasons for the deviation in roll angle results were due to neglecting the transfer of forces through linkages during cornering.

The MATLAB/SIMULINK computer program was modified by replacing the original roll formula with the modified roll formula illustrated in Section 3.1.2; while the remaining formula were still used. The final simulation results from MATLAB/SIMULINK and ADAMS/car showed that the roll angle prediction was then in agreement overall with each other.

The selection of parameters for the power boost characteristic curve were identified by simulating the full vehicle ADAMS/car software model fitted with conventional hydraulic power assisted steering (HPAS) and using the iteration technique. The parameters to be selected and optimized were the starting curve corresponding to vehicle zero-speed, α_o and the distance between each individual curve, *d*; the remaining variables followed manufacturer's recommendation. The analysis showed that suitable values were $\alpha_o = 0.5^o$ and $d = 0.125^0$; these were determined based on the output reactive torques which during normal driving should be about 2 Nm.

The first step in developing SAS EPAS was to calibrate the reactive torque of the system with the conventional HPAS. This was done by determining the constant K_f which corresponding reactive torque equalled the conventional HPAS at 50 km/h. The torsion bar of the HPAS system has a stiffness of 120 Nm/rad and a damping of 0.2 Nm.s/rad. The calibrated value of K_f at 50 km/h was found to be 106 Nm/rad.

After the calibration was conducted, the SAS EPAS software model was simulated and the results were compared with simulation results of the conventional HPAS for assessment of performance. It was found that the activation of power assistance for HPAS of each case of vehicle speed occurred at a later time and the behaviour was inversely proportional to speed; while for SAS EPAS system it occurred at the same time for all the cases. Similar characteristics were also observed for the steering wheel torque where the activation was found to delay with the increase in speed for the HPAS case. The explanation to these phenomena was owing to the configuration of each system. For the HPAS, the required energy for operation was provided by both the driver and the system; while for the case of SAS EPAS, all the energy was provided by the system.

The reactive torque for SAS EPAS was low at low vehicle speed and high at high vehicle speed, with a non-linear relationship; and the HPAS reactive torque had a linear relationship. The total torque required by the SAS EPAS was found to be slightly higher than HPAS because the driver provided some portion of the total torque required to steer. SAS EPAS can still offer energy saving advantages in the long run because such additional energy is only required during cornering, unlike HPAS which requires its hydraulic pump to be running all the time when a vehicle is running.

The last task which completed the design of SAS was the addition of active control to the system. An example of a control to change vehicle understeer gradient based on vehicle speed was selected. The simulation results showed that the selected control which was implemented on the SAS full vehicle model could change the original vehicle characteristics to the desired characteristics. The characteristics of the original vehicle could be changed to either being oversteer or understeer by applying additional power-assisted torque or applying less power assistance to steer the front road wheels. The disturbance torque due to the presence of LSRS was eliminated by the reaction motor which applied equal and opposite torque to the disturbance source. During active control, the reaction motor applied torque which consisted of reactive torque and counter-disturbance torque. The reaction motor provided more torque during oversteer than during understeer. The steering feel can be enhanced during active control by allowing some amount of disturbance to be felt by the driver.

8.2. Conclusions

Based on the results and findings presented in this research, several conclusions can be drawn about the design proposal for a Semi-Active Steering (SAS) system for passenger cars:

*i. **Literature Review of Previous Work***

- Based on the previous work and main disadvantages found in active-steering (with the presence of a rigid shaft) and steer-by-wire, it was concluded SAS should be designed to possess a low stiffness resilience shaft (LSRS) that combined the advantages offered by active-steering and steer-by-wire. The LSRS provided basic steering in the event of system failure; and its flexibility allows steering intervention to be performed.
- The control algorithm of the SAS system would be segregated into power assistance and active control, to be separately developed.
- The SAS power assistance would operate using Electrical Power-Assisted Steering (EPAS) which power boost characteristics would follow the ideal curve of a Hydraulic Power Assisted Steering (HPAS).
- For the implementation of active control, any types of control strategies implemental on either active steering or steer-by-wire should be applicable to the SAS system.

*ii. **Simulation Results of Mathematical Models***

<u>Modelling of a cornering car fitted with hydraulic power assisted steering</u>

- The graphical results of steering gear stiffness and feel versus lateral acceleration and yaw velocity have enhanced understanding in analyzing the performance and characteristics of a hydraulic power-assisted steering.
- The performance of the hydraulic power-assisted steering system fitted on the Jaguar car was found to assist the driver during parking, provide more steering gear

stiffness at high lateral acceleration and yaw velocity, increase the driver's feel at the steering wheel during low speed manoeuvring, and prevent forces from being transmitted through the steering column at high lateral acceleration as well as yaw velocity.

- The characteristics of the power boost curve of the Jaguar car had some similarities to the ideal hydraulic power assisted steering presented in Section 2.5.1.2.

Detailed modelling of a cornering vehicle fitted with a flexible steering column

- Preliminary results showed that the suitable steering shaft stiffness for the experimental work were 5 Nm/rad, 10 Nm/rad and 15 Nm/rad which were determined based on the range of overshoots.
- The shaft with a minimum acceptable stiffness value which causes the vehicle to be stable without overshoot during system failure was found to be the best of all mainly due to the flexibility of the shaft enables it to have packaging advantage. The characteristics of the curves are also similar to the conventional vehicle but with different magnitudes.
- The best choice of damping properties was either to have a minimum or a maximum acceptable value. The advantage of a high damping value was that vehicle behaviour tends to follow the behaviour of the conventional vehicle during failure. The main disadvantage was that the packaging benefit was sacrificed. It was therefore concluded that the minimum damping value was the most preferable.
- Although having acceptable low stiffness and low damping values are preferable, the steering ratios are increased and this requires faster response time to control the steering wheel.
- Further analysis showed that the steering wheel speed would adjust automatically depending on the torque applied at the steering wheel. If the stiffness is low, the

turning of the steering wheel will be light and the steering wheel speed will increase. The car is definitely safe to be driven under this condition but the performance may be under par as compared to the conventional system during failure.

Simplified modelling of a cornering vehicle fitted with a flexible steering column

- The simplified mathematical model of a cornering vehicle fitted with a flexible shaft was accurate to predict vehicle behaviour in this research with less than 5% relative error compared to the detailed model.
- The trend of error may be different for other vehicles due to the difference in parameters. However, the magnitude of error is very small and the same may apply to vehicle of different parameters. The derived simplified formula is convenient for use during preliminary design stage where quick results are expected.

iii. Experimental Results

Cornering along a medium curve

- The experimental results have shown that an experimental vehicle fitted with a flexible shaft of stiffness as low as 5 Nm/rad could provide stability and be safe to drive during cornering tests, judging from the plots of yaw velocity and lateral acceleration which behaved similarly to the conventional vehicle.
- The test vehicle became more stable as vehicle speed was increased. These results verified the proposal of implementing LSRS. However, further testing at higher speeds would be recommended as the maximum permissible speed during the experiment was only 30 km/h.

Single lane change in the verge of skidding

- Based on the experimental results which agreed with the theoretical formula, it was concluded that the derived mathematical formula were valid for predictions in order to obtain better understanding of vehicle behaviour during SAS failure when fitted with different properties of steering shaft.

- The theoretical formula could also be used to predict vehicle performance at extreme conditions where it was impossible or impractical to perform experiments.

iv. Concepts and Design of SAS

- The embodiment of the SAS system is similar to the Electrical Power-Assisted Steering system which is simple in construction.
- The semi-active steering (SAS) for a passenger car has more advantages than the steer-by-wire (SBW) in terms of the safety aspects.
- The SAS system could also offer similar advantages as SBW and any control that could be implemented on SBW could also be implemented on SAS but with some constraints depending on the design of LSRS.
- The disturbance rejection concept of using a reaction motor which supplied equal and opposite torque to counter the source was very practical since the information of torque could be obtained from the rotation of power motor.
- The SAS system might become a stepping stone for SBW to prove its ground, and the process would take a very long time until customers fully gain their confidence levels.

v. Full Vehicle Software Model Development

- The full vehicle software model was validated using the mathematical model of a cornering vehicle fitted with hydraulic power-assisted steering. The software models and the MATLAB/SIMULINK models were in close agreement. The model would be used to demonstrate the working concepts of the SAS system and to show how the system performance can meet the requirements of a robust steering system.

- The power boost curve of HPAS was converted to represent a specified mathematical formula so that it could be implemented on EPAS efficiently.
- The selected control strategy was to vary the understeer gradient of a car depending on its forward speed. At low vehicle speed, the vehicle was required to oversteer for quick response during parking. At common driving speed, neutral steer was preferable. While at high speed, the vehicle was required to understeer to eliminate driving sensitivity.

vi. Simulation Results of the SAS System

Power Boost Curve optimisation

- Suitable values for α_0 and d had been determined from an optimisation process involving iterative method; and also based on the knowledge of the required steering wheel torque during normal driving.
- The complete system may be able to be optimized by considering the slope m as one of the parameters and adding a constraint that the sum of power-assisted torque and steering wheel torque should be constant.

Performance of Power Assistance

- The characteristic of power assistance for SAS EPAS was similar to HPAS, but SAS EPAS required higher torque for operation because it was a fully power-assistance system. Although this is the case, SAS EPAS can still offer energy saving advantages because additional power is only required during cornering. HPAS requires its hydraulic pump to be running all the time when a vehicle is being driven.

- The reactive torque of SAS EPAS had a better characteristic in terms of steering requirements; viz. low steering wheel torque at low speed and high steering wheel torque at high speed. The characteristic of steering wheel torque was also changed from linear to non-linear behaviour. The SAS EPAS system also allows improvement of reactive torque through active control depending on requirements.

Implementation of Active Control

- The simulation results had shown that a selected control implemented on the SAS full vehicle software model could change the original vehicle characteristics to desired vehicle characteristics. The original vehicle (which had an understeer characteristic at low speed and medium speed) could be changed to be over-steer and neutral steer by applying additional power-assisted torque to turn the front steered wheels. Likewise, an under-steer characteristic at high vehicle speed could be achieved by applying less power assistance to turn the front road wheels.
- During active control, disturbance torque was eliminated by the reaction motor which applied equal and opposite torque to the disturbance source. The reaction motor applied the sum of reactive torque and counter-disturbance torque during control; it would provide more torque during over-steer than during under-steer.
- The steering feel could be enhanced by allowing some amount of disturbance to be felt by the driver so that the driver could judge on what was happening at the road wheels.

vii. General

- This research had provided some fundamental knowledge and proposals on the design of SAS system which could be used for the development of prototypes in the future.

- Due to its better safety aspects than SBW and its capability to maintain most advantages offered by SBW, SAS might be fitted to most passenger cars in the future.

8.3. Recommendations for Future Research

There are many opportunities for further research in this field and the recommendations for future work are as follows:

i. Construct an actual prototype of the complete SAS system based on the design presented in this thesis.

ii. Perform experiments on the prototype stated above.

iii. Design and fabricate a LSRS based on the recommendation stated in Chapter 5.

iv. Optimize all parameters used to construct the power boost characteristic curve.

v. Evaluate different types of active control to be implemented in the SAS.

vi. Perform different types of testing for vehicle performance assessment and also at higher vehicle speeds.

References

Ackermann, J. (1998). Active Steering for Better Safety, Handling and Comfort. *Proceedings of Advances in Vehicle Control and Safety*, (pp. 1-10). Amiens, France, July 1-3,1998.

Ackermann, J. (1994). Robust Decoupling of car Steering Dynamics with Arbitrary Mass Distribution. *Proceedings of the 1994 American Control Conference.* Baltimore, Maryland, TPI-5:00.

Ackermann, J., & Bünte, T. (1998). Handling Improvement of Robust Car Steering. *Proc. International Conference on Advances in Vehicle Control and Safety*, (pp. 112-117). Amiens, France, July 1998.

Ackermann, J., & Bünte, T. (1999). Robust Prevention of Limit Cycles for Robustly Decoupled Car Steering Dynamics. *Kybernetica, 35(1)* , 105-106.

Ackermann, J., & Bunte, T. (1997). Automatic Car Steering Control Bridges Over the Driver Reaction Time. *Kybernetika, Number 1* , 61-74.

Ackermann, J., & Bunte, T. (1996). Yaw Disturbance Attenuation by Robust Decoupling of Car Steering. *Proceedings of the IFAC World Congress*, (pp. 1-6). San Francisco, CA, 1996.

Ackermann, J., Bunte, T., & Odenthal, D. (1999). Advantages of Active Steering for Vehicle Dynamics and Control. *Proc. 32nd International Symposium on Automotive Technology and Automation*, (pp. 263-270). Vienna, 1999.

Ackermann, J., T. Bünte, T., Sienel, W., Jeebe, H., & Naab, K. (1996). Driving Safety by Robust Steering Control. *Proc. Int. Symposium on Advanced Vehicle Control.* Aachen, germany, June 1996.

Ackermann, J., Walter, W., & Bunte, T. (2004). Automatic Car Steering Using Robust Unilateral Decoupling. *International Conference on Advances in Vehicle Control and Safety.* Genoa, Italy October 2004.

ADAMS. (2005). MSC ADAMS 2005 Online Help, ADAMS/car, ADAMS/tire – Tire Models.

Adams, F. J. (1983). Power Steering 'Road Feel' . *SAE Technical Paper Series, 830998* .

Agebro, M., Nilsson, A., & Stensson Trigell, A. (2006). Driver Preferences of Steering Gear ratio and Steering Wheel Effort – A Driving Simulator Study. *F2006V079, FISITA 2006* . Japan.

Amberkar, S., Bolourchi, F., Demerly, J., & Millsap, S. (2004). A Control System Methodology for Steer-by-Wire Systems. *SAE Technical Paper Series* , 2004-01-1106.

Aneke, N., Ackermann, J., Bünte, T., & Nijmeijer, H. (1999). Application of Nonlinear Disturbance Decoupling to Active Car Steering. *Proc. European Control Conference.* Karlsruhe, Germany 1999.

Augustine, M. J. (2006). Mechanically linked active steering system. *United States Patent No.: 7063636.* www.freepatentsonline.com/7063636. html.

Badawy, A., Zuraski, J., Bolourchi, F., & Chandy, A. (1999). Modelling and Analysis of an Electric Power Steering System. *SAE Technical paper Series, 1999-01-0399* .

Baharom, M. B., Hussain, K., & Day, A. J. (2006). Mathematical Modelling of a Cornering Vehicle Fitted with Hydraulic-Power Assisted Steering. *FISITA 2006.* Japan, F2006V019.

Baxter, J. (1988). Analysis of Stiffness and Feel for a Power-Assisted Rack and Pinion Steering Gear. *SAE Technical Paper Series 880706* .

BMW. (2008). *www.bmw.com, "BMW Technology Guide", Active Steering.*

BRITISH STANDARD. (2003). *Road Vehicles – Lateral Transient Response Test Methods – Open-Loop Test Methods* . BS ISO 7401:2003.

Bunte, T., Odenthal, D., & Aksun-Guvenc, B. (2002). Robust Vehicle Steering Control Design Based on the Disturbance Observer. *PERGAMON, Annual Reviews in Control 26(2002)* , 139-149.

Camuffo, I., Caviasso, G., Pascali, L., & Pesce, M. (2002). Simulation Tools and Evaluation Criteria for Steering Wheel Feel Improvement of an Electric Power Steering System. *SAE Technical Paper Series 2002-01-1593* .

Cesiel, D., Gaunt, M. C., & Daugherty, B. (2006). Development of a Steer-by-Wire System for the GM Sequel. *SAE Technical Paper Series* , 2006-01-1173.

Chai, Y. W. (2004). A study of Effect of Steering Gain and Steering Torque on Driver's Feeling for SBW Vehicle. *FISITA 2004.* Barcelona.

Coudon, J., Canudas-de-Wit, C., & Claeys, X. (2006). A New Reference Model for Steer-by-Wire Applications with Embedded Vehicle Dynamics. *American Control Conference, 14-16 June 2006.*

Data, S., Pesce, M., & Reccia, L. (2004). Identification of Steering System Parameters by Experimental Measurements Processing. *Proceedings of the Institution of Mechanical Engineers, IMechE 2004, Vol. 218 Part D: J. Automobile Engineering D05403* .

Davis, F. W. (1945). Power Steering for Automotive Vehicles. *SAE Journal, 1945* , VOL LIII, 239-254.

Dorf, R. C., & Bishop, R. H. (2005). *Modern Control System.* International Edition, 10th Edition, Prentice Hall, c 2005.

Gadda, C. D., Yih, P., & Gerdes, J. C. (2004). Incorporating a Model of Vehicle Dynamics in a Diagnostic System for Steer-by-Wire Vehicles. *Proceedings of the International Symposium on Advanced Vehicle Contol (AVEC).* Arnhem, Netherlands.

Gaspar, P., Szaszi, I., & Bokor, J. (2003). Rollover Avoidance for Steer-by-Wire Vehicles by Using Linear Parameter Varying Methods. *Mediterranean Conference on Control and Automation, 2003.*

Genta, G. (1997). *Motor Vehicle Dynamics-Modelling and Simulation.* Series for Advances in Mathematics for Applied Sciences-Vol. 43, World Scientific.

George, G., Lendaris, G., Schultz, L., & Shannon, T. (2000). Adaptive Critic Design for Intelligent Steering and Speed Control of a 2-Axle Vehicle. *IJCNN'2000 (Jan 2000).* Italy.

Gillespie, T. D. (1992). *Fundamentals of Vehicle Dynamics.* Society of Automotive Engineers (SAE), 1992.

Gjurkov, I., Danev, D., & Kosevski, M. Study of the Effect of Active Rear Steering on Vehicle's Response in Co-Simulation Environment. *BEOGRAD 2005 EAEC European Automotive Congress.* EAEC05YU-AS13.

Guldner, J., Sienel, W., Tan, H.-S., Ackermann, J., Patwardhan, S., & Bünte, T. (1999). Robust Automatic Steering Control for Look-Down Reference Systems with Front and Rear Sensors. *IEEE Trans. on Control Systems Technology, 7, no. 1:2-11,1999.*

Guldner, J., W., S., Ackermann, J., & al, e. Robust Control Design for Automatic Steering Based on Feedback of Front and Tail Lateral Displacement. *Proc. 4th European Control Conference.* Brussels, Belgium, 1997.

Hac, A. (2006). Control of Brake-and Steer-by-Wire Systems during Brake Actuator Failure. *SAE Technical Paper Series* , 2006-01-0923.

Harrer, M., Pfeffer, P. E., & Johnston, D. N. Steering Feel – Objective Assessment of Passenger cars Analysis of Steering Feel and Vehicle Handling. *F2006V165, FISITA 2006* . Japan.

Huh, K., Seo, C., Kim, J., & Hong, D. (1999). Active Steering Control Based on the Estimated Tyre Forces. *Proceedings of the American Control Conference.* San Diego, California, June 1999.

Husain, M., Daugherty, B., & Oynoian, J. (2004). Motor Vehicle Steering System. *United States Patent Application Publication.* Pub. No.: US 2004/0262073 A1, 2004, Appl. No.: 10/610,123.

Itoh, K. (2006). Steering Apparatus for Vehicle. *United States Patent Application Publication.* Pub. No.: US 2006/0042859 A1, 2006, Appl. No.: 11/206,944.

John C. Dixon, J. C. (1996). *Tires, suspension and handling.* London: Society of Automotive Engineers, c1996. 2nd edition.

Kader, A. (2006). *Steer-by-Wire Control System.* Engineering Senior Design Project, Swarthmore College Department of Engineering, May 2006, USA, http://www.engin.swarthmore.edu/academics/courses/e90/2005_6/E90Reports/AK_Final.pdf.

Kanagawa, N. F., Kanagawa, T. N., Kanagawa, K. S., Kanagawa, S. T., Kanagawa, Y. K., & Saitama, M. (2005). Steering Control System. *United States Patent Application Publication.* Pub. No.: US 2005/0016791 A1, 2005, Appl. No.: 10/897,125.

Kasselmann, J., & Keranen, T. (1969). Adaptive Steering. *Bendix Technical Journal, 1969* , 26-35.

Kerr, J. (2003, Nov 12). *CanadianDriver, 'BMW's Active Steering', Canada's Online Auto magazine*. Retrieved from www.canadiandriver.com/articles/jk/031112.htm.

Krautstrunk, A., & Mutschler, P. (2000). Fault Tolerant Force Feedback Actuator for Steer-by-Wire. *MECHATRONICS 2000.* Atlanta, Georgia, USA.

Li, D., Shen, X., & Yu, F. (2006). Study on the Chassis Control Integration Based on Tyre Slip Ratio Regulation and Active Steering Control. *F2006V177, FISITA 2006.* Japan.

Liao, Y. B., & Du, H. I. (2003). Modelling and Analysis of Electric Power Steering System and its Effect on Vehicle Dynamic Behaviour. *Int. Journal of Vehicle Autonomous Systems (IJVAS), Vol. 1, No.2, 2003.*

McCann, R. (2000). Variable Effort Steering for Vehicle Stability Enhancement Using an Electric Power Steering System. *SAE Technical Series, 2000-01-0817* .

Milliken, W. F., & Milliken, D. L. (1995). *Race car vehicle dynamics.* Society of Automotive Engineers, c1995.

Mitsuhiro, M., & Yoshiteru, M. (2001). Vehicular Steering Gear. *Japanese Patent Application Publication.* Patent No.: JP2001001907, 2001, Application No.: JP19990176538 19990623.

National Science and Technology Council Committee on Technology. (Nov 2000). *Review of Federal Program of Wire System Safety, Final Report.* USA: Wire System Safety Interagency Working Group, http://www.ostp.gov/pdf/wire_rpt.pdf.

O'Brien, R., Urban, T., & Iglesias, P. (1995). Lane Change Maneuver via Modern Steering Control Methods. *1995 IVHS America Conference.*

Odenthal, D., Bünte, T., & Ackermann, J. (1999). Nonlinear Steering and Braking Control for Vehicle Rollover Avoidance. *Proc. European Control Conference.* Karlsruhe, Germany 1999.

Oh, S., Chae, H., Yun, S., & Han, C. (2004). The Design of A Controller for th Steer-by-Wire System. *JSME International Journal* , Series C, Vol.47, No.3.

Pacejka, H. B. (2002). *Tire and Vehicle Dynamics.* Oxford : Butterworth Heinemann, Society of Automotive Engineers, 2002.

Pang, D.-Y., Jang, B.-C., & Lee, S.-C. (2005). Steering Wheel Torque Control of Electric Power Steering by PD-Control. *ICCAS2005, June 2005, KINTEX.* Gyeonggi-Do, Korea.

Pfeffer, P. E., Harrer, M., Johnston, D., & Shinde, R. P. (2006). Modelling of a Hydraulic Steering System. *F2006V164, FISITA 2006.* Japan.

Pimentel, J. (2004). An Architecture for a Safety-Critical Steer-by-Wire System. *SAE Technical Paper Series* , 2004-01-0714.

Pimentel, J. R. (2006). Verification and Validation of a Safety-Critical Steer-by-Wire System Using DO-178B. *SAE Technical Paper Series* , 2006-01-1447.

Post, J. W., & Law, E. H. (1996). Procedure for the Characterization of Friction in Automobile Power Steering Systems. *SAE Technical Paper Series, 960933* .

Reimpell, J., Stoll, H., & Betzler, J. (2001). *The Automotive Chassis, Engineering Principles.* Second Edition, Butterworth Heinemann.

Riccardo, M., Stefano, S., & Fabio, C. (2006). Active Front and Rear Steering Control in Four Wheel Steering Vehicles. *F2006V089, FISITA 2006.* Japan.

Rossetter, E., & Gerdes, J. (2002). A Study of Lateral Vehicle Control under a 'Virtual' Force Framework. *In Proc. Int'l Symp. Advanced Vehicle Control, Jan 2002.*

Rossetter, E., Switkes, J., & Gerdes, J. (2003). A Gentle Nudge Towards Safety: Experimental Validation of the Potential Field Driver Assistance System. *American Control Conference, 2003.* Proceedings of the 2003, Volume 5, Issue, 4-6 June 2003.

Rosth, M. (2007). *Hydraulic Power Steering Design in Road Vehicles: Analysis, Testing and Enhanced Functionality.* PhD Dissertation No. 1068, Linkoping University, Sweden, www.diva-portal.org.

Sawyer, C. (2008). *Nearly Steer-by-Wire.* Retrieved from Automotive Design and Production,Gardner Publications Ltd.: www.autofieldguide.com

Segawa, M., Kimura, S., Kada, T., & Nakano, S. (2002). A Study of Reactive Torque Control for Steer by Wire System. *Proc. of the Intl. Symp. on Advanced Vehicle Control (AVEC)*, (pp. 653-657).

Segawa, M., Nakano, S., Nishihara, O., & Kumamoto, H. (2001). Vehicle Stability Control Strategy for Steer-by-Wire System. *Society of Automotive Engineers of Japan, Inc. and Elsevier Science B. V.* , PII: S0389-4304(01) 00144-8.

Sharp, R., & Valtetsiotis, V. (2001). Optimal Preview Car Steering Control. *Vehicle System Dynamics, May 2001*, (pp. 101-117).

Sherwin, K. A., & DuCharme, R. T. (2003). Steer-by-Wire Steering Apparatus with Actuatable Mechanism. *United States Patent Application Publication.* Pub. No.: US 2003/0141134 A1, 2003, Appl. No.: 10/059,983.

Shutto, S., & LeRoy, D. (2006). MR Technology, Tactile Feedback, and Application in By-Wire Systems. F2006V191, FISITA 2006 Japan.

Song, Y., Simonot-Lion, F., & Clement, T. (2001). Song, YQ.; SimoEvaluating Quality of Service and Behavioural Reliability of Steer-by-Wire Systems. *LORIA-PSA Peugeot-Citroen.* http://www.iestcfa.org/bestpaper/etfa03/etfa03_simonot.pdf.

Sugiyama, A., Kurishige, M., Hamada, H., & Kaifuku, T. (2006). An EPS Control Strategy to Reduce Steering Vibration Associated with Vibrations from Road Wheels. *F2006V133, FISITA 2006*. Japan.

Switkes, J. P., Coe, I. A., & Gerdes, J. C. (2004). Using MEMS Accelerometers to Improve Automobile Handwheel State Estimation for Force Feedback. *2004 ASME International mechanical Engineering Congress and Exposition, Proceedings of IMECE '04.* Anaheim, CA, USA, IMECE2004-62183.

Switkes, J. P., Rossetter, E. J., Coe, I. A., & Gerdes, J. C. (2004). Handwheel Force Feedback for Lanekeeping Assistance: Combined Dynamics and Stability. *Proceedings of the International Symposium on Advanced Vehicle Control (AVEC).* Arnhem, Netherlands.

Ueki, N., Kubo, J., Takayama, T., Kanari, I., & Uchiyama, M. (n.d.). Vehicle Dynamics Electric Control Systems for Safe Driving. *The Automotive Systems, Hitachi, Ltd., www.hitachi.com/ICSFiles/afieldfile/2004/11/26/r2004_04_104_3.pdf.*

VISTEON, www.visteon.com, "Electric Power Assisted Steering" . (n.d.). Retrieved from www.visteon.com/products/automotive/media/power_steering_spec.pdf.

Wittmeijer, H. H. (2004). Electric Steering System with Mechanical Back-up Device. *United States Patent Application Publication.* Pub. No.: US 2004/0007418 A1, 2004, Appl. No.: 10/332,694, PCT No.: PCT/NL01/00538.

Wong, J. Y. (2001). *Theory of Ground Vehicles.* Third Edition, John Wiley & Sons, Inc., 2001.

Wong, T. (2001). Hydraulic Power Steering System Design and Optimization Simulation. *SAE Technical Paper Series, 2001-01-0479* .

Yamakawa, H., Sakai, Y., Yamamoto, Y., Barber, A., & Wakabayashi, Y. (2002). An Application of Full Vehicle ADAMS Modelling with Detailed Force Elements: Collaborative Activity Among Design, Experiment & CAE in the Field of Vehicle Dynamics. *Neosimulation Engineering.* http://www.neosim.com/publications.htm.

Yao, Y. (2006). Vehicle Steer-by-Wire System Control. *SAE Technical Paper Series* , 2006-01-1175.

Yasui, Y., Kodama, H., Momiyama, M., & Kato, H. (2006). Electronic Stability Control (ESC) Coordinated with Electric Power Steering (EPS). *F2006V195, FISITA 2006.* Japan.

Yih, P. (2005). *Steer-by-Wire: Implications for Vehicle Handling and Safety.* PhD Dissertation, Stanford University, http://gradworks.umi.com/31/53/3153217.html.

Yih, P., & Gerdes, J. C. (2004). Steer-by-Wire for Vehicle State Estimation and Control. *Proceedings of the International Symposium on Advanced Vehicle Control (AVEC), Arnhem, Netherlands.*

Yih, P., Ryu, J., & Gerdes, J. (2004). Vehicle State Estimation Using Steering Torque. *American Control Conference, 2004* (pp. 2116-2121 Vol.3). Issue June 30 - July 2 2004.

Yoshiyuki, S. (2006). Steer-by-Wire System. *Japanese Patent Application.* Pub. No.: 2006-027494, 2006, Appl. No.: 2004-211019.

You, S.-S., & Jeong, S.-K. (2002). Controller Design and Analysis for Automatic Steering of Passenger Cars. *PERGAMON, Mechatronics 12 (2002)* , 426-446.

Zaremba, A. T., Liubakka, M. K., & Stuntz, R. M. (1998). Zaremba, A. T.; Liubakka,Control and Steering Feel Issues in the design of An Electric Power Steering System. *Proceedings of the American Control Conference.* Philadelphia, June 1998.

APPENDIX 1

1 (a) Simplified Data of JAGUAR car (X-Type 2.2L TD) for Mathematical Models

Constants	Descriptions	Value	Unit
m	Total vehicle mass	*	kg
m_s	Total sprung mass	*	kg
m_{uf}	Total front unsprung mass	*	kg
m_{ur}	Total rear unsprung mass	*	kg
F_{fl}	Front left static axle load	*	N
F_{fr}	Front right static axle load	*	N
F_{rl}	Rear left static axle load	*	N
F_{rr}	Rear right static axle load	*	N
L	Wheelbase	*	m
a	Distance from c.g. to front contact patch	*	m
b	Distance from c.g. to rear contact patch	*	m
$c_{c.g}$	Offset distance of c.g. from vehicle centreline	*	m
c	Unsprung mass offset from vehicle centreline	*	m
e	Unsprung mass longitudinal offset from c.g.	*	m
h_s	Height of sprung mass from ground	*	m
h	Height of sprung mass to the roll axis	*	m
V_x	Longitudinal forward speed	*	$\frac{m}{s}$
$C_{F\alpha f}$	Total front lateral force cornering stiffness due to slip angle	*	$\frac{N}{rad}$
$C_{F\alpha r}$	Total rear lateral force cornering stiffness due to slip angle	*	$\frac{N}{rad}$
$C_{F\gamma f}$	Total front lateral force cornering stiffness due to camber angle	*	$\frac{N}{rad}$

APPENDIX 1

$C_{F\gamma r}$	Total rear lateral force cornering stiffness due to camber angle	*	$\frac{N}{rad}$
$C_{M\alpha f}$	Total front self aligning moment cornering stiffness due to slip angle	*	$\frac{Nm}{rad}$
$C_{M\alpha r}$	Total rear self aligning moment cornering stiffness due to slip angle	*	$\frac{Nm}{rad}$
$C_{M\gamma f}$	Total front self aligning moment cornering stiffness due to camber angle	*	$\frac{Nm}{rad}$
$C_{M\gamma r}$	Total rear self aligning moment cornering stiffness due to camber angle	*	$\frac{Nm}{rad}$
$k_{f\gamma\phi}$	Front roll-camber coefficient	*	$\frac{rad}{rad}$
$k_{r\gamma\phi}$	Rear roll-camber coefficient	*	$\frac{rad}{rad}$
$I_{xx\,S}$	Sprung mass roll inertia	*	$kg \cdot m^2$
$I_{xz\,S}$	Sprung mass x-z product inertia	*	$kg \cdot m^2$
I_{zz}	Total yaw inertia	*	$kg \cdot m^2$
h_{uf}	c.g. height of front unsprung mass	*	m
h_{ur}	c.g. height of rear unsprung mass	*	m
h_f	Height of front roll centre	*	m
h_r	Height of rear roll center	*	m
θ_r	Approximated roll axis slope	*	rad
T_f	Front track width	*	m
T_r	Rear track width	*	m
r_{statf}	Average front static loaded tyre radius	*	m
r_{statr}	Average rear static loaded tyre radius	*	m
r_{dyn}	Calculated front dynamic loaded tyre radius	*	m

APPENDIX 1

K_{fx}	Average front spring stiffness	*	$\frac{N}{m}$
K_{rx}	Average rear spring stiffness	*	$\frac{N}{m}$
C_{fx}	Average front damper constant	*	$\frac{Ns}{m}$
C_{rx}	Average rear damper constant	*	$\frac{Ns}{m}$
d_f	Length from front inner lower control arm joint to tyre contact patch	*	m
d_r	Length from rear inner lower control arm joint to tyre contact patch	*	m
d_{2f}	Length from front spring lower joint to inner lower control arm joint	*	m
d_{2r}	Length from rear spring lower joint to inner lower control arm joint	*	m
h_{jf}	Height from sprung mass attached to front jounce control to the tyre contact patch.	*	m
h_{jr}	Height from sprung mass attached to rear jounce control to the tyre contact patch.	*	m
w_{sf}	Length of front sprung mass joint to joint of jounce orientations	*	m
w_{sr}	Length of rear sprung mass joint to joint of jounce orientations	*	m
w_{af}	Length of front axle	*	m
w_{ar}	Length of rear axle	*	m
h_{lf}	Height of front lower arm inner joint	*	m
h_{lr}	Height of rear lower arm inner joint	*	m

* These data are company confidential and can only be accessed by their permission. Please contact the author for more information.

APPENDIX 1

1 (b) Tyre File (source - ADAMS 2005 R1)

```
                                     pac2002_195_65R15
[MDI_HEADER]
FILE_TYPE                  ='tir'
FILE_VERSION               =3.0
FILE_FORMAT                ='ASCII'
! : TIRE_VERSION :         PAC2002
! : COMMENT :              Tire                     195/65 R15
! : COMMENT :              Manufacturer
! : COMMENT :              Nom. section with  (m)   0.195
! : COMMENT :              Nom. aspect ratio  (-)   65
! : COMMENT :              Infl. pressure    (Pa)   220000
! : COMMENT :              Rim radius         (m)   0.19
! : COMMENT :              Measurement ID
! : COMMENT :              Test speed       (m/s)   16.6
! : COMMENT :              Road surface
! : COMMENT :              Road condition           Dry
! : FILE_FORMAT :          ASCII
! : Copyright MSC.Software, Fri Jan 23 15:21:20 2004
!
! USE_MODE specifies the type of calculation performed:
!       0: Fz only, no Magic Formula evaluation
!       1: Fx,My only
!       2: Fy,Mx,Mz only
!       3: Fx,Fy,Mx,My,Mz uncombined force/moment calculation
!       4: Fx,Fy,Mx,My,Mz combined force/moment calculation
!     +10: including relaxation behaviour
!      *-1: mirroring of tyre characteristics
!
!    example: USE_MODE = -12 implies:
!       -calculation of Fy,Mx,Mz only
!       -including relaxation effects
!       -mirrored tyre characteristics
!
$----------------------------------------------------------------units
[UNITS]
LENGTH                     ='meter'
FORCE                      ='newton'
ANGLE                      ='radians'
MASS                       ='kg'
TIME                       ='second'
$----------------------------------------------------------------model
[MODEL]
PROPERTY_FILE_FORMAT       ='PAC2002'
USE_MODE                   = 14                 $Tyre use switch (IUSED)
VXLOW                      = 1
LONGVL                     = 16.6               $Measurement speed
TYRESIDE                   = 'LEFT'             $Mounted side of tyre at vehicle/test bench
$-----------------------------------------------------------dimensions
[DIMENSION]
UNLOADED_RADIUS            = 0.312              $Free tyre radius
WIDTH                      = 0.195              $Nominal section width of the tyre
ASPECT_RATIO               = 0.65               $Nominal aspect ratio
RIM_RADIUS                 = 0.19               $Nominal rim radius
RIM_WIDTH                  = 0.1524             $Rim width
$----------------------------------------------------------------shape
[SHAPE]
{radial width}
 1.0    0.0
 1.0    0.4
 1.0    0.9
 0.9    1.0
$------------------------------------------------------------parameter
[VERTICAL]
VERTICAL_STIFFNESS         = 2e+005             $Tyre vertical stiffness
VERTICAL_DAMPING           = 50                 $Tyre vertical damping
BREFF                      = 6.1                $Low load stiffness e.r.r.
DREFF                      = 0.45               $Peak value of e.r.r.
FREFF                      = 0.01               $High load stiffness e.r.r.
FNOMIN                     = 4000               $Nominal wheel load
$-------------------------------------------------------long_slip_range
[LONG_SLIP_RANGE]
KPUMIN                     = -1.5               $Minimum valid wheel slip
KPUMAX                     = 1.5                $Maximum valid wheel slip
$------------------------------------------------------slip_angle_range
[SLIP_ANGLE_RANGE]
ALPMIN                     = -1.5708            $Minimum valid slip angle
ALPMAX                     = 1.5708             $Maximum valid slip angle
```

APPENDIX 1


```
$------------------------------------------------inclination_slip_range
[INCLINATION_ANGLE_RANGE]
CAMMIN                   = -0.26181           $Minimum valid camber angle
CAMMAX                   = 0.26181            $Maximum valid camber angle
$--------------------------------------------------vertical_force_range
[VERTICAL_FORCE_RANGE]
FZMIN                    = 200                $Minimum allowed wheel load
FZMAX                    = 9000               $Maximum allowed wheel load
$---------------------------------------------------------------scaling
[SCALING_COEFFICIENTS]
LFZO                     = 1                  $Scale factor of nominal (rated) load

LCX                      = 1                  $Scale factor of Fx shape factor
LMUX                     = 1                  $Scale factor of Fx peak friction
coefficient
LEX                      = 1                  $Scale factor of Fx curvature factor

LKX                      = 1                  $Scale factor of Fx slip stiffness
LHX                      = 1                  $Scale factor of Fx horizontal shift

LVX                      = 1                  $Scale factor of Fx vertical shift
LGAX                     = 1                  $Scale factor of camber for Fx
LCY                      = 1                  $Scale factor of Fy shape factor
LMUY                     = 1                  $Scale factor of Fy peak friction
coefficient
LEY                      = 1                  $Scale factor of Fy curvature factor

LKY                      = 1                  $Scale factor of Fy cornering stiffness

LHY                      = 1                  $Scale factor of Fy horizontal shift

LVY                      = 1                  $Scale factor of Fy vertical shift
LGAY                     = 1                  $Scale factor of camber for Fy
LTR                      = 1                  $Scale factor of Peak of pneumatic trail

LRES                     = 1                  $Scale factor for offset of residual torque

LGAZ                     = 1                  $Scale factor of camber for Mz
LXAL                     = 1                  $Scale factor of alpha influence on Fx

LYKA                     = 1                  $Scale factor of alpha influence on Fx

LVYKA                    = 1                  $Scale factor of kappa induced Fy
LS                       = 1                  $Scale factor of Moment arm of Fx
LSGKP                    = 1                  $Scale factor of Relaxation length of Fx

LSGAL                    = 1                  $Scale factor of Relaxation length of Fy

LGYR                     = 1                  $Scale factor of gyroscopic torque
LMX                      = 1                  $Scale factor of overturning couple
LVMX                     = 1                  $Scale factor of Mx vertical shift
LMY                      = 1                  $Scale factor of rolling resistance torque

$----------------------------------------------------------longitudinal
[LONGITUDINAL_COEFFICIENTS]
PCX1                     = 1.839              $Shape factor Cfx for longitudinal force

PDX1                     = 1.1387             $Longitudinal friction Mux at Fznom
PDX2                     = -0.11999           $Variation of friction Mux with load

PDX3                     = -2.2142e-005       $Variation of friction Mux with camber

PEX1                     = 0.62727            $Longitudinal curvature Efx at Fznom

PEX2                     = -0.12336           $Variation of curvature Efx with load

PEX3                     = -0.03448           $Variation of curvature Efx with load
squared
PEX4                     = -1.5066e-005       $Factor in curvature Efx while driving

PKX1                     = 18.886             $Longitudinal slip stiffness Kfx/Fz at Fznom

PKX2                     = -3.988             $Variation of slip stiffness Kfx/Fz with
load
PKX3                     = 0.21542            $Exponent in slip stiffness Kfx/Fz with load
```

APPENDIX 1


```
PHX1                    = -0.00033912          $Horizontal shift Shx at Fznom
PHX2                    = -8.5877e-006         $Variation of shift Shx with load
PVX1                    = -4.638e-006          $Vertical shift Svx/Fz at Fznom
PVX2                    = 1.9874e-005          $Variation of shift Svx/Fz with load

RBX1                    = 5.9945               $Slope factor for combined slip Fx reduction

RBX2                    = -8.2609              $Variation of slope Fx reduction with kappa

RCX1                    = 1.7816               $Shape factor for combined slip Fx reduction

REX1                    = 1.644                $Curvature factor of combined Fx
REX2                    = -0.0064359           $Curvature factor of combined Fx with load

RHX1                    = 0.008847             $Shift factor for combined slip Fx reduction

PTX1                    = 1.85                 $Relaxation length SigKap0/Fz at Fznom

PTX2                    = 0.000109             $Variation of SigKap0/Fz with load
PTX3                    = 0.101                $Variation of SigKap0/Fz with exponent of
load
$------------------------------------------------------------------overturning
[OVERTURNING_COEFFICIENTS]
QSX1                    = 0                    $Lateral force induced overturning moment

QSX2                    = 0                    $Camber induced overturning couple
QSX3                    = 0                    $Fy induced overturning couple
$----------------------------------------------------------------------lateral
[LATERAL_COEFFICIENTS]
PCY1                    = 1.3223               $Shape factor Cfy for lateral forces

PDY1                    = 1.0141               $Lateral friction Muy
PDY2                    = -0.12274             $Variation of friction Muy with load

PDY3                    = -1.0426              $Variation of friction Muy with squared
camber
PEY1                    = -0.63772             $Lateral curvature Efy at Fznom
PEY2                    = -0.050782            $Variation of curvature Efy with load

PEY3                    = -0.27333             $Zero order camber dependency of curvature
Efy
PEY4                    = -8.3143              $Variation of curvature Efy with camber

PKY1                    = -19.797              $Maximum value of stiffness Kfy/Fznom

PKY2                    = 1.7999               $Load at which Kfy reaches maximum value

PKY3                    = 0.0095418            $Variation of Kfy/Fznom with camber
PHY1                    = 0.0011453            $Horizontal shift Shy at Fznom
PHY2                    = -6.6688e-005         $Variation of shift Shy with load
PHY3                    = 0.044112             $Variation of shift Shy with camber
PVY1                    = 0.031305             $Vertical shift in Svy/Fz at Fznom
PVY2                    = -0.0085749           $Variation of shift Svy/Fz with load

PVY3                    = -0.092912            $Variation of shift Svy/Fz with camber

PVY4                    = -0.27907             $Variation of shift Svy/Fz with camber and
load
RBY1                    = 6.2238               $Slope factor for combined Fy reduction

RBY2                    = 3.0734               $Variation of slope Fy reduction with alpha

RBY3                    = 0.016076             $Shift term for alpha in slope Fy reduction

RCY1                    = 1.0051               $Shape factor for combined Fy reduction

REY1                    = 0.019749             $Curvature factor of combined Fy
REY2                    = -0.0020691           $Curvature factor of combined Fy with load

RHY1                    = -0.0010319           $Shift factor for combined Fy reduction

RHY2                    = 7.4123e-006          $Shift factor for combined Fy reduction with
load
RVY1                    = 0.02962              $Kappa induced side force Svyk/Muy*Fz at
Fznom
RVY2                    = -0.011053            $Variation of Svyk/Muy*Fz with load
```

APPENDIX 1


```
RVY3                    = -0.0009317    $Variation of Svyk/Muy*Fz with camber
RVY4                    = 11.842        $Variation of Svyk/Muy*Fz with alpha
RVY5                    = 1.9           $Variation of Svyk/Muy*Fz with kappa
RVY6                    = 0             $Variation of Svyk/Muy*Fz with atan(kappa)
PTY1                    = 1.9           $Peak value of relaxation length SigAlp0/R0
PTY2                    = 2.25          $Value of Fz/Fznom where SigAlp0 is extreme
$----------------------------------------------------------rolling resistance
[ROLLING_COEFFICIENTS]
QSY1                    = 0.01          $Rolling resistance torque coefficient
QSY2                    = 0             $Rolling resistance torque depending on Fx
QSY3                    = 0             $Rolling resistance torque depending on
speed
QSY4                    = 0             $Rolling resistance torque depending on
speed ^4
$-------------------------------------------------------------------aligning
[ALIGNING_COEFFICIENTS]
QBZ1                    = 7.5088        $Trail slope factor for trail Bpt at Fznom
QBZ2                    = -1.9428       $Variation of slope Bpt with load
QBZ3                    = 0.61681       $Variation of slope Bpt with load squared
QBZ4                    = 0.12231       $Variation of slope Bpt with camber
QBZ5                    = 0.50016       $Variation of slope Bpt with absolute camber
QBZ9                    = 5.5144        $Slope factor Br of residual torque Mzr
QBZ10                   = 0             $Slope factor Br of residual torque Mzr
QCZ1                    = 1.2237        $Shape factor Cpt for pneumatic trail
QDZ1                    = 0.062582      $Peak trail Dpt" = Dpt*(Fz/Fznom*R0)
QDZ2                    = 0.00052585    $Variation of peak Dpt" with load
QDZ3                    = -0.60661      $Variation of peak Dpt" with camber
QDZ4                    = 8.634         $Variation of peak Dpt" with camber squared
QDZ6                    = -0.0048467    $Peak residual torque Dmr" = Dmr/(Fz*R0)
QDZ7                    = 0.0034983     $Variation of peak factor Dmr" with load
QDZ8                    = -0.11032      $Variation of peak factor Dmr" with camber
QDZ9                    = 0.021277      $Variation of peak factor Dmr" with camber
and load
QEZ1                    = -5.3971       $Trail curvature Ept at Fznom
QEZ2                    = 1.1207        $Variation of curvature Ept with load
QEZ3                    = 0             $Variation of curvature Ept with load
squared
QEZ4                    = 0.14942       $Variation of curvature Ept with sign of
Alpha-t
QEZ5                    = -1.1429       $Variation of Ept with camber and sign
Alpha-t
QHZ1                    = -0.00069905   $Trail horizontal shift Sht at Fznom
QHZ2                    = 0.0055192     $Variation of shift Sht with load
QHZ3                    = 0.065953      $Variation of shift Sht with camber
QHZ4                    = 0.11393       $Variation of shift Sht with camber and load
SSZ1                    = 0.022576      $Nominal value of s/R0: effect of Fx on Mz
SSZ2                    = 0.024754      $Variation of distance s/R0 with Fy/Fznom
SSZ3                    = 0.0014697     $Variation of distance s/R0 with camber
SSZ4                    = 0.0014801     $Variation of distance s/R0 with load and
camber
QTZ1                    = 0.2           $Gyration torque constant
```



```
MBELT                   = 4.9           $Belt mass of the wheel
```

APPENDIX 1

1 (c) PAC-2002 Magic Formula

Formulas for the Longitudinal Force at Pure Slip

$F_x = F_{x0}(\kappa, F_z, \lambda)$

$F_{x0} = D_x \sin[C_x \tan^{-1}\{B_x\kappa_x - E_x(B_x\kappa_x - \tan^{-1}(B_x\kappa_x))\}] + S_{Vx}$

with the following coefficients:

$\gamma_x = \gamma \cdot \lambda_{\gamma x}$

$df_z = \dfrac{F_z - F_{z0}\cdot\lambda_{Fz0}}{F_{z0}\cdot\lambda_{Fz0}}$

$D_x = F_z \cdot (p_{Dx1} + p_{Dx2}df_z)\cdot(1 - p_{Dx3}\cdot\gamma_x^2)\cdot\lambda_{\mu x}\cdot\varsigma_1$

$C_x = P_{Cx1}\cdot\lambda_{Cx}$

$K_x = F_z\cdot(p_{Kx1} + p_{Kx2}df_z)\cdot\exp(p_{Kx3}df_z)\cdot\lambda_{Kx}$ *(The Longitudinal Slip Stiffness)*

$B_x = \dfrac{F_z\cdot(p_{Kx1} + p_{Kx2}df_z)\cdot\exp(p_{Kx3}df_z)\cdot\lambda_{Kx}}{C_x D_x}$

$\kappa_x = \kappa + S_{Hx}$

$E_x = (p_{Ex1} + p_{Ex2}df_z + p_{Ex3}df_z^2)\cdot(1 - p_{Ex4}\cdot sign(\kappa_x))\cdot\lambda_{Ex}$ with $E_x \le 1$

$S_{Hx} = (p_{Hx1} + p_{Hx2}\cdot df_z)\cdot\lambda_{Hx}$

$S_{Vx} = F_z(p_{Vx1} + p_{Vx2}df_z)\cdot\lambda_{Vx}\cdot\lambda_{\mu x}\cdot\varsigma_1$

Formulas for the Lateral Force at Pure Slip

$F_y = F_{y0}(\alpha, \gamma, F_z)$

$F_{y0} = D_y \sin[C_y \tan^{-1}\{B_y\alpha_y - E_y(B_y\alpha_y - \tan^{-1}(B_y\alpha_y))\}] + S_{Vy}$

with the following coefficients:

$\gamma_y = \gamma\cdot\lambda_{\gamma y}$

$\alpha_y = \alpha + S_{Hy}$

$C_y = P_{Cy1}\cdot\lambda_{Cy}$

$D_y = F_z\cdot(p_{Dy1} + p_{Dy2}df_z)\cdot(1 - p_{Dy3}\cdot\gamma_y^2)\cdot\lambda_{\mu y}\cdot\varsigma_2$

$E_x = (p_{Ey1} + p_{Ey2}df_z)\cdot\{1 - (p_{Ey3} + p_{Ey4}\cdot\gamma_y)\cdot sign(\alpha_y)\}\cdot\lambda_{Ey}$ with $E_y \le 1$

$K_{y0} = p_{Ky1}\cdot F_{z0}\cdot\sin[2\tan^{-1}\{\dfrac{F_z}{p_{Ky2}F_0\lambda_{Fz0}}\}]\cdot\lambda_{Fz0}\cdot\lambda_{Ky}$ *(The Cornering Stiffness)*

$K_y = K_{y0}\cdot(1 - p_{ky3}|\gamma_y|)\cdot\zeta_3$

$B_y = \dfrac{K_y}{(C_y\cdot D_y)}$

$S_{Hy} = (p_{Hy1} + p_{Hy2}\cdot df_z)\cdot\lambda_{Hy} + p_{Hy3}\cdot\gamma_y\cdot\zeta_0 + \zeta_4 - 1$

APPENDIX 1

$$S_{Vy} = F_z \cdot \{(p_{Vy1} + p_{Vy2} df_z) \cdot \lambda_{Vy} + (p_{Vy1} + p_{Vy2} \cdot df_z) \cdot \gamma_y\} \cdot \lambda_{\mu y} \cdot \zeta_4$$

$$K_{y\gamma 0} = p_{Hy3} \cdot K_{y0} + F_z \cdot (p_{vy3} + p_{vy4} \cdot df_z) \qquad \textit{(The Camber Stiffness)}$$

<u>Formulas for the Aligning Moment at Pure Slip</u>

$$M_z = M_{z0}(\alpha, \gamma, F_z)$$

$$M_{z0} = -t \cdot F_{y0} + M_{zr}$$

where $t(\alpha_t) = D_t \cdot \cos[C_t \tan^{-1}\{B_t\alpha_t - E_t(B_t\alpha_t - \tan^{-1}(B_t\alpha_t))\}] \cdot \cos(\alpha)$

$$\alpha_t = \alpha + S_{Ht}$$

$$\gamma_z = \gamma \cdot \lambda_{\gamma z}$$

$$B_t = (q_{Bz1} + q_{Bz2} df_z + q_{Bz3} df_z^2) \cdot (1 + q_{Bz4} \cdot \gamma_z + q_{Bz5} \cdot |\gamma_z|) \cdot \frac{\lambda_{Ky}}{\lambda_{\mu y}}$$

$$C_t = q_{Cz1}$$

$$D_t = F_z \cdot (q_{Dz1} + q_{Dz2} df_z) \cdot (1 + q_{Dz3}\gamma_z + q_{Dz4} \cdot \gamma_z^2) \cdot \frac{R_0}{F_{z0}} \cdot \lambda_t \cdot \varsigma_5$$

$$E_t = (q_{Ez1} + q_{Ez2} df_z + q_{Ez3} df_z^2) \cdot \{1 + (q_{Ez4} + q_{Ez5} \cdot \gamma_z) \cdot \frac{2}{\pi} \cdot \tan^{-1}(B_t \cdot C_t \cdot \alpha_t)\} \text{ with } E_t \le 1$$

$$S_{Ht} = q_{Hz1} + q_{Hz2} df_z + (q_{Hz3} + q_{Hz4} df_z)\gamma_z$$

$$M_{zr}(\alpha_r) = D_r \cdot \cos[C_r \tan^{-1}(B_r\alpha_r)] \cdot \cos(\alpha)$$

$$\alpha_r = \alpha + S_{Hf}$$

$$S_{Hf} = S_{Hy} + \frac{S_{Vy}}{K_y}$$

$$B_r = (q_{Bz9} \cdot \frac{\lambda_{Ky}}{\lambda_{\mu y}} + q_{Bz10} \cdot B_y \cdot C_y) \cdot \zeta_6$$

$$C_r = \zeta_7$$

$$D_r = F_z \cdot [(q_{Dz6} + q_{Dz7} df_z) \cdot \lambda_r + (q_{Dz8} + q_{Dz9} \cdot df_z) \cdot \gamma_z] \cdot R_0 \cdot \lambda_{\mu\gamma} + \zeta_8 - 1$$

$$K_z = -t \cdot K_y \quad (\approx -\frac{\partial M_z}{\partial \alpha}) \text{ at } \alpha = 0 \qquad \textit{(The Aligning Moment Stiffness)}$$

APPENDIX 1

1 (d) SIMULINK Program for a Cornering Vehicle fitted with HPAS

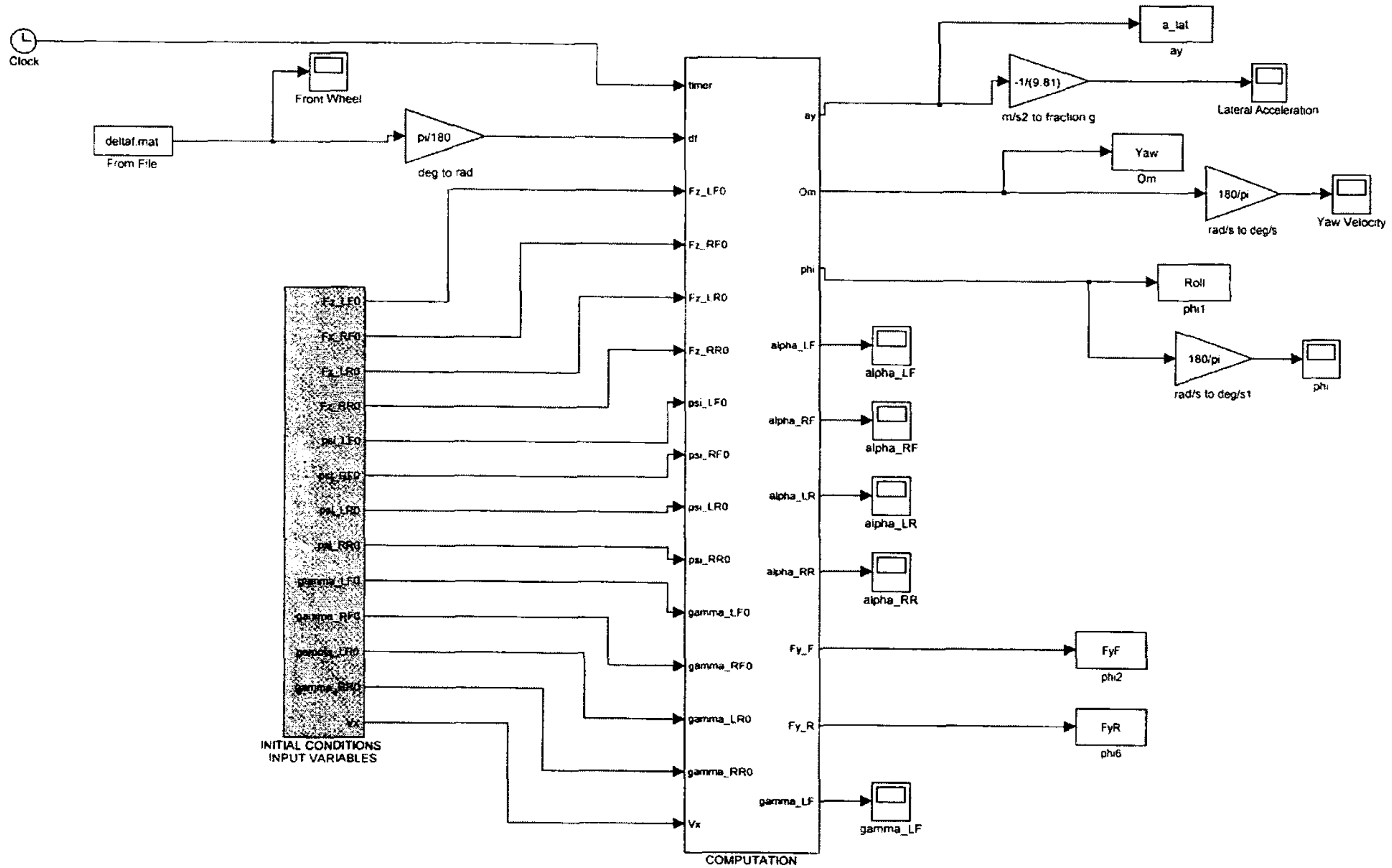

APPENDIX 1

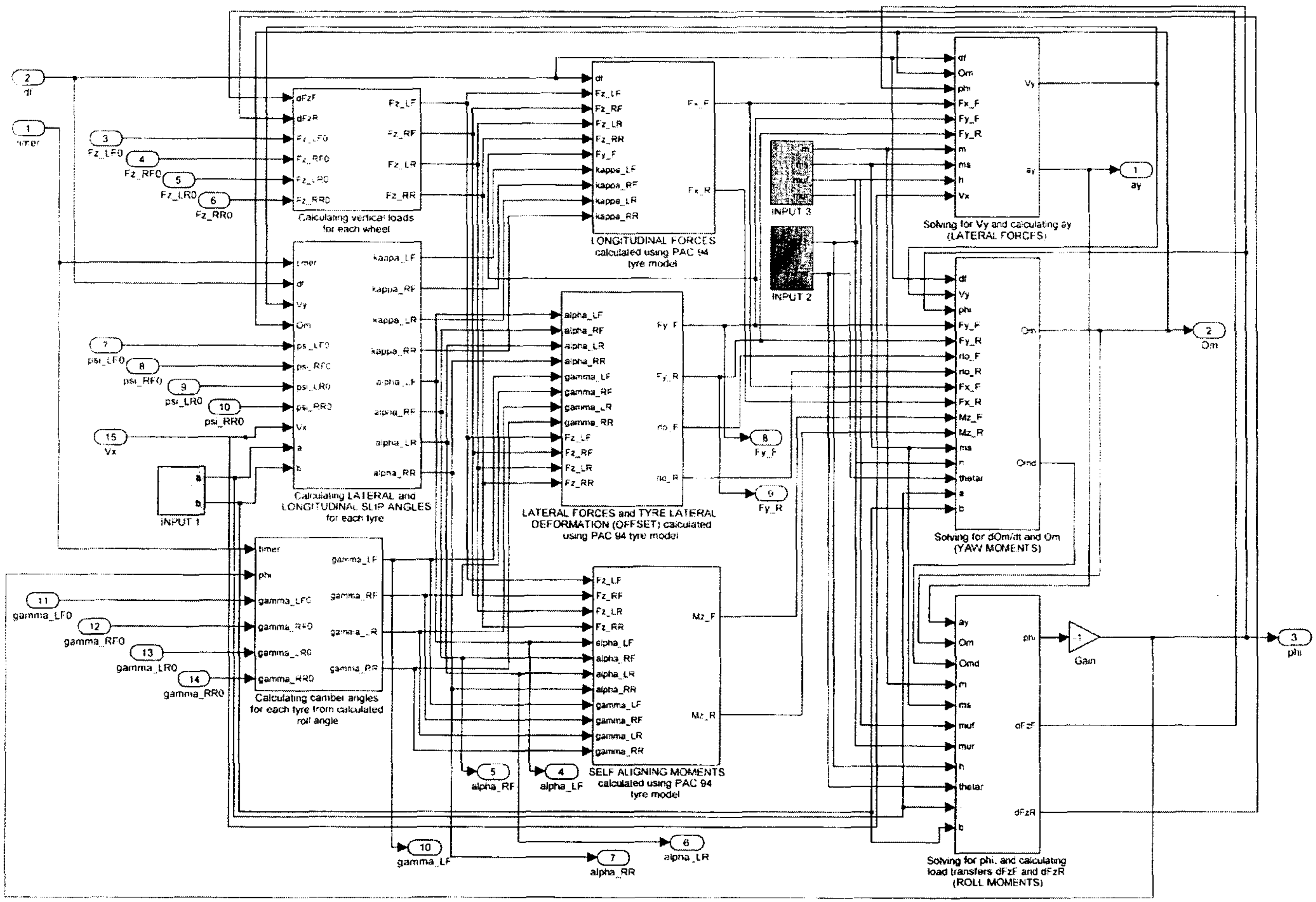

df
timer
Fz_LF0
Fz_RF0
Fz_LR0
Fz_RR0
Calculating vertical loads for each wheel
LONGITUDINAL FORCES calculated using PAC 94 tyre model
INPUT 3
INPUT 2
Solving for Vy and calculating ay (LATERAL FORCES)
ay
Calculating LATERAL and LONGITUDINAL SLIP ANGLES for each tyre
INPUT 1
psi_LF0
psi_RF0
psi_LR0
psi_RR0
Vx
LATERAL FORCES and TYRE LATERAL DEFORMATION (OFFSET) calculated using PAC 94 tyre model
Fy_F
Fy_R
Solving for dOm/dt and Om (YAW MOMENTS)
Om
Calculating camber angles for each tyre from calculated roll angle
gamma_LF0
gamma_RF0
gamma_LR0
gamma_RR0
SELF ALIGNING MOMENTS calculated using PAC 94 tyre model
alpha_RF
alpha_LF
alpha_LR
alpha_RR
gamma_LF
Gain
phi
Solving for phi, and calculating load transfers dFzF and dFzR (ROLL MOMENTS)

APPENDIX 1

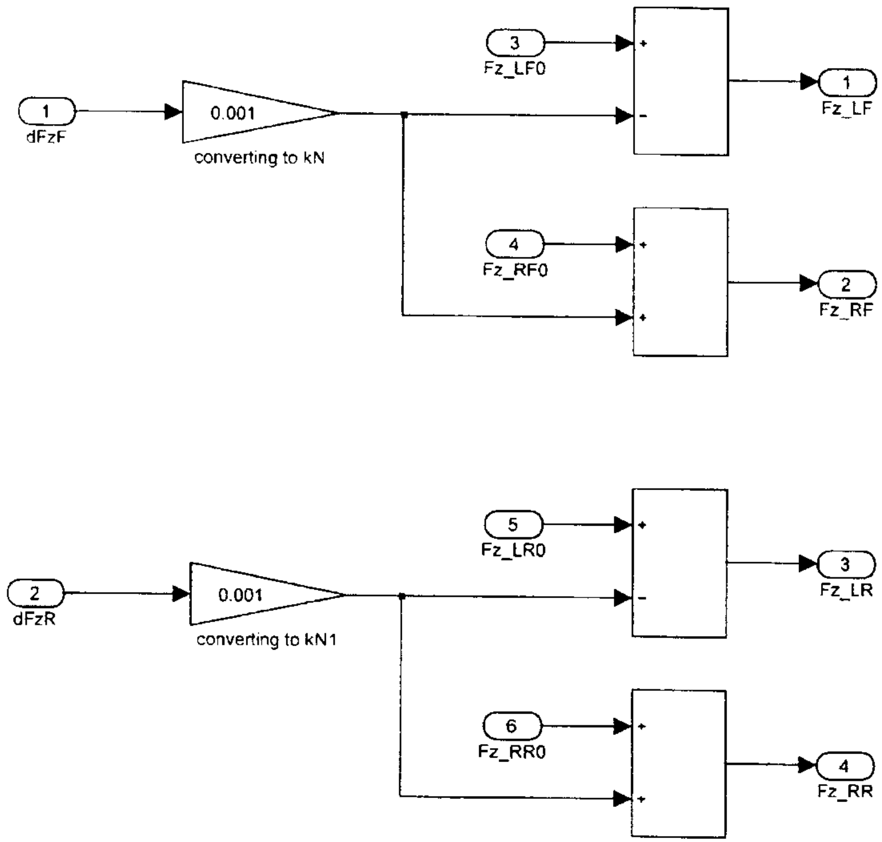

1
dFzF
0.001
converting to kN
3
Fz_LF0
4
Fz_RF0
1
Fz_LF
2
Fz_RF
2
dFzR
0.001
converting to kN1
5
Fz_LR0
6
Fz_RR0
3
Fz_LR
4
Fz_RR

APPENDIX 1

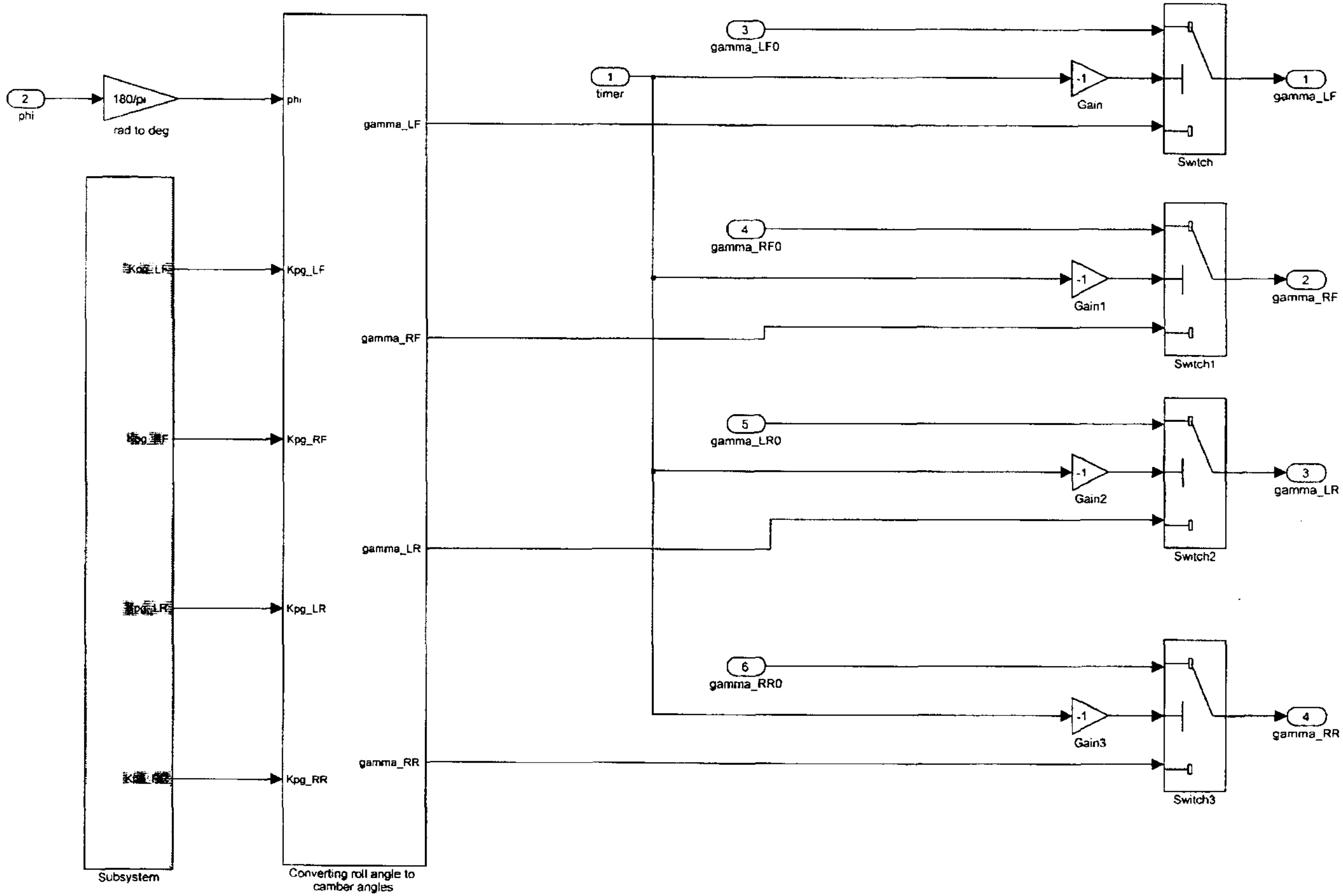

2
phi
180/pi
rad to deg
phi
Kpg_LF
Kpg_RF
Kpg_LR
Kpg_RR
gamma_LF
gamma_RF
gamma_LR
gamma_RR
Subsystem
Converting roll angle to camber angles
1
timer
3
gamma_LF0
4
gamma_RF0
5
gamma_LR0
6
gamma_RR0
-1
Gain
Gain1
Gain2
Gain3
Switch
Switch1
Switch2
Switch3
1
gamma_LF
2
gamma_RF
3
gamma_LR
4
gamma_RR

APPENDIX 1

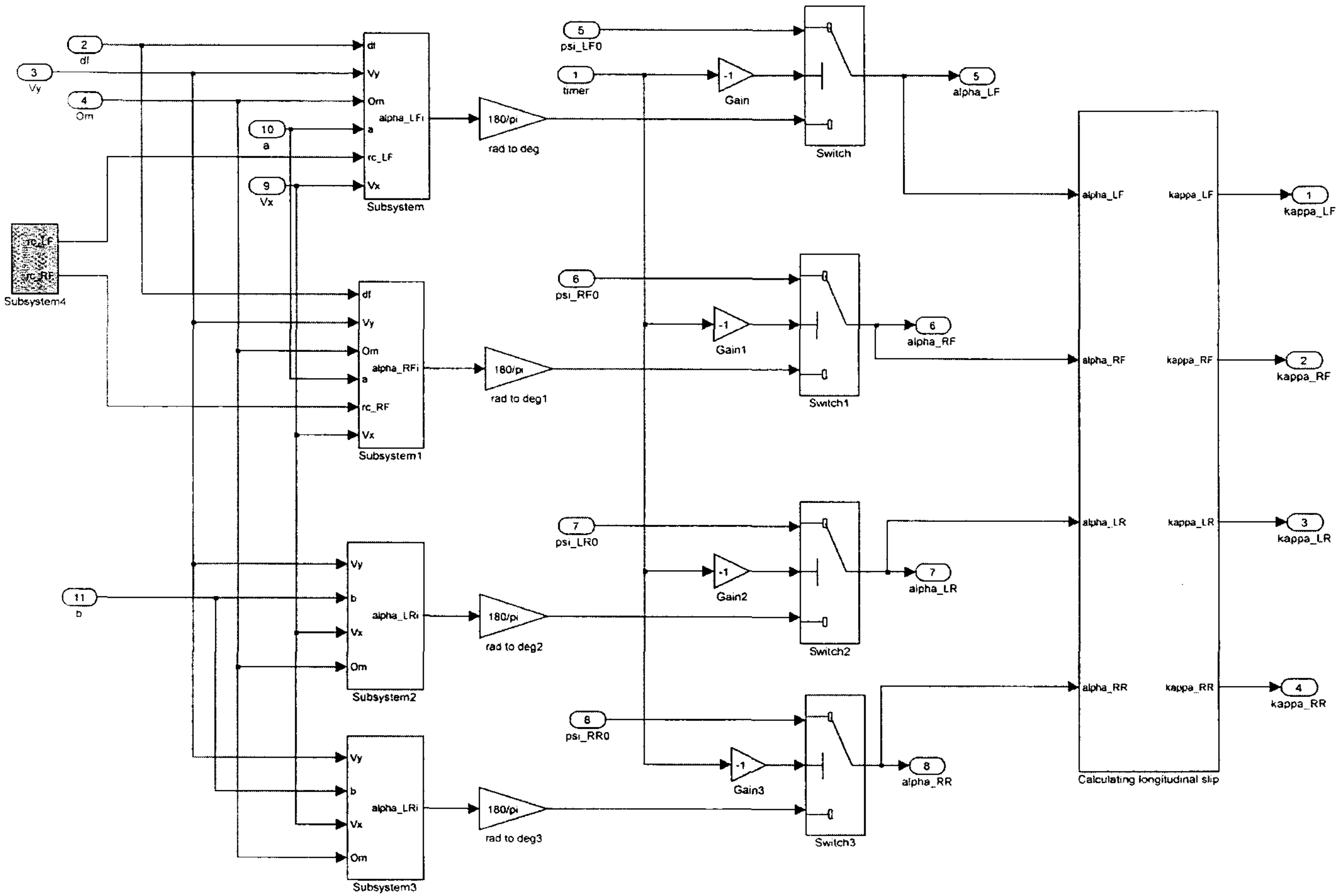

2
df
3
Vy
4
Om
10
a
9
Vx
11
b
Subsystem4
rc_LF
rc_RF
df
Vy
Om
a
rc_LF
Vx
alpha_LF
Subsystem
rc_RF
alpha_RF
Subsystem1
alpha_LR
Subsystem2
Subsystem3
180/pi
rad to deg
rad to deg1
rad to deg2
rad to deg3
5
psi_LF0
1
timer
-1
Gain
Gain1
Gain2
Gain3
Switch
Switch1
Switch2
Switch3
6
psi_RF0
7
psi_LR0
8
psi_RR0
5
alpha_LF
6
alpha_RF
7
alpha_LR
8
alpha_RR
alpha_RR
kappa_LF
kappa_RF
kappa_LR
kappa_RR
Calculating longitudinal slip
1
kappa_LF
2
kappa_RF
3
kappa_LR
4
kappa_RR

APPENDIX 1

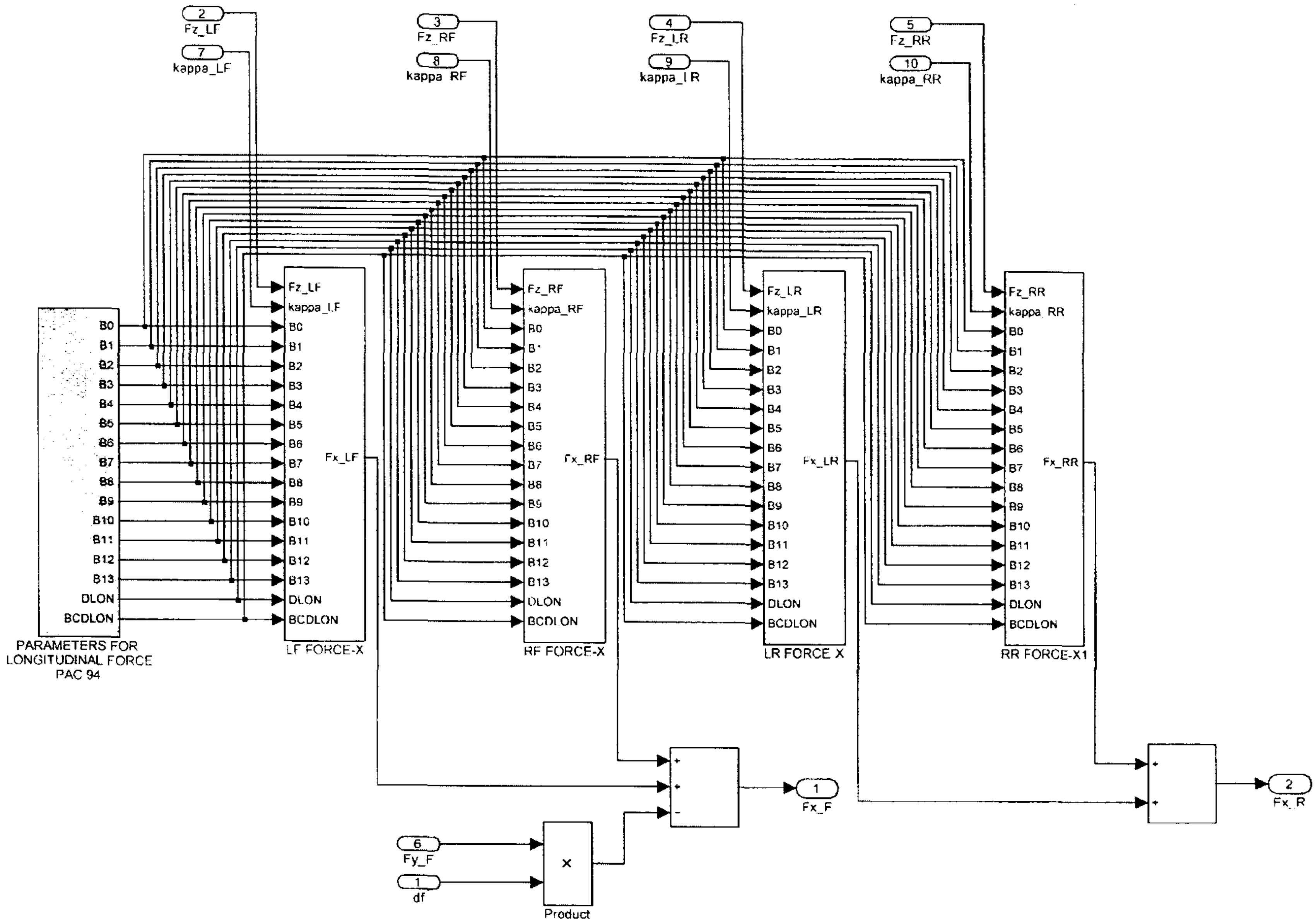

Fz_LF
kappa_LF
Fz_RF
kappa_RF
Fz_LR
kappa_LR
Fz_RR
kappa_RR
PARAMETERS FOR LONGITUDINAL FORCE PAC 94
B0
B1
B2
B3
B4
B5
B6
B7
B8
B9
B10
B11
B12
B13
DLON
BCDLON
Fx_LF
Fx_RF
Fx_LR
Fx_RR
LF FORCE-X
RF FORCE-X
LR FORCE X
RR FORCE-X1
Fy_F
df
Product
Fx_F
Fx_R

APPENDIX 1

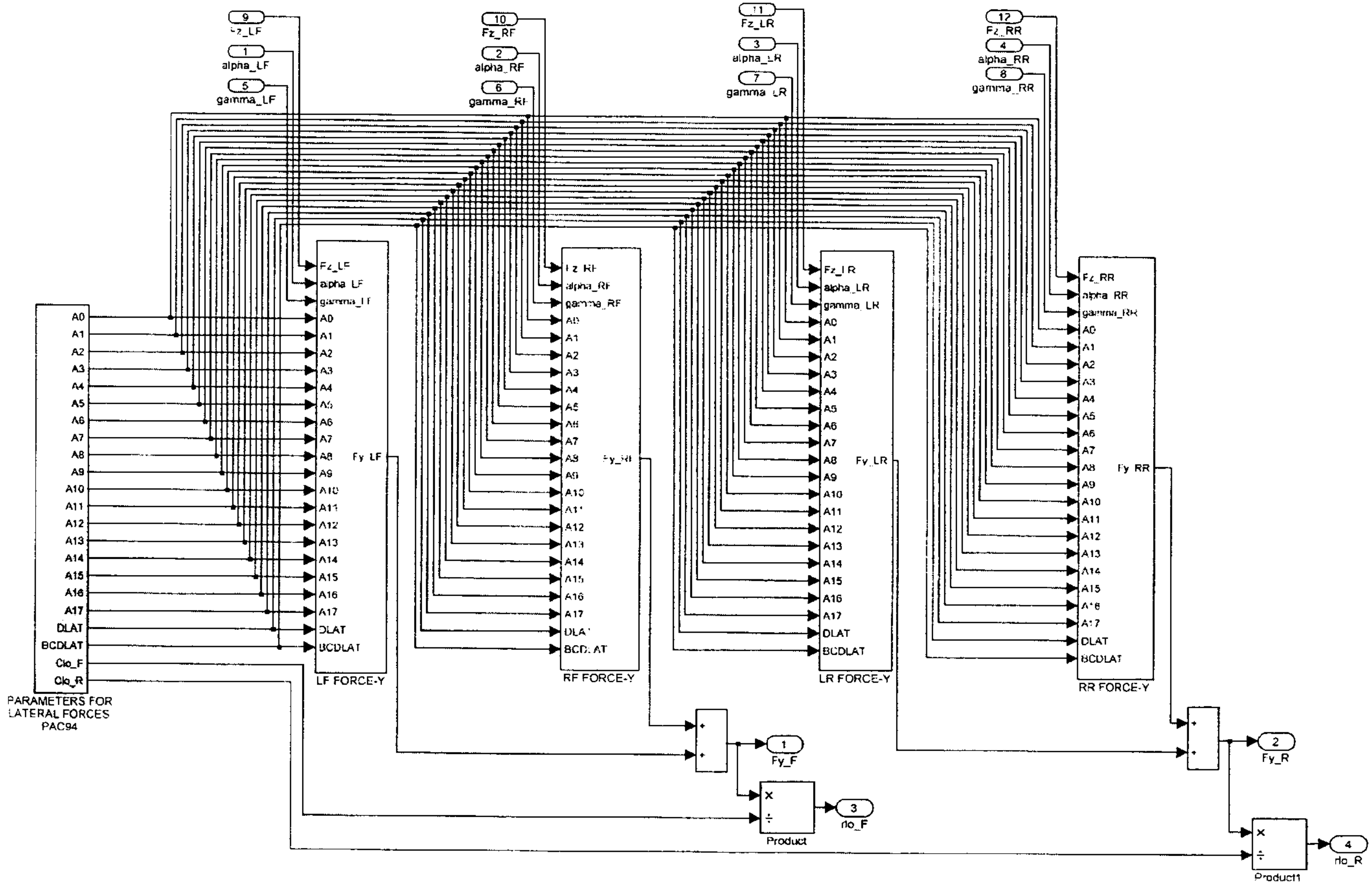

Fz_LF
alpha_LF
gamma_LF
Fz_RF
alpha_RF
gamma_RF
Fz_LR
alpha_LR
gamma_LR
Fz_RR
alpha_RR
gamma_RR
A0
A1
A2
A3
A4
A5
A6
A7
A8
A9
A10
A11
A12
A13
A14
A15
A16
A17
DLAT
BCDLAT
Clo_F
Clo_R
PARAMETERS FOR
LATERAL FORCES
PAC94
Fy_LF
LF FORCE-Y
Fy_RF
RF FORCE-Y
Fy_LR
LR FORCE-Y
Fy_RR
RR FORCE-Y
Fy_F
Fy_R
Product
rlo_F
Product1
rlo_R

APPENDIX 1

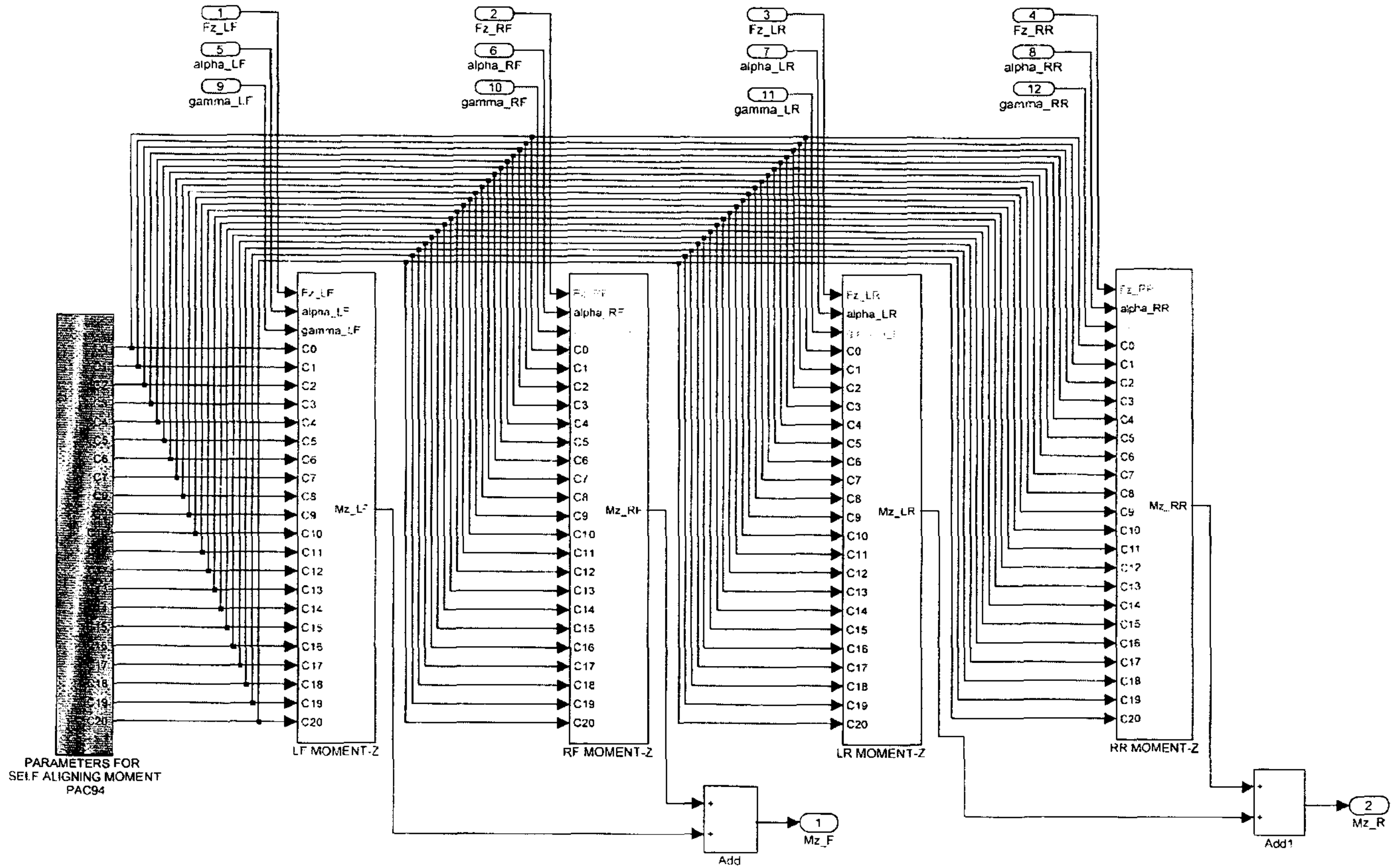

1
Fz_LF
5
alpha_LF
9
gamma_LF
2
Fz_RF
6
alpha_RF
10
gamma_RF
3
Fz_LR
7
alpha_LR
11
gamma_LR
4
Fz_RR
8
alpha_RR
12
gamma_RR
Fz_LF
alpha_LF
gamma_LF
C0
C1
C2
C3
C4
C5
C6
C7
C8
C9
C10
C11
C12
C13
C14
C15
C16
C17
C18
C19
C20
Mz_LF
LF MOMENT-Z
alpha_RF
Mz_RF
RF MOMENT-Z
Fz_LR
alpha_LR
Mz_LR
LR MOMENT-Z
alpha_RR
Mz_RR
RR MOMENT-Z
PARAMETERS FOR
SELF ALIGNING MOMENT
PAC94
Add
1
Mz_F
Add1
2
Mz_R

APPENDIX 1

1 (e) Vehicle Data for FORD FIESTA V6 1.25L 5-DOORS

Constants	Descriptions	Value	Unit
m_{wd}	Total vehicle mass without driver	*	kg
m	Total vehicle mass with a driver and passenger	*	kg
F_R	Front static axle load (without driver)	*	N
F_R	Rear static axle load (without driver)	*	N
L	Wheelbase	*	m
T	Wheel Track	*	m
a	Distance from c.g. to front contact patch	*	m
b	Distance from c.g. to rear contact patch	*	m
V_x	Longitudinal forward speed	*	m/s
$C_{F\alpha F}$	Total front lateral force cornering stiffness	*	N/rad
$C_{F\alpha r}$	Total rear lateral force cornering stiffness	*	N/rad
$C_{M\alpha F}$	Total front SAM cornering stiffness	*	Nm/rad
$C_{M\alpha R}$	Total rear SAM cornering stiffness	*	Nm/rad
I_{zz}	Total yaw inertia	*	$kg \cdot m^2$

* These data are company confidential and can only be accessed by their permission. Please contact the author for more information.

APPENDIX 1

1 (f) SIMULINK Program for Detailed Modelling of a Cornering Vehicle Fitted with Flexible Shaft

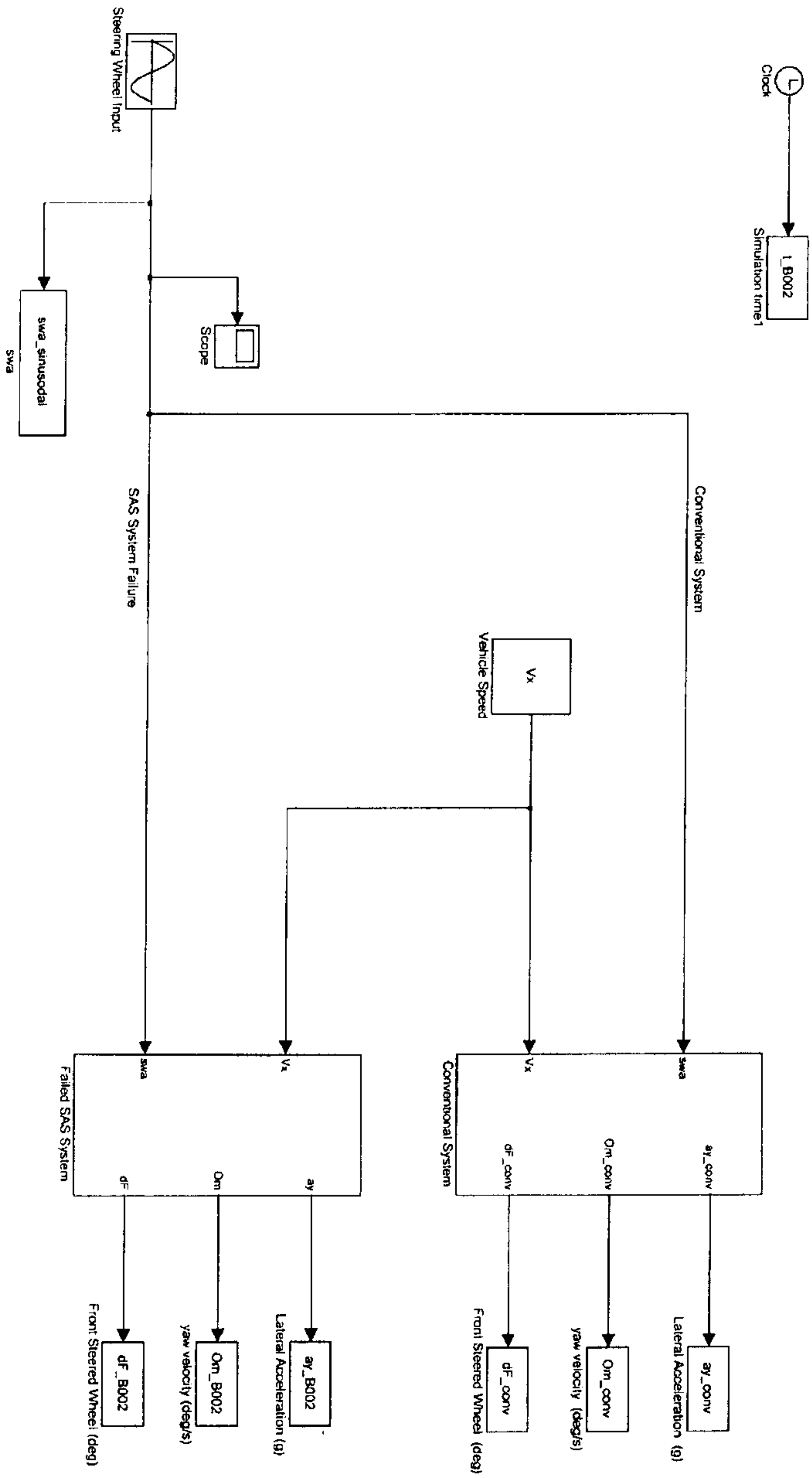

APPENDIX 1

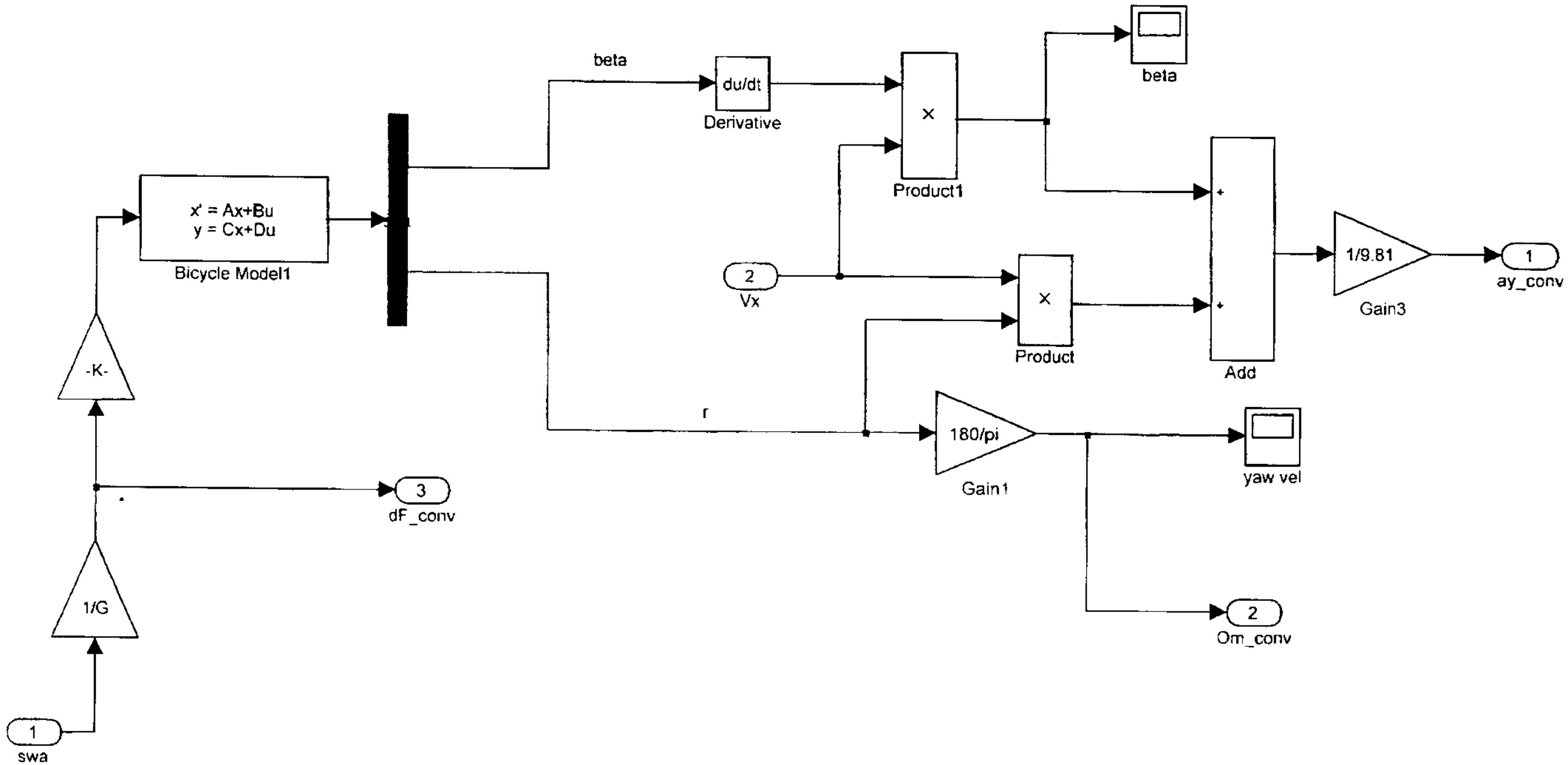

beta
du/dt
Derivative
Product1
beta
x' = Ax+Bu
y = Cx+Du
Bicycle Model1
2
Vx
Product
Add
1/9.81
Gain3
1
ay_conv
-K-
r
180/pi
Gain1
yaw vel
3
dF_conv
1/G
2
Om_conv
1
swa

APPENDIX 1

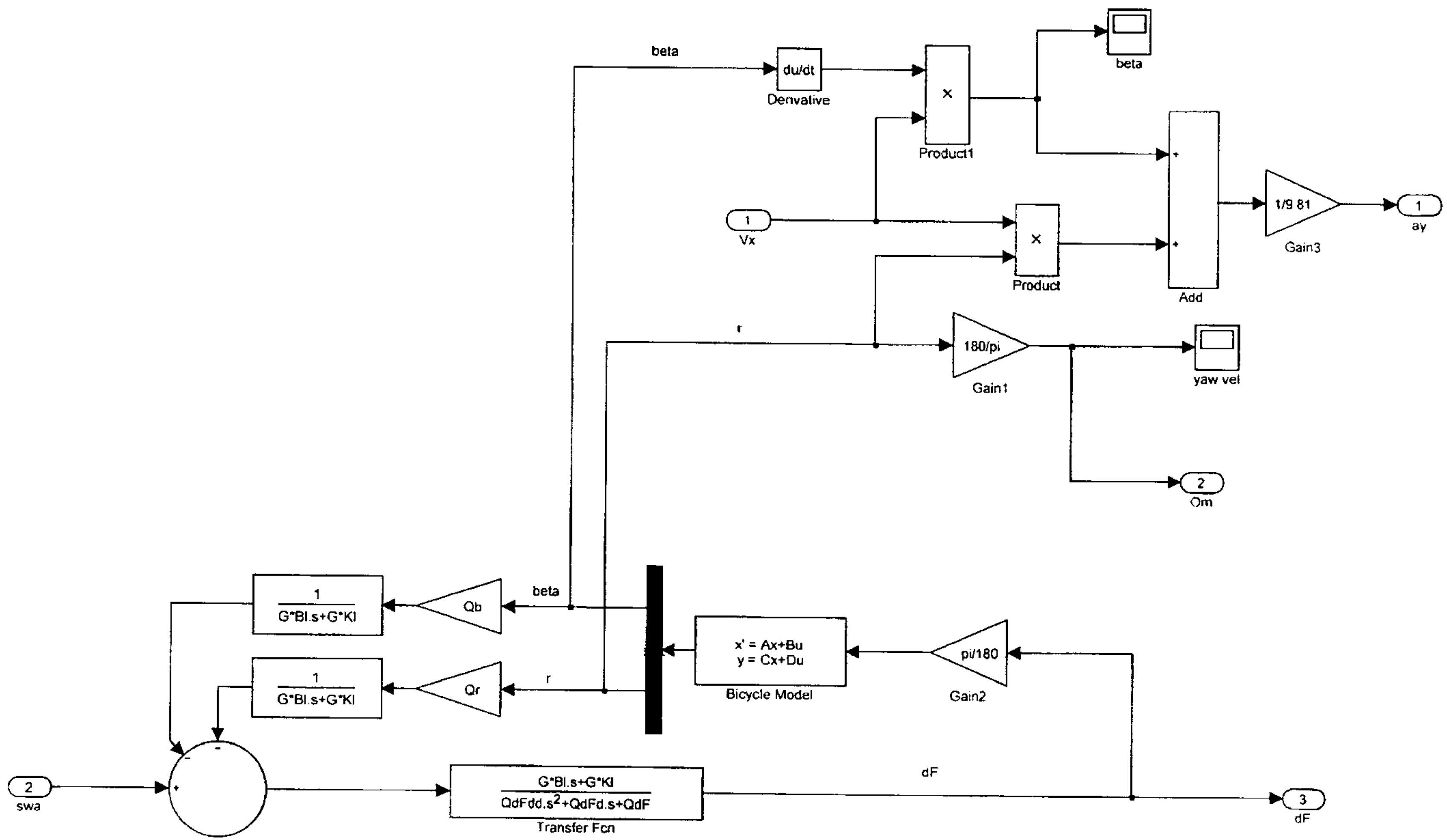

beta
du/dt
Derivative
×
Product1
beta
+
+
Add
1/9 81
Gain3
1
ay
1
Vx
×
Product
r
180/pi
Gain1
yaw vel
2
Om
1
G*BI.s+G*KI
Qb
beta
1
G*BI.s+G*KI
Qr
r
x' = Ax+Bu
y = Cx+Du
Bicycle Model
pi/180
Gain2
2
swa
-
-
+
G*BI.s+G*KI
QdFdd.s2+QdFd.s+QdF
Transfer Fcn
dF
3
dF

APPENDIX 2

a) Experimental Vehicle – Ford Fiesta V6 1.25L

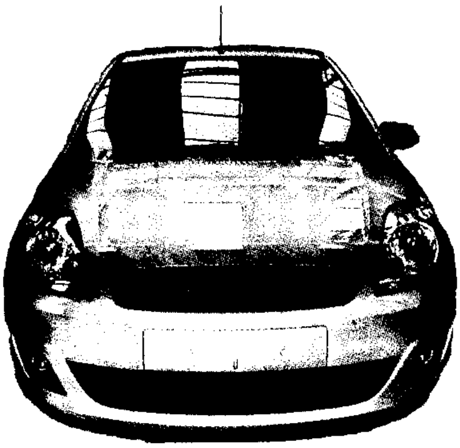

a) Front View

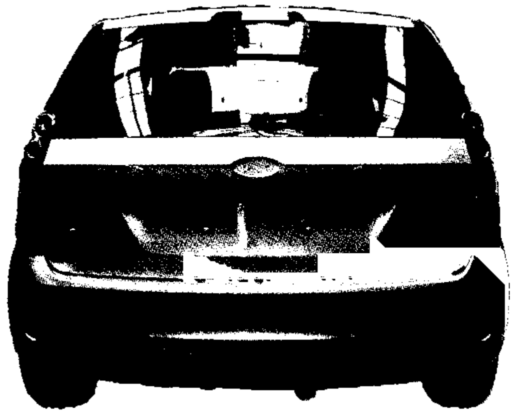

b) Rear View

c) Partial 3D View

APPENDIX 2

) Determination of Steering Ratios and Lock-to-lock Number of Turns

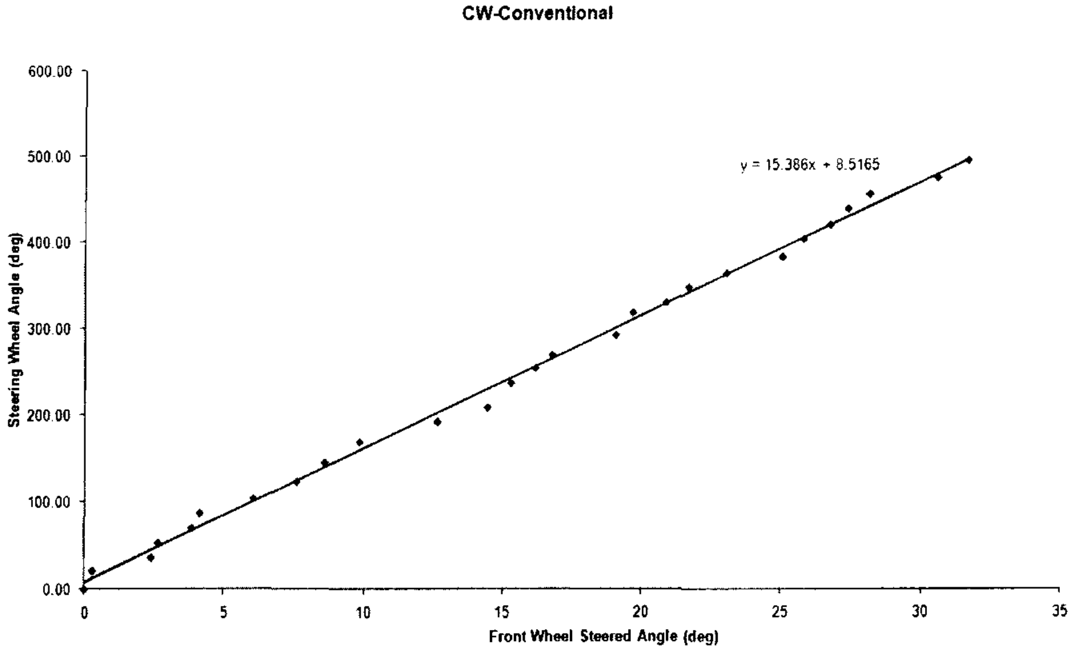

a) Turning in clockwise direction

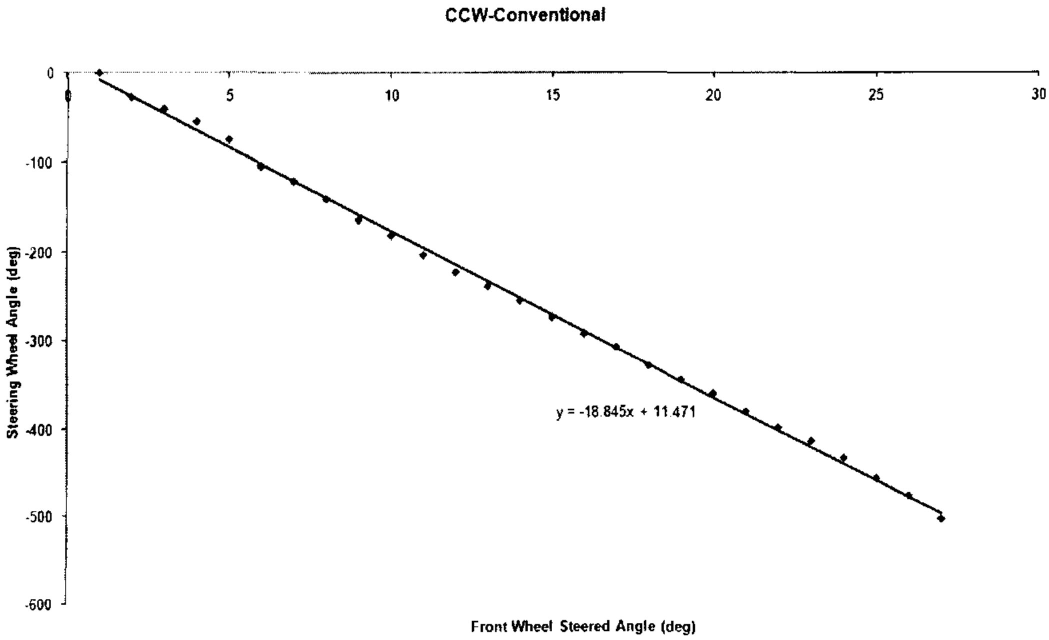

b) Turning in counter clockwise direction

rage Steering Ratio = (15.4 + 18.8)/2 = 17.1

nber of lock-to-lock turns = 500/360 = 1.4 turns

APPENDIX 2

) Steering Shaft Assembly

Nith compliments from ,

VIN:
WF0HXXJAJH5D75007

:atalogue: Fiesta/Fusion CBK (GCAT) 2001-
;ection: 211-04/05 STEERING COLUMN (FROM 30/11/2001)

Build Date
11/2005

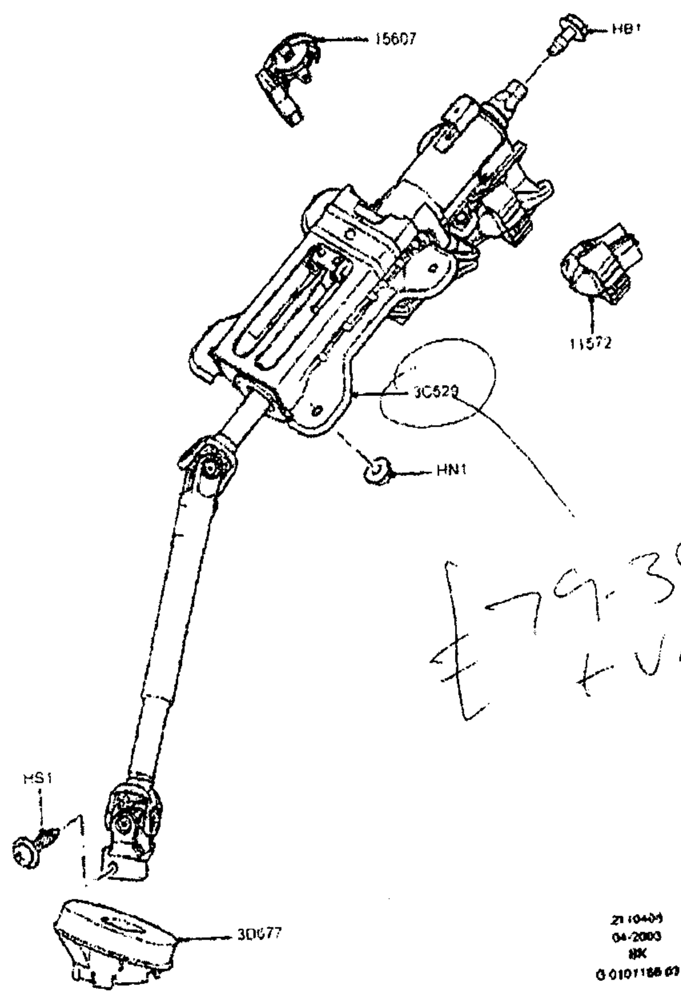

£79.38
+ VAT

APPENDIX 2

) PARTS OF FLEXIBLE SHAFTS

) i) PART 1, K = 5 Nm/rad

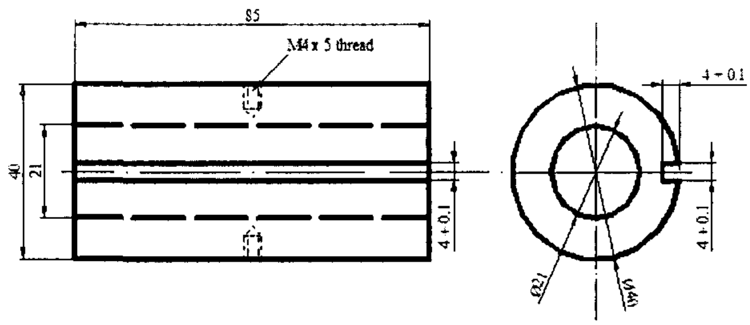

PART 1 (A) : Double Spring Holder

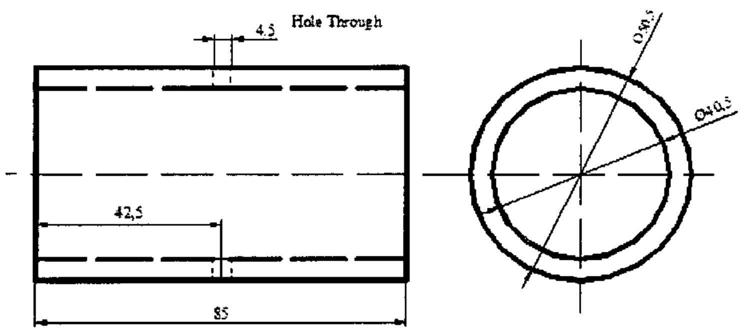

PART 1 (B) : Sleeve Holder

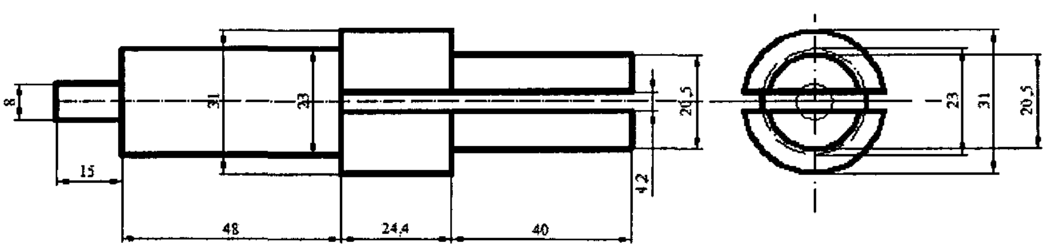

PART 1 (C) Upper Shaft

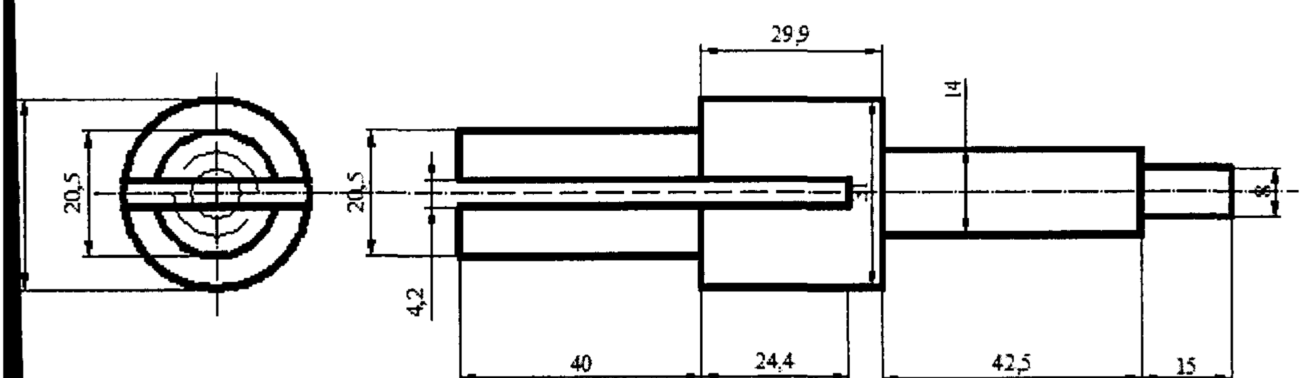

PART 1 (D) Lower Shaft

APPENDIX 2

) ii) PART 2, K = 10 Nm/rad

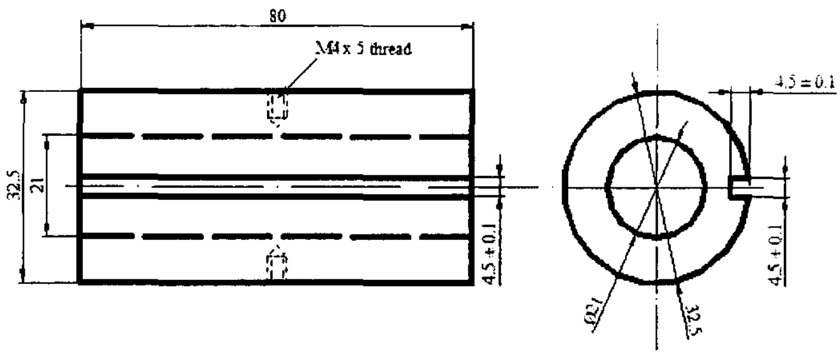

PART 2 (A) : Double Spring Holder

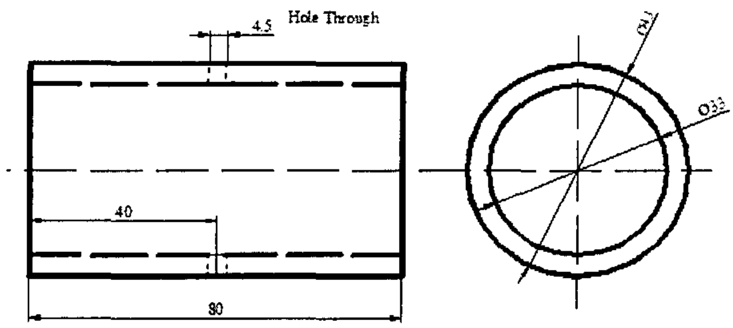

PART 2 (B) : Sleeve Holder

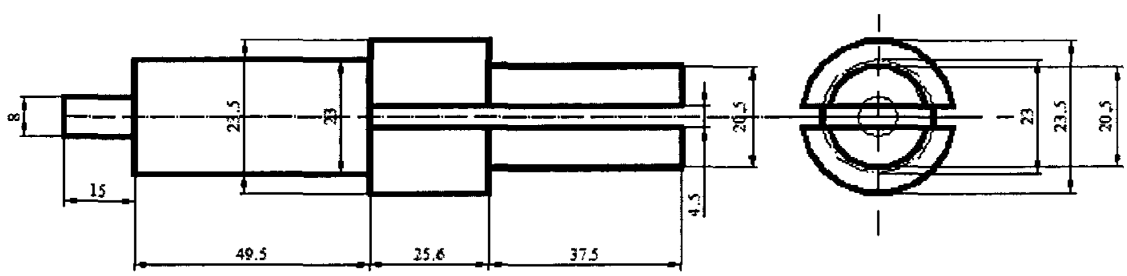

PART 2 (C) Upper Shaft

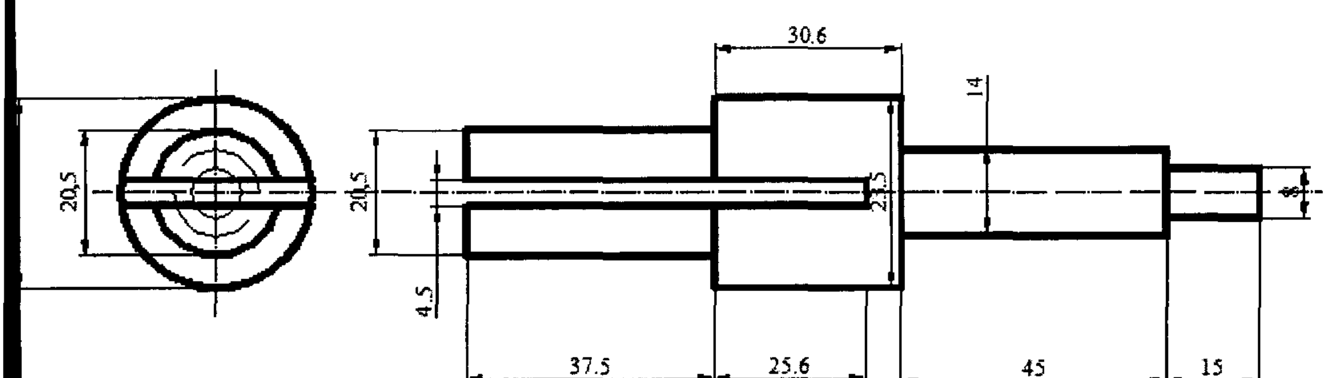

PART 2 (D) Lower Shaft

APPENDIX 2

) iii) Detailed of PART 3, K = 15 Nm/rad

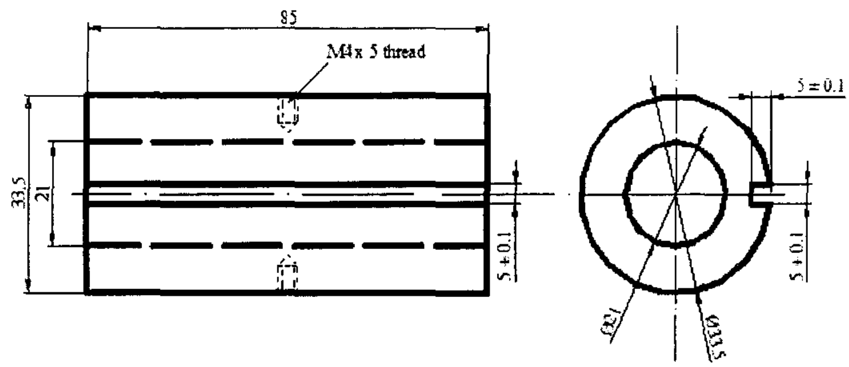

PART 3 (A) : Double Spring Holder

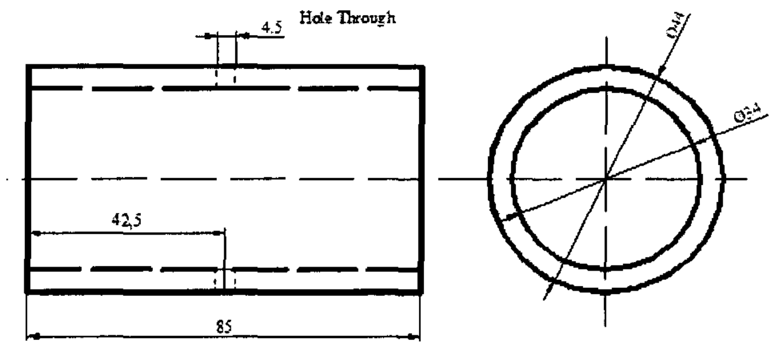

PART 3 (B) : Sleeve Holder

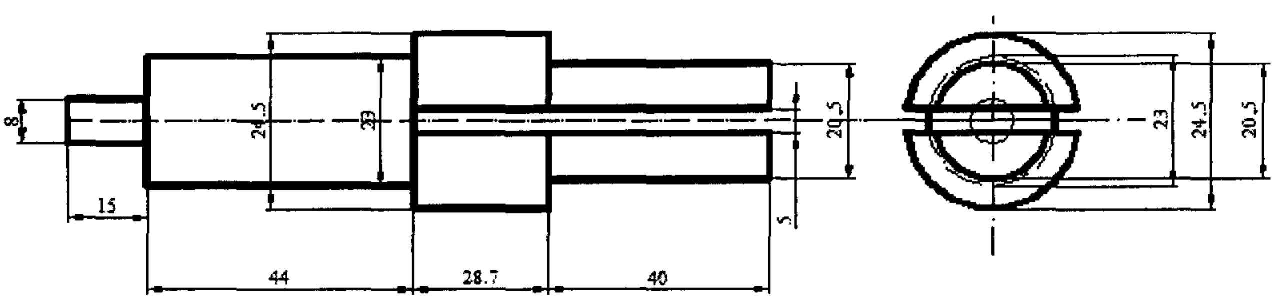

PART 3 (C) Upper Shaft

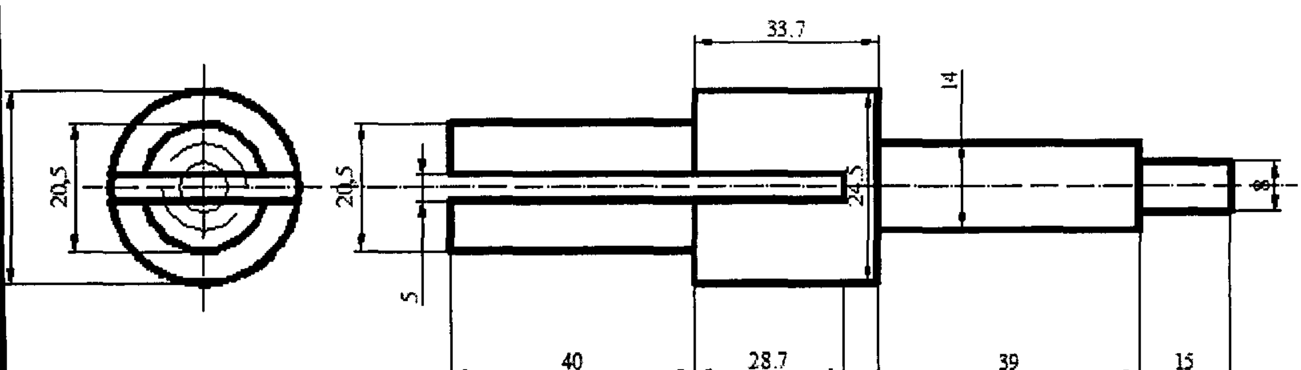

PART 3 (D) Lower Shaft

APPENDIX 2

i) Computer Program to Compute Required Wire Diameters

Editor - C:\PhD Related Documents\2007 PhD PAPERS #3\sprcom.m

```
%sprcom
function f = sprcom(K,N,Dp,E,d)
    f = 10.8*K*((Dp/0.9)+d)*N - E*(d^4);
```

a) MATLAB function

Editor - C:\PhD Related Documents\2007 PhD PAPERS #3\spring_design.m

```
%spring_design
clc
disp('This program computes spring wire diameter,d when the the following data are provided:');
disp('a) The required torsion stiffness, K');
disp('b) The number of spring body turns, N');
disp('c) The desired pin diameter, Dp');
disp('d) The modulus of elasticity of wire material, E');
disp(' ');
K = input('K (Nm/rad) = ');
K = 2*pi*1000*K;%Converting from Nm/rad to Nmm/turn
N = input('N (turns) = ');
Dp = input('Dp (mm) = ');
E = input('E (Gpa) = ');
E = 1E3*E;
%
Di = Dp/0.9;
d = fzero(@(d) sprcom(K,N,Dp,E,d),1);
D = Di + d;
%
% Calculating maximum angle of twist
theta_max = (((N*D)/Dp)-N)*(360);
%
disp(' ');
disp('For Rough Calculation when the Pin Diamater is Specified:');
fprintf('Wire Diameter, d = %6.4f mm \n',d);
fprintf('Spring Mean Diamater, D = %6.4f mm \n',D);
%
disp(' ');
disp('Calculation for the Round Value of Wire Diamater Based on above:');
d = round(d);
D = ((d^4)*E)/(10.8*K*N);
if D <= Dp
    d = d + 0.5;
    D = ((d^4)*E)/(10.8*K*N);
end
fprintf('Wire Diameter, d = %6.4f mm \n',d);
fprintf('Spring Mean Diamater, D = %6.4f mm \n',D);
%
```

a) MATLAB Program

APPENDIX 2

) ii) A Sample of a Running Programme

```
mmand Window
his program computes spring wire diameter,d when the the following data are provided:
) The required torsion stiffness, K
) The number of spring body turns, N
) The desired pin diameter, Dp
) The modulus of elasticity of wire material, E

 (Nm/rad) = 22
 (turns) = 4
p (mm) = 22
 (Gpa) = 207

or Rough Calculation when the Pin Diamater is Specified:
ire Diameter, d = 5.4176 mm
pring Mean Diamater, D = 29.8621 mm

alculation for the Round Value of Wire Diamater Based on above:
ire Diameter, d = 5.5000 mm
pring Mean Diamater, D = 31.7201 mm
>
```

APPENDIX 2

) Samples of Hand Calculations for Results Verification

art No.	d (mm)	L (mm)	A (mm)	B (mm)	ID (mm)	OD (mm)	D (mm)	N_b (turns)	k (Nm/rad)
1	4.0	85	133.7	21	31	40	35.5	4	5.5
2	4.46	80	131.2	24	23.5	32.5	28	4	10.7
3	5	85	142.3	25	24.5	33.5	29	4	16.4

$(\frac{1}{2\pi})\frac{d^4E}{10.8DN_b} Nm/rad$; where $E = 207\ E{+}09\ N/m^2$

$\frac{-D_p}{D_i} = 0.1 \qquad \Rightarrow D_p = 0.9D_i; \qquad D' = \frac{N_b D}{N_b + \theta_c'} \qquad \Rightarrow \theta_c' = \frac{N_b D - N_b D'}{D'}$

RT 1:

$$(\frac{1}{2\pi})\frac{d^4E}{10.8DN_b} Nm/rad = (\frac{1}{2\pi})\frac{(0.004)^4(207E+09)}{10.8\times 0.0355\times 4} = 5.5\frac{Nm}{rad}$$

$$D_p = 0.9(31) = 27.9\ mm$$

$$= 27.9 + 4.1 = 32\ mm$$

$$\frac{(3.75)(35.5)-(3.75)(32)}{32} = 0.41\ turns = 148^o$$

$$\left(\frac{(3.75+0.41)}{3.75}\right)\times 24.4 = 27.07$$

$$l = 27.07 - 24.4 \approx 3\ mm$$

T 3:

$$\frac{1}{2\pi})\frac{d^4E}{10.8DN_b} Nm/rad = (\frac{1}{2\pi})\frac{(0.00489)^4(207E+09)}{10.8\times 0.029\times 4} = 16.4\frac{Nm}{rad}$$

$$_p = 0.9(24.5) = 22\ mm$$

$$22 + 4.89 = 26.89\ mm$$

$$\frac{(3.75)(29)-(3.75)(26.89)}{26.89} = 0.294\ turns = 106^o$$

$$\left(\frac{(3.75+0.294)}{3.75}\right)\times 26.5 = 28.6$$

$$= 28.6 - 26.5 \approx 2.1\ mm$$

APPENDIX 2

) A Sample of Quotation Form for Fabrication of Double Springs

ATTENTION : MR. C MISTRY , Tel :- 01274 234[redacted]1C
UNIVERSITY OF BRADFORD
Fax : 01274 235790
e-mail :i) m.b.baharom@bradford.ac.uk
ii) cmistry@bradford.ac.uk

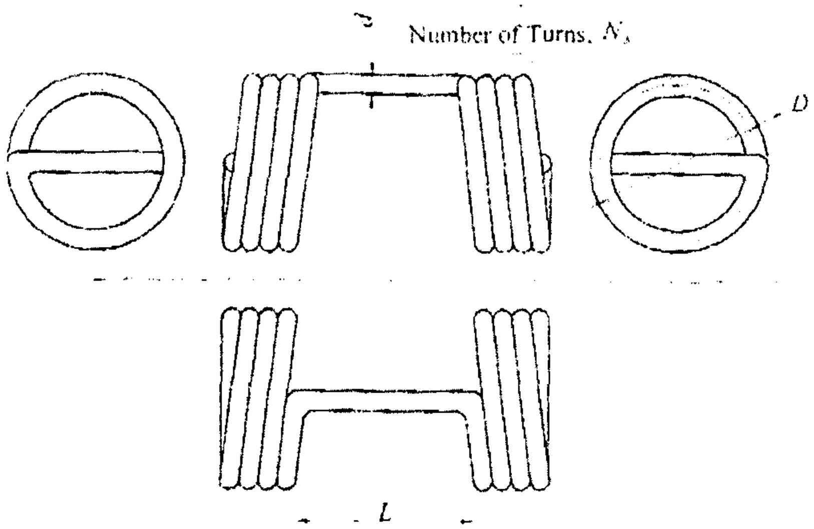

d = Wire Diameter

D = Spring Coil Mean Diameter

N_t = Number of Spring Body Turns

End Type: Hinged Ends with Long Legs as Shown above

Wire Material : Chromed Steel, possessing roughly, E = 207 Gpa

No	Wire Dia. (d) mm	Spring Mean Dia. (D) mm	(L) mm	Spring Body Turns (N_t)	Expected Stiffness Nm/rad	Price / 1 piece	Price / 10 pieces
1	4	35.5	50	4	5.5 210 Nmm/Deg	£55	£9.5 each
2	~~4.5~~ 4.46mm	28.43	50	4	11 382 Nmm/Deg	£55	£9.5 each
3	5	28.89	50	4	16.5 596 Nmm/Deg	£55	£4.5 each
4	~~5.5~~ 5.30	31.72	50	4	22 824 Nmm/Deg	£55	£9.5 each

Note: *1) The expected stiffness should be as exactly as possible*

2) The Spring Mean Diameter should not be less than 25 mm

LEEMING & PEEL
SPRINGS
☎ 01274 491434

DELIVERY 10 WORKING DAYS

Regards

APPENDIX 2

i) Detailed Drawing of Torsion Test Jig

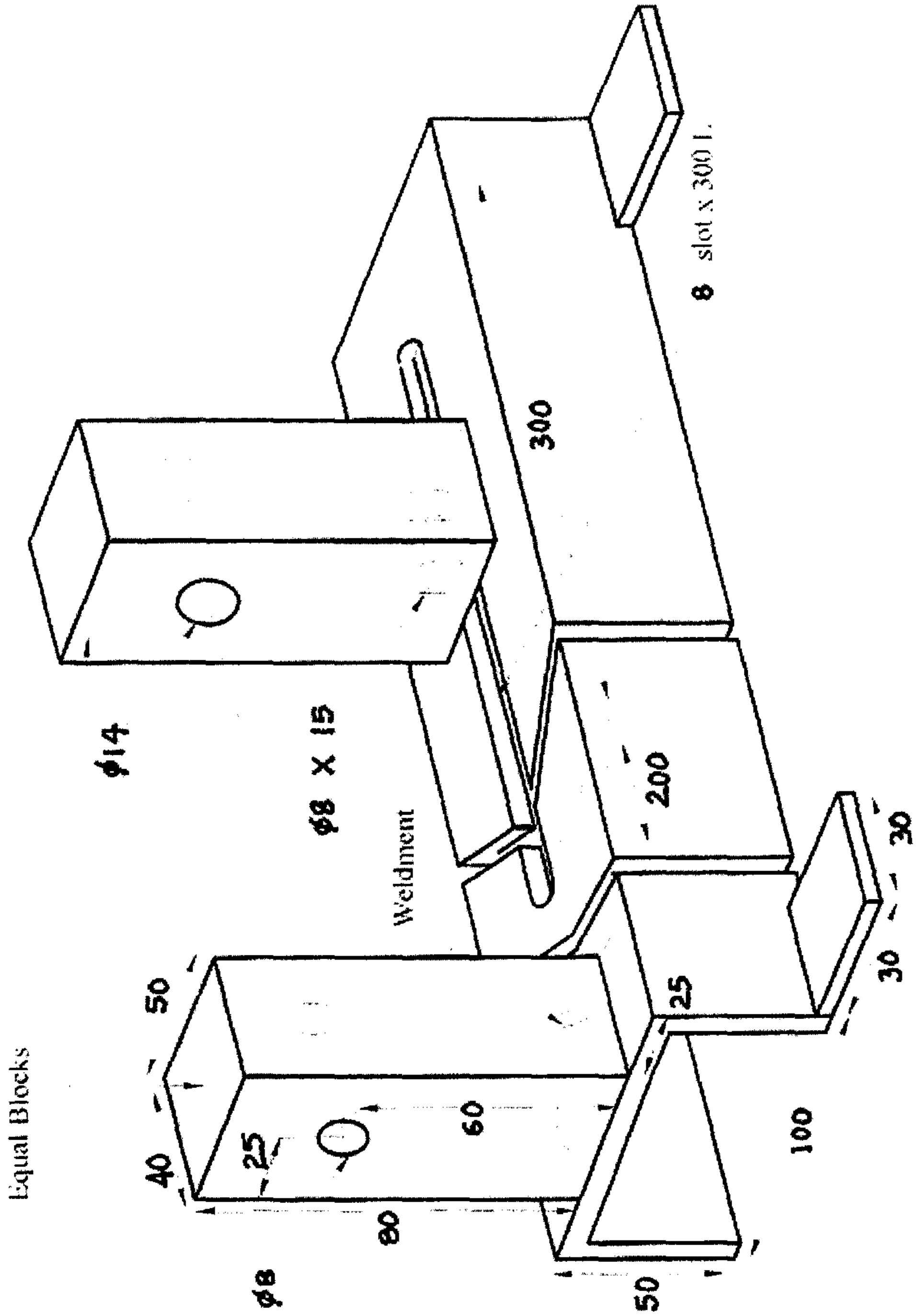

APPENDIX 2

) i) Part 1 Stiffness Measurement

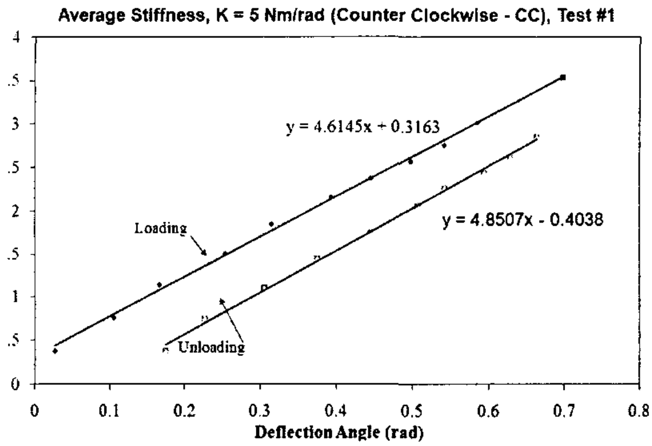

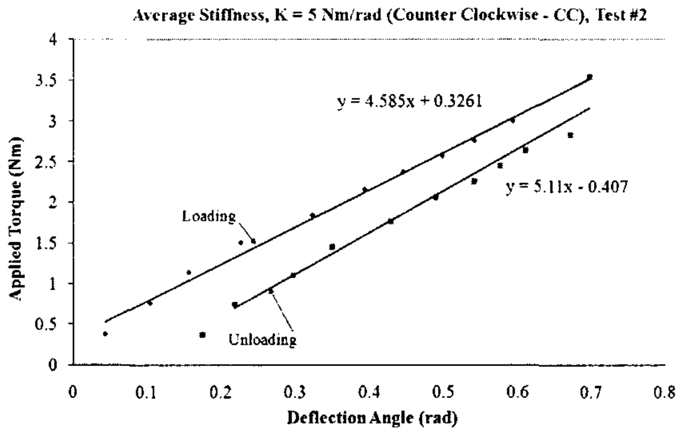

i) Counter Clockwise

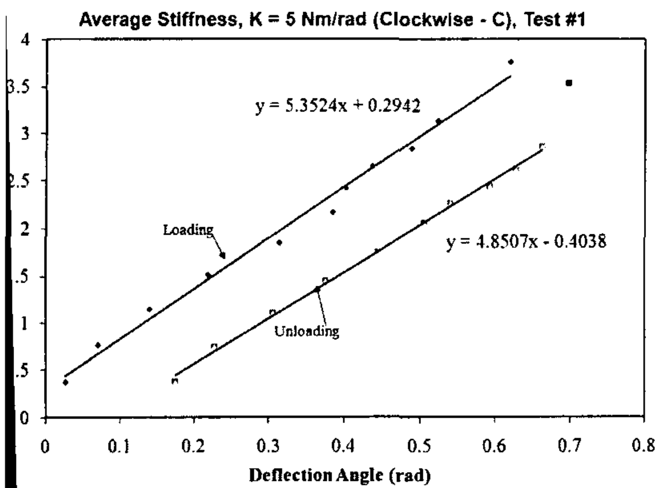

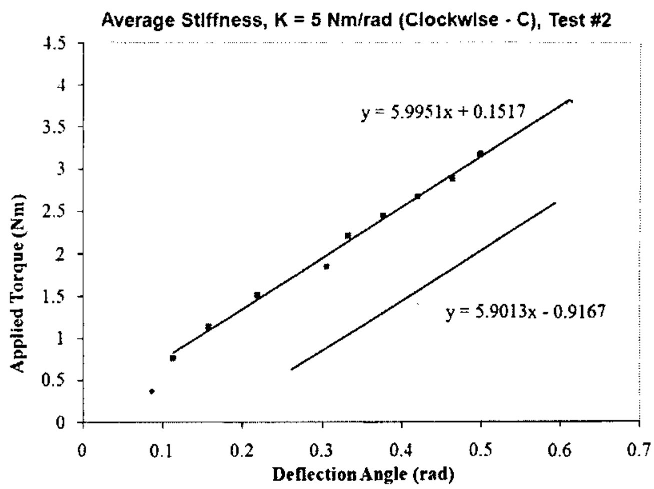

ii) Clockwise

$$\left(\frac{4.61+4.85+4.58+5.11+5.35+4.85+5.99+5.9}{8}\right)=5.2\,Nm/rad$$

APPENDIX 2

) ii) Part 2 Stiffness Measurement

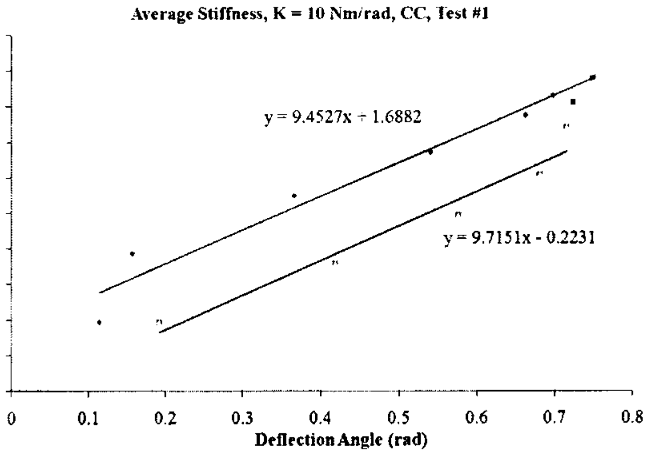

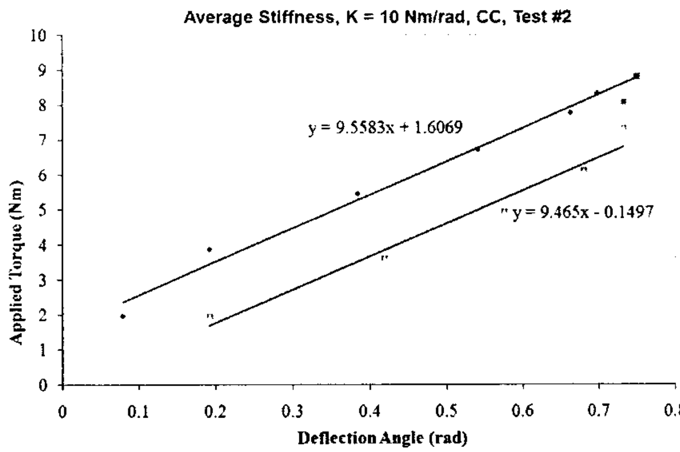

i) Counter Clockwise

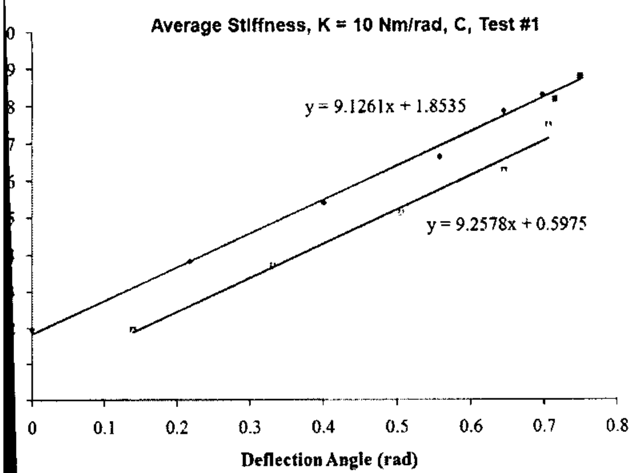

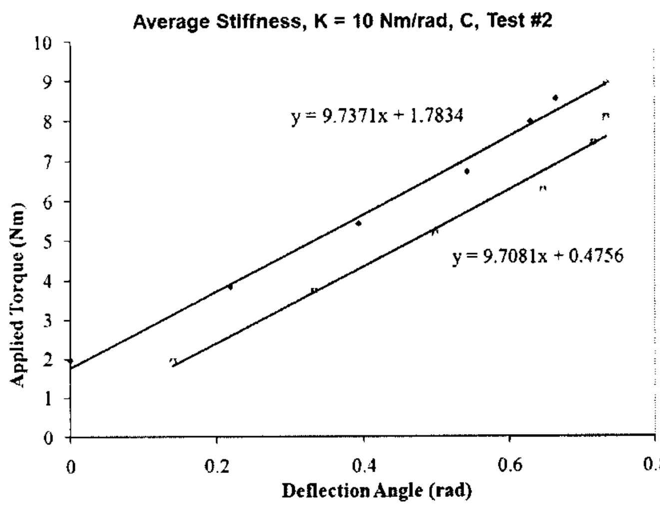

ii) Clockwise

$$= \left(\frac{9.45+9.72+9.56+9.47+9.13+9.26+9.74+9.71}{8}\right) = 9.5\ Nm/rad$$

APPENDIX 2

iii) Part 3 Stiffness Measurement

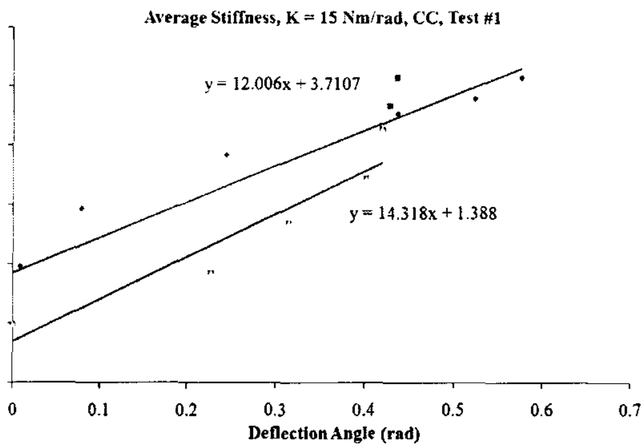

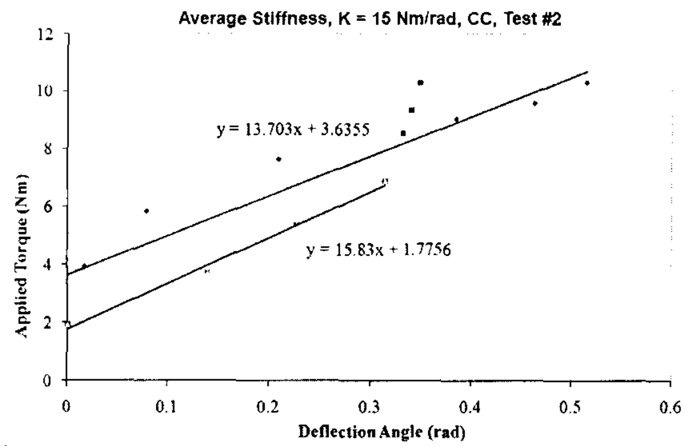

i) Counter Clockwise

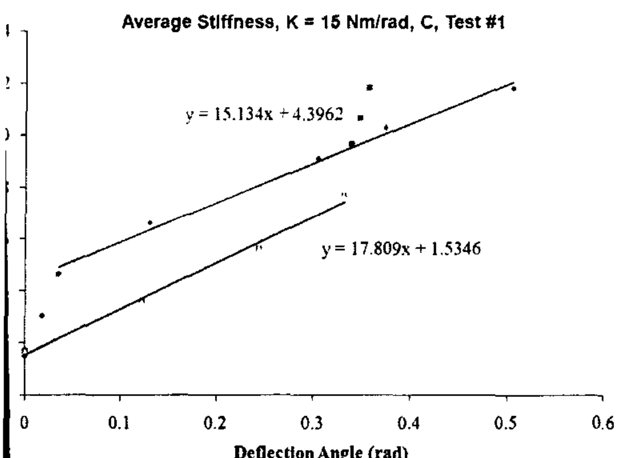

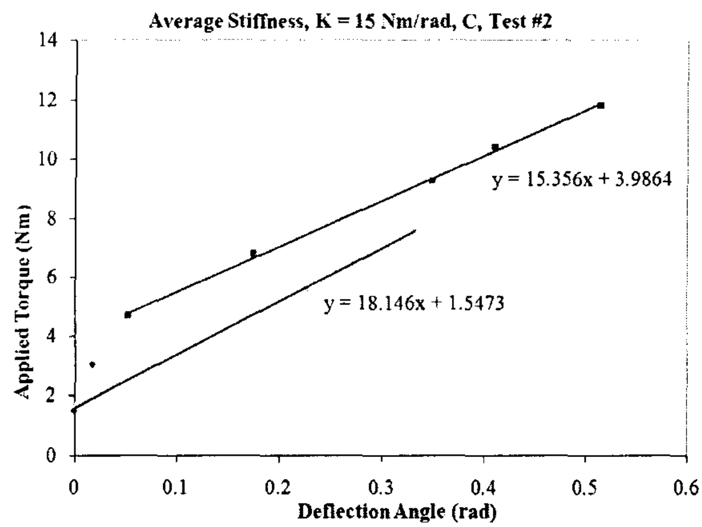

ii) Clockwise

$$K_3 = \left(\frac{12.0+14.32+13.7+15.83+15.13+17.81+15.36+18.15}{8}\right) = 15.3\ Nm/rad$$

<u>Summary of Results</u>

No.	Category/Class	Calculation	Measurement
1	5 Nm/rad	5.5 Nm/rad	5.2 Nm/rad
2	10 Nm/rad	10.7 Nm/rad	9.5 Nm/rad
3	15 Nm/rad	16.4 Nm/rad	15.3 Nm/rad

APPENDIX 2

) Locations of Data Logging Apparatus

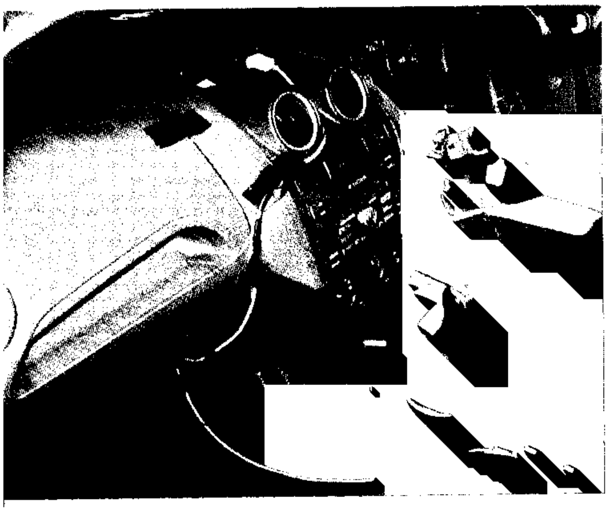

a) Location of DL1

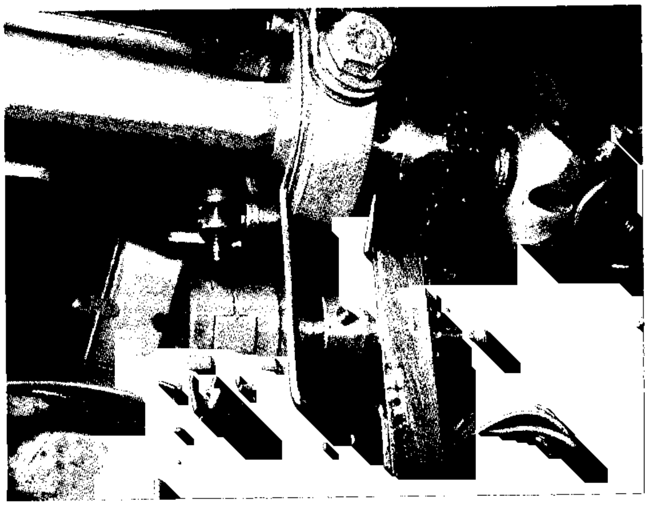

b) Location of Potentiometer

c) Location of Antenna

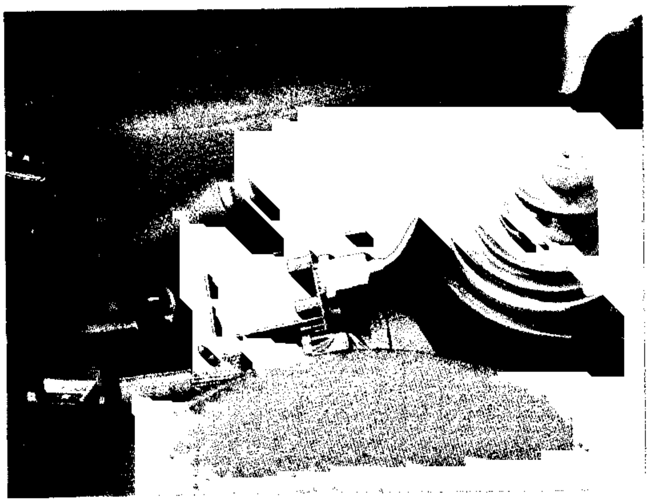

d) Location of Accelerometer

APPENDIX 2

k) Experimental Test Track

TMD Friction UK Limited

Lennerton Lane
Sherburn-in-Elmet
North Yorkshire LS25 6JE
United Kingdom

Tel +44 (0) 1977 683026
+44 (0) 1977 682644
Fax +44 (0) 1977 684171

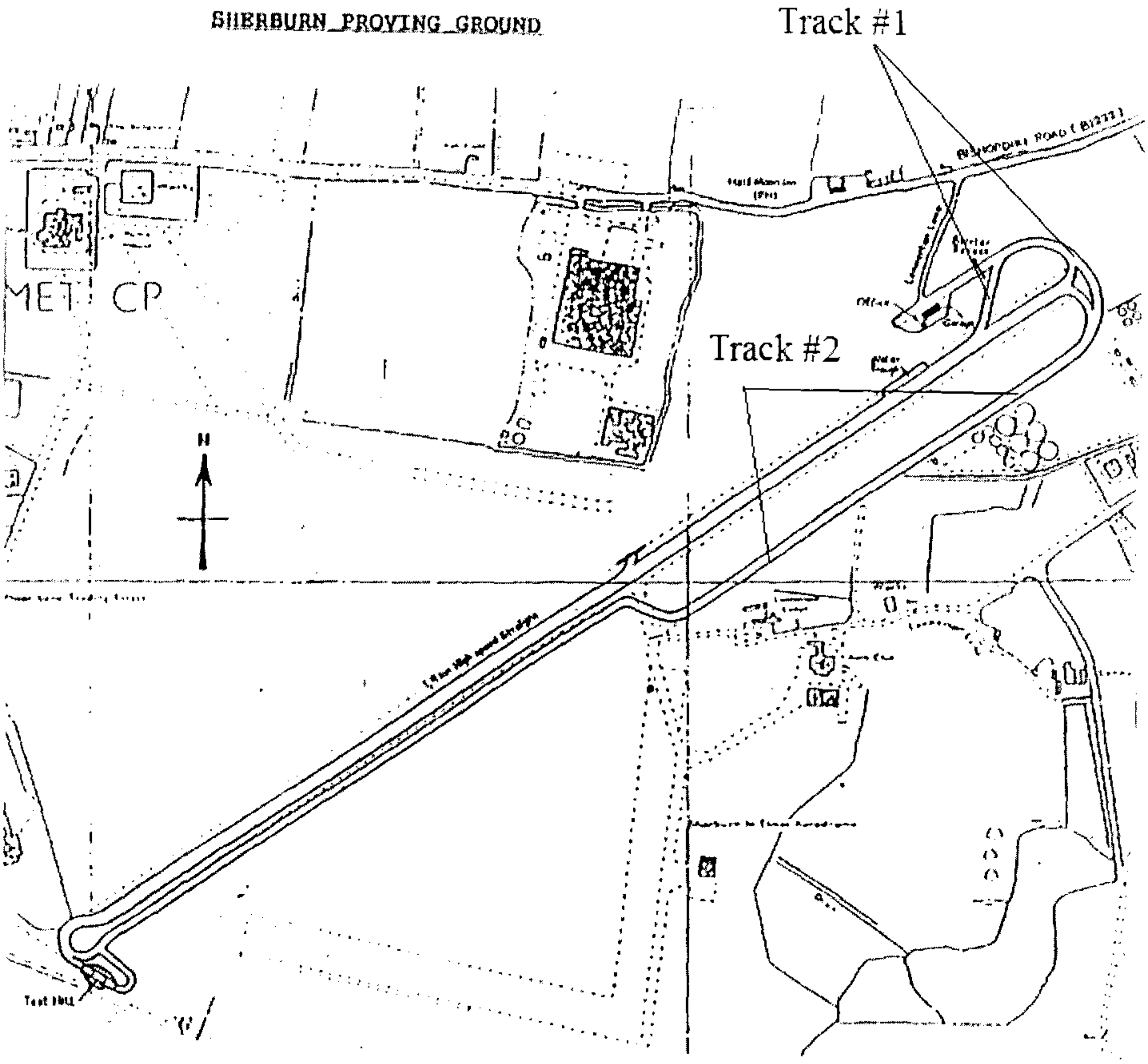

APPENDIX 2

I) Experimental Procedure for Vehicle Testing

Constant Velocity Cornering

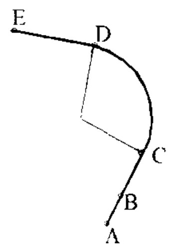

Procedure:

i. Accelerate vehicle from rest at A to achieve a constant speed, V at B.
ii. Maintain at speed V from B to C.
iii. Start cornering at constant speed V along the curve CD. Ensure that the vehicle speed is constant during cornering by pressing the accelerator if vehicle slows down.
iv. Start slowing down vehicle speed starting from D and stop at E.

Overtaking

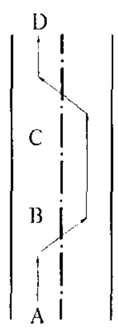

Procedure:

i. Drive at constant speed V from A and overtakes road barriers BC starting from appropriate distance
ii. Change to left lane after successfully passing C and slow down vehicle to a stop at D.

es:

Vehicle speed V is to be increased by every 5 mph; e.g. 5, 10, 15 , ...

The above tests are to be performed for every type of installed modified steering shaft stiffness (i.e. 5 Nm/rad, 10 Nm/rad, 15 Nm/rad) and for the conventional shaft without hydraulic power assisted system.

During testing, vehicle should be in second gear.

The maximum speed is 20 mph but can be increased to 30 mph if confidence persists.

Vehicle condition especially the modified parts should be inspected every time before proceeding with increased vehicle speed.

APPENDIX 2

m) Load Cell Housings for Measuring of Vehicle Weights

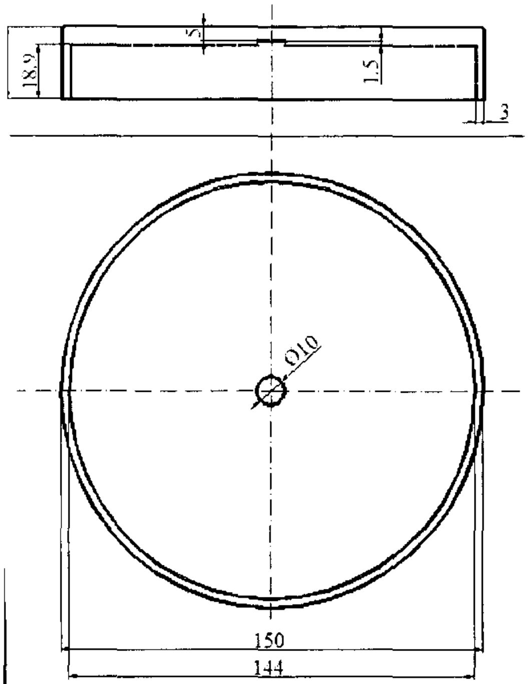

Load Cell Top Housing

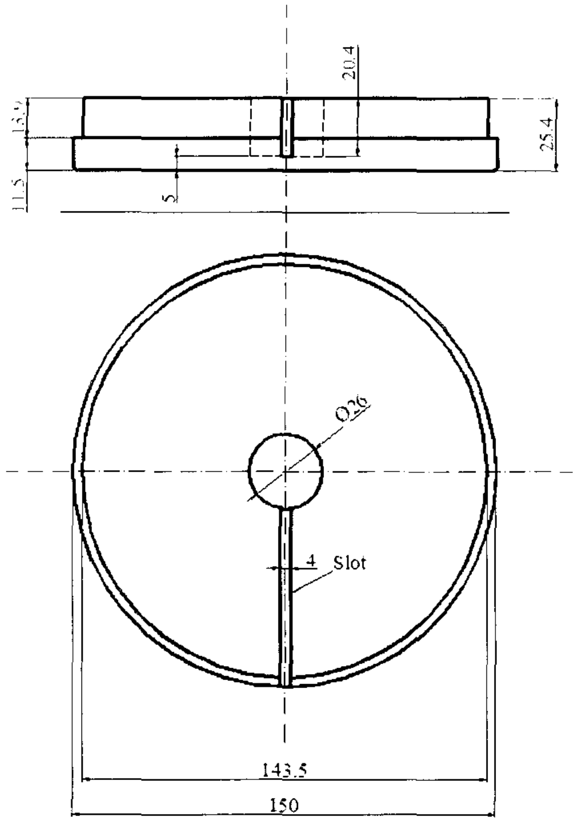

Load Cell Bottom Housing

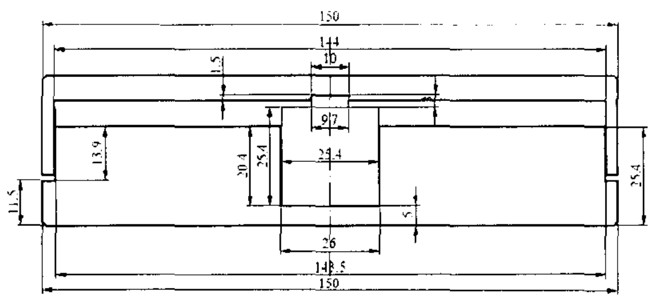

Assembly

APPENDIX 3

3(a) Front Suspension Details of JAGUAR X404 3L

*

3(b) Rear Suspension Details of JAGUAR X404 3L

*

3(c) Details of Rack and Pinion Steering for JAGUAR X404 3L

*

3(d) Power Boost Characteristics

*

3(e) Details of Rigid Chassis

*

3(f) Wheels Subsystem Configuration

*

3(g) Details of Antiroll Bar for SLA suspension

*

3(h) Details of Power-train

*

* These data are company confidential and can only be accessed by their permission. Please contact the author for more information.

APPENDIX 4

4(a) SPEED CLASS 10mph

Average Stiffness, K = 5 Nm/rad

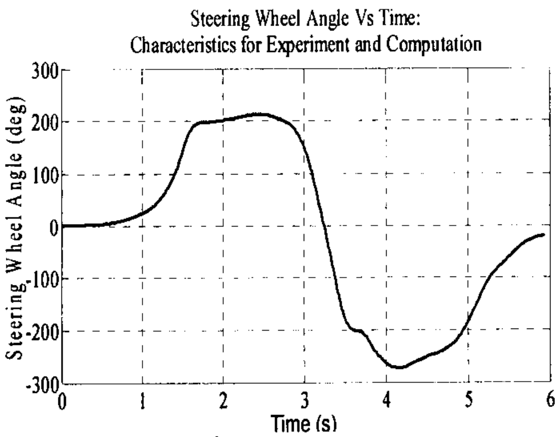

Figure 1

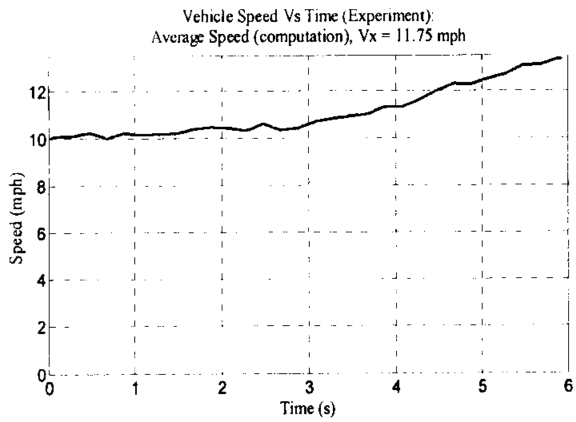

Figure 2

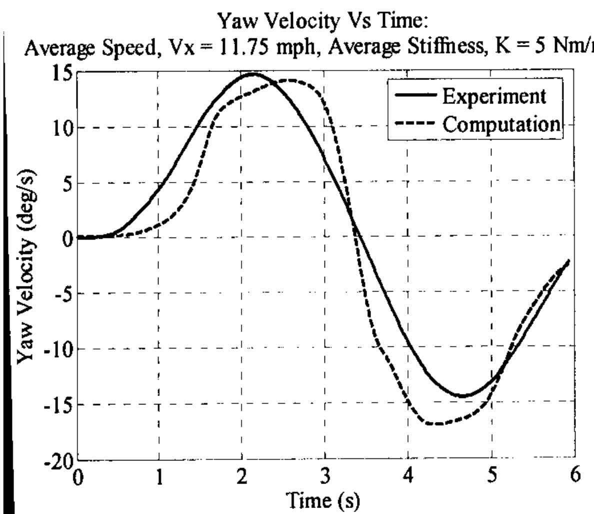

Figure 3

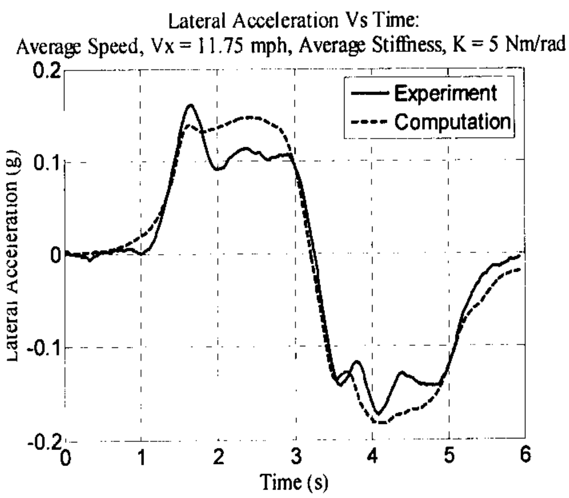

Figure 4

APPENDIX 4

Average Stiffness, K = 10 Nm/rad

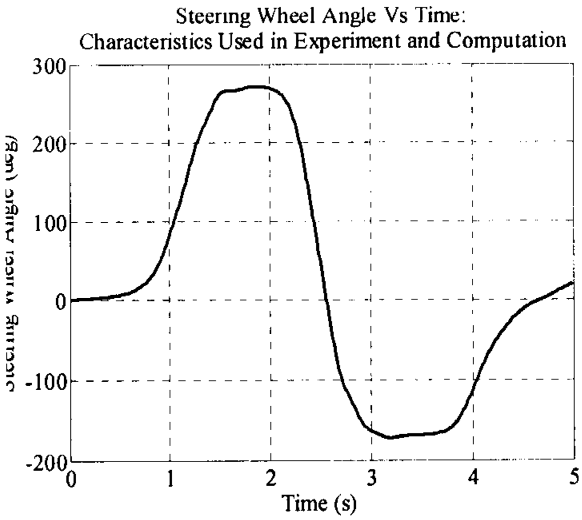

Figure 1

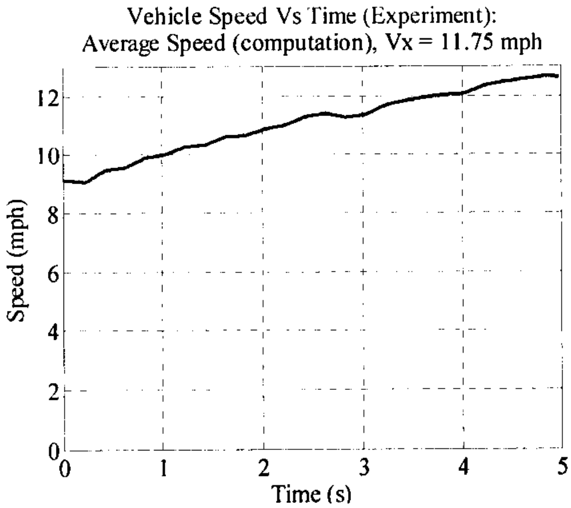

Figure 2

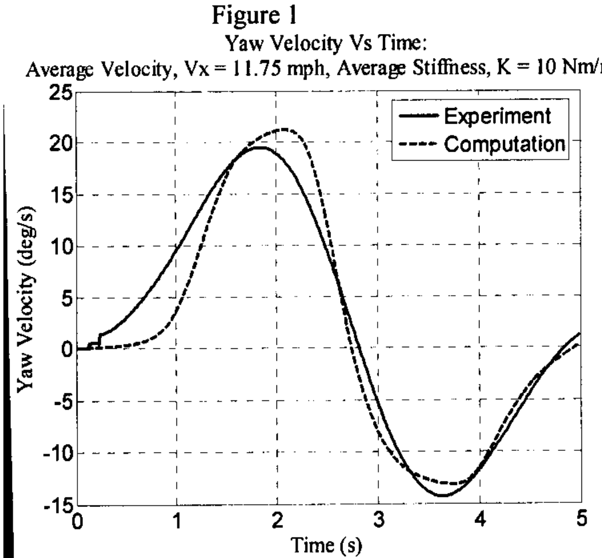

Figure 3

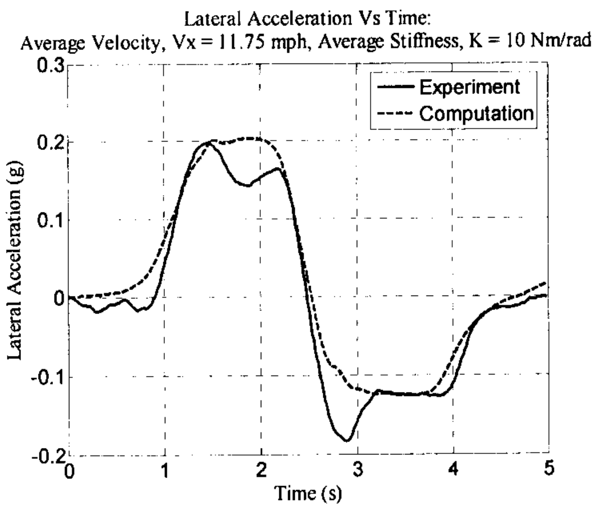

Figure 4

APPENDIX 4

Average Stiffness, K = 15 Nm/rad

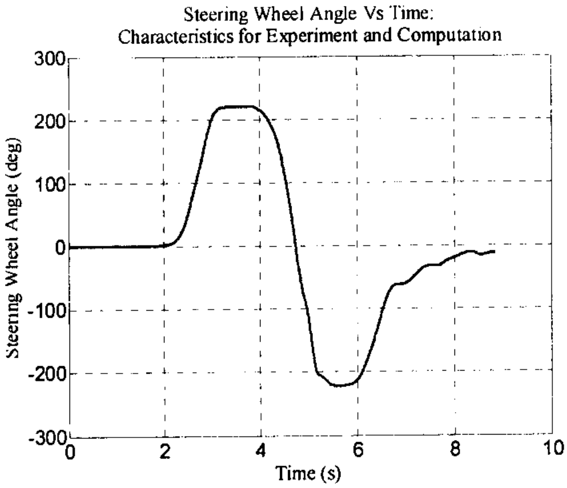

Figure 1

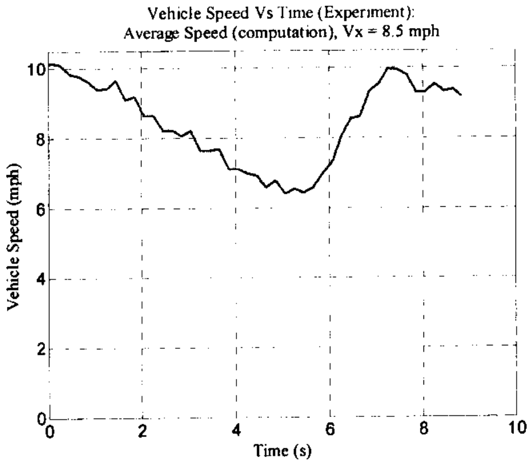

Figure 2

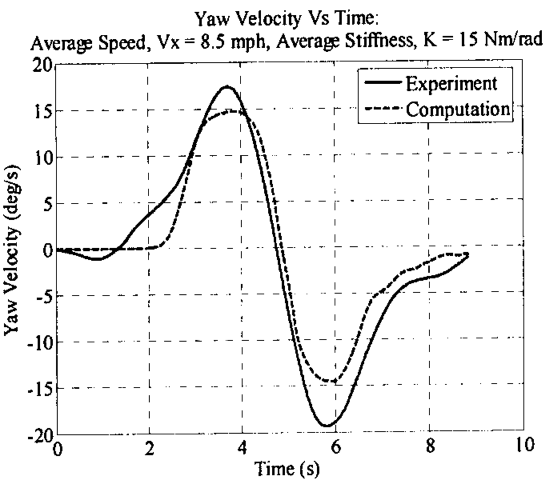

Figure 3

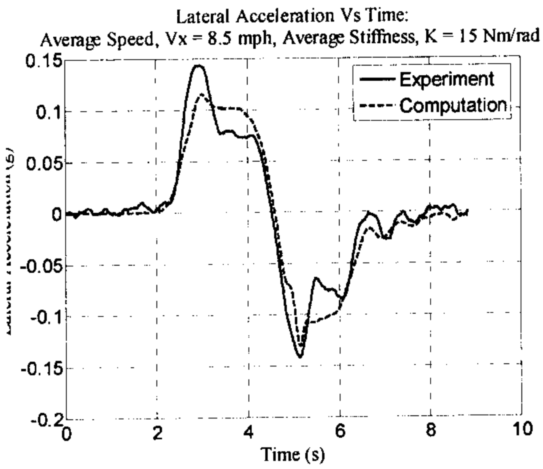

Figure 4

APPENDIX 4

CONVENTIONAL

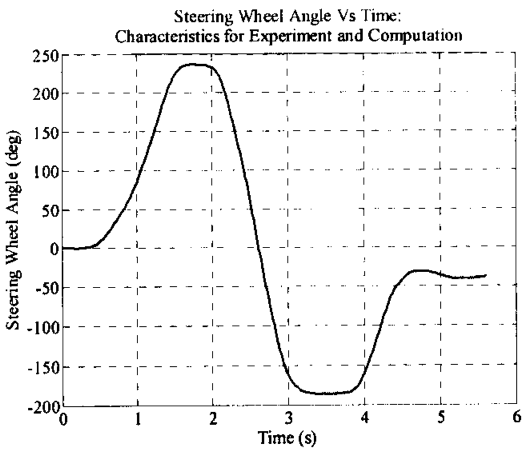

Figure 1

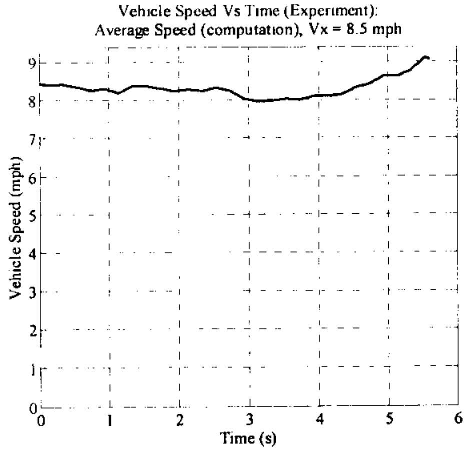

Figure 2

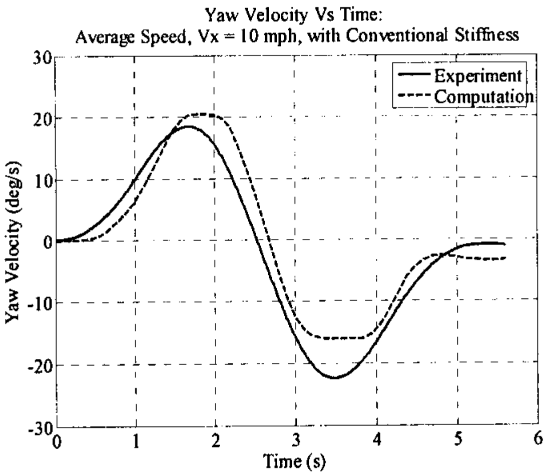

Figure 3

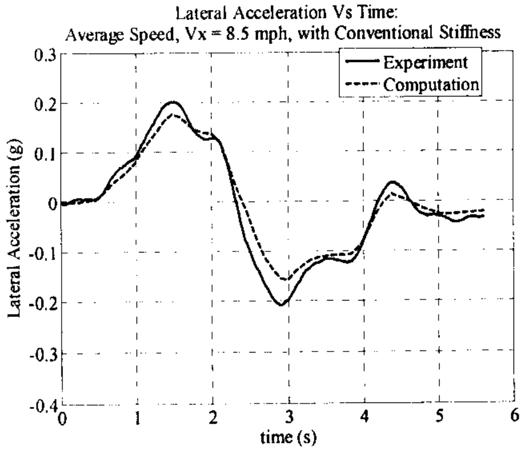

Figure 4

APPENDIX 4

4(b) SPEED CLASS 15mph

Average Stiffness, K = 5 Nm/rad

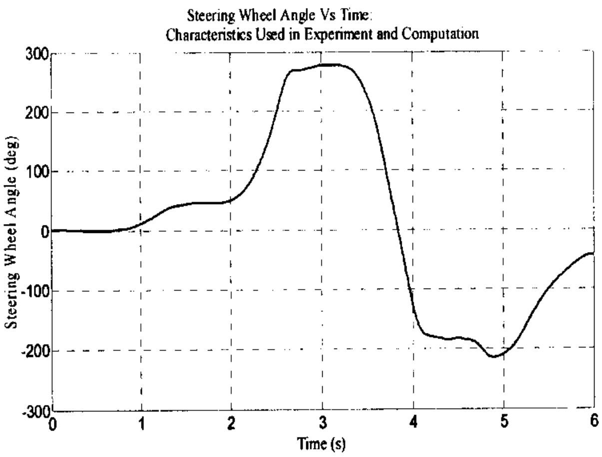

Figure 1

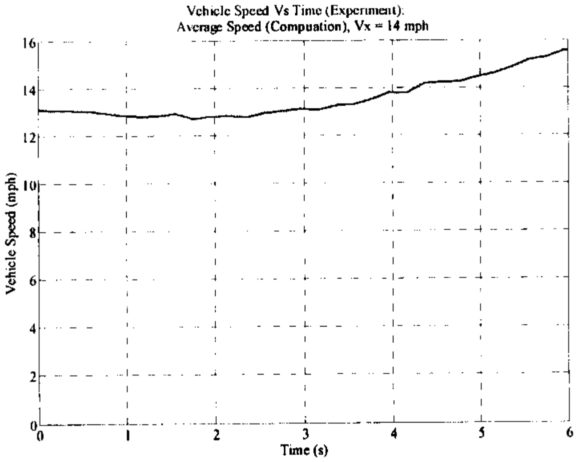

Figure 2

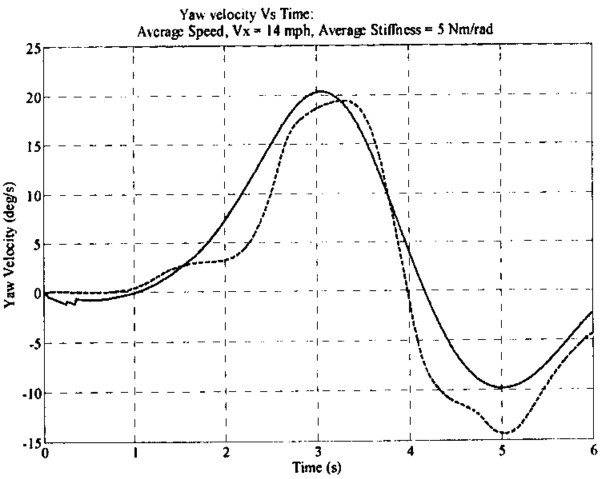

Figure 3

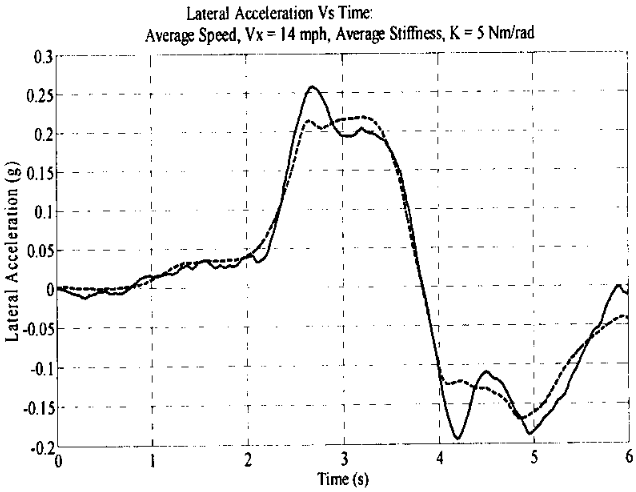

Figure 4

APPENDIX 4

Average Stiffness, K = 10 Nm/rad

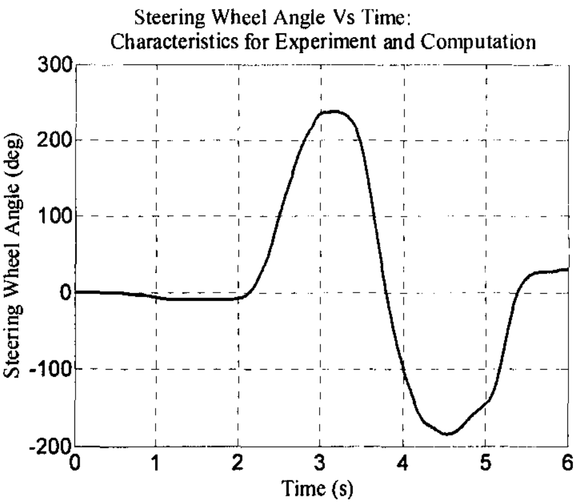

Figure 1

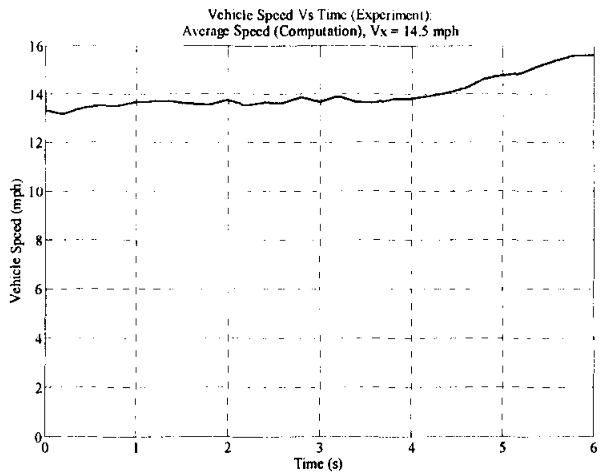

Figure 2

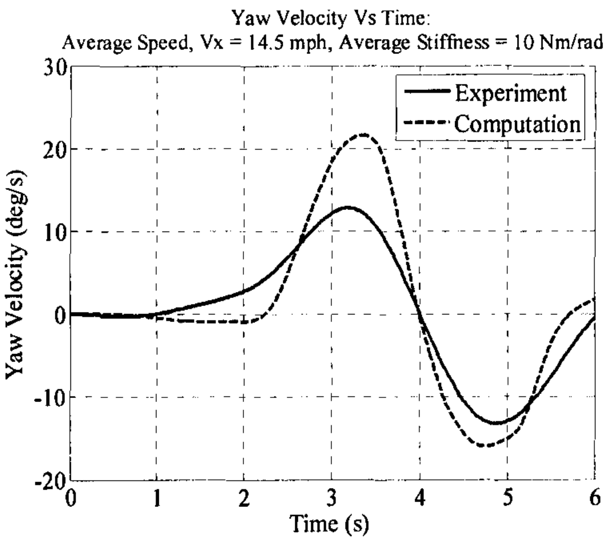

Figure 3

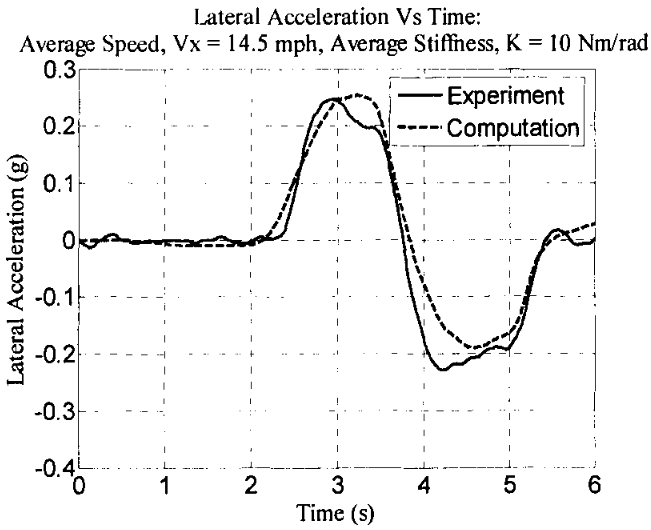

Figure 4

APPENDIX 4

Average Stiffness, K = 15 Nm/rad

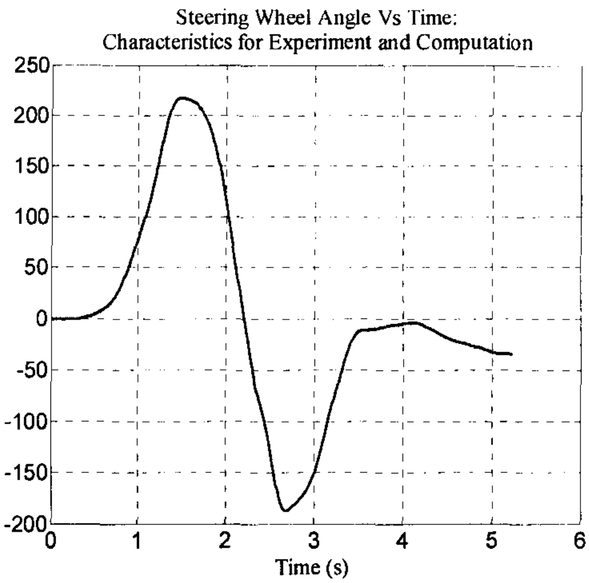

Figure 1

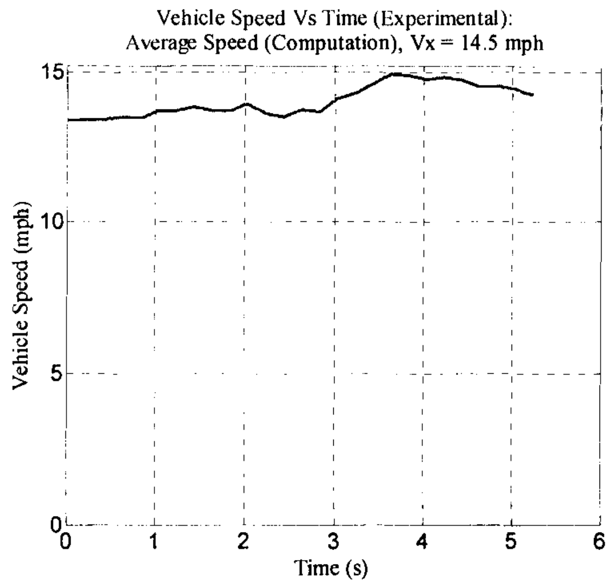

Figure 2

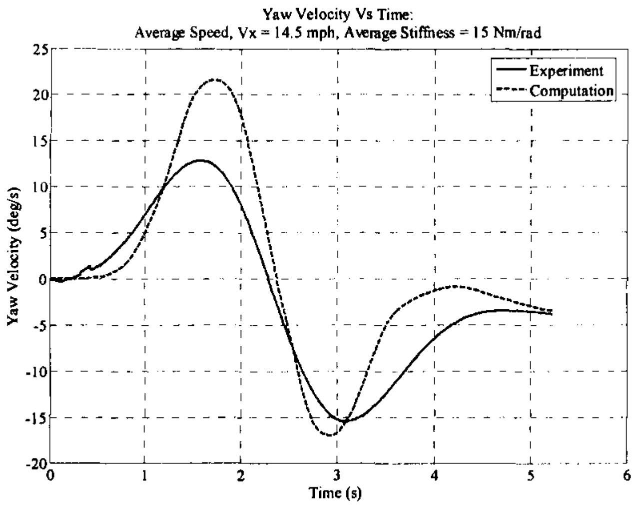

Figure 3

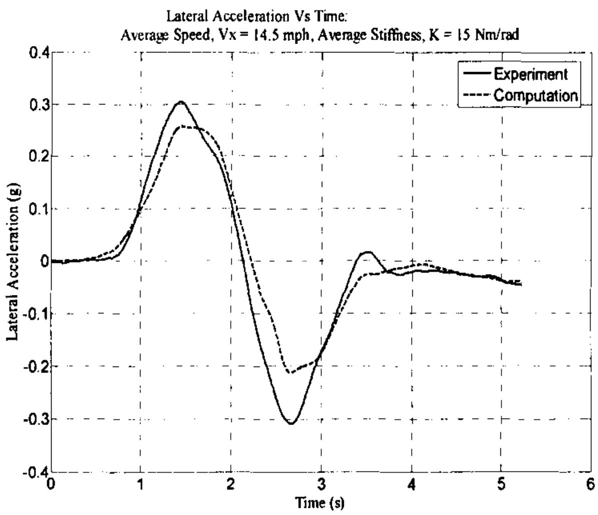

Figure 4

APPENDIX 4

CONVENTIONAL

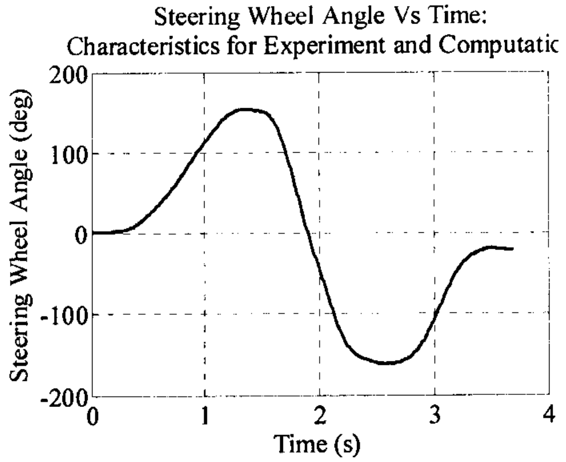

Figure 1

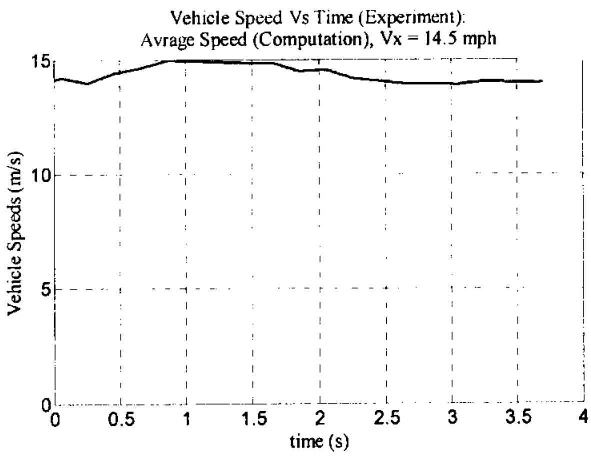

Figure 2

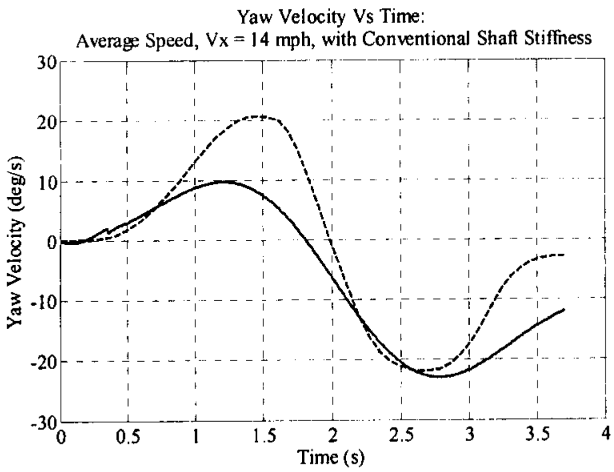

Figure 3

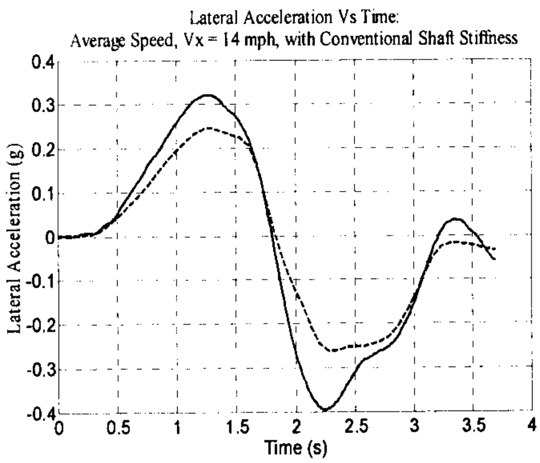

Figure 4

APPENDIX 4

4(c) SPEED CLASS 20mph

Average Stiffness, K = 5 Nm/rad

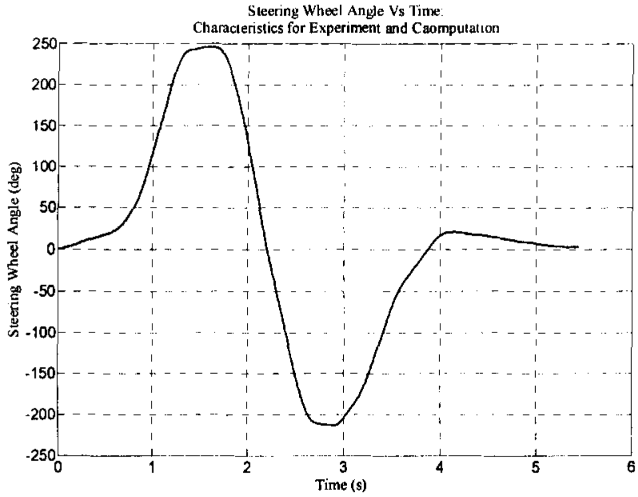

Figure 1

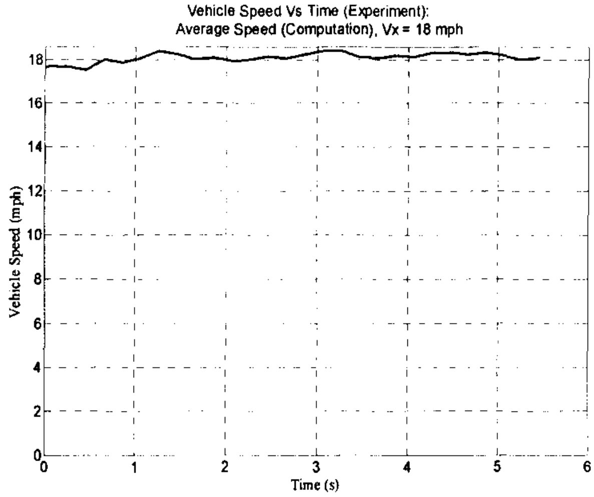

Figure 2

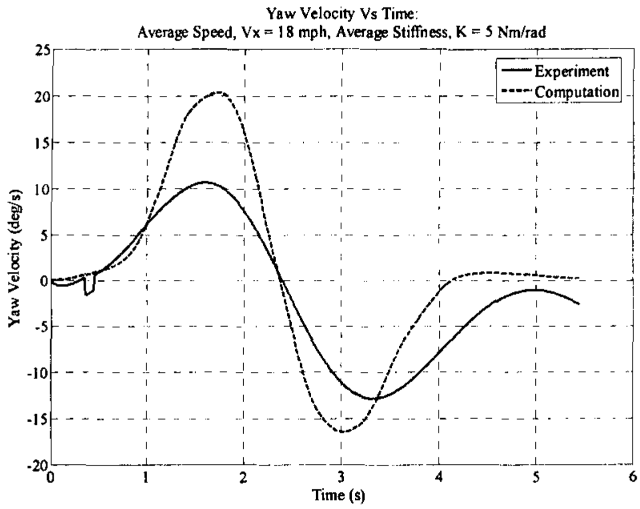

Figure 3

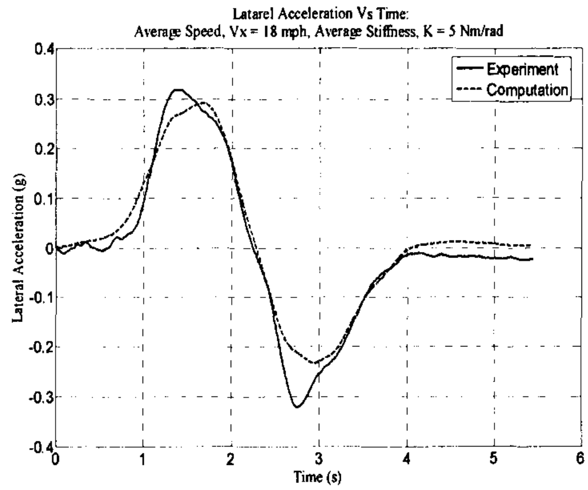

Figure 4

APPENDIX 4

Average Stiffness, K = 10 Nm/rad

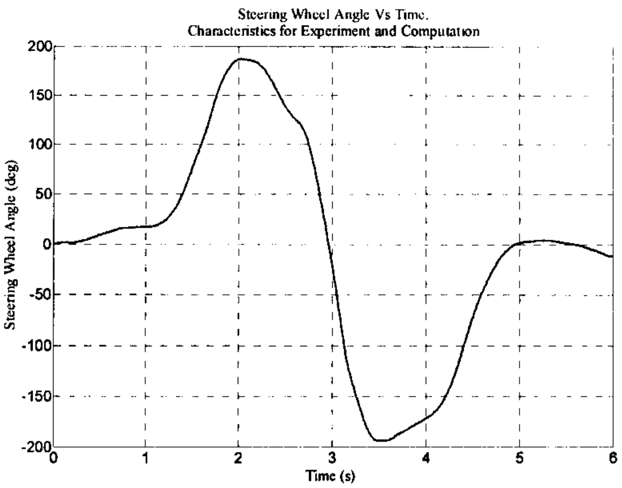

Figure 1

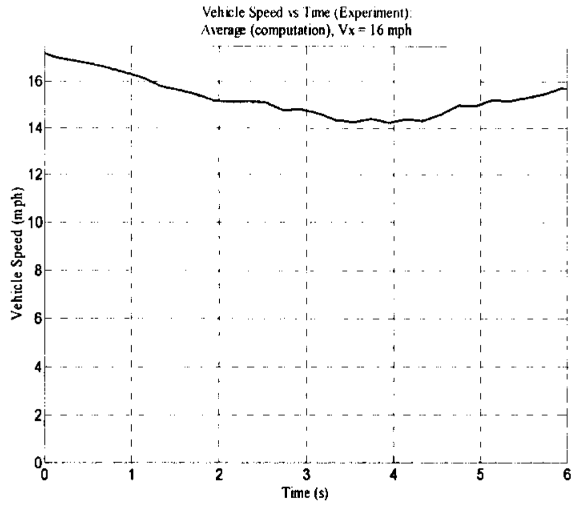

Figure2

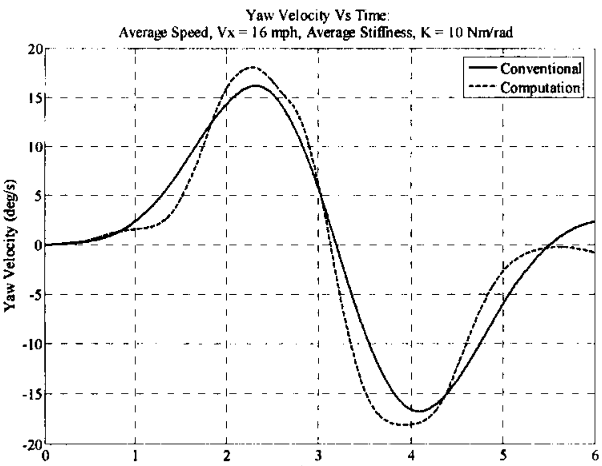

Figure 3

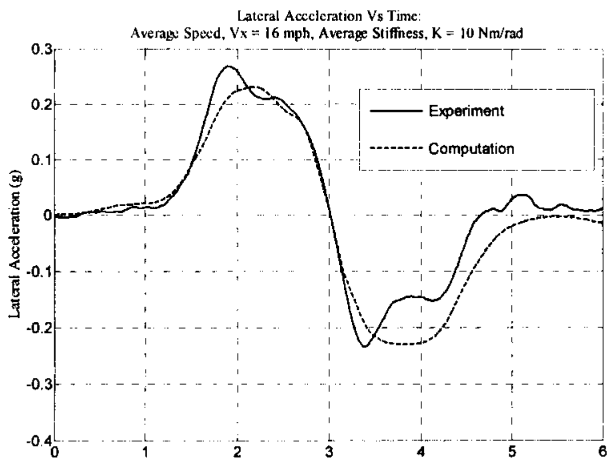

Figure 4

APPENDIX 4

Average Stiffness, K = 15 Nm/rad

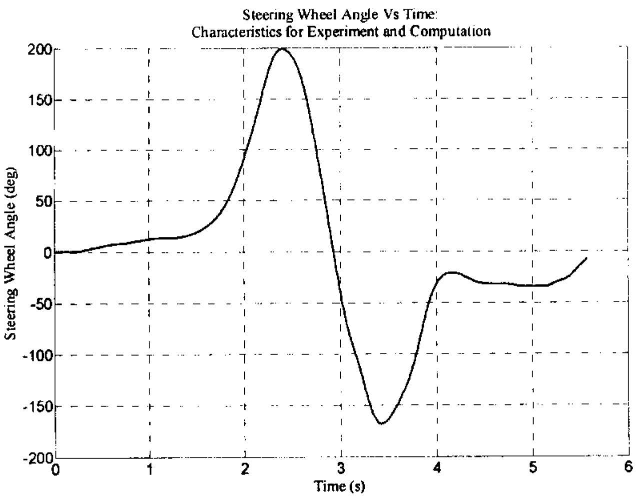

Figure 1

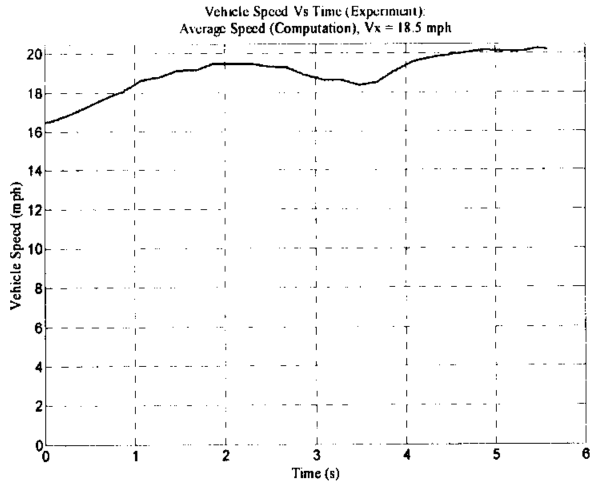

Figure 2

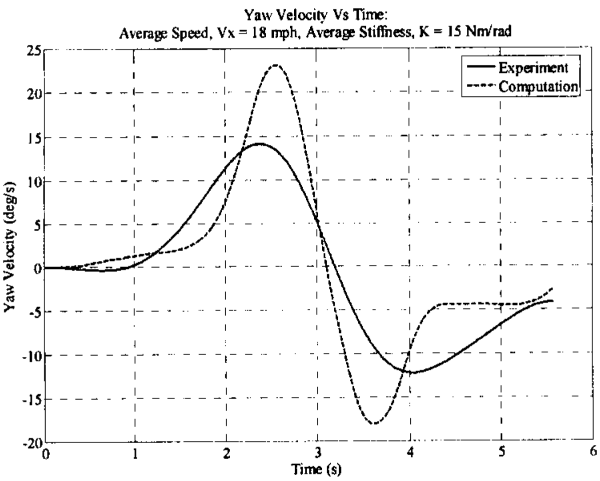

Figure 3

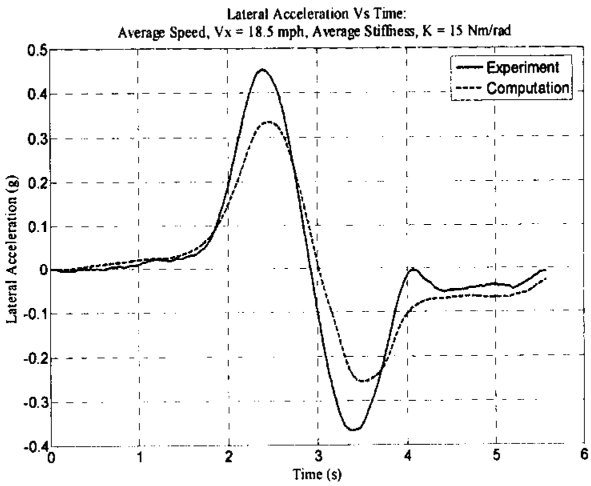

Figure 4

APPENDIX 4

CONVENTIONAL

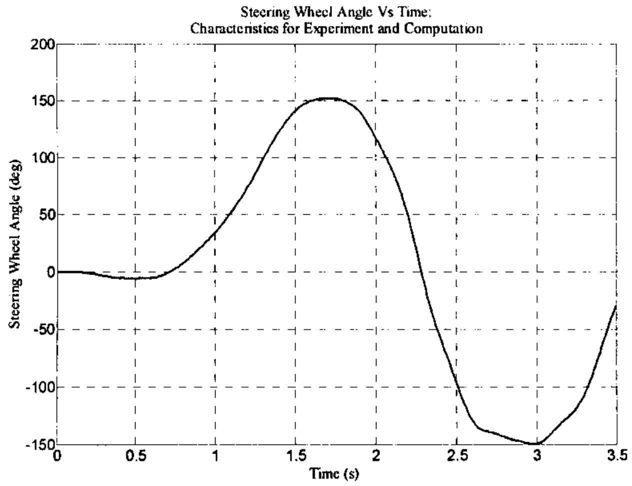

Figure 1

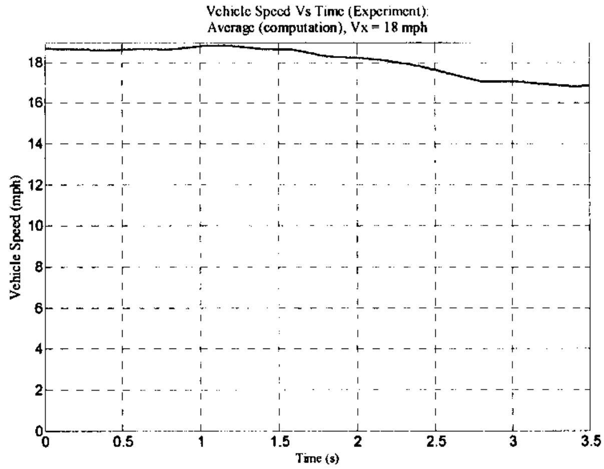

Figure 2

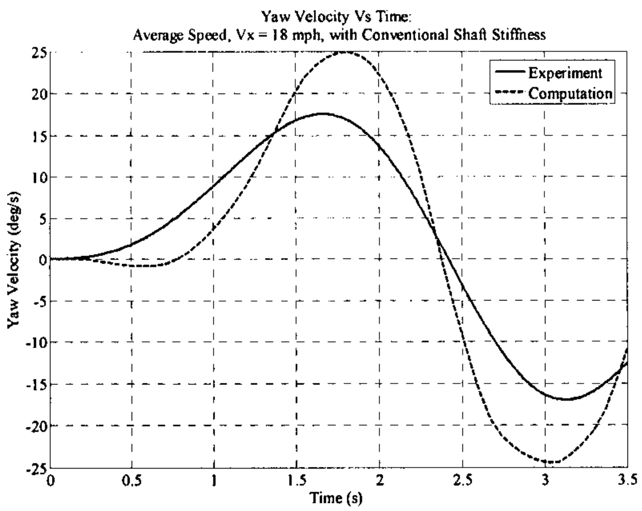

Figure 3

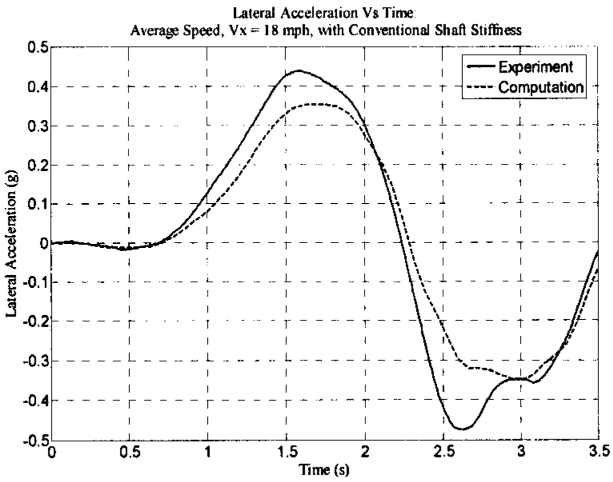

Figure 4